Naphthalene Hydrogenation with Water-Gas Shift in Model Oil/Water Emulsion Slurry over MoS_2

by

Christopher Choy

A thesis
presented to the University of Waterloo
in fulfillment of the
thesis requirement for the degree of
Master of Applied Science
in
Chemical Engineering

Waterloo, Ontario, Canada, 2009

I hereby declare that I am the sole author of this thesis. This is a true copy of the thesis, including any required final revisions, as accepted by my examiners.

I understand that my thesis may be made electronically available to the public.

Abstract

Catalytic naphthalene hydrogenation to tetralin in water/hydrocarbon emulsions with simultaneous water gas shift as the hydrogen source was performed in a 300 ml batch autoclave as a model for aromatic hydrogenation in water/bitumen emulsions. The catalyst utilized was an unsupported and dispersed type based on molybdenum sulfide (MoS_2). Distinguishing the fate of hydrogen from water as opposed to molecular hydrogen in hydrogenation and water gas shift was accomplished by utilizing deuterium oxide (D_2O) with NMR spectroscopy. The use of D_2O allowed determination of isotope effects when compared with H_2O. Diffuse Reflectance Infrared Fourier Transform Spectroscopy was performed to observe CO adsorption on the MoS_2 sulfide surface. Ruthenium was tested as a potential candidate to enhance the activity of the Mo catalyst. Iron, nickel and vanadium were utilized in combination with molybdenum to test promotional/inhibitive activity during naphthalene hydrogenation and water gas shift since Ni and V are found in significant quantities in real bitumen feed. Finally, a multifactorial experiment was performed to test the hydrogenation and water gas shift activity of a binary VNiMo-sulfide catalyst towards H_2S partial pressure, temperature and H_2 versus CO atmospheres.

Deuterium from D_2O was incorporated into both saturated and aromatic hydrogen positions in tetralin products. Calculation of a Hydrogenation Index and Exchange Index indicated the extent of H-exchange is greater than hydrogenation. Exchange between D_2O and organic products was enhanced with the MoS_2 catalyst under H_2 or CO compared to N_2. A kinetically measured isotope effect of 1.58 was in agreement with a quasi-equilibrium thermodynamic isotope effect for O-H dissociations measured in the

literature. A true kinetic isotope effect may be masked by transient surface concentrations occurring under batch conditions. Two strong vibrational bands associated with adsorbed CO were observed over MoS_2 above 160 °C. Activation of the MoS_2 surface with CO produces COS, suggesting an analgous mechanism to the production of H_2S during reduction in H_2. In the presence of H_2S, Ru displayed low catalytic activity for both water gas shift and naphthalene hydrogenation, attributed to incomplete sulfidation to active RuS_2. FeMo and VMo exhibited lower hydrogenation activity than Mo, but the water gas shift activity of VMo was high. A ternary VNiMo displayed lower hydrogenation activity than NiMo and Mo but was higher than VMo, implying Ni could offset the inhibition caused by V. Recycle of V and Ni rich asphaltene residues in catalytic slurry upgrading may therefore be feasible. An analysis of the effect of H_2S pressure, temperature and type of reduction gas (CO vs. H_2) concluded that temperature had the greatest positive effect on rate, followed by a small interaction effect of temperature/gas type and P_{H2S}/gas type. The proximity to equilibrium conversions in WGS limited the analysis, while equilibrium limited the conversion of naphthalene at 380 °C in the batch reactor.

Acknowledgements

My sincere thanks to Dr. F.T.T. Ng for her supervision, encouragement and guidance throughout this research. To members of the Ng laboratory at the University of Waterloo: Aziz Alghamdi, Aijaz Baig, Kamalakar Gunda, Amir Irivani, Justin Jia, Kun Liu, Jennifer Moll, Bill O'Keefe, Prem Pal, Zhiwen Qi, Yinmei Ye and Keir Thomas for their support, encouragement and enlightening discussions.

A special thanks also to Peter Byrne, Bert Habicher and Rick Hecktus for their technical expertise and patience. Ralph Dickhout and Jan Venne (Chemistry) provided invaluable assistance with analytical and Nuclear Magnetic Resonance. A special thank you also to Dr. Zhongwei Chen and Dr. Bill Epling for their insightful comments during their review of this document.

Finally, my thanks to the staff of the Department of Chemical Engineering at the University of Waterloo for their help and my fellow students who endured long meetings in the Graduate House.

Dedication

To Sylvia, Janice and Jonathan and in loving memory of Lawrence.

Table of Contents

List of Figures

List of Tables

List of Schemes

Nomenclature

Latin letters

acac	acetylacetonate $(C_5H_7O_2)^-$
ATTM	ammonium tetrathiomolybdate (NH_4MoS_4)
c (prefix)	cis-isomer
C	Concentration (mol/g-liq)
CI	Confidence Interval
D	Deuterium Isotope of Hydrogen (^2H)
DBT	Dibenzothiophene ($C_{12}H_8S$)
DEC	both isomers of decalin ($C_{10}H_{16}$)
df	degrees of freedom
DRIFTS	Diffuse Reflectance Infrared Fourier Transform Spectroscopy
EDX	Energy Dispersive X-Ray
f	number of factors in an experimental design
$F_{i,j,1-\alpha}$	In the F-test, the ratio of two means or measurements, $\frac{\overline{X_i}}{\overline{Y_j}}$, where i and j are the degrees of freedom associated with each mean and α is the confidence level.
$F_{critical}$	from the F-tables, the value of F that $F_{i,j,\alpha}$ must exceed for $\overline{X}$ and $\overline{Y}$ to be considered significantly different.
^1H	protium isotope of Hydrogen
HDN	Hydrodenitrogenation
HDS	Hydrodesulfurization
HR-TEM	High Resolution Transmission Electron Microscopy
HYD	Hydrogenation
IR	Infrared Spectroscopy
k_i	pseudo-first order rate constant of species I (s^{-1})
$k"_i$	pseudo-second order rate constant (g-liq/mol-s)
KIE	Kinetic Isotope Effect
m_i	mass of species or sample I (g)
$N_{i,t}$	number of mols of species i at reaction time t
MS_e	Mean Square Error (variance)
MS_i	Mean Square of the effect of parameter i
NAPH	naphthalene ($C_{10}H_8$)
NPT	naphthalene ($C_{10}H_8$)
NMR	Nuclear Magnetic Resonance Spectroscopy
$P_{i,t}$	Pressure of species i at reaction time t (psig or Pa)
PMA	Phosphomolybdic Acid ($H_3PMo_{12}O_{40}$)
R	Ideal Gas Constant (8.314 Pa-m^3/mol-K) or (0.082061 atm-L/mol-K)
s	standard deviation
s^2	Variation
s_p^2	pooled variance

SS_i	Sum of Squares of factor i
t	reaction time (min); trans-isomer (prefix)
T	temperature (K) or (°C)
TET	tetralin ($C_{10}H_{12}$)
TPR	Temperature Programmed Reduction
Volts	Voltage (Volts)
V_g	Volume of gas in reactor (ml)
V_l	Volume of liquid in reactor (ml)
V_{SB}	Volume of sampling bomb (ml)
WGS	Water-gas Shift
XRD	X-ray Diffraction

Greek Letters

A	level of confidence interval, where percentage of measurements will lie between $2s \leq \overline{X} \leq 2s$
Δ	change in a measurement or calculation
υ_i	wavenumber; Infrared vibrational absorption of species i (cm^{-1})
χ_i	Dry basis normalized gas phase composition (mol%)

Chapter 1: Background

1. 1 Introduction

Increasing energy demands coupled with a plateau in discovery of new oil reserves has emphasized the need to further develop known hydrocarbon reserves. The Athabasca Oil Sands deposit in northern Alberta has an estimated reserve of 1.7 billion barrels of oil that is second only to Saudi Arabia. Bitumen is extracted from oil sand as,

1) Bitumen froth from Surface Mining and Hot Water Extraction
2) Bitumen emulsions extracted from in-situ methods such as Cyclic Steam Simulation (CSS)

Both bitumen froth and emulsions have significant amounts of entrained water. The bitumen emulsion must be broken and dewatered before further processing which can be difficult since the emulsions can be very stable. The crude bitumen is a highly viscous product that is high in sulfur, nitrogen, metals and asphaltene content (Table 1.1.1). Upgrading of the bitumen into a light, sweet product that is easier for conventional refineries to process is required.

Table 1.1. 1: Properties of a Cold Lake Bitumen (Environment Canada)

API Gravity	9.8
Sulfur (wt%)	6.9
Density at 25 °C (kg/m^3)	994.3
Dynamic Viscosity at 0 °C (cP)	> 3 000 000
Asphaltenes (wt%)	13
Boiling Point Distribution above 550 °C (wt%)	65
Iron (ppm)	15.2
Nickel (ppm)	69
Vanadium (ppm)	190

1. 2 Residue Upgrading: Hydroprocessing and Hydrotreating

The hydroprocessing of bitumen or heavy oil achieves several goals, including (Speight 2006):

- reduction of metals, organic sulphur and nitrogen content
- conversion of low value, high boiling Conradson Carbon Residues (CCR) to distillate and naphtha through hydrogen addition
- increase API gravity and reduce viscosity

Sulphur removal is important as new emissions standards for gasoline and diesel in Canada have been mandated at 80 ppm and 15 ppm placing additional strain on downstream hydrotreaters. An advantage of hydroprocessing over more conventional carbon rejection processes such as delayed coking and fluid coking is the higher yield of liquid products obtained (Rana et al. 2007). For high value fractions such as naphtha and

distillate, hydrotreating reduces organosulfur, organonitrogen and aromatics with high yields. The main disadvantage of hydroprocessing is the requirement for expensive H_2. The requirement for hydrotreating of diesel is dictated by environmental rather than economic factors.

1. 3 Catalytic Slurry Phase Upgrading

Supported hydroprocessing catalysts such as Co-Mo/Al_2O_3 and Ni-Mo/Al_2O_3 in bitumen upgrading applications have mass transfer limitations. Large asphaltene molecules must diffuse into the porous support structure to the active sites for hydrogenation and cracking to occur. Aggregation and condensation of asphaltenes and maltenes can cause coke deposition. The presence of V and Ni impurities in bitumen feed deactivates the catalyst. Catalyst deactivation occurs due to the deposition of vanadium sulfides and nickel sulfides on active molybdenum sulfide particles while deposition of metal sulfides and coke in the pores block access to the active sites.

An alternative is the use of un-supported, dispersed catalysts. These can be homogeneous or slurry catalysts (Rana et al. 2007). A novel slurry catalyst developed by ExxonMobil, known as M-coke, incorporates an active catalytic metal sulfide phase into a hydrocarbonaceous matrix formed from feedstock oil (Bearden 1981). Its purpose is to control coking reactions by hydrogenating hydrocarbon radical species, preventing their oligomerization to asphaltenes and increasing liquid yields from heavy feeds. Conversions of 100+ vol% were achieved in pilot scale operations. Mo displayed the best hydrodesulfurization (HDS) and CCR conversion compared to Ti, Mn, Cr, V and Fe.

Phosphomolybdic acid (PMA) was found to give an excellent compromise between effectiveness and cost at catalyst concentrations as low as 100 ppmw of Mo; addition of phosphoric acid for a P:Mo atom ratio of 0.5-3.5 was found to enhance the activity even more (Bearden 1981).

The similarity in size of the catalyst particles compared to asphaltene molecules is believed to allow rapid diffusion of the catalyst into asphaltene aggregates resulting in better reaction rates and conversions. Effective catalysts may be introduced as homogenous precursor solutions into a bitumen/heavy oil feed and are formed in-situ under reaction conditions (Zhang et al. 2007). The $(HC)_3$ technology developed by Alberta Research Council was compared with a commercial supported catalyst for upgrading performance. Overall bitumen conversion and asphaltene conversion were similar, in comparison to a supported catalyst where asphaltene conversion plateaued as the overall bitumen conversion continued to increase. This indicates mass transfer limitations for the supported catalyst whereas the unsupported catalyst shows no such inhibition (Zhang et al. 2007).

Organic free-radicals formed at high temperatures can agglomerate to form high molecular weight molecules and produce coke. Reducing coke production by preventing free-radical condensation can maximize hydrocarbon yields from bitumen. In hydroprocessing, this is achieved through dissociation of H_2 to form hydrogen radicals at high hydrogen pressure which combine with organic free radicals to prevent their polymeriziation. Alternatively, in the presence of solvent with high H/C ratio, thermolytic dissocation of C-H can form hydrogen radicals which can transfer to substrate radicals. An interesting process developed jointly by UOP, Foster-Wheeler and the Venezuelan

organization Intevep is titled Aquaconversion™ (Rana et al. 2007). This visbreaking process aims to reduce the viscosity of heavy oil while reducing coke formation compared to traditional delayed coking technologies. Steam is injected with the heavy oil, and an alkali catalyst is introduced as a metal salt. Marzin et al. suggested the catalyst promotes dissociation of H_2O to form hydrogen radicals which can add to organic free-radicals and prevent polymerization to ashphaltene (Marzin et al. 1986); however dissociation into H^+ and HO^- is more likely due to a lack of evidence for radical formation. CO_2 is also formed in the process. The process apparently enjoys mild pressure and temperature conditions which can be adapted to conventional visbreaking units with little difficulty. Table 1.3.1 exhibits properties of a Pilon crude upgraded using Aquaconversion™ technology.

Table 1.3.1: Characteristics of Pilon Crude after Aquaconversion™ (Marzin et al. 1986)

Improvement in API Gravity	6
Reduction in Viscosity at 50 °C (%)	99
Hydrodesulfurization Conversion (wt%)	17
Hydrodenitrogenation Conversion (wt%)	20
Conradson Carbon Conversion (wt%)	15
C_7-insoluble Asphaltene Conversion (wt%)	10
Acidity Reduction (%)	93

Use of metal-rich residues from upgrading units could represent an economic alternative to the use of Mo-based catalyst although Ni and V sulfides are not as effective catalysts. Bitumen asphaltenes contain high concentrations of vanadium and nickel (Table 1.3.2). Dunn et al. (Dunn et al. 2003) utilized V and Ni-rich carbonaceous Venturi fines (~12 wt% total metals) and flexicoker ash (~50 wt% total metals) obtained from an ExxonMobil flexicoking unit, to upgrade a simulated Cold Lake bitumen. Sulfidation

with H_2S at 420 °C significantly increased sulfur incorporation into the solids compared to elemental sulfur at 385 °C, but showed no benefits in hydroconversion (Dunn et al. 2003). The highest API conversion was achieved on a once-through basis, with notable deactivation on subsequent catalyst recycle runs due to coke deposition. Removal of coke via thermal oxidation led to a decrease in catalytic activity caused by sintering and loss of surface area compared to the fresh catalyst. Retention of surface area should accompany removal of carbon deposits in order to preserve catalytic activity of the flexicoker solids (Dunn et al. 2003).

Table 1.3.2: Nickel and Vanadium in Cold Lake Asphaltene (Semple et al. 1990)

Metal Concentration (ppm)		V in Porphyrin concentration
Ni	V	(wt%)
820	320	12

1. 4 Coupling of Water-Gas Shift, Hydrodesulfurization (HDS) and Hydrogenation (HYD)

The production of H_2 from CO in synthesis gas (CO/H_2) to replenish H_2 is one route for hydroprocessing of bitumen emulsions/froths. Use of syngas for bitumen upgrading is feasible since asphaltenes and pitch recovered from the upgraded product can be gasified to produce synthesis gas (Ng 1989; Hook 1986). The primary goal of substituting synthesis gas for pure hydrogen may be economic. However, the most significant cost-savings can be achieved by eliminating the operational and capital requirements for hydrogen purification.

Ng and Tsakiri developed a novel bitumen emulsion breaking and upgrading process using in-situ generated H_2 from water gas shift of syngas (Ng 1989). Use of syngas is feasible because molybdenum sulfide can also catalyze the Water-Gas Shift (WGS) reaction to produce hydrogen from CO and H_2O (Ng 1989; Hou et al. 1983). Moll found that during upgrading of a Cold Lake bitumen emulsion that in-situ generated hydrogen was more active than molecular H_2 in water and produced a higher quality oil product (Moll 1999). In-situ generated hydrogen resulted in increased conversion of pitch to gas oils and distillates. Water was found to significantly inhibit hydrogenation and hydrodesulfurization, while direct desulfurization (hydrogenolysis) in HDS was favoured during model compound (Lee 2004) and bitumen hydrocracking studies (Moll 1999) under in-situ generated hydrogen. Takemura et al. performed HDS of residual oil over sulfided-CoMo/Al_2O_3 using CO and H_2O and found catalyst promoted desulfurization but excess water and CO_2 inhibited desulfurization (Takemura et al. 1981).

Siewe and Ng compared desulfurization of a Cold Lake diesel fraction in water using in-situ generated and molecular H_2 (Siewe and Ng 1998). The activity of in-situ versus molecular hydrogen was comparable, but HDS activity in the absence of water was considerably higher (Siewe and Ng 1998).

Hook and Akgermann studied HDS of DBT using in-situ generated hydrogen from water gas shift and concluded in-situ hydrogen was as effective as molecular hydrogen (Hook 1986). Their results indicated the HDS rate of DBT using in-situ generated hydrogen was higher due to nascent hydrogen on the catalyst surface.

Lee and Ng used DBT in toluene/water as a model system for diesel and found that water inhibits HDS but blocks the hydrogenation pathway more than hydrogenolysis (Lee

2006). At an optimal H_2O:CO ratio of 1.35, in-situ generated hydrogen was better than molecular H_2 in the HDS of DBT. In the HDS of DBT over unsupported, dispersed MoS_2, the direct desulfurization pathway was favoured with in-situ generated hydrogen (Liu et al. 2007).

Abusaido conducted naphthalene hydrogenation under $CO/H_2O/H_2S$ over unsupported, dispersed MoS_2 prepared from PMA (Abusaido 1999) while similar studies over NiMo from $NiSO_4$ and PMA were performed by Zhang (Zhang 2005). In-situ generated hydrogen was more active for Mo sulfides while over a NiMo catalyst in-situ and molecular H_2 activity was comparable (Abusaido 1999; Zhang 2005).

Isotopic labeling has been utilized to determine hydrogen incorporation from D_2O. Incorporation of isotopic hydrogen from H_2O during phenanthrene hydrogenation and dibenzothiophene (DBT) HDS under synthesis gas (CO:H_2O ratio from 0 to 1) was studied by Fu et al. over sulfided $NiMo/Al_2O_3$ (Fu et al. 1995). Fu et al. observed deuterium incorporation in HDS products and identified an isotopic mixture (HD, D_2, H_2) in the gas phase (Fu et al. 1995). Phenanthrene conversion under syngas was only slightly lower than for H_2. The hydrogenation sequence of phenanthrene, determined by evaluation of hydrogenated intermediates via GC, was similar whether performed under syngas or H_2. The water-gas shift rate was faster than hydrogenation and HDS, so WGS could replenish H_2 for hydrogenation (Fu et al. 1995).

Liu et al. hydrogenated diesel under supercritical $D_2O/CO/H_2$ at 400 °C using ATTM as catalyst (Liu et al. 2006). The product distribution was analyzed by deuterium Nuclear Magnetic Resonance Spectroscopy (D-NMR) to determine deuterium incorporation from water. Deuterium was incorporated into alkyl, benzyl and aromatic

species. Incorporation into saturated alkyls was suggested to be due to HDS of mercaptans and aromatic ring saturation. Deuterium incorporation into alkyl, benzyl and aromatic species correlated with the diesel fraction, ie. naphtha contained significant deuterated-alkyls while heavy arenes displayed little deuterated-alkyls but more deuterated-aromatics. Using supercritical water-syngas for upgrading diesel yielded a higher quality product with less sulfur (Liu et al. 2006, 1283-1289).

1. 5 Improving the activity of catalysts for simultaneous water-gas shift and hydrogenation

The difference in activity while using in-situ generated hydrogen versus molecular hydrogen has been attributed to nascent hydrogen produced via the WGS. Study of the relative kinetics between nascent hydride hydrogenation (from H_2O) and molecularly dissociated hydrogen (from H_2) may give important insight into the surface mechanisms on the catalyst. Coupling of hydrogenation to water gas shift should result in interaction between adsorption of different molecules. The activation of catalyst under CO and observation of surface species during water gas shift may allow elucidation of important mechanistic steps.

One route to improve hydrogenation would be to utilize metal species with good hydrogenation characteristics as substitutes for MoS_2 or in conjunction with MoS_2 as promoters. One of the main detriments to hydrogenation in emulsions is that water tends to inhibit hydrogenation. Therefore, a metal with good resistance to inhibition from water would be an ideal candidate. A high activity for WGS is also desired if the metal was to substitute for MoS_2. Rhodium and ruthenium metal on activated carbon have been shown

to have good aromatic hydrogenation activity in water, more so than other noble metals such as Pt and Pd (Maegawa et al. 2006). Of particular interest is Ru since ruthenium sulfides have been shown to be very active for hydrodesulfurizaion and aromatic hydrogenation (Castillo-Villalon et al. 2008). $Ru_3(CO)_{12}$ is active for WGS under alkaline conditions in toluene/water emulsions and catalyzes WGS in acidic solutions (Ng 1992; Fachinetti et al. 1996; Payne et al. 1991; Ng 1993). Ru has also been extensively studied as a high temperature steam reforming catalyst for hydrogen production from a variety of substrates including biomass (Osada et al. 2008). If Ru can significantly enhance the hydrogenation of aromatics in the presence of water over MoS_2 this may compensate for the inhibition by water.

Ru is very expensive compared to Mo and Ni and therefore any commercial process utilizing Ru as a catalyst would require an efficient catalyst separation and recycle process to completely recover the spent Ru. For commercial utilization, economics dictates the use of a cheaper metal. Nickel sulfided with molybdenum has good hydrogenation ability and is utilized extensively in hydrotreating. Certain forms of vanadium sulfides display good hydrogenation activity (Castillo-Villalon et al. 2008; Hubaut 2007). Both vanadium and nickel are found in substantial amounts in bitumen. If both vanadium and nickel could be incorporated into unsupported, dispersed MoS_2 to provide a positive catalytic synergy this would reduce the amount of molybdenum required for a slurry hydroprocessing process. In a slurry-based process, the metal-rich upgrading residue can be sent to a gasification unit where the coke and organic-matrix are gasified to CO, CO_2 and H_2. The resulting gasification solid would contain residual metal

oxides such as Mo, Ni and V which may be recycled into the upgrading process with H_2S to form catalytic metal sulfides.

Iron is an extremely cheap metal and has been utilized in the CANMET upgrading process at PetroCanada's Montreal refinery (Zhang et al. 2007). The disadvantage with iron is that activity is low compared to molybdenum and nickel and high metal dosages are required.

1. 6 Objective

Understanding the mechanism of in-situ hydrogenation may help in developing active catalysts. Isotopic labeling of water may yield a direct comparison between molecular H_2 and in-situ generated hydrogenation with CO/D_2O. The use of CO to probe the catalyst surface at reaction temperatures can be followed using Diffuse Reflectance Infrared Fourier Transform Infrared Spectroscopy.

In order to increase the hydrogenation activity using in-situ generated H_2, promoters such as Ru will be used. The effect of Fe and V on unsupported, dispersed Mo and NiMo sulfides will be studied since these metals are found in significant concentrations in bitumen. If Ni and V are effective, the use of residue containing Ni, V and spent Mo catalyst may be feasible for hydroprocessing of bitumen emulsions.

The objectives of this study are to:

i) Probe catalyst characteristics under reaction temperatures using DRIFTS, kinetic and isotope studies

ii) Determine effects of Ru, Fe, V on sulfided-Mo and NiMo unsupported, dispersed catalysts in water gas shift and naphthalene hydrogenation in toluene/water emulsions

iii) Determine parameter effects of temperature, P_{H2S} and P_{CO} versus P_{H2} on the water gas shift and naphthalene hydrogenation over the sulfided-VNiMo unsupported, dispersed catalysts in toluene/water emulsions.

Chapter 2: Literature Review

2. 1 Aromatics Hydrogenation

Organic sulfur-containing and nitrogen-containing compounds, and aromatics in diesel and gasoline fractions have significant environmental impacts. While sulfur-containing and nitrogen-containing compounds contribute to acid rain and smog, aromatics can increase the emission of particulates in exhaust (Hochhauser 2008). In several regions such as Europe and California, aromatics content in gasoline and diesel fuels is regulated in order to reduce the emissions of particulate matter (Table 2.1.1) (Hochhauser 2008). High levels of aromatics are found in gas oils and distillates (Table 2.1.2).

Table 2.1. 1: Diesel Specifications

Year	2006 (Canada)	2006 (California) (California Air Resources Board , 2009)	2009 (Europe) (Hochhauser 2008)
Sulfur, max (ppm)	15	15	10
Polynuclear Aromatics (wt%)		1.4	11

Hydrodearomatization (HDA), or removal of aromatics is accomplished via hydrogenation of the aromatic rings. Aromatic hydrogenation also plays a vital role in other processes. It is believed that in deep hydrodesulfurization and hydrodenitrogenation, partial hydrogenation of the aromatic rings facilitates the cleavage of C-S and C-N bonds to liberate H_2S and NH_3 respectively (Ho 2004). Aromatics

hydrogenation can also enhance hydrocracking through intermediate production of saturated polycyclic hydrocarbons, which can undergo ring cleavage over metal and acid catalysts (McVicker et al. 2002). Hydrogenation of polynuclear aromatics to mononuclear aromatics can enhance diesel quality while reducing particulate emissions.

Table 2.1. 2: Aromatics Distribution in Distillation Fractions (Cooper 1996)

Property	Heavy FCC Gasoline	Light Coker Gasoil	Light atmospheric Gasoil	Light Cycle Oil	Heavy Atmospheric Gasoil
IBP (°C)	195	259	289	291	322
Specific Gravity, 15 °C	0.84	0.861	0.846	0.997	0.864
Aromatics (vol %)					
Mono	38.8	16.3	16.5	8.2	22.5
Di	5.5	16.4	7.0	69.8	8.5
Tri	0.5	8.0	0.1	4.0	0.7
Total	44.8	40.7	23.6	82.0	31.7

Sapre and Gates reported mononuclear aromatics such as benzene and benzene derivatives are the most difficult species to hydrogenate (Sapre and Gates 1981). The hydrogenation rate for naphthalene conversion to tetralin is an order of magnitude larger than for tetralin hydrogenation to decalins; a similar trend is observed for benzene to

cyclohexane (Sapre and Gates1981). Ho found that hydrogenation of tetralin was twice as fast as hydrogenation of m-xylene over sulfided-NiMo/Al_2O_3 (Ho 1994).

2.1. 1 Reaction Mechanism

The hydrogenation of naphthalene is a multi-step reaction, where tetralin is formed from naphthalene; tetralin can subsequently be hydrogenated to cis and trans-decalin (Scheme 2.1.1.1). The initial hydrogenation to tetralin is the fastest step. The second hydrogenation to decalins is also fast over noble metal catalysts but is much slower over molybdenum sulfides, where trans-decalin was the major product (Sapre and Gates 1981). Although naphthalene hydrogenation is equilibrium limited at higher temperatues,

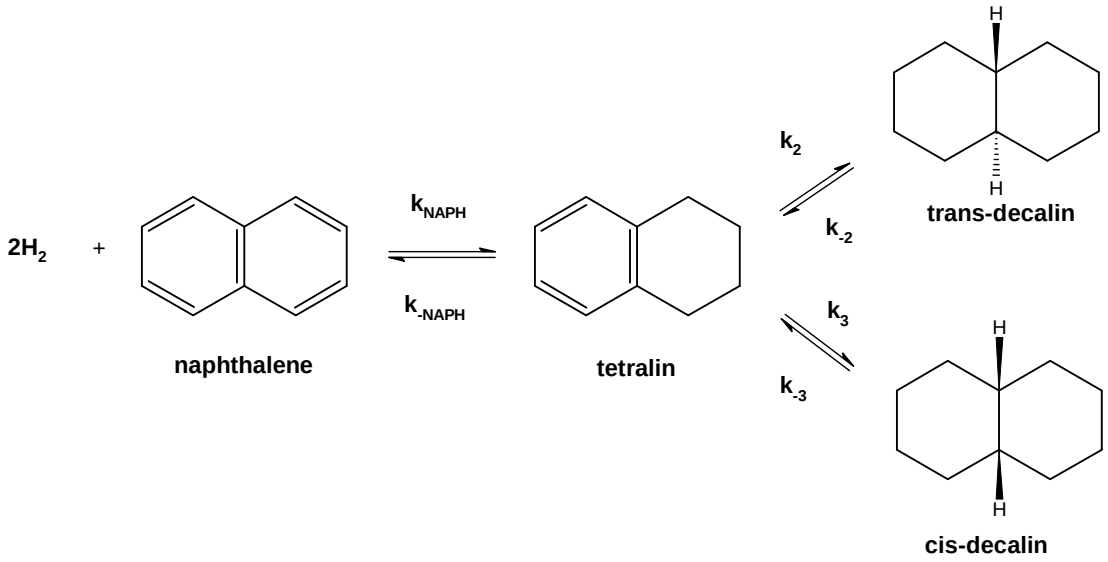

Scheme 2.1.1. 1: Hydrogenation of Naphthalene

over a $CoMo/Al_2O_3$ catalyst, the thermodynamic equilibrium is not reached until approximately 400 °C and can be coerced through higher H_2 pressure (Sapre and Gates 1981).

Hydrogenation over homogeneous metal complexes and heterogeneous reduced-metal catalysts occurs via metal-hydride species (Cotton 1988). Formation of metal hydrides under H_2 is followed by π-adsorption of aromatics to adjacent active sites; insertion of hydride into the aromatic species occurs followed by reductive elimination of the hydrogenated product. Coordinatively unsaturated sites (CUS) or vacancies are formed by product desorption allowing the catalytic cycle to continue (Cotton 1988).

When MoS_2 is treated under H_2, sulfur vacancies are formed liberating gaseous H_2S (Jacobsen et al. 1999). Coordination of heteroaromatic and aromatic substrates to these vacancies is believed to be essential for catalytic activity of MoS_2. Jacobsen et al. performed TPR studies of various metal sulfide catalysts presulfided in H_2/H_2S, and suggested that the surface sulfidation/reduction reaction (Jacobsen et al. 1999)

$$*S + H_2 \Leftrightarrow H_2S + *$$

was a reversible equilibrium, where * are surface vacancies. H_2S inhibits hydrodesulfurization by driving the equilibrium towards surface sulfur and H_2 reducing the number of vacant active sites. S-H surface groups have been identified at 2640 and 2500 cm^{-1} using FT-IR after exposure of MoS_2 to H_2 (Ratnasamy 1970).

Fundamental studies suggest that hydrogenation may also occur through formation of reactive S-H edge species. Lauritsen et al. studied triangular MoS_2 nanoclusters on Au

support by Surface Tunneling Microscopy (Lauritsen et al. 2004). They observed the existence of a metallic brim site near the edge of clusters composed of reactive S edge with metallic character. Treatment of the clusters with atomic H resulted in slight changes to edge sites adjacent to the brim which was interpreted as formation of S-H edge species. Adsorption of thiophene to the brim with subsequent hydrogenation of the thiophene ring occurring via the S-H edge was inferred from STM images of H-treated MoS_2 clusters exposed to thiophene. The STM images also suggested some thiophene could be coordinated end-on through sulfur to edge site sulfur vacancies. End-on coordination of thiophene to sulfur vacancies on the edge was proposed to occur after adsorption of thiophene on the brim site and removal of edge sulfur (Lauritsen et al. 2004). End-on coordination of aromatic sulfur species is considered a crucial step in HDS via hydrogenolysis.

For in-situ HDS and HYD of emulsions where water gas shift occurs, the system becomes complex due to adsorption of CO onto sulfur vacancies. Infrared (IR) adsorption studies of CO at low temperatures (100 K) onto metal sulfides reduced in H_2/H_2S have revealed relevant information about the vacant active sites on supported and unsupported HDS catalysts (Mauge 1992; Muller et al. 1993; Travert et al. 2001). DRIFTS experiments of CO hydrogenation to methane and alcohols on sulfided-Mo/Al_2O_3 indicated that CO adsorption to Mo vacancies occurs under reaction conditions(Koizumi et al. 2004). Theoretical calculations performed for ideal molybdenum sulfide clusters in CO hydrogenation suggest that formation of sulfur vacancies in the presence of CO is energetically favourable compared to H_2-only atmospheres (Zeng et al. 2005a; Zeng et al. 2005b; Zeng et al. 2005c).

2.1. 2 Hydrodesulfurization (HDS)

Hydrodesulfurization (HDS) is another reaction of importance in hydroprocessing (Scheme 2.1.2.1). In addition to a hydrogenation pathway, in HDS a hydrogenolysis pathway is also operative where the C-S bonds are cleaved directly before any hydrogenation of aromatic rings. In hydrogenative HDS, initial hydrogenation of the aromatic ring is a key step.

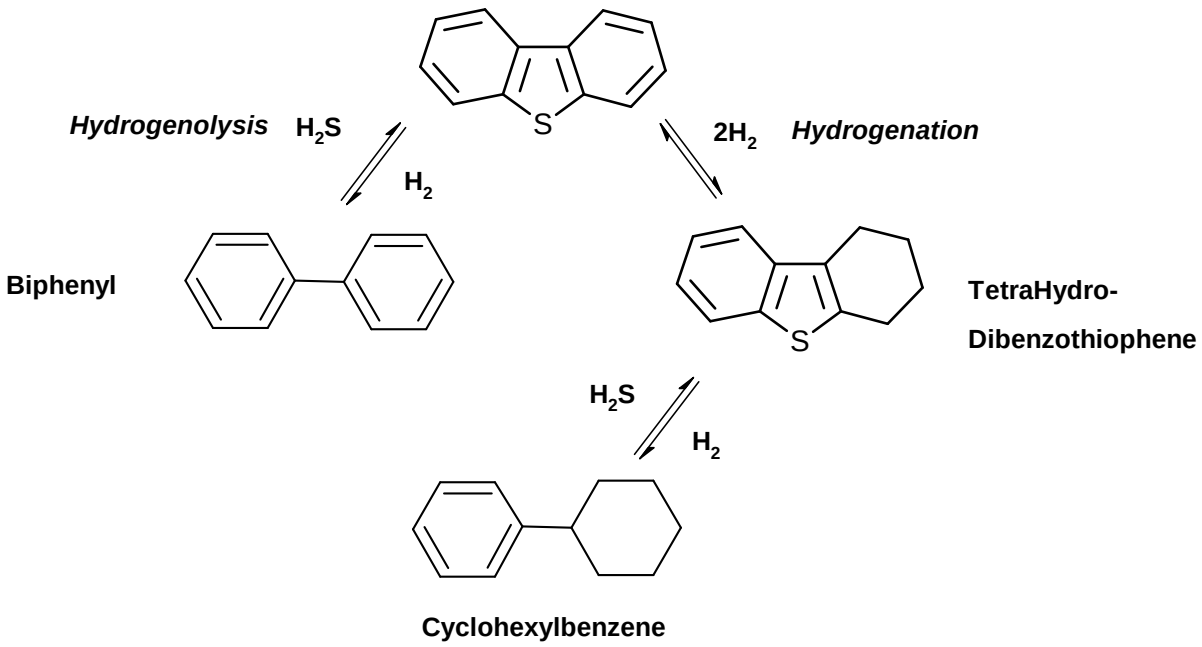

Scheme 2.1.2. 1: Hydrodesulfurization of Dibenzothiophene

2.1. 3 Hydrocracking and Asphaltene reduction

A brief mention of hydrocracking is warranted although this study does not specifically address this topic. The formation of asphaltene residue is believed to begin when thermal cleavage of C-C bonds form free-radical species which polymerize into larger aggregate asphaltenes. The formation of asphaltene aggregates is prevalent under low pressure, high temperature conditions such as those found in delayed and fluid cokers. Appreciable portions of the heavy oil feed are lost as coke compared to hydrocracking processes.

Hydrocracking results in much less asphaltene production since in the presence of catalyst under high hydrogen pressures, addition of dissociated H_2 can prevent polymerization into asphaltenes/coke. Although hydrocracking operates at lower temperatures, there is a trade-off since high hydrogen pressures are required. The high hydrogen pressures involved in hydrocracking can also promote ring opening of hydroaromatics and lighter alkanes leading to high gas production (Vernon 1980). The catalyst may be rapidly deactivated by the heavy hydrocarbon feed is also a disadvantage. However, a higher conversion of feed into a better quality product is achievable with hydrocracking than with thermal coking.

Although hydrocracking is an effective method of reducing coke yields, inhibition of free-radical polymerization can also be achieved by H-atom transfer from so-called donor solvents. Donor solvents, for example tetralin, have a higher H/C ratio than the coal or heavy oil substrates. Other processes have utilized gases such as methane or water as H-atom donors (*vide supra*).

2. 2 Catalysts for Aromatics Hydrogenation

Aromatics hydrogenation is exothermic and equilibrium limited at higher temperatures. The best catalysts for aromatics hydrogenation are noble metals such as Pt, Pd, Rh and Ru. These are typically supported on Al_2O_3 or activated carbon and give excellent hydrogenation activity when reduced. Hydrogenation is close to zero-order in the reactant hydrocarbon due to strong adsorption of aromatic species on the noble metal sites (Cooper 1996). Noble metals also show good hydrogenation activity in water. Maegawa et al. studied Ru/C and Rh/C for the hydrogenation of mononuclear aromatics in water at low temperatures(Maegawa et al. 2006). Greater than 50% hydrogenation conversion was achieved for various alkyl and heteromononuclear aromatics using Ru/C, Pt/C and Rh/C at 60 °C in water for 3 hours. Although mixed Pd/Pt catalysts show improved resistance to sulfur deactivation, the main difficulty with using noble metal catalysts in petroleum and fuel processing is their extreme sensitivity towards poisoning by sulfur compounds.

Metal sulfides also catalyze aromatic hydrogenation but are not as active as noble metal catalysts. The kinetics are approximately first-order in both hydrogen and reactant hydrocarbon (Cooper 1996). Because metal sulfides require higher temperatures in order to achieve satisfactory reaction rates, aromatics conversion with metal sulfides will always be lower due to the smaller equilibrium values at higher temperatures. This can be overcome through use of higher H_2 pressures albeit at a cost penalty. $CoMo/Al_2O_3$ is utilized commercially for HDS, while for processes requiring high hydrogenation activity with reasonable cost $NiMoS_2/Al_2O_3$ is utilized. Currently, the NEBULA type of unsupported catalysts which was jointly commercialized by ExxonMobil and Albemarle, achieves significant improvements over earlier catalysts in deep HDS for distillate and

diesel fuels (Kerby et al. 2005; Eijsbouts et al. 2007). Good aromatics hydrogenation ability is thought to be partially responsible for the excellent activity of NEBULA in deep hydrodesulfurization and hydrodenitrogenation (Kerby et al. 2005; Eijsbouts et al. 2007).

Pecoraro and Chianelli studied various bulk transition metal sulfides for hydrodesulfurization of dibenzothiophene and found that the Group VIII metal sulfides (RuS_2 and OsS_2) give the highest specific HDS activity (Pecoraro 1981). Mo and W sulfides displayed lower activity than Ru and Os but were highest among non-noble metals (Pecoraro 1981). First-row transition metals such as V and Fe were found to have low HDS activity. Lacroix et al. (Lacroix et al. 1989) studied biphenyl hydrogenation over several metal sulfides and reported that while RuS_2 had the highest specific activity, the specific activity of V_2S_3 was higher than that for MoS_2. They attributed this to preparation of the sulfide from thiovanadate under carefully controlled conditions to form an active V_2S_3, where contact with air was avoided since V is easily oxidized. Certain forms of bulk vanadium sulfides have been suggested to be very active hydrogenation catalysts (Lacroix et al. 1992; Hubaut 2007; Lacroix et al. 1989).

Regardless, under commercial operation with heavy oils and residues present coke and metals deposition deactivate hydroprocessing catalysts. Studies on metals deposition concluded vanadium sulfide deposits deactivated a commercial catalyst for HYD and HDS, while deposits of nickel sulfide did not severely affect the hydrogenation rate (Kim 1993; Yumoto et al. 1996). In HDS, vanadium deposits deactivated the hydrogenation pathway more than than hydrogenolysis. Yumoto et al. also observed an increase in the cracking activity with increasing vanadium content which was ascribed to the acidity of vanadium sulfides (Yumoto et al. 1996). In model studies, Kim and Massoth sulfided a

supported $NiMo/Al_2O_3$ catalyst with both a vanadium salt and vanadium tetraphenylporphyrin (V-TPP), similar to the organo-vanadium species found in heavy oils (Semple et al. 1990). The V salt deactivated the catalyst more than did V-TPP.

Ruthenium sulfides present the highest activity of all transition metal sulfides for hydrodesulfurization due to the relatively weak Ru-S bond energy (Pecoraro 1981). Although ruthenium is prohibitively expensive to be used commercially as a single-pass slurry catalyst for bitumen upgrading, with efficient catalyst recycle it could be used as a promoter with MoS_2. Furthermore, study of RuS_2 could provide fundamental insight on surface structure interplay between water gas shift, HDS and hydrogenation. Castillo-Villalon et al. characterized supported ruthenium sulfide (sulfided in H_2S/N_2 at 873 K) on proton and alkaline-cation exchanged BEA zeolites (Castillo-Villalon et al. 2008). Thiophene HDS activity increased with the Bronsted acidity of the catalysts, as did coke production. A remote effect on acidic sites from alkaline cations was proposed to be responsible for improved HDS behaviour. From Temperature Programmed Reduction (TPR), the atomic ratio of S/Ru was estimated at 1.5 possibly due to partial reduction of Ru in the zeolite which suggests these catalysts may suit hydrogenation rather than hydrodesulfurization (Castillo-Villalon et al. 2008).

Breysse et al. prepared supported RuS_2 using ion exchange with HY, KY, dealuminated HY (HYd) and dealuminated KHY (KHY-d) zeolites of varying acidity (Breysse et al. 1997). Sulfidation was performed in 15% H_2S/H_2 at 673 K for 4 hours. Low temperature CO adsorption observed via IR spectroscopy and isooctane hydrocracking were used as acidity tests. The hydrogenation rate of tetralin to decalins and toluene to methylcyclohexane was compared over the various supports at 300 °C, 4.5

MPa of H_2 and 2 % H_2S. For both hydrogenations, an increase in support acidity increased catalytic activity in the order,

$$RuHYd > RuKHYd > RuHY >> RuKY \sim NiMo/Al_2O_3$$

Electron microscopy revealed that well dispersed RuS_2 particles were in close proximity to acidic zeolite sites.

Mitchell et al. studied sulfided-Ru/Al_2O_3 and $RuMo/Al_2O_3$ catalysts in thiophene HDS. Calcination of $RuMo/Al_2O_3$ before sulfidation deactivated catalyst compared to individual Ru and Mo catalysts (Mitchell et al. 1987). However, with no calcination $RuMo/Al_2O_3$ displayed a synergistic effect in thiophene HDS, attributed to the absence of Ru-O-Mo bonds formed during calcination. Both calcined and uncalcined catalysts promoted the hydrogenation function in HDS.

Fe has been studied in coal liquefaction and residue upgrading since it is cheap. However, FeS_2 has a much lower activity for HDS and HYD compared with MoS_2 and therefore requires higher concentrations as catalyst. Commercial applications include the CANMET Process utilizing $FeSO_4$ for visbreaking of heavy oil and residue. It is occasionally used when economic conditions warrant at PetroCanada's Montreal refinery and achieves satisfactory removal of sulfur and nitrogen (Zhang et al. 2007).

Abusaido studied naphthalene hydrogenation on unsupported, dispersed MoS_2 and found that phosphomolybdic acid (PMA) had the best activity for *in-situ* naphthalene hydrogenation via water gas shift (Abusaido 1999). Zhang studied the in-situ hydrogenation of naphthalene via water gas shift using dispersed, unsupported NiMo

sulfide which achieved the highest conversion to tetralin compared to cobalt, palladium and unpromoted MoS_2 (Zhang 2005). The presence of organic N-containing compounds, but not S-containing organics, significantly inhibited the hydrogenation activity while at lower water concentrations the hydrogenation activity improved substantially.

2. 3 Water Gas Shift Reaction

The Water Gas Shift reaction is utilized in steam reforming, ammonia manufacture and Fischer-Tropsch synthesis to vary the $CO:H_2$ ratio,

$$CO_{(g)} + H_2O_{(g)} \rightleftharpoons CO_{2(g)} + H_{2(g)}$$

$$\Delta H^0_{298} = -41.2 \text{ kJ mol}^{-1}$$

The water gas shift is important since it produces active in-situ hydrogen necessary for hydrogenation.

2.3. 1 Water Gas Shift Mechanism

Two mechanisms have been proposed for the water gas shift reaction over supported transition metal catalysts. The redox mechanism involves dissociation of water to form adsorbed oxygen and molecular or atomic H on surface sites (*), where the metal centre

shuttles between an oxidized and reduced state to dissociate H_2O and form CO_2 and H_2 (Chinchen and Spencer 1988; Bunluesin et al. 1998).

$$* + CO \rightarrow CO* \quad (2.3.1\text{-}1)$$
$$* + H_2O \rightarrow H_2O* \quad (2.3.1\text{-}2)$$
$$H_2O* \rightarrow OH* + H* \quad (2.3.1\text{-}3)$$
$$OH* \rightarrow O* + H* \quad (2.3.1\text{-}4)$$
$$CO* + O* \rightarrow CO_2* \quad (2.3.1\text{-}5)$$
$$H* + H* \rightarrow H_2* \quad (2.3.1\text{-}6)$$
$$H_2* \rightarrow H_2 + * \quad (2.3.1\text{-}7)$$
$$CO_2* \rightarrow CO_2 + * \quad (2.3.1\text{-}8)$$

The second mechanism proposed is the Associative Mechanism which occurs through a formate-type intermediate after dissociation of H_2O into surface *OH and *H (Chinchen 1988; Bunluesin et al. 1998). Insertion of dissociated surface water to *OH occurs, followed by *OH insertion into adsorbed CO followed by rearrangement to HCO_2^-; cleavage of C-H releases CO_2 and H_2.

$$* + CO \rightarrow CO* \quad (2.3.1\text{-}1)$$
$$* + H_2O \rightarrow H_2O* \quad (2.3.1\text{-}2)$$
$$H_2O* \rightarrow OH* + H* \quad (2.3.1\text{-}3)$$
$$CO* + OH* \rightarrow COOH* \quad (2.3.1\text{-}9)$$
$$COOH* \rightarrow HCOO* \quad (2.3.1\text{-}10)$$
$$HCOO* \rightarrow CO_2* + H* \quad (2.3.1\text{-}11)$$
$$2H* \rightarrow H_2* \quad (2.3.1\text{-}6)$$
$$H_2* \rightarrow H_2 + * \quad (2.3.1\text{-}7)$$
$$CO_2* \rightarrow CO_2 + * \quad (2.3.1\text{-}8)$$

WGS occurs under acid, neutral and alkaline conditions. Studies of the WGS using homogeneous catalysts have elucidated proposed mechanistic pathways under alkaline, neutral and acidic conditions (Laine 1988). Under neutral conditions, adsorption of CO to a low oxidation state metal centre results in back-donation of electrons from metal d-orbitals to CO anti-bonding orbitals. The activated CO is susceptible to nucleophilic attack by ^{-}OH coordinated to the metal or stabilized by an alkaline environment. Under acidic conditions, electropositive coordinated CO can react with water to form formic acids or formates which can decompose to CO_2 and H_2. Decomposition of formate may occur through metal hydrides, where either reductive elimination of two hydride ligands or reaction of hydride to abstract a proton from water can produce H_2 (Laine 1988).

Due to the heterogeneity of supported metal surfaces, mechanistic studies over supported catalysts are more complex. Gines et al. studied kinetics of the reverse water gas shift (RWGS) over $CuO/ZnO/Al_2O_3$ and observed evidence that a regenerative mechanism was active whereby active sites are successively oxidized by H_2O and reduced by H_2(Gines et al. 1997). They also found that at high initial P_{H2}/P_{CO2} (large surface coverage of H_2) CO_2 dissociation was rate limiting. As P_{H2}/P_{CO2} decreased, surface reconstruction occurred where the RWGS rate was positive order in P_{H2} and both CO_2 dissociation and water formation determined the overall reaction rate (Gines et al. 1997). This highlights the complexity of the reaction network over heterogeneous catalysts.

2.3. 2 Water Gas Shift Catalysts

Two commercial types of catalysts used are high temperature shift catalysts (HTS), typically magnetite Fe_3O_4/Cr_2O_3 and CuO/ZnO low temperature shift catalysts (LTS). HTS catalysts operate in the temperature range of 320-400 °C and are slightly tolerant towards sulfur compounds in the synthesis gas. Copper LTS catalysts have the advantage of high activity at lower temperatures (200 - 250 °C) which enhances equilibrium conversion, but are poisoned even by slight amounts of sulfur compounds. Sulfur tolerant water gas shift catalysts are sought after since they can process CO/H_2 streams from gasifiers reforming "dirty" feeds such as coal or petroleum residues. Insensitivity towards sulfur is necessary for catalysis of WGS under hydrotreating conditions. Removal of sulfur compounds can be accomplished downstream for processes requiring low or no sulfur.

Yu et al. gasified an Fe-impregnated Victorian Brown Coal under steam and utilized the product char for WGS (Yu et al. 2007). They observed that the conversion of char affected catalyst activity due to agglomeration of active Fe_3O_4 particles. A char conversion of 35 wt% was found to be optimal and suggests that gasification char impregnated with metal can form active catalysts for WGS; gasification of carbonaceous residue produces catalytically active char in addition to CO and H_2 which can be utilized in bitumen or diesel upgrading (Siewe 1998; Fu et al. 1995; Yu et al. 2007).

MoS_2 and $NiMoS_2$ are known to catalyze the WGS in the presence of feeds containing sulfur compounds. The presence of sulfur is required in the feed since pure MoO_3 does not show any significant activity toward WGS (Hou et al. 1983). Exchange of

surface sulfur with oxygen from water to form an oxidized Mo centre is thought to initiate the catalytic process.

From kinetic data Hou et al. suggested a redox cycle involving Mo^{4+} and Mo^{5+} centres for water gas shift (Scheme 2.3.1.1) and reported that the presence of H_2S was required to maintain catalytic activity for conversion of CO and H_2O (Hou et al. 1983).

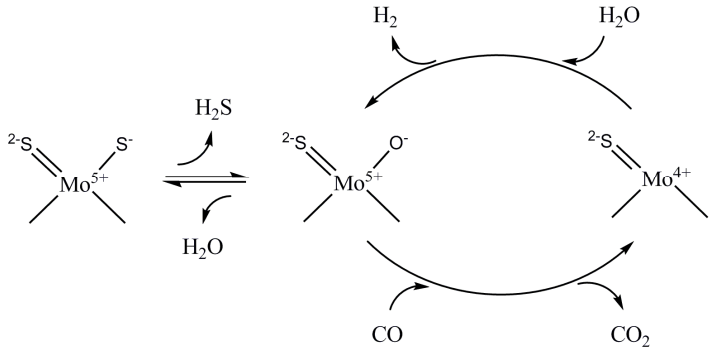

Scheme 2.3.1.1: Proposed Water Gas Shift Mechanism

Lund (Lund 1996) developed a qualitative microkinetic model of WGS over sulfided Mo/Al_2O_3 catalyst and proposed its lack of quantitative agreement with experimental studies (Hou et al. 1983) highlighted the interplay between H_2O, H_2S and surface structure on activity.

MoS_2 differs from traditional WGS catalysts in that dynamic exchange of surface sulfur and oxygen is necessary to maintain activity (Hou et al. 1983). WGS on supported transition-metal/oxides is believed to begin when CO adsorbs to the transition metal active centres. Various side or main reactions may also occur on the oxide support. On metal sulfides, sulfur vacancies can form through which gas phase CO can access Mo active sites and then possibly react with adjacent hydroxyl species, forming either carboxylic,

formate or carbonate surface species. The key step here is then formation of sulfur vacancies in MoS_2 under CO with adsorption of CO to Mo.

Heterogeneous and homogeneous ruthenium species catalyze reactions such as water gas shift and hydrogenation of aromatics in water (Maegawa et al. 2006; Ng 1992; Fachinetti et al. 1996; Payne et al. 1991; Monteiro-Gezork et al. 2008). Ng and Tsakiri studied HDS of DBT and WGS in toluene/water emulsions using $Ru_3(CO)_{12}$, $Mo(CO)_6$ and $W(CO)_6$ and found ruthenium carbonyl to be 20 times more active for water gas shift than Mo or W but with much lower HDS activity (Ng 1992). The catalysts were not sulfided prior to reaction. Exchange between O and S on RuS_xO_y should be facilitated if the metal-oxygen and metal-sulfur bonds strengths are weak enough to allow for exchange, such as on MoS_xO_y (Hou et al. 1983). Since the Ru-S bond strength is weak (Pecoraro 1981), whether or not RuS_2 exhibits high activity for WGS may depend upon the relative strength of the Ru-O bond in ruthenium oxysulfides.

Chapter 3: Experimental

3. 1 Experimental Setup

Experiments were conducted on an Autoclave Engineers 300 ml HC-276 Bolted Closure Batch Autoclave. The experimental set-up is shown in Figure 3.1.1. The inside diameter

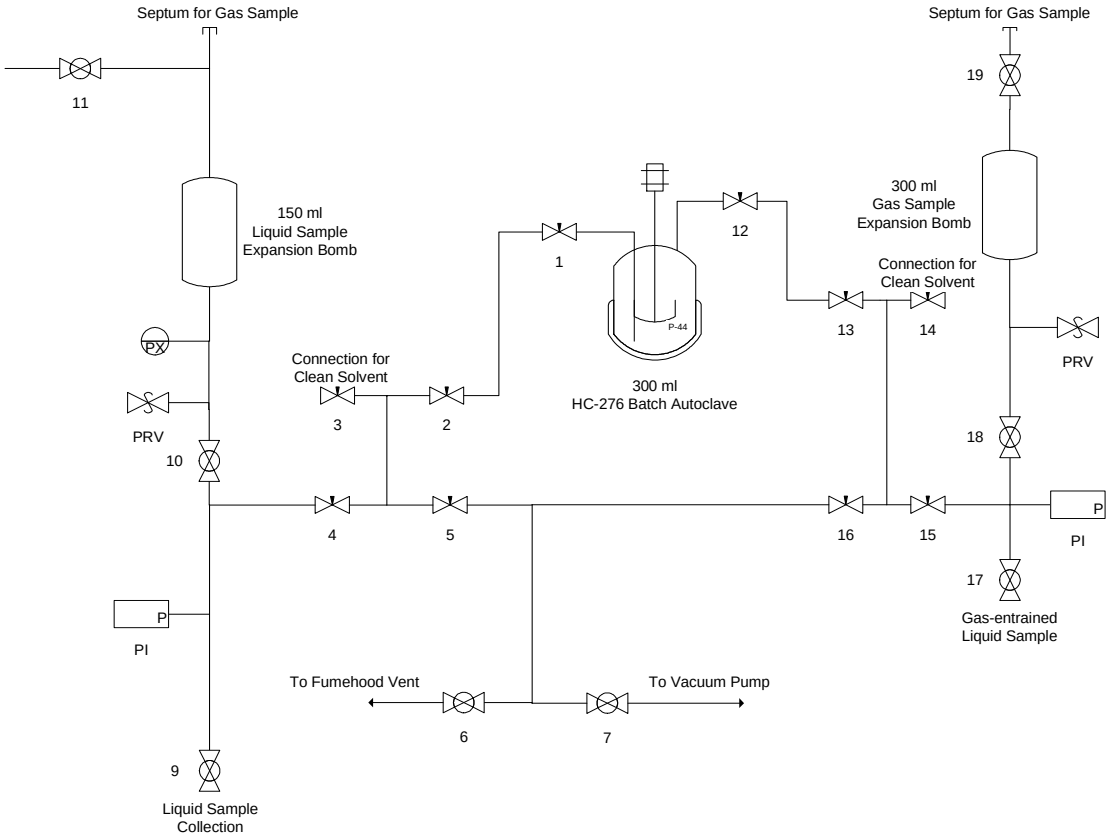

Figure 3.1. 1: Experimental Setup of Autoclave Engineers 300 ml HC-276 Bolted Closure Autoclave and Sampling System

of the vessel is 1.5 inches. The reactor is equipped with a rupture disc designed to burst at 4941 psig and prevent overpressure. Originally the autoclave was equipped with a gas inlet, gas sparger tube, gas vent and a liquid sampling tube. However, due to residual catalyst penetrating the sparger tube and the difficulty of cleaning, the sparger tube was removed and the inlet plugged with a SS 316 plug and gland. Reactor internals also include a baffle, cooling coil (air coolant) and thermowell. Additional parts not installed include a liquid sampling tube with filter; however, because catalyst sulfidation requires formation of solids from the homogeneous precursor, the filter clogs regularly and was replaced with an open-bore sampling tube. Molybdenum sulfide can be cleaned from the liquid sample tube filter with the use of dilute hydrogen peroxide to oxidize MoS_2 to molybdic acid and water. An estimate of the reactor volume was made by filling the reactor with water and measuring the mass collected; the actual estimated working volume is 257 ml. The autoclave is equipped with a Magnedrive stirrer which eliminates traditional problems with rotating seals. However, the Magnedrive should be periodically disassembled and cleaned to ensure residual catalyst and reactants do not deposit on the Magnedrive bearings. Autoclave instrumentation includes a temperature controller with alarms for over-temperature and over-pressure. Two thermocouples provide the furnace and thermowell temperatures; both temperatures and the pressure transducer have alarm set-points that can be programmed on the temperature controller. The pressure transducer is connected to the controller and the Data Acquisition System (Appendix F).

The sampling system allows sample collection from the reactor lower phase. All valves and lines from the reactor to valve 1 and valve 12 are Hastelloy-C 276 medium pressure Autoclave Engineers fittings. Valves 2, 3, 4, 5 and 13, 14, 15, 16 have HC-276

Autoclave Engineers Speedbite fittings. All fittings downstream of valve 5 on the liquid line and valve 16 on the gas line are Swagelok SS316 compression fittings.

The volume of the liquid sampling system was estimated from the ideal gas law by pressurizing the reactor and then opening the sample valve to allow gas to expand inside the sample volume. The estimated volume is 156 ml. Both liquid and gas sample systems are equipped with pressure indicators and proportional relief valves designed to open at 85 psig. The liquid system is equipped with a pressure transducer (Omega) with a range from -14.7 to 85 psig. If necessary the gas sample system can be similarly fitted. The pressure transducer is connected to the Data Acquisition System (DAQ) run from the computer in DWE 1521B. A thermocouple inserted via septum into the 150 ml Liquid Sample Expansion bomb measures the sample temperature.

3. 2 Catalyst Preparation

3.2. 1 Reagents

Naphthalene (99+ %, Sigma-Aldrich), n-octane (98+ %, Alfa Aesar), toluene (Omnisolve), Formic Acid (97% Sigma-Aldrich) and deuterium oxide (99.9%, Cambridge Isotopes) were used as received. H_2S (Praxair), CO (2.5 Grade, Praxair), H_2 (4.5 Grade, Praxair), 50 % CO/H_2 (Linde, Standard) and N_2 (4.8 Grade, Praxair) cylinders supplied gas to the reactor through a common manifold. Phosphomolybdic acid (PMA) hydrate (ACS, Sigma-Aldrich), $NiSO_4 \cdot 6H_2O$ (Sigma-Aldrich), $VO(C_5H_8O_2)_2$ (99% Strem

Chemicals) and $FeSO_4$ (Sigma-Aldrich) were used as received. De-ionized water produced via ion exchange was provided by the Department of Chemical Engineering.

3.2. 2 Deuterium Labeling Studies

For consistency in catalyst preparation between deuterium oxide (D_2O) and H_2O, 3 g of PMA hydrate was stirred in approximately 25 ml of D_2O or H_2O for 4 hours (to exchange PMA protons with deuterium) and water subsequently evaporated overnight at 80 °C. This procedure was repeated three times and the final dry, deuterium exchanged PMA was dissolved in 50 ml of D_2O (H_2O) and diluted in 100 ml volumetric flasks. Atomic absorption (Perkin Elmer AAS 3100) was used to quantify Mo content for both D_2O and H_2O catalyst solutions. Kinetic experiments consisted of charging the 300 ml Autoclave Engineers batch autoclave (HC-276) with 10 ml H_2O or D_2O, 100 ml of n-octane, 5.0 wt% (3.7 g) of naphthalene and appropriate volumes of PMA solution to make 500 ppmw Mo with respect to total organics.

Six samples per experiment were collected using a high pressure sampling system which allowed separation of a gas and liquid sample. For ^1H quantification, collected liquid samples were dissolved in $CDCl_3$ (99.9% Cambridge Isotopes) as an NMR lock solvent and analyzed by ^1H-NMR in n-octane and quantified by ^1H-NMR (verified by H^2-NMR). Overall liquid organic concentrations were then determined by GC-FID.

3.2. 3 Preparation of MoS_2 from PMA for DRIFTS

MoS_2 was prepared from an aqueous solution of phosphomolybdic acid (PMA) under CO/H_2S in a toluene/water emulsion at 340 °C. 4.09 g of PMA hydrate (ACS, Sigma-Aldrich), 25 ml of de-ionized H_2O and 100 ml of toluene were charged to a 300 ml batch autoclave (working volume 257 ml, Autoclave Engineers). 180 psi of H_2S was charged sequentially with stirring in order to absorb H_2S into solution. After the final H_2S charge, the pressure was 104 psig. CO was then charged for a total pressure of 600 psig. The reactor was heated at 4.1 °C/min until the target of 340 °C was reached and the temperature maintained for 2 hours. After 2 hours the reaction was stopped and allowed to cool to room temperature. The gas was collected into a gas bag and analyzed by GC, while the slurry of catalyst and liquid was removed from the autoclave under N_2 by cannulation. Degassed (N_2) reagent alcohol was then used to rinse the reactor wall and internals and cannulated into the Schlenk under N_2 purge. The collected slurry was then filtered through a porous frit under N_2 and the solids dried in vacuo overnight. The dried black solids were transferred via Schlenk into a glovebag under Ar. Samples were loaded into the DRIFTS cell in the glovebag and the DRIFTS cell sealed under Ar.

3.2. 4 Catalyst Preparation for $Ru(acac)_3$ and $Ru_3(CO)_{12}$ experiments

500 ppm based on metal for 91 g of total organics was used, either in the form of phosphomolybdic acid, $Ru_3(CO)_{12}$ or $Ru(C_5H_7O_2)_3$. PMA was added to the reactor in an

aqueous solution, while both Ru precursors were added as solids ($Ru_3(CO)_{12}$ is insoluble in toluene). 100 ml of toluene was added and the total volume of water used was 10 ml. 4.5 g of naphthalene comprising 5.0 wt% of organics was introduced, and the batch autoclave sealed. 15 psi of H_2S and balance of CO up to 600 psig were used to test simultaneous water gas shift and naphthalene hydrogenation. Because of the low activity of the Ru precursors for water gas shift, $Ru(acac)_3$ (where acac = acetylacetonate = $C_5H_7O_2^-$) was tested separately after catalyst preparation under H_2/H_2O to determine the activity for hydrogenation of naphthalene.

3.2. 5 Catalyst Preparation for Me-Mo sulfides (Me = Fe, V, Ni)

Experimental conditions were similar to those used in previous studies performed in a 1000 ml autoclave (Abusaido 1999; Zhang 2005). Table 3.2.5.1. lists the conditions for the 1000 ml and 300 ml autoclave. The conditions in the 300 ml autoclave were chosen such that the molar ratios of CO:H_2O:Solvent:Naphthalene were equal between the two reactors. A stirring speed of 1500 RPM in the 300 ml autoclave was chosen versus 1300 RPM for the original reactions since it was suggested by Peter Byrne (Autoclave Engineers) that a higher stir speed may be required for good gas dispersion due to the smaller impeller size compared to the older 300 ml SS-316 and 1 L SS-316 batch autoclave. 52 ml of toluene and 18 ml of water were used with 11.17 g of naphthalene (20 wt% naphthalene to approximate diesel). The precursors used were $FeSO_4$, $NiSO_4 \cdot 6H_2O$ and $VO(C5H_7O_2)_2$ and PMA. The total amount of metal was based on 1500 ppmw of Mo for 74.20 g total liquid, or 1.16 mmoles metal (0.87 mmoles Mo, 0.29 mmoles Ru). 15 psi

Table 3.2.5. 1: Comparison of Experimental Conditions between 1 L and 300 ml Autoclaves

	1-L SS Batch Autoclave	300 ml HC-276 Batch Autoclave
Total Working Volume (ml)	995	257
Solvent Volume (ml)	200 (Toluene)	52 (Toluene)
Water Volume (ml)	70	18
Liquid Volume Fraction (Oil:H_2O)	0.35	0.35
Gas Volume (ml)	725	187
Mass of Naphthalene (g)	43.25	11.17
L/G Volume Fraction (Liquid:Gas)	0.37	0.37
Catalyst Concentration (ppmw Mo wrt Oil)	1500	1500
Final Temperature (°C)	340	340
Temperature Ramp during Heating (°C / min)	3.0	3.0
Stir Speed (RPM)	1300	1500
Batch Autoclave Material	SS-316	HC-276

of H_2S and balance of CO up to 600 psig were used to test simultaneous water gas shift and naphthalene hydrogenation.

3.2. 6 Catalyst Preparation for Multifactorial study of Fe, V and Ni-doped Mo sulfides

1500 ppmw (with respect to 96.6 g organic) of Mo was used in the form of Phosphomolybdic acid (PMA). Dopant metals (Fe, Ni and V) were added to make an atomic ratio, Dopant:Mo of 0.6 (1.5 mmole Mo, 0.91 mmole V, 0.91 mmole Ni). PMA was added to the reactor in an aqueous solution, while both $NiSO_4 \cdot 6H_2O$ and $VO(C_5H_7O_2)$ precursors were added as solids. 100 ml of toluene was added and the total

volume of water used was 10 ml. 10 g of naphthalene were introduced, and the batch autoclave sealed.

3. 3 Operational Procedure

Autoclave seal rings were sprayed with Molykote dry lubricant to aid in sealing. The autoclave was pressure tested at 1200 psig under N_2 for 30 minutes to determine proper sealing. The reactor was then stirred at 500 RPM for approximately 1 minute to dissolve any solids. The autoclave was then purged with the balance gas (CO, H_2 or 50% CO/H_2) 3 times (~200 psig) under stirring (~300 RPM). After purging the inlet lines through the H_2S absorption column, H_2S was then charged to the reactor and balance gas up to total pressure of 600 psig was charged. After purging, H_2S was introduced and CO or other balance gas was charged to a total pressure of 600 psig. Stirring to 1500 rpm was started, and the reactor temperature ramp rate was set. An operational flowchart is shown in Figure 3.3.1. The start of reaction was taken at the time the reactor thermocouple stabilized at 340 °C. Six samples in total were recovered for kinetic analysis. Before sampling, a purge volume was taken to account for dead volume in the sampling lines. Gas and liquid samples were separated by flash depressurization in an expansion bomb. Gas samples were transferred from the autoclave via a medium pressure gas-tight syringe with valve and analyed by GC-TCD on an Agilent 3000A (Appendix A). Liquid samples were weighed and transferred to GC vials for analysis by GC-FID on a Varian CP-3800 (Appendix A). A detailed procedure for sampling is included in Appendix E. A sampling flowchart is shown in Figure 3.3.2. Pressure and temperature in the reactor and sample bombs was measured with Omega thermocouples and pressure transducers.

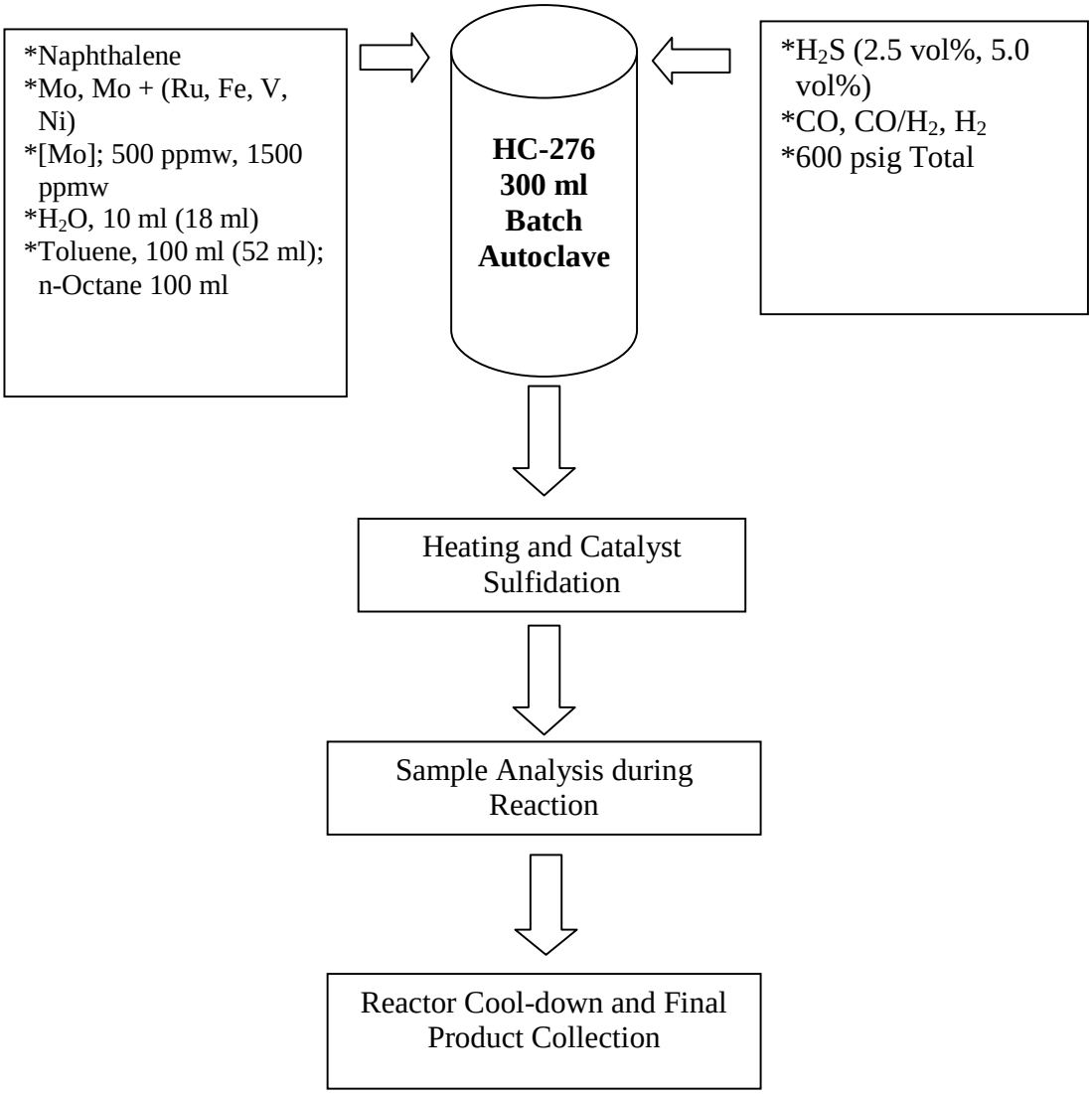

Figure 3.3. 1: Reactor Operation Flowchart

Concentrations of gases in the sample were obtained by calculating total number of mols in the sample bomb via the ideal gas law and dividing by the mass of liquid collected.

3. 4 Analytical Procedures

3.4. 1 Liquid Phase Analysis

Samples were collected at regular intervals during reaction and analyzed to determine hydrogenation and WGS rate constants. The HC-276 reactor internals also catalyze the WGS and hydrogenation reactions, and an estimate of the blank "wall effect" is given in Table D.2, Appendix D (Experiments #6, #12, #30). The organic liquid product was analyzed on a Varian CP-3800 GC-FID with a 30 m x 0.32 mm VF-5MS column. The analysis conditions are listed in Appendix A. Kinetic rate constants were determined through regression analysis of the data in Excel. Solid catalyst particles were removed via filtration or by allowing the solids to settle by gravity.

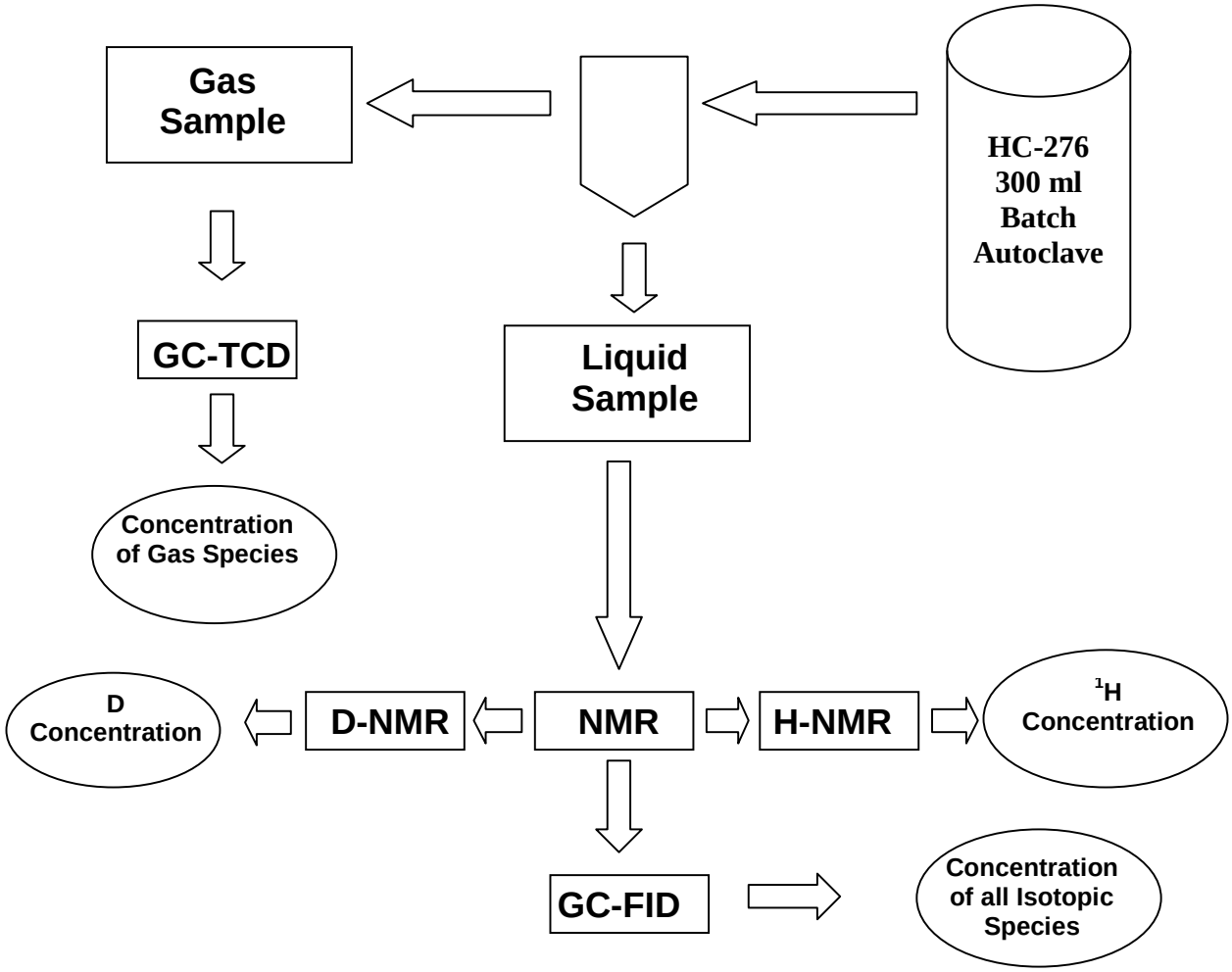

Figure 3.3. 2: Sampling and Analysis Flowchart

3.4. 2 Gas Phase Analysis

Gas Phase samples were collected in a 5 mL gas-tight syringe with valve. An Agilent 3000A MicroGC was utilized for analysis. The conditions are listed in Appendix A. H_2, N_2, O_2, CO were analyzed on a 5A Molecular Sieve column using Argon as carrier gas for enhanced detector sensitivity to H_2. CO_2, methane, propane, propylene, H_2S and COS were fractionated on a PLOT U column running Helium carrier gas. An RGA Calibration

mixture supplied by Agilent was used to calibrate the Agilent 3000A GC bi-weekly. H_2S and COS were calibrated using a Certified Standard supplied by Praxair of 2.54 vol% H_2S and 5.02 vol% COS. Kinetic rate constants were from regression analysis of data in Excel (Appendix B).

3.4. 3 ^{1}H-NMR and ^{2}H-NMR (D-NMR) Analysis

^{1}H and D Nuclear Magnetic Resonance Spectroscopy (NMR) were performed under the supervision of Jan Venne in the Department of Chemistry on a Bruker AVANCE 300. Quantification was accomplished via integration of proton and deuterium resonances using Bruker X-Winnmr software. d_6-acetone (^{2}H) or n-octane solvent was utilized as an internal reference. The quantification from ^{1}H-NMR spectra was then compared to total organic concentrations from GC-FID analysis to determine the percent of ^{1}H-incorporation. Since ^{1}H and D are the only hydrogen isotopes present in the reaction in significant quantities, the deuterated-naphthalene concentration can be calculated from,

$$[NAPH]_{GC} - [NAPH]_{1H} = [NAPH]_{D}$$

3.4. 4 Procedure for Recording DRIFTS Spectrum

The DRIFTS setup is shown in Figure 3.3.3.1. In addition to the cell (Harrick Praying Mantis, ZrSe windows) a vacuum attachment and liquid holder to introduce vapour are included.

Sample (ATTM or MoS_2 prepared ex-situ) was loaded into the DRIFT cell under Ar in a glovebag. The sample holder was filled so that fine powder was flush with the top of the sample. After connecting the DRIFTS cell to the gas lines, the cell was flushed with N_2 for approximately 20 minutes.

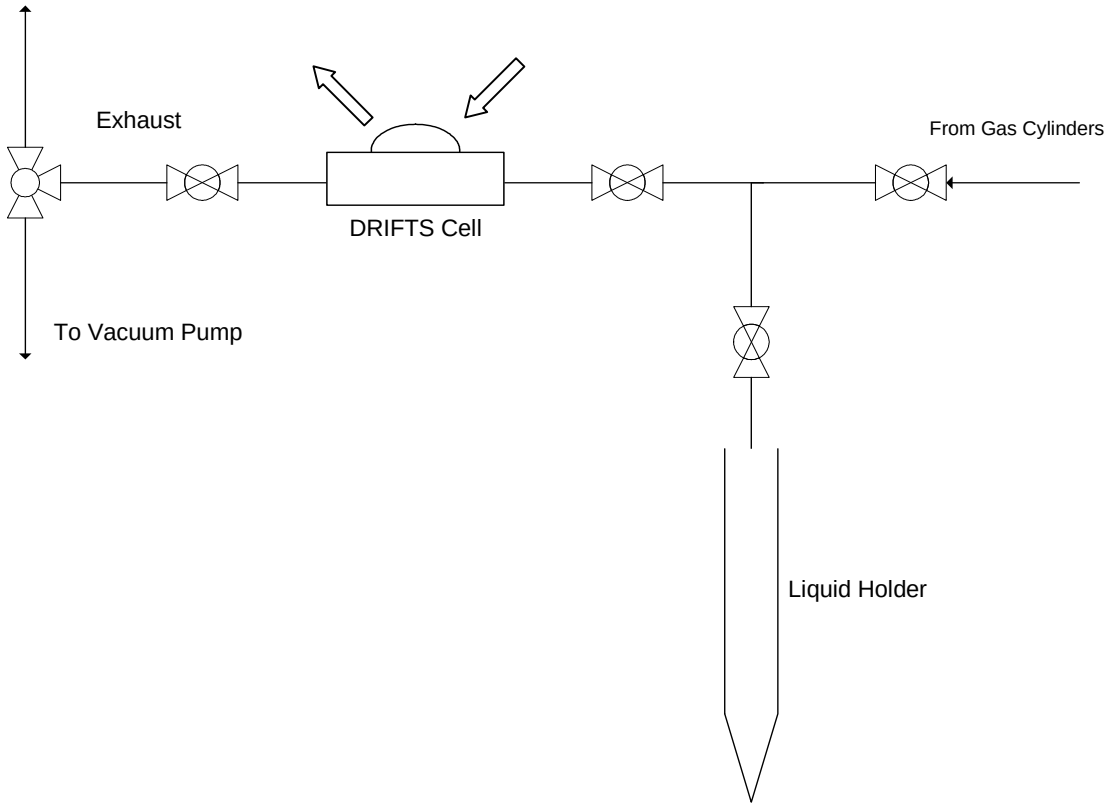

Figure 3.4.4. 1: Diagram of the Diffuse Reflectance Infrared Fourier Transform Spectroscopy (DRIFTS) Set-up

For liquid vapours (formic acid and water), the cell was loaded using vacuum techniques. After evacuating the cell for 30 minutes to remove moisture and air, the liquid holder was evacuated to reduce the pressure and heated with hot water (~90 °C) to allow

the liquid to partially vapourize. After waiting several seconds for vapour to permeate through the gas lines, the gas inlet valve was opened (4 ml/min) to introduce vapour into the cell. This was repeated several times if necessary. After introducing the vapour, the selected reactant gas was introduced and after flushing the cell for a short time the gas flow gas flow was stopped. DRIFTS spectra were recorded with 128 scans with a resolution of 4 cm^{-1}. A background scan (usually N_2 flow at room temperature) was subtracted from the recorded spectrum to give a difference spectrum. Spectra were recorded in absorbance units, therefore an upward shift in intensity corresponds to the appearance of a particular molecular vibration. For variable temperature runs, the sample was heated incrementally and spectra were recorded 10 minutes after the thermocouple reached the specified temperature in order to ensure thermal equilibrium of the sample.

3. 5 Formulas and Calculations (for sample calculations see Appendix C)

3.5. 1: Pseudo-First Order Rate Constant

A pseudo-first order rate constant for WGS was determined for CO since H_2O is in excess. An analagous rate constant for naphthalene was calculated during hydrogenation. The reactant concentrations were fitted to the exponential equation below through regression analysis in Excel.

$$k_i C_i = -\frac{dC_i}{dt}$$

$$-\int k_i dt = \int \frac{dC_i}{dt}$$

$$-k_{i0}^{\ t} = Ln\, C_{i\ C_{io}}^{\ C_{it}}$$

$$\exp^{-k_i t} = \frac{C_{it}}{C_{i0}}$$

$$C_{i0} \exp^{-k_i t} = C_{it}$$

3.5. 2: Calculation for gas concentration in liquid

Pressure, temperature and mass of flashed reactor samples were recorded and used to calculated gas concentrations [mol / g-liquid]. Mols of gas were calculated from pressure and temperature via the Ideal Gas Law.

Calculation of Molar Gas Quantities from Ideal Gas Law

$$n_{gas} = \frac{PV}{RT}$$

where,

P	=	pressure (Pa)
V	=	Volume (m^3)
R	=	8.314 (J/(mol-K)
T	=	Temperature (K)

The reactor sample is flashed at ambient temperature (25-27 °C) and low pressure (~10 psig) to separate light gases (CO, H_2, CO_2, H_2S) and condensing liquids (toluene, water, naphthalene, tetralin). A sample from each phase is collected for analysis.

The pressure data for the sampling vessel must be converted from a raw voltage reading. The pressure range of the transducer is 0-100 psia, while the measured voltage range is from 1-5 Volts. For details of the actual instrumentation set-up see Appendix F.

$$P_{SB} = \frac{(Volts - 1)(100\,psia - 0\,psia)}{(5Volts - 1Volts)}$$

$$P_{SB,gauge} = P_{SB} - 14.7$$

$$P'_{SB} = P_{SB}\frac{(101325\ Pa\ atm^{-1})}{(14.7\ psi\ atm^{-1})}$$

$$n_{gas} = \frac{(P'_{SB}V_{SB})}{(RT)}$$

$$[Gas]\,(mol\ g - Liq^{-1}) = \frac{n_{gas}}{m_{sample}}$$

m_{sample} = mass of collected sample liquid sample (g-Liq)

P_{SB} = Pressure in the sampling bomb (Pa)

R = Molar Gas Constant (8.314 J-K^{-1}-mol^{-1})

T = Sampling bomb temperature (K)

V_{SB} = Volume of the sampling bomb (157 x 10^{-6} m^3)

Volts = Pressure transducer voltage (Volts)

$$N_{gas} = \frac{(P'_{SB}V_{SB})}{(RT)}$$

to determine the gas concentration:

$$[GAS] = \frac{(mol\% - GAS)x(total - moles - in - sample - bomb)}{(mass - of\ - liquid - sample)}$$

mol%-H_2 = mol% measurement calculated by External Standard (ESTD) from Gas Chromatogram

3.5. 3: Naphthalene Conversions

Naphthalene conversion was calculated from the sample concentrations as analyzed by GC-FID.

$$X(\%) = 100x\frac{[NAPH]_0 - [NAPH]_t}{[NAPH]_0}$$

Where,

$[NAPH]_i$ = Initial Naphthalene Concentration (mol/g-liq)

$[NAPH]_t$ = Naphthalene Concentration at t minutes (mol/g-liq)

3.5. 4: Calculation of second order rate constant for hydrogenation

For hydrogenation in a stirred autoclave, the solubility of H_2 in the reacting medium is important and therefore a second-order rate constant was calculated (Sections 4.4 and 6.3.5).

$$r_{NAPH} = k_{NAPH}[NAPH]$$
$$r_{NAPH} = k_{NAPH}"\overline{[H_2]}[NAPH]$$
$$k_{NAPH}" = \frac{k_{NAPH}}{\overline{[H_2]}}$$

3.5. 5: Reversible WGS Rate Constant

If CO conversion is high in a batch reaction the WGS may approach equilibrium thereby falsifying the true kinetics. To measure a true pseudo-first order rate constant under conditions where equilibrium is limiting, the calculation derived by Rintjema was used (Rintjema 1992),

$$Ln(A) = Ln\left\{\frac{[CO]_0{}^2 - [CO]_e[CO]_t}{([CO]_t - [CO]_e)[CO]_0}\right\}$$

where,

$[CO]_0$ = initial concentration of CO

$[CO]_e$ = equilibrium concentration of CO

$[CO]_t$ = measured concentration of CO at reaction time t

A plot of Ln A versus time should yield a straight line with slope m, where

$$m = k_i x\left[\frac{[CO]_0 + [CO]_e}{[CO]_0 - [CO]_e}\right]$$

In order to calculate $[CO]_e$, we need K_{eq}^{WGS} at 340 °C. A simple equilibrium calculation was published by Moe (Moe 1962),

$$K_{eq} = \exp\left\{-4.33 + \frac{4577.8}{T(K)}\right\}$$

Calculation of [CO]e during WGS was performed as follows. Consider an overall mole balance on the WGS reaction:

$$CO(g) + H_2O(g) \Leftrightarrow H_2(g) + CO_2(g)$$

As one can see, for every mole consumed one mole is produced, therefore the change in total number of moles is 0. However, H_2 is consumed in hydrogenation. Furthermore, the analyzed sample is flashed to separate liquid and gases at ambient temperature and pressure (27 °C, 1 atm). Toluene, naphthalene, tetralin, decalins and water condense to liquids at these conditions. Therefore, we may assume two conditions when analyzing the gas sample;

i) H_2O vapour condenses out of the gas sample
ii) All other gas species (H_2S, light hydrocarbons) are present in negligible quantities

Because the water vapour content is difficult to measure during the reaction and will condense into the liquid phase, we can consider as a basis the gas mol% on a dry basis (CO,H_2,CO_2,H_2S) and calculate a theoretical equilibrium conversion:

Calculation for Pure CO feed:

The calculation of CO equilibrium conversion, X_{eq} for an initial atmosphere of CO only occurs as follows:

$[CO]_e$ = theoretical equilibrium dry mol% CO

$[CO]_0$ = normalized mol% CO at 0 minutes

$[CO]_t$ = normalized mol% CO at t minutes

K_{eq} = Equilibrium constant for WGS

$N_{CO,i}$ = Initial mols of CO loaded into reactor (mol)

N_j = mols of species j

N_{H2}^C = hydrogen consumed in hydrogenation (mol); 2 mol required to form tetralin, 5 mol for decalin

X = Conversion of CO

X_{eq} = Equilibrium conversion of CO

w = initial molar ratio of H_2O:CO, $\frac{molH_2O}{molCO}$

χ_{CO} = normalized dry mol% CO from GC analysis

At some time t,

$N_{CO} = (1-X)*N_{CO,0}$

$N_{H2} = X*N_{CO,0} - N_{H2}^c$

$N_{CO2} = X*N_{CO,0}$

$N_T = (1-X)* N_{CO,0} + (X* N_{CO,0}) – N_{H2}^c + (X* N_{CO,0})$

$N_T = (1-X)*N_{CO,0} + 2*X*N_{CO,0} – N_{H2}^c$

$N_T = (1+X)*N_{CO,0} – N_{H2}^c$

where,

N_T is the total mols of dry gas (normalized to CO, H_2, CO_2).

At this point, $N_{CO,0}$ is known, $N_{H2}{}^c$ can be calculated from the conversion of naphthalene to tetralin and decalins and the only unknown is X,

$$X = \frac{(N_{CO,0} - Nco)}{N_{CO,0}}$$

$$\chi_{CO} = \frac{N_{CO}}{N_T} = \frac{(1-X)N_{CO,0}}{(1+X)N_{CO,0} - N_{H2}^{C}}$$

where,

The calculation of K_{eq} is thus:

$$K_{eq} = \frac{N_{CO2}N_{H2}}{N_{CO}N_{H2O}}$$

$$K_{eq} = \frac{[N_{CO,i}X_{eq}][N_{CO,i}X_{eq} - N_{H2}^{C}]}{[N_{CO,i}(1-X_{eq})][N_{CO,i}(w-X_{eq})]}$$

$$K_{eq} = \frac{[N_{CO,i}X_{eq}]^2 - [N_{CO,i}X_{eq}N_{H2}^{C}]}{[N_{CO,i}{}^2(1-X_{eq})(w-X_{eq})]}$$

X_{eq} can be solved by trial and error or using software such as GOALSEEK in Excel.

3.5. 6: Calculation of Variance

To obtain an estimate of the experimental variability, the variance was calculated,

$$s_p{}^2 = \sum_{i=1}^{n} \frac{(X_i - \overline{X})^2}{n-1}$$

s_p = variance

X_i = measurement for the i^{th} replicate

$\overline{X}$ = mean value over all the replicated measurements

n = number of replicates

3.5. 7: Calculation of Pooled Variance

The pooled variance was calculated for sets of experiments where more than one experimental condition was replicated but the number of replicates for each condition was low (ie. 3 experimental conditions each with 2 replicates).

$$^{naph}s_p^2 = \frac{\sum_i^n \nu_i s_i^2}{\sum_i^n \nu_i}$$

ν_i = $n_i - 1$ (n is the same as in 3.6.7).

s_i = variance for the i^{th} mean

3.5. 8: Confidence Interval Calculation

The 90% Confidence Interval was calculated for the two-factor study in Section 4.4.

$$CI = t_{df,\frac{1-\alpha}{2}}\sqrt{\frac{s^2}{n}}$$

n = # of measurements = 3

s^2 = variance = $9.17*10^{-11}$

df = degrees of freedom = n-1 = 2

α = Confidence Level = 90 %

3.5. 9 ANOVA Calculations

An error estimate is calculated from the centre-point replicate results. 3 centre-point replicates were performed at periodic intervals during the reaction sequence to check for experimental drift. The error is taken as the variance of the 3 centre-point results. The degrees of freedom (df) for the error is n-1,

$$n - 1 = 3 - 1 = 2$$

where n is the number of replicates. For the calculation of effects, the average of results at the high (+) factor level is subtracted from the average of results at the low factor level (-).

$$\textit{Effect of } A = \frac{(1+3+5+7)}{4} - \frac{(2+4+6+8)}{4}$$

For interaction factors, the level of the interaction effect is taken from the product of the interactions, ie. for A x B interaction (experiment #1)

A(+) x B(-) = (A x B)(-)

Table 3.5.3.1 displays representative main and interaction levels for a full 2^3 multifactorial experiment.

To calculate the Sum of Squares of Effects, we use:

$$SS = 2^{(f-1)}(effect)^2$$

where f is the number of experimental factors (A,B,C), in this case 3.

The Mean Squares of Effects (MS_i) is simply the SS_i divided by the df of effect i,

$$MS_i = \frac{(SS_i)}{df_i}$$

Table 3.5.3. 1: Level of Factor for ANOVA Analysis

Experiment Number	A	B	C	AB	AC	BC	ABC
1	+	-	-	-	-	+	+
2	-	-	-	+	+	+	-
3	+	+	-	+	-	-	-
4	-	+	-	-	+	-	+
5	+	-	+	-	+	-	-
6	-	-	+	+	-	-	+
7	+	+	+	+	+	+	+
8	-	+	+	-	-	+	-

Because each effect is measured at two levels, (+) and (-), $df_i = n-1 = 2-1 = 1$.

To test for significance, an F-test is used. The analyzed ratio is,

$$\frac{(MS_i)}{(MS_e)} = F_{\exp erimental}$$

where,

MS_i = mean square of effect

MS_e = mean square of error (variance)

F-critical is taken from F-tables, ie. $F_{1,2,0.05}$, where

1 is the df of effects

2 is the df of the error

0.05 = α, and 1-α = 0.95 is the confidence level

ex. $F_{1,2,0.05}$ = 18.51

$F_{critical}$ represents the minimum F-value where MS_i is considered significantly different than MS_e. If,

$$F_{experimental} > F_{critical}$$

then the effect can be considered significant.

3.5. 10: Calculation of Hydrogenation Equilibrium Constant

Hydrogenation is exothermic with conversions thermodynamically limited at high temperatures. The naphthalene/tetralin/H_2 equilibrium constant (Frye 1969);

$$K_P = \frac{N_{TET}}{N_{NAPH} * (P_{H2} + 0.00033\ P_{H2}{}^2)^2}$$

$$X_{eq} = 1 - [1 + \frac{N_{TET}}{N_{NAPH}}]^{-1}$$

$$P_{H2} = hydrogen \quad pressure \quad (atm)$$

$$P_{H2} = \frac{[H_2\ mol\ /\ g] * mass_{rxn}(g) * RT}{V_{reactor}}$$

The equilibrium conversion, X_{eq} calculated was compared to the experimental conversion to determine if the reaction was equilibrium limited.

3.5. 11: ^{1}H-percentage of ^{1}H incorporation into organic products

The percentage of ^{1}H isotope incorporated into the organic product was calculated from the ^{1}H-NMR spectrum integrations.

$$[NAPH]_{NMR,t} = [NAPH]_{GC,t}\ x\left[\frac{(mass-of-GC-sample)}{mass-of-NMR-sample}\right] = [0.0114g/g-liq]x\left[\frac{(3.1968-2.4903)g}{(2.9198-2.4903)g}\right]$$

$$[NAPH]_{NMR,t} = 0.011361g/g-liq$$

$$\left[\frac{mol-NAPH}{mol-n-Octane}\right]_{total} = \frac{\left\{\frac{[NAPH]_{NMR,t}}{MW_{NAPH}}\right\}}{\left\{\frac{1-[NAPH]_{NMR,t}-[TET]_{NMR,t}-[c-DEC]_{NMR,t}-[t-DEC]_{NMR,t}-[Acetone]_{NMR,t}}{MW_{n-Octane}}\right\}}$$

$[NAPH]_{NMR,t}$ = Concentration of Naphthalene in the NMR sample measured by GC-FID at reaction time t

$[TET]_{NMR,t}$	=	Concentration of Tetralin in the NMR sample measured by GC-FID at reaction time t
$[c\text{-}DEC]_{NMR,t}$	=	Concentration of c-Decalin in the NMR sample measured by GC-FID at reaction time t
$[t\text{-}DEC]_{NMR,t}$	=	Concentration of t-Decalin in the NMR sample measured by GC-FID at reaction time t
$[Acetone]_{NMR,t}$	=	Concentration of in the NMR sample measured by GC-FID at reaction time t
Subscript t	=	Reaction time sample was collected, t (min)
NMR	=	Sample from NMR tube

Integration of distinct hydrogen resonances in the NMR spectrum corresponds to relative molar quantities of molecules. For instance, consider n-octane ($CH_3(CH_2)_6CH_3$) and tetralin ($C_{10}H_{12}$; 4 aromatic protons resonate at same frequency). There are six methyl (-CH_3) protons in one molecule of n-octane; likewise there are 4 aromatic protons for each molecule of tetralin. Dividing the integral of the n-octane –CH_3 resonances by 6 gives the relative moles of n-octane. Similarly, dividing the integral of naphthalene aromatic protons by 4 gives the relative moles of naphthalene. Then, dividing:

$$\left[\frac{\mathrm{Re}\,lative\ moles\ naphthalene}{\mathrm{Re}\,lative\ moles\ n-oc\tan e}\right]=\left[\frac{mol-NAPH(^1H)}{mol-n-Oc\tan e(^1H)}\right]$$

mol-NAPH(^{1}H)	=	mols of ^{1}H naphthalene determined from NMR integration
mol-n-Octane(^{1}H)	=	mols of ^{1}H n-octane determined from NMR integration

gives the molar ratio of naphthalene to n-octane (recall only ^{1}H resonances are observed in ^{1}H-NMR). Since deuterium incorporation into n-octane is insignificant, the percentage of ^{1}H-incorporation into naphthalene is,

$$\%(^1H) - Incorporation_{NAPH-A} = \left[\frac{\left[\frac{mol - NAPH(^1H)}{mol - n - Oc\tan e(^1H)} \right]_{NAPH-A}}{\left[\frac{mol - NAPH}{mol - n - Oc\tan e} \right]_{total}} \right]$$

where,

$\left[\frac{mol - NAPH}{mol - n - Oc\tan e} \right]_{total}$ = molar ratio of total naphthalene ($^1H + ^2H$) versus n-octane from GC-FID analysis (n-octane is all ^1H since exchange with D_2O is negligible).

3.5. 12: Calculation of Hydrogenation Index (HI) and Exchange Index (EI)

The HI and EI method developed by Skowronski et al. to compare the extent of hydrogenation and exchange in coal liquefaction was used (Skowronski et al. 1984):

$$n_H = \{\frac{8\ moles - H)}{mol - NAPH} * [NAPH] + \frac{12\ moles - H}{mol - TET} * [TET]\} * mass_{rxn}$$

$$n_{1H}{}^\circ = \frac{\left[\frac{8\ moles - H}{mol - NAPH} \right] * mass_{NAPH,i}}{MW_{NAPH}}$$

$$n_{2H} = mass_{rxn} * \{\{ (1 - [\%^1H - NAPH - A]) + (1 - [\%^1H - NAPH - B])\} * \left[\frac{4\ moles - H}{mol - NAPH} \right] * [NAPH]$$
$$+ \{(1 - [\%^1H - TET - AROM]) + (1 - [\%^1H - TET - SAT] * 2\} * \left[\frac{4\ moles - H}{mol - TET} \right] * [TET]\}$$

$$HI = \frac{H}{H + E}$$

$$EI = \frac{E}{H + E}$$

$mass_{rxn}$	=	mass of liquid in reactor (g)
n_H	=	total moles of hydrogen including D in all products (NAPH and TET)
$n_{1H}°$	=	moles of hydrogen in starting naphthalene
n_{2H}	=	total moles of deuterium in products by hydrogenation and exchange
H	=	net amount of hydrogen added to form tetralin, $n_H - n_{1H}°$
E	=	amount of deuterium incorporated by exchange, $n_{2H} - H$
$\%^1$H-NAPH-A	=	percentage of ^{1}H on the naphthalene α- position
$\%^1$H-NAPH-B	=	percentage of ^{1}H on the naphthalene β-position
$\%^1$H-TET-AROM	=	percentage of ^{1}H on the tetralin aromatic ring
$\%^1$H-TET-SAT	=	percentage of ^{1}H on the tetralin saturated ring

(for the various hydrogen-positions in tetralin and naphthalene refer to Scheme 4.2.1.1)

Chapter 4: Isotope Effects and CO adsorption

4. 1 Introduction

In order to compare the rates of in-situ hydrogen and molecular hydrogen utilization under CO/H_2, we might distinguish between hydrogen originating from water and molecular hydrogen through isotopic labeling with D_2O and H_2. Isotopic tracing techniques utilizing Nuclear Magnetic Resonance (NMR) of deuterium have been applied to analyze D incorporation into coal liquefaction products and model compounds (Young et al. 1984; Schweighardt et al. 1976). Simple analysis detailing relative incorporation into aromatics, ring saturates and alkyl groups is possible.

Isotopic labeling using D_2O was utilized to determine deuterium incorporation from water into hydrogenated products and compared to molecular hydrogen incorporation. Kinetics under D_2O were compared with kinetics under H_2O to determine possible apparent kinetic isotope effects. Diffuse Reflectance Infrared Fourier Transform Spectroscopy (DRIFTS) was performed to analyze adsorption of CO on the catalyst surface at reaction temperature.

4. 2 Isotopic Labeling of Water

4.2. 1 ^{1}H-NMR Analysis of Liquid Phase Products

Deuterium incorporation into liquid products was quantified by NMR spectroscopy. The processed ^{1}H-NMR spectra are shown in Appendix B. Protons at chemically unique sites

on naphthalene and tetralin resonate in a magnetic field at different frequencies; their chemical shifts (ppm) are shown in Scheme 4.2.1.1. n-Octane was used as solvent rather than toluene since aromatic protons exchange with D_2O at reaction conditions. ^1H incorporation into naphthalene and tetralin was quantified by ^1H-NMR; these results were then compared with quantification of total organic species concentrations (^1H and ^2H (D)) by GC-FID analysis to determine the ^1H incorporation (as ^1H-percentage) into naphthalene and tetralin. Deuterium incorporation was determined by subtracting the ^1H-percentage. The accuracy of this method was confirmed by quantifying a control sample

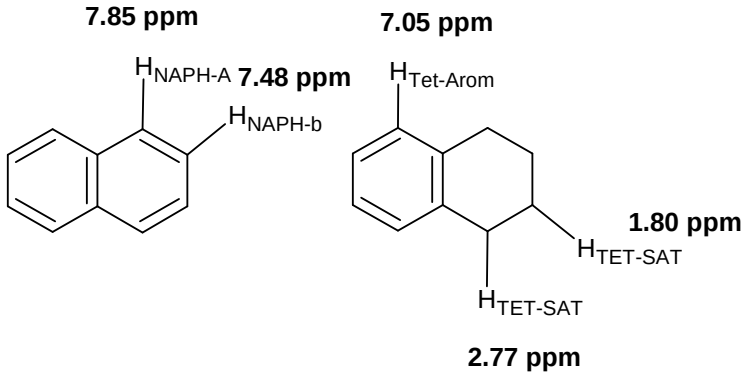

Scheme 4.2.1. 1: Chemical Shifts of Naphthalene and Tetralin Protons in ^1H-NMR

prepared with measured quantities of h_6-acetone and d_6-acetone in n-octane with ^1H-NMR, ^2H-NMR and GC-FID analysis. It was hoped that measuring the deuterium incorporation over reaction time would allow differentiation between the in-situ and molecular hydrogenation pathways. Scheme 4.2.1.2 displays the possible hydrogenation mechanisms. Incorporation of deuterium from D_2O can occur through,

i) direct exchange between aromatic species and protons/deuterons from water or

ii) hydrogenation and dehydrogenation.

Molecular $^1H_2$ which can also exchange ^1H with D_2O and naphthalene (Scheme 4.2.1.3). Exchange between molecular hydrogen and water in catalytic environments in part due to reactor wall effects is well established (Roland et al. 2006). The reactor wall may also catalyze WGS and hydrogenation; an estimate of the blank "wall effect" kinetics under $CO/H_2/H_2O$ (Experiment #6) is shown in Table D.2, Appendix D.

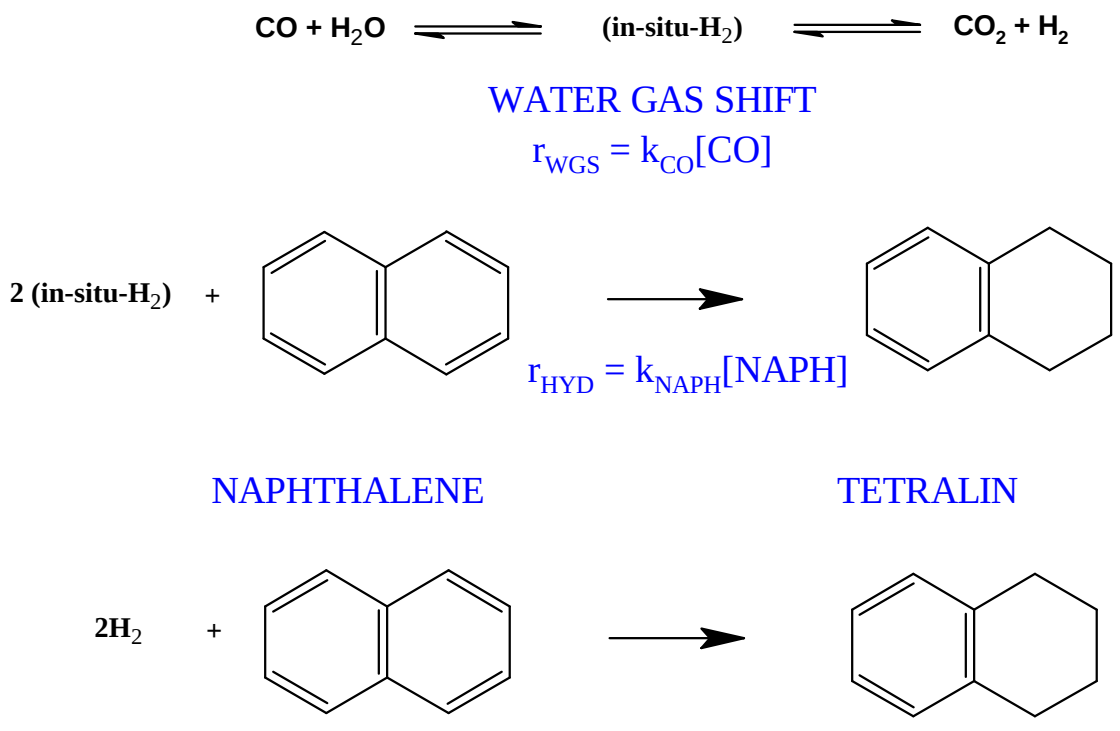

Scheme 4.2.1. 2: Hydrogenation of Naphthalene in Water

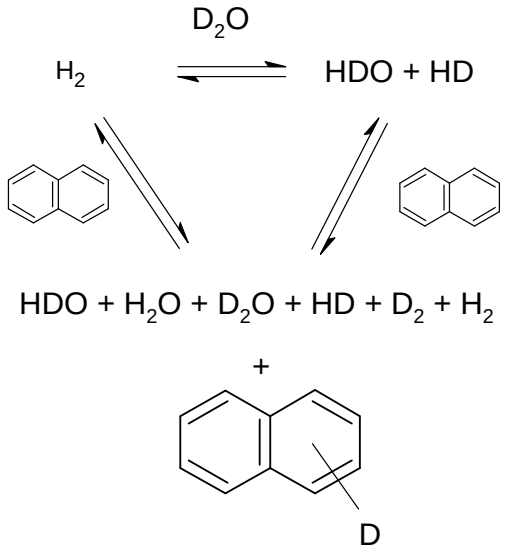

Scheme 4.2.1. 3: Hydrogen Exchange Pathways between molecular-H_2, naphthalene and water

Hydrogen-exchange between D_2O and naphthalene was confirmed by performing an experiment under $N_2/D_2O/H_2S$ with PMA as the Mo precursor (Figure 4.2.1.1). The naphthalene ^{1}H-percentage for both α-hydrogen and β-hydrogen decrease over the reaction time indicating that deuterium is incorporated from D_2O. The lower ^{1}H-percentage at a given reaction time for α-hydrogens versus β-hydrogens suggests a faster rate of H-exchange for naphthalene α-hydrogen sites. Under $N_2/D_2O/H_2S$ a decrease in ^{1}H-percentage is observable over reaction time while the rate of exchange is different for naphthalene α-hydrogens versus β-hydrogens.

Figure 4.2.1.2 shows the ^{1}H-percentage for naphthalene and tetralin with reaction time under $CO/D_2O/H_2S$. The initial sample (not shown) was lost before complete

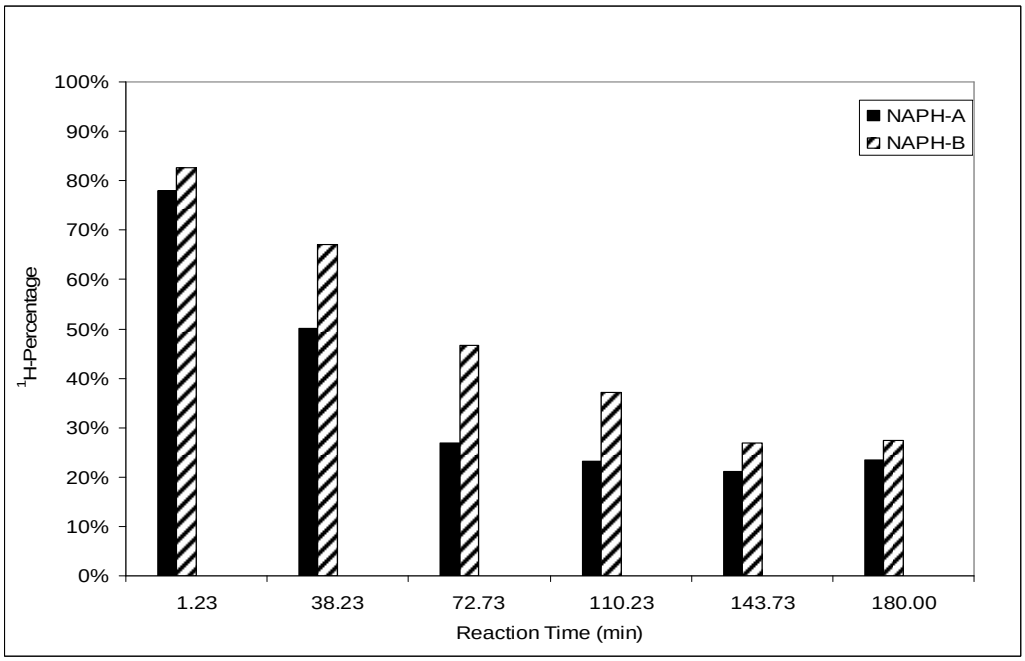

Figure 4.2.1.1: Experiment #19, ^{1}H-isotope percentage into naphthalene and tetralin in hydrogenation($N_2/D_2O/H_2S$, 600 psig, 15 psi H_2S, 4.0°C/min, 340 °C for 3 hrs, 10 ml H_2O, 100 ml n-octane, 28.9 mmol Naphthalene, 0.39 mmole Mo, 1500 rpm impeller speed)

analysis could be performed. The ^{1}H-percentage reaches a pseudo-steady state value early in the reaction due to hydrogen-exchange and hydrogenation. The low naphthalene and tetralin ^{1}H-percentage is due to the high ratio of overall D/H since deuterium is the only H-isotope available for hydrogenation and the relative molar amount of D_2O (1.10 moles D) compared to naphthalene (0.2312 moles ^{1}H) is large (D/H = 4.76, $D_2O/C_{10}H_8$ = 20). The D/H ratio depends upon the molar amounts of naphthalene, H_2 and D_2O in the batch system. For comparison, the ^{1}H percentage in naphthalene and tetralin under an initial atmosphere of $H_2/D_2O/H_2S$ is shown in Figure 4.2.1.3. Hydrogenation with $^1H_2$ produces ^{1}H-tetralin. HD (and D_2) can be produced via H-exchange between H_2 and D_2O. Exchange between H_2 and D_2O scrambles the molecular hydrogen into H_2 and HD

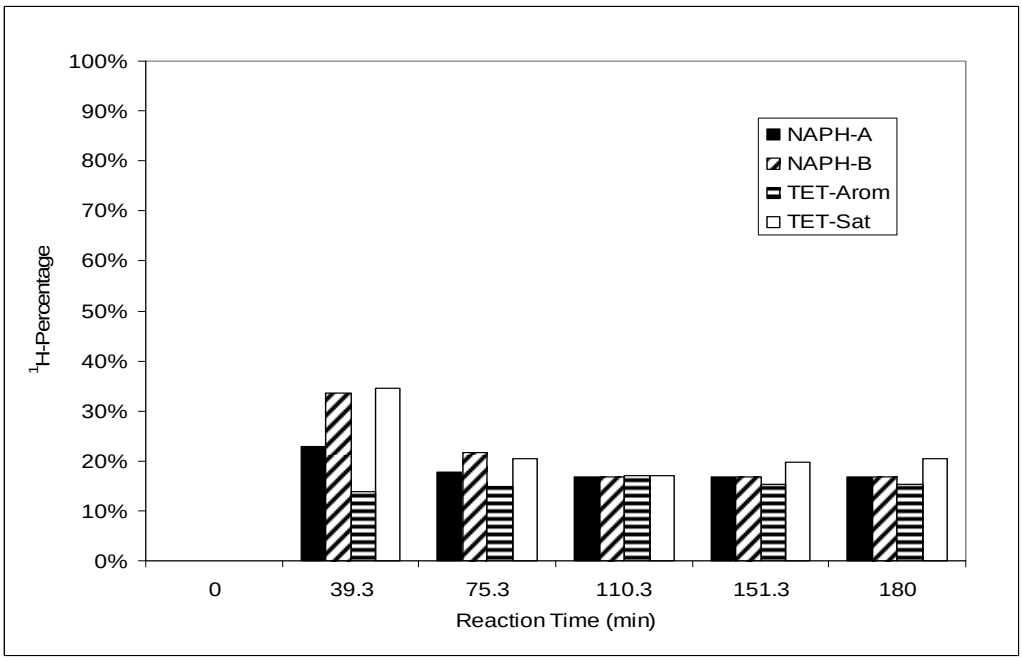

Figure 4.2.1.2: Experiment #5R1, ^{1}H-isotope percentage into naphthalene and tetralin in hydrogenation (($CO/D_2O/H_2S$, 600 psig, 15 psi H_2S, 4.0°C/min, 340 °C for 3 hrs, 10 ml H_2O, 100 ml n-octane, 28.9 mmol Naphthalene, 0.39 mmole Mo, 1500 rpm impeller speed)

(possibly D_2). Fu et al. found that hydrogenation of phenanthrene over sulfided $NiMo/Al_2O_3$ under syngas ($CO/H_2/D_2O$) resulted in a mixture of H_2 and HD in the gas mixture (Fu et al. 1995). Therefore, in addition to direct exchange between D_2O and aromatic hydrogen, deuterium can be incorporated into tetralin from molecular hydrogen (HD or D_2) through hydrogenation. In our case the relative concentrations of H_2, HD and D_2 could not be quantified, but the information could be provided using suitable MS techniques and may be useful to determine the isotopic distribution between water, naphthalene, tetralin and molecular hydrogen at 340 °C for various D/H ratios. Comparison between the case with CO (Figure 4.2.1.2) and H_2 (Figure 4.2.1.3) indicates a

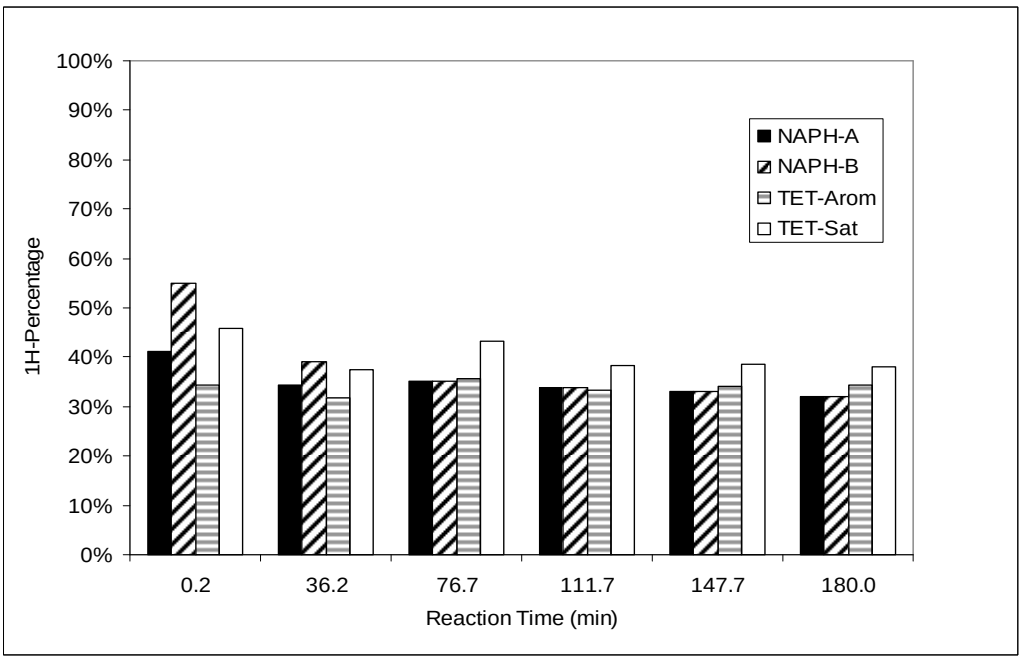

Figure 4.2.1.3: Experiment #2R1, (1:2) ^{1}H-isotope percentage into naphthalene and tetralin in hydrogenation ($H_2/D_2O/H_2S$, 600 psig, 15 psi H_2S, 4.0°C/min, 340 °C for 3 hrs, 10 ml H_2O, 100 ml n-octane, 28.9 mmol Naphthalene, 0.39 mmole Mo, 1500 rpm impeller speed)

higher steady-state ^{1}H- percentage (naphthalene and tetralin) with H_2. Since under $H_2/D_2O/H_2S$ the overall atomic ratio of D/H is lower than under $CO/D_2O/H_2S$, the higher steady-state naphthalene and tetralin ^{1}H-percentage under H_2 is not surprising.

Hydrogenation of naphthalene in n-octane under $CO/H_2/D_2O/H_2S$ is shown in Figure 4.2.1.3. The D/H ratio under an initial $CO/H_2/D_2O$ lies between that for CO/D_2O and H_2/D_2O. The steady-state naphthalene and tetralin ^{1}H-percentage for an initial atmosphere of $CO/H_2/D_2O/H_2S$ also falls between the values for CO and H_2 (Figures 4.2.1.2, 4.2.1.3 and 4.2.1.4).

It is difficult to directly compare the rates of in- situ vs. molecular hydrogenation directly since significant proton exchange occurs between D_2O, naphthalene and H_2.

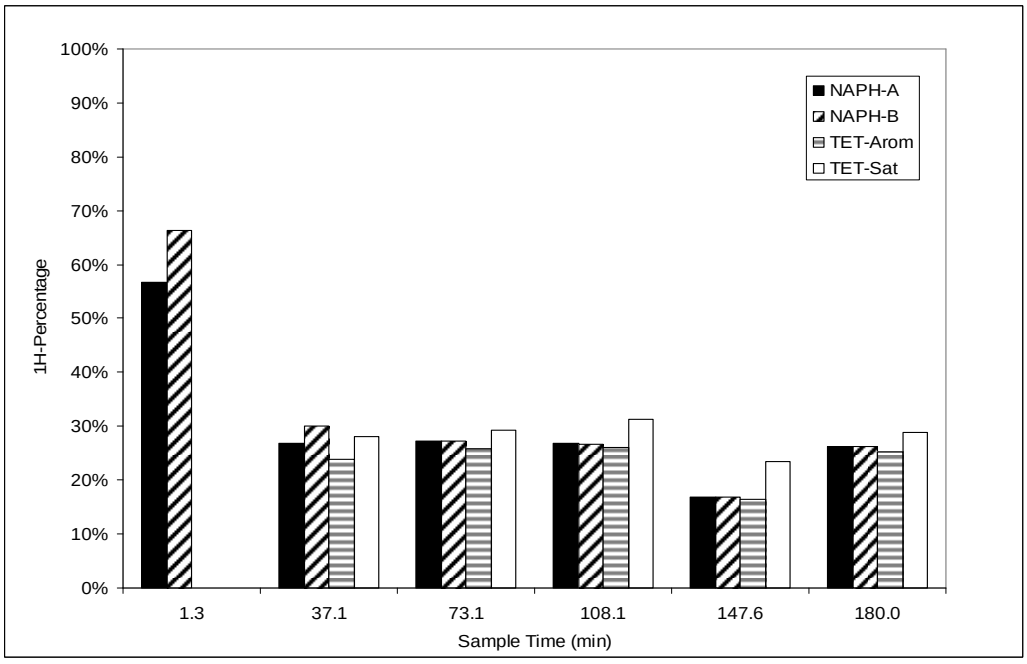

Figure 4.2.1.4: Experiment #14, ^{1}H-isotope percentage into naphthalene and tetralin in hydrogenation ((molar 1:1 CO/H_2)/D_2O/H_2S, 600 psig, 15 psi H_2S, 4.0°C/min, 340 °C for 3 hrs, 10 ml H_2O, 100 ml n-octane, 28.9 mmol Naphthalene, 0.39 mmole Mo, 1500 rpm impeller speed)

Therefore, without knowledge of the gas phase isotope distribution, it is not possible to kinetically distinguish between deuterogenation from water and hydrogenation from molecular hydrogen in n-octane/water emulsions. Under $N_2/D_2O/H_2S$, only exchange occurs, and a steady-state ^{1}H-percentage is reached at the end of reaction (Figure 4.2.1.4). During reaction under $N_2/D_2O/H_2S$, the ^{1}H-percentage for naphthalene is different for α-hydrogen than for β-hydrogen. A greater percentage of deuterium incorporation is observed under CO and H_2 compared with N_2. In contrast to N_2, under CO and H_2, the deuterium incorporation between α-hydrogen and β-hydrogen is similar. Over dispersed, unsupported MoS_2 deuterium incorporation from D_2O appears enhanced under reducing (CO, H_2) versus inert (N_2) atmospheres. Under a reducing atmosphere (CO and/or H_2) sulfur vacancies on the MoS_2 surface are formed. It is thought that hydrogenation,

hydrodesulfurization and hydrodenitrogenation occur at these sulfur vacancies. Hydrogenation catalysts have been observed to dissociate water and catalyze H-exchange; therefore sulfur vacancies on MoS_2 created by reduction under CO or H_2 may also catalyze H_2/D_2O exchange (Garnett 1966).

Skowronski et al. studied deuterium incorporation during coal liquefaction with Ni/kieselguhr (Skowronski et al. 1984). They formulated a Hydrogenation Index (HI) and Exchange Index (HI) to compare the extent of deuterium incorporated into coal through hydrogenation ($^2H_2$) and solvent exchange (tetralin-d_{12}). The formulation of HI and EI are covered in Section 3.5.12. As defined, HI and EI are valid for conditions where deuterium is present in the hydrogenation ($^2H_2$) and exchange (solvent) source. Table 4.2.1.1 displays the values of HI and EI for naphthalene hydrogenation under $CO/D_2O/H_2S$. The values indicate the strong extent of exchange compared to hydrogenation occurring with the MoS_2 catalyst. Under coal liquefaction, the activation energy for H-exchange is less than for hydrogenation (Skowronski et al. 1984). A dissociative type mechanism has been proposed for exchange between D_2O and aromatic molecules (Garnett 1966). The

Table 4.2.1. 1: Hydrogenation Index (HI) and Exchange Index (EI) under $CO/D_2O/H_2S$ (($CO/D_2O/H_2S$, 600 psig, 15 psi H_2S, 4.0°C/min, 340 °C for 3 hrs, 10 ml H_2O, 100 ml n-octane, 28.9 mmol Naphthalene, 0.39 mmole Mo, 1500 rpm impeller speed)

Reaction Time (min)	*39.3*	*75.3*	*110.3*	*151.3*	*180*	*Average over reaction*
Hydrogenation Index (HI)	0.191	0.208	0.194	0.207	0.402	0.241
Exchange Index (EI)	0.809	0.792	0.806	0.793	0.598	0.759

* sample at 0 minutes was lost

dissociation of H_2O is implicated as a key factor in coke inhibition for the Aquaconversion™ process jointly developed by Intevep, UOP and Foster-Wheeler (Marzin et al. 1986; Rana et al. 2007). The alkali salts (K, Na) used are thought to catalyze H_2O dissociation to produce some form of hydrogen which can then add to the thermally formed hydrocarbon free-radicals terminating their oligomerization into coke (Marzin et al. 1986). Moll suggested that the presence of water during upgrading of bitumen emulsion with MoS_2 may reduce condensation reactions that form coke solids (Moll 1999). The presence of unsupported MoS_2 may enhance the dissociation of H^+ from water at high temperature serving to inhibit coke formation similar to the Aquaconversion™ process.

4. 3 Effect of Solvent Type

4.3. 1 Effect of Solvent Type on WGS: n-octane versus toluene

HDS, HDN and HYD reactions occur during hydroprocessing of bitumen and heavy oils. Inhibition of certain pathways may therefore exist if the substrate contains a mix of sulfur-containing , nitrogen-containing and aromatic hydrocarbons. The presence of nitrogen-containing compounds is known to significantly inhibit both HDS and HYD, while for sulfur-containing compounds the presence of aromatics has been suggested to inhibit HDS pathways (Song et al. 2006).

MoS_2 enhances the rate of exchange between protons on water and aromatic hydrocarbon species. When toluene is used as solvent for naphthalene HYD using D_2O as the hydrogen source, deuterated toluene was observed in significant amounts from the D-

NMR spectrum (not shown). Since aromatic exchange and water gas shift reactions involve dissociation of protons from water and may occur on similar or adjacent active sites, these mechanistic interactions may impact the kinetics of various pathways. A practical consideration then is whether an inhibitory effect on water gas shift and hydrogenation is observed in the presence of an aromatic solvent.

The pseudo-first order rate constants for water gas shift and naphthalene hydrogenation were measured while keeping other parameters constant. However, in order to maintain the same liquid/gas ratio in the batch autoclave, the same volumes of n-octane and toluene solvents were used. The catalyst concentration (3.70×10^{-3} g Mo / ml water) was kept constant with respect to H_2O rather than with total organics since it is the WGS rate we are interested in comparing.

The CO concentrations versus time are shown in Figures 4.3.1.1 and 4.3.1.2 for n-octane and toluene solvents. Reported pseudo-first order rate constants for CO are shown in Table 4.3.1.1. The type of solvent appears to affect the water gas shift rate. At the start of reaction, more CO has been consumed in the toluene solvent compared with n-octane as can be seen from the CO concentrations (Figures 4.3.1.1, 4.3.1.2). It is possible this is due to phase effects; the three-phase critical point of water/n-octane (267 °C) is 18 °C lower than the three-phase critical temperature of water/toluene (285 °C) (Roof 1970). Segregation of water and hydrocarbon phases below the critical point may enhance the water gas shift rate if catalyst particles preferentially reside in the water phase or at the emulsion interface. A minimum in the surface free energy occurs for particles adsorbing to a three-phase interface. More facile dissociation of water in toluene (influenced by H-exchange with aromatics) versus minimal exchange with n-octane (aliphatic solvent) may

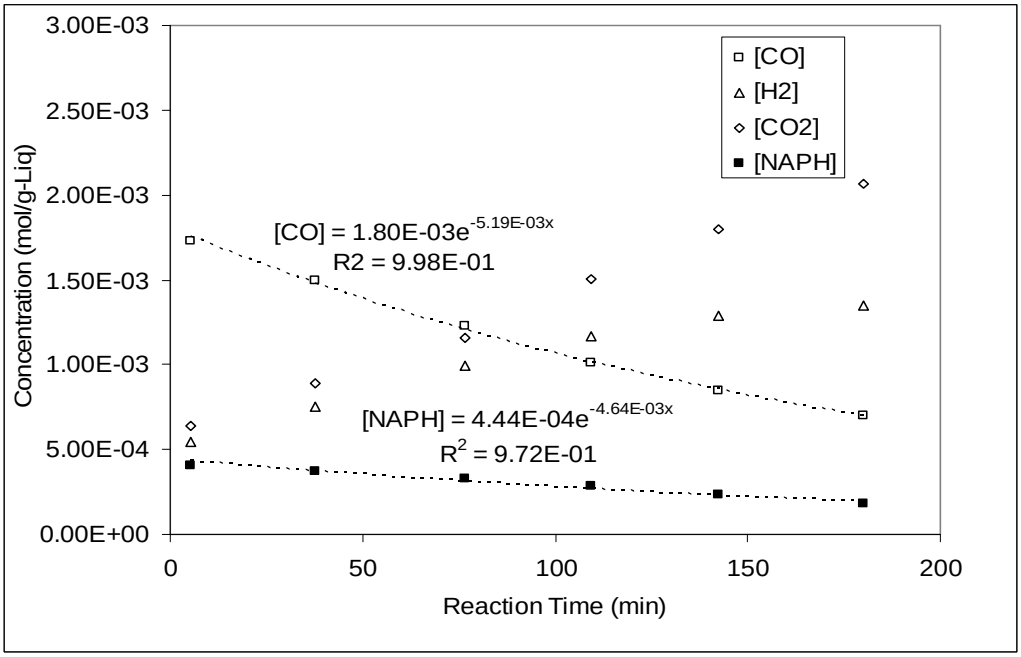

Figure 4.3.1.1: Experiment #7, CO, H_2, CO_2 and Naphthalene Concentrations in n-octane/water ($CO/H_2O/H_2S$, 600 psig, 15 psi H_2S, 4.0°C/min, 340 °C for 3 hrs, 10 ml H_2O, 100 ml n-octane, 28.9 mmol Naphthalene, 0.39 mmole Mo, 1500 rpm impeller)

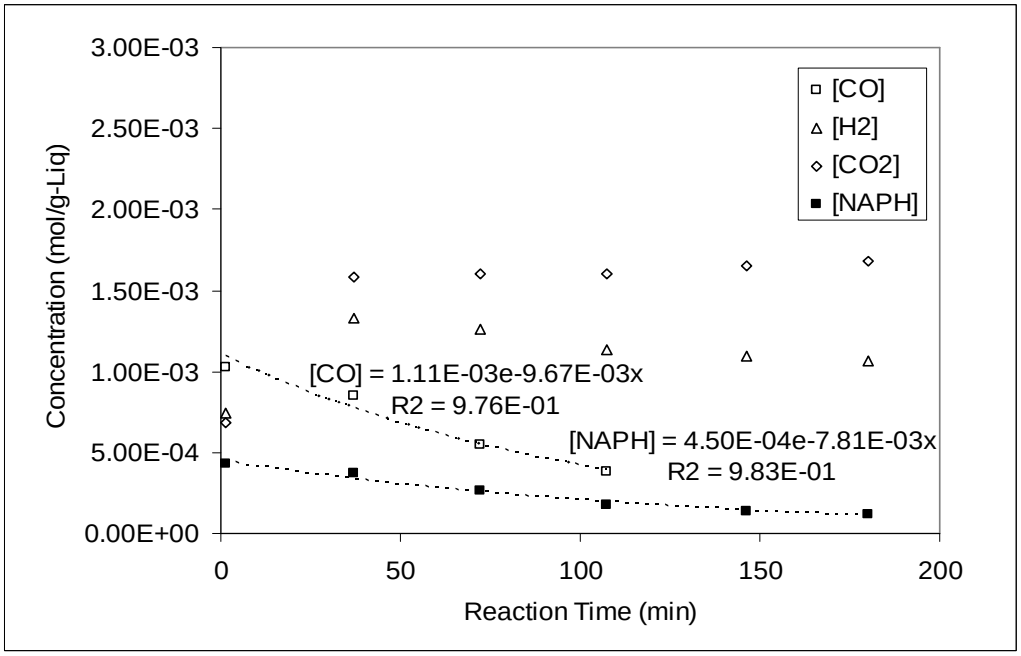

Figure 4.3.1. 2: Experiment #25, CO, H_2, CO_2 and Naphthalene Concentrations in toluene/water ($CO/H_2O/H_2S$, 600 psig, 15 psi H_2S, 4.0°C/min, 340 °C for 3 hrs, 10 ml H_2O, 100 ml toluene, 28.9 mmol Naphthalene, 0.39 mmole Mo, 1500 rpm impeller)

account for the increase in isothermal pseudo-first order rate constant, but phase effects in the three-phase critical regime cannot be ruled out. An aromatic solvent (toluene) does not inhibit WGS over MoS_2 compared to an aliphatic solvent (n-octane).

Table 4.3.1. 1: Pseudo-first order rate constants for WGS and naphthalene HYD under n-octane and toluene ($CO/H_2O/H_2S$, 600 psig, 15 psi H_2S, 4.0°C/min, 340 °C for 3 hrs, 10 ml H_2O, 100 ml Solvent, 28.9 mmol Naphthalene, 0.39 mmole Mo, 1500 rpm impeller)

Solvent	k_{CO}, (s^{-1})	k_{NAPH}, (s^{-1})
n-Octane (Experiment #7)	$8.65*10^{-5}$	$7.73*10^{-5}$
Toluene (Experiment #25)	$1.61*10^{-4}$	$1.30*10^{-4}$

4.3. 2 Effect of Solvent type on Hydrogenation: n-octane vs. toluene

For n-octane, H_2 is limiting until about 100 minutes, however the measured rate fits a pseudo-first order rate relationship for naphthalene quite well. For toluene, H_2 is in excess at 40 minutes due to the fast rate of water gas shift initially. Gas concentrations were calculated from pressure and composition measurements of the gases flashed from a high-pressure reactor sample. The excess of H_2 present occurs because water gas shift begins at a lower temperature than hydrogenation. The higher rate constant of HYD in toluene/water (1.30×10^{-4} s^{-1}) compared to n-octane/water (7.73×10^{-5} s^{-1}) may be due to the higher concentration of hydrogen in the toluene/water system. An aromatic solvent (toluene) does not inhibit hydrogenation compared to an aliphatic solvent (n-octane).

4. 4 Effect of Gas Atmosphere and Isotope of Water on Naphthalene Hydrogenation in n-octane/water

Taking the deuterium labeling experiments as a basis, additional experiments were performed under similar conditions but substituting normal water for heavy water. This was done to determine if an isotope substitution for hydrogen in water had a significant effect on HYD activity. Rate constants are presented in Table 4.4.1. In addition a

Table 4.4. 1: Measured pseudo-first order rate constants for Isotope and Gas Type (600 psig, 15 psi H_2S, 4.0°C/min, 340 °C for 3 hrs, 10 ml Water, 100 ml n-octane, 28.9 mmol Naphthalene, 0.39 mmole Mo, 1500 rpm impeller speed)

Run Order	Water Isotope, H_2O (-) D_2O (+)	Gas Type, CO (-) H_2 (+)	Pseudo-First Order Naphthalene Rate Constant, $k_{NAPH}(10^{-5}\ s^{-1})$	Pseudo-First Order Irrev. WGS Rate Constant, $k_{CO}(10^{-5}\ s^{-1})$
2	D_2O	H_2	21.0	
2R1	D_2O	H_2	19.8	
17	H_2O	H_2	24.3	
28	H_2O	H_2	20.2	
5	D_2O	CO	8.67	
5R1	D_2O	CO	7.42	7.50
5R2	D_2O	CO	7.33	6.83
7	H_2O	CO	8.55	11.30
14	D_2O	CO/H_2 (mol ratio = 1:1)	7.83	9.58
1	D_2O	CO/H_2 (mol ratio = 1:1)	2.02	8.50
1R1	D_2O	CO/H_2 (mol ratio = 1:1)	5.33	7.67

comparison between in-situ generated hydrogen and molecular hydrogen can be performed. From the ANOVA results only the type of gas has a significant effect on the HYD rate in n-octane/water (Table 4.4.2). Molecular hydrogen gives a significant increase in rate over in-situ generated H_2 under n-octane/water at 340 °C, while the opposite was observed in toluene/water (Zhang 2005).

Table 4.4.2: ANOVA Table for Hydrogenation pseudo-first order rate constant, k_{NAPH} (Gas Type, Hydrogen Isotope in Water) (600 psig, 15 pis H_2S, 4.0°C/min, 340 °C for 3 hrs, 10 ml Water, 100 ml n-octane, 28.9 mmol Naphthalene, 0.39 mmole Mo, 1500 rpm impeller speed)

Source	Effect on k_{NAPH} (10^{-5} s^{-1})	SS_i (10^{-10} s^{-2})	DF	MS_i (10^{-10} s^{-2})	$F_{experimental}$ = MS_i / MS_e
Main Effect					
Gas Type CO (-) or H_2 (+)	13.155	173.1	1	173.1	67.86
Isotope H_2O (-) or D_2O (+)	-1.285	1.651	1	1.651	< 1
Interaction Effects					
Gas x Isotope	-0.545	0.297	1	0.297	< 1
Error			4	2.55	
$F_{critical}$ = $F_{1,4,\ 0.05}$					7.71

4.4. 1 Hydrogenation under $CO/H_2O/H_2S$ and $H_2/H_2O/H_2S$ in n-octane/water

The pseudo-first order rate constants k_{CO} and k_{NAPH} under various gas atmospheres are shown in Table 4.4.1.1. For $CO/H_2/H_2O$ and H_2/H_2O, the hydrogen concentration over

reaction time does not change considerably (Figures 4.4.1.1-4.4.1.3). For molecular H_2, dividing k_{NAPH} by the hydrogen concentration yields a pseudo-second order rate constant, $k"_{NAPH}$ (Table 4.4.1.1). $k"_{NAPH}$ for both the $H_2/H_2O/H_2S$ and $N_2/H_2/H_2O/H_2S$ runs (experiments #17 and #29) are very similar (average 9.39 x 10^{-2} g s^{-1} mol^{-1}) which suggests that under molecular H_2 the pseudo-second order rate constant is relevant. Water is known to inhibit HDS (Lee 2006). Generation of in-situ hydrogen consumes water, while the water content of the emulsion under ex-situ hydrogen should remain constant. Under synthesis gas, the hydrogen initially present is supplemented by in-situ generated

Table 4.4.1 1: Comparison of pseudo-first order rate constants for water gas shift and hydrogenation under different initial gas atmospheres (600 psig, 15 psi H_2S, 4.0°C/min, 340 °C for 3 hrs, 10 ml Water, 100 ml n-Octane, 28.9 Naphthalene, 0.39 mmole Mo, 1500 rpm impeller speed)

Initial Gas Charge	**k_{CO}, (10^{-5} s^{-1})**	**k_{NAPH}, (10^{-5} s^{-1})**	*** Pseudo-steady state [H_2] (10^{-4} mol/g-Liq)**	**$k"_{NAPH}$ (g s^{-1} mol^{-1})**
$CO/H_2O/H_2S$ (mol $CO:H_2O$ = 1:2) Experiment #7	8.65	8.55	pseudo-steady state n/a	
$CO/H_2/H_2O/H_2S$ (mol $CO:H_2:H_2O$ = 1:1:4) Experiment #15	11.2	9.50	15.0	0.0598
$N_2/H_2/H_2O/H_2S$ (mol $N_2:H_2:H_2O$ = 1:1:4) Experiment #29		8.67	9.5	0.0955
$H_2/H_2O/H_2S$ (mol $H_2:H_2O$ = 1:2) (Experiment #17 & 28)		22.3	20.0	0.0922

* Appendix B

hydrogen thereby increasing the hydrogen concentration. However, when CO is present in syngas k"$_{NAPH}$ is considerably lower (5.98 x 10^{-2} g s^{-1} mol^{-1}) in n-octane/water than when CO is absent. This may indicate that CO competes with H_2 or naphthalene for adsorption to active sites.

Competitive adsorption between CO, H_2 and aromatic species on sulfur vacancies may inhibit the various reactions. This assumes that significant adsorption occurs on sulfur vacancies. Theoretical studies of ideal triangular MoS_x nanoclusters indicate removal of surface sulfur via H_2S desorption in the presence of CO is energetically favourable while

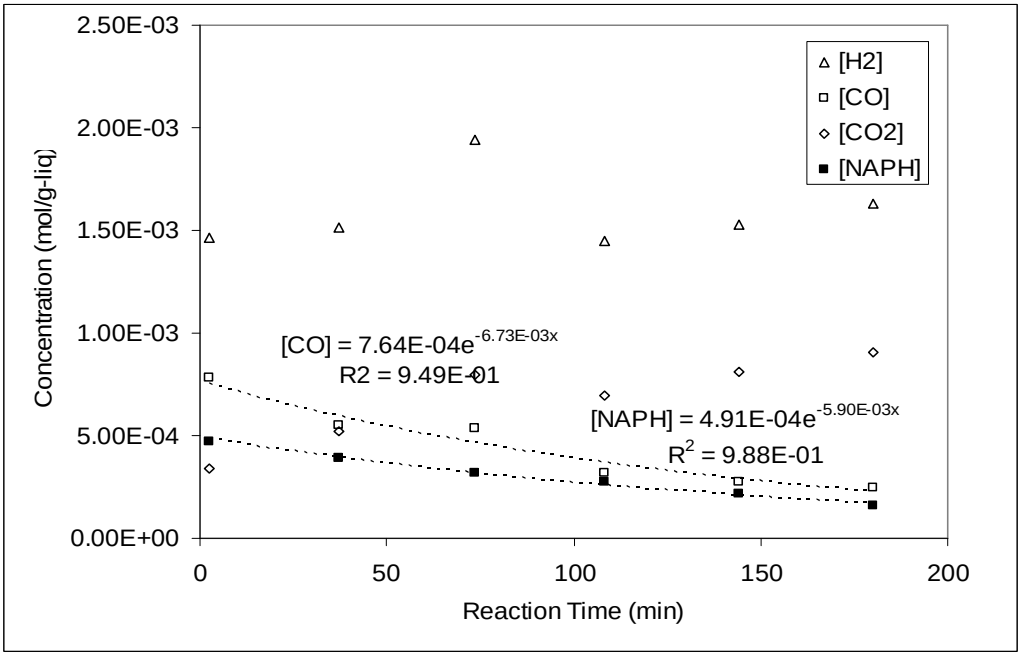

Figure 4.4.1.1: Experiment #15, CO, CO_2, H_2 and Naphthalene Concentrations ((1:1 molar CO/H_2)/H_2O/H_2S), 600 psig, 15 H_2S, 4.0°C/min, 340 °C for 3 hrs, 10 ml Water, 100 ml n-Octane, 28.9 mmol Naphthalene, 0.39 mmole Mo, 1500 rpm impeller speed)

H_2S adsorption is favoured without CO (Zeng et al. 2005; Zeng et al. 2005). Production of COS from CO and liberated surface sulfur to form sulfur vacancies on the catalyst may occur analogous to H_2S formation from H_2 and surface sulfur. Liu and Ng found that HDS of dibenzothiophene increased as the ratio of CO:H_2 increased and the rate of HDS was higher with in-situ generated hydrogen (Liu 2008). In contrast to hydrogenation, the initial step in direct desulfurization may be adsorption of thiophenic sulfur to sulfur

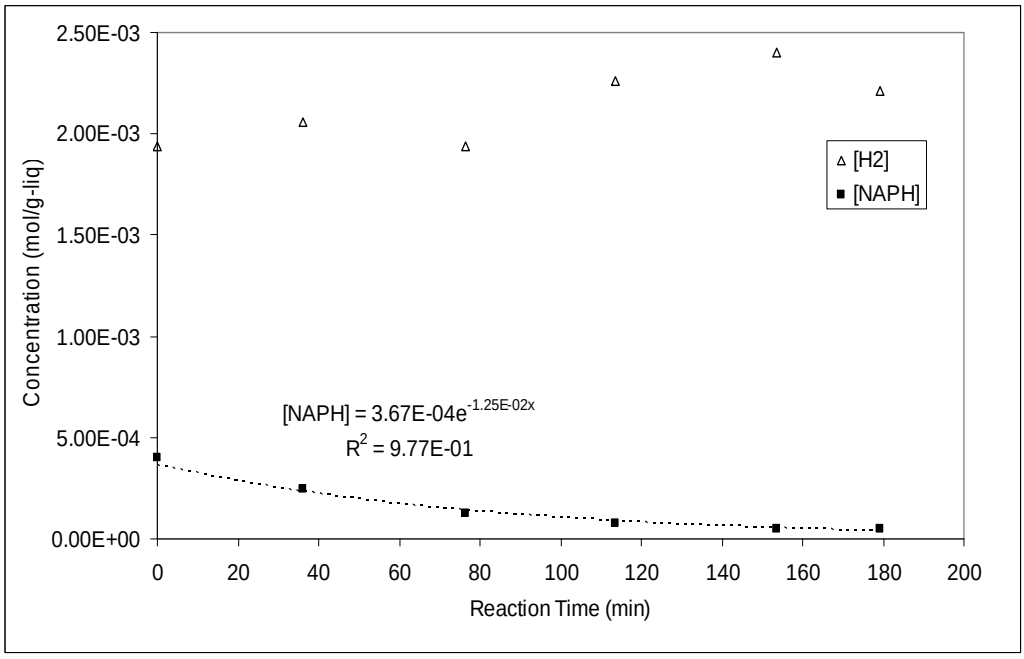

Figure 4.4.1.2: Experiment #28, H_2 and Naphthalene Concentrations ($H_2/H_2O/H_2S$), 600 psig, 15 psi H_2S, 4.0°C/min, 340 °C for 3 hrs, 10 ml Water, 100 ml n-Octane, 28.9 mmol Naphthalene, 0.39 mmole Mo, 1500 rpm impeller speed)

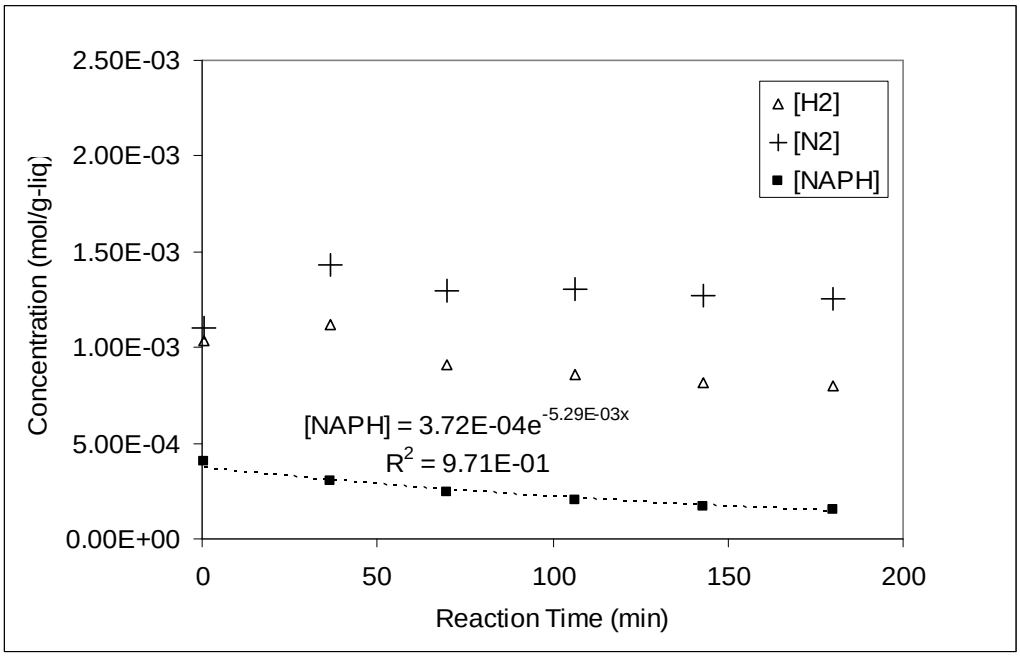

Figure 4.4.1.3: Experiment #29, N_2, H_2 and Naphthalene Concentrations ((1:1 molar N_2/H_2)/H_2O/H_2S), 600 psig, 15 psi H_2S, 4.0°C/min, 340 °C for 3 hrs, 10 ml Water, 100 ml n-Octane, 28.9 mmol Naphthalene, 0.39 mmole Mo, 1500 rpm impeller speed)

vacancies followed by hydrogenation to H_2S and cleavage of C-S bonds. More facile removal of surface sulfur by CO to generate sulfur vacancies may enhance direct desulfurization.

4. 5 Deuterium Substitution in Water: Effect on the WGS Rate in n-octane/water

When D_2O is used a decrease in the WGS rate is observed compared to H_2O. The measured apparent isotope effects for water gas shift are shown in Table 4.5.1.1, while the rate constants are displayed in Figure 4.5.1.1. An apparent normal isotope effect (k_{H2O} /

k_{D2O}) of 1.58 was observed for n-octane/water, which suggests that the rate determining step is not inconsistent with dissociation of a bond containing hydrogen.

Table 4.5.1. 1: Normal Kinetic Isotope Effect (k_{H2O}/k_{D2O}) for Pseudo-First Order WGS Rate Constant (CO) (600 psig, 15 pis H_2S, 4.0°C/min, 340 °C for 3 hrs, 10 ml Water, 100 ml n-Octane, 28.9 mmol Naphthalene, 0.39 mmole Mo, 1500 rpm impeller speed)

Initial Gas Composition	***Pseudo-First Order Irrev. WGS Rate Constant, $k_{CO,H2O}$ (10^{-5} s^{-1})***	***Pseudo-First Order Irrev. WGS Rate Constant, $k_{CO,D2O}$ (10^{-5} s^{-1})***	***WGS Rate Based CO KIE ($k_{CO,H2O}/k_{CO,D2O}$)***
CO	11.3[A]	7.17[B]	1.58
CO/H_2 (1:1 molar)	11.2[C]	8.58[D]	1.30

A – Expt. #7; B – Expt. #5, 5R1, 5R2; C-Expt. 15; D – Expt. #1, 1R1, 14

Kinetic isotope studies have been performed on various water gas shift catalysts including Pt/CeO_2 and $Rh/PtCeO_2$. Shido and Iwasawa, using combinations of isotopically labelled formates and D_2O or H_2O found the rate of bidentate formate decomposition to depend only on the C-H hydrogen isotope in the formate over Rh/CeO_2 (Shido 1993). The apparent kinetic isotope effect (k_{C-H} / k_{C-D}) was between 1.4 – 1.5. Using a Pt/CeO_2 catalyst, Jacobs et al. compared CO conversion between H_2O and D_2O in a flow reactor and found a normal apparent kinetic isotope effect of 1.3 – 1.4, by which the rate controlling step was observed to be decomposition of formate C-H/C-D by Diffuse

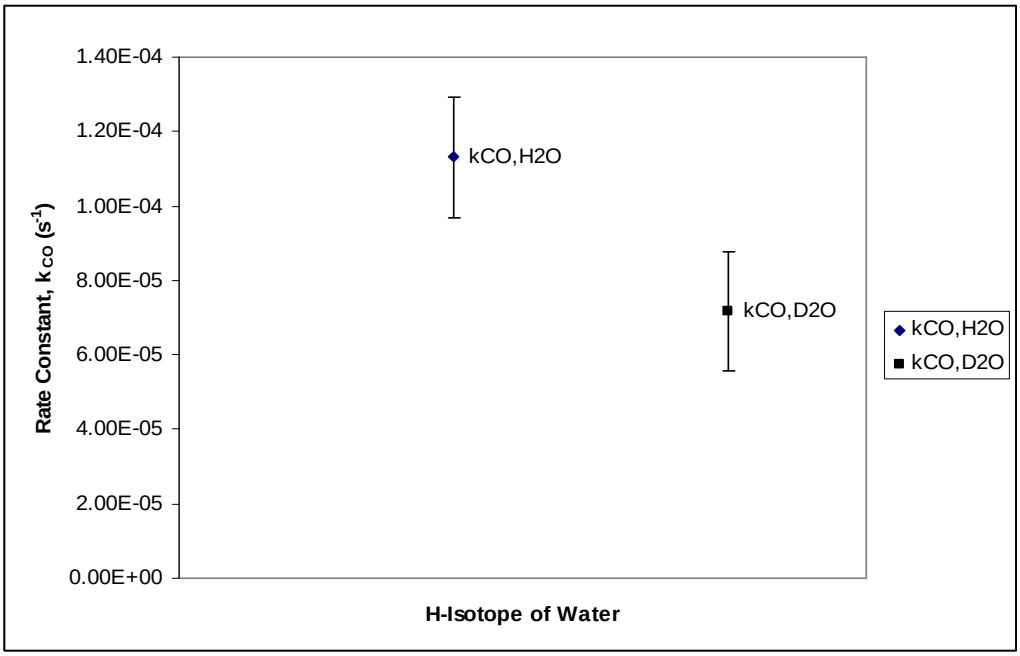

Figure 4.5.1.1: Measured pseudo-first order rate constants for k_{CO} under H_2O and D_2O at a 90% Confidence Interval ($CO/H(D)_2O/H_2S$, 600 psig, 15 psi H_2S, 4.0°C/min, 340 °C for 3 hrs, 10 ml Water, 100 ml n-Octane, 28.9 mmol Naphthalene, 0.39 mmole Mo, 1500 rpm impeller speed)

Reflectance Infrared Fourier Transform Spectroscopy (DRIFTS) (Jacobs et al. 2004). Similar values of k_H/k_D were found by comparing the apparent kinetic isotope effects of deuterated formate decomposition with WGS rate using CO/D_2O. Jacobs et al. observed an apparent correlation between the intensity of the C-H(D) bond vibration through IR spectroscopy and WGS conversion over Pt/CeO_2 catalysts and concluded formate decomposition was the rate determining step over this catalyst (Jacobs et al. 2004). Meunier et al. utilized a custom-built DRIFTS cell that eliminated complications due to cell dead-volumes and residence times which they used to quantify rates of ^{13}CO exchange to differentiate between carbonate and formate decomposition (Meunier et al. 2007). Analysis of their data suggested that formate formation was much slower than CO_2

formation and concluded that formate could not be a significant pathway over a $Au/LaCeO_2$ WGS catalyst. Kim and Iglesia isotopically assessed the kinetics of CH_3OH-H_2O reforming reactions over supported Cu catalysts (Kim 2008). Reaction rates were measured for various deuterated mixtures. The kinetic isotope effect (KIE) of CH_3OH/CD_3OH was 2.6 versus 1.5 for CH_3OH/CH_3OD. They concluded C-H bond activation leading to methoxide decomposition was irreversible and kinetically significant while for hydroxyl dissociation the measured rates represented a thermodynamic isotope effect due to quasi-equilibrium on the surface (Kim 2008). Other studies noted similar effects of 2.5 – 4.0 were measured for the methyl C-H activation during methanol dehydrogenation (Kim 2008). A (C-H)/(C-D) KIE of 2.9 was reported for formic acid decomposition over Cu(110) at 460 K (Madix 1992). The measured isotope effect of 1.58 over MoS_2 prepared from PMA is close to the isotope effects measured by DRIFTS from Jacobs et al. and Shido and Iwasawa (Shido 1993; Jacobs et al. 2004). However, these isotope effects are very similar to the hydroxyl dissociation pseudo-equilibrium effect determined by Kim and Iglesia (Kim 2008) and may indicate that a single rate determining step in the DRIFTS reactor studies was not dominant. Gines et al. suggested for the reverse water gas shift over Cu that under different ratios of P_{H2}/P_{CO2} a different limiting step was operative (Gines et al. 1997). Under batch conditions the concentration of surface species may be transient since the ratio $\frac{P_{CO}P_{H2O}}{P_{H2}P_{CO2}}$ changes as the reaction proceeds. Therefore, any kinetically rate limiting steps may be masked by side reactions or a change in relevant surface mechanism.

During water gas shift in a hydrocarbon emulsion, Milad et al. found that an increase in catalyst concentration and water content led to greater CO_2 absorption

(compared to H_2) in the liquid phase (Milad 1994). Increased gas absorption occurs in liquids with dispersed solids and this could indicate that CO_2 is more strongly adsorbed to the MoS_2 surface than H_2 (Milad 1994). However, CO_2 is also more soluble in water than CO. Strong adsorption of CO_2 on the catalyst surface may also contribute to throttling the rate of water gas shift. A detailed kinetic and spectroscopic analysis could be performed to determine if desorption or chemical reaction is rate limiting.

4. 6 In-situ DRIFTS of MoS_2 from thermal decomposition of ATTM and hydrothermally sulfided PMA

Adsorption of CO and H_2 may result in a competitive relationship between WGS and HYD. Diffuse Reflectance Infrared Fourier Transform Spectrsocopy (DRIFTS) was performed to probe CO adsorption on unsupported MoS_2.

4.6. 1 Thermal Decomposition of ATTM under vacuum

$(NH_4)_2MoS_4$ (ATTM) was thermally decomposed in the DRIFTS cell under vacuum at 300 °C according to the procedure utilized by Tsganenko et al. (Tsyganenko et al. 2004). The decomposition of ATTM to MoS_2 occurs via MoS_3 and liberates ammonia; formation of MoS_2 occurs at 573 K (300 °C) (Tsyganenko et al. 2004). During decomposition under high vacuum NH_3, H_2S and sulfur are evacuated from the cell as they are generated (Tsyganenko et al. 2004).

$$(NH_4)_2MoS_4 \rightarrow 2NH_3 + H_2S + MoS_3 \rightarrow MoS_2 + S$$

The DRIFTS spectrum of decomposed ATTM at 300 °C under vacuum is shown (Figure 4.6.1.1). Absorptivity changes in the powdered sample may be reflected by broad changes in absorbance over large wavenumber regions, while molecular absorption features may appear better resolved with defined, sharp absorbances. Two broad absorptions between 2800 – 3000 appear in the spectrum which is within the absorption region indicative of C-H stretching, but no carbon source should be present. S-H absorptions occur between 2400 – 2700 cm^{-1} below the range of these features. Figure 4.6.1.1 is included as a reference spectrum for the adsorption studies.

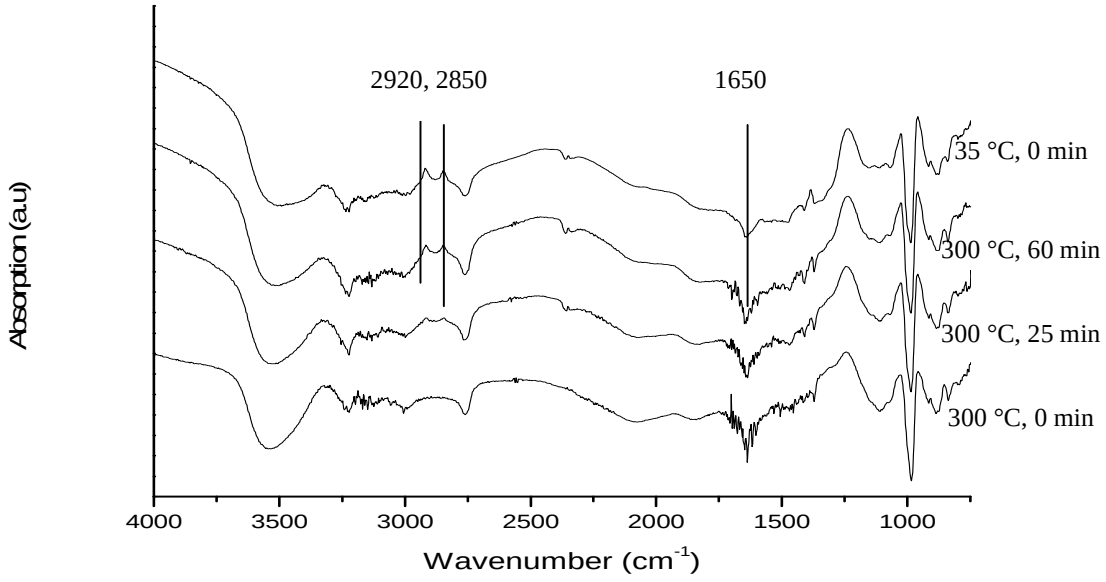

Figure 4.6.1.1: DRIFTS Spectrum of ATTM thermally decomposed under vacuum at 300 °C (300 °C at 0 minutes; 300 °C at 25 min; 300 °C at 60 minutes; 35 °C) (background from ATTM under N_2 at room temperature subtracted)

4.6. 2 CO adsorption onto MoS_2 prepared from thermal decomposition of ATTM

MoS_2 prepared from decomposition of ATTM was heated to 300 °C and subsequently exposed to a 9.94% CO/He flow. After confirming the presence of CO gas (2170 and 2143 cm^{-1}) in the cell via DRIFTS, the cell was isolated. The recorded spectra at increasing time are shown in Figure 4.6.2.1. Exposure to CO at 300 °C results in adsorbed CO, with sharp vibrational absorptions occurring at 2070 cm^{-1} and a slightly broader less intense absorption at 2052 cm^{-1} (Figure 4.6.2.1). The observed values agree well with literature data for bulk MoS_2 (Table 4.6.2.1). For supported catalysts the most intense υ_{CO} absorption occurs at higher wavenumbers (2157 cm^{-1}) and corresponds

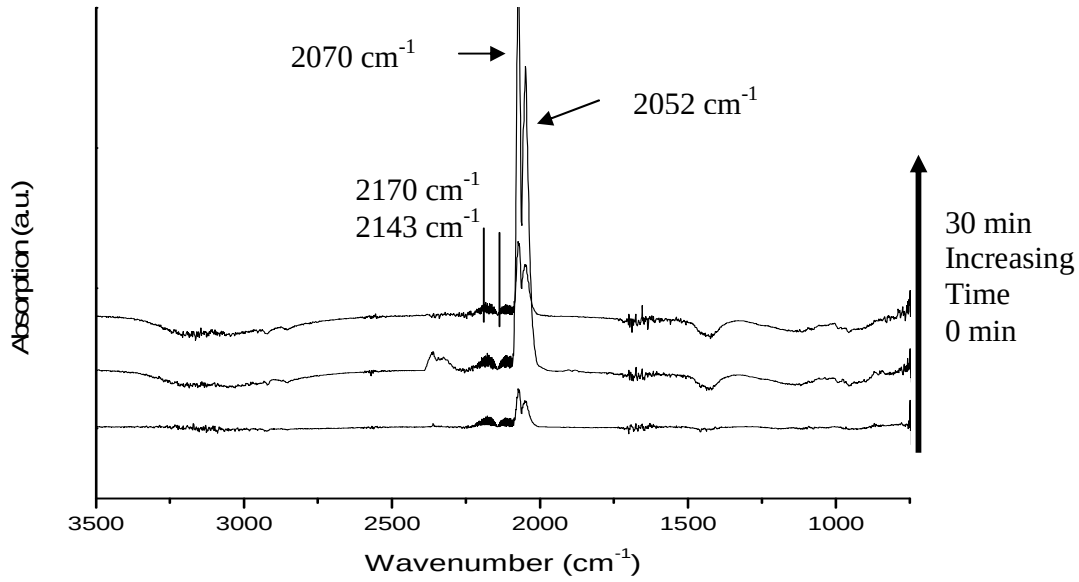

Figure 4.6.2.1: DRIFTS Spectra of MoS_2 from ATTM reduced at 300 °C under CO (0 min; 15 min; 30 min) (background spectrum at 300 °C subtracted)

to increased acidity due to support interactions resulting in less back-donation of electrons from metal to CO (Mauge et al. 2001). In contrast, for unsupported MoS_2 the most intense absorption occurs around 2070 – 2060 cm^{-1} (Mauge et al. 2001). Interestingly, CO adsorption at lower wavenumbers (2050 – 2060 cm^{-1}) appears as a shoulder in the low temperature spectrum but is better resolved at higher temperatures (Mauge et al. 2001; Sarbak 2005). CO adsorption at decreasing wavenumbers indicates adsorption to more reduced coordinatively unsaturated sites (CUS). The different vibration bands of CO may

Table 4.6.2. 1: Vibrational Frequencies of CO, CO_2 and COS over unsupported and supported MoS_2

Conditions	***CO (cm^{-1})***	***CO_2 (cm^{-1})***	***COS***
Gas	*2170, 2143*	*2352* *1337* *649*	*2062* *859* *520*
100 K *Adsorbed on MoS_2 from thiomolybdate prepared in-situ* (Tsyganenko et al. 2004, 189-197)	*2165, 2135* *(physisorbed) 2100*	*2326*	*2038* *854*
100 K *Adsorbed on MoS_2 from thiomolybdate prepared ex situ (H_2/H_2S)* (Mauge et al. 2001, 271-284)	*2157, 2134, 2086, 2070*	*2331 (high coverage)* *2326 (low coverage)*	*2032* *857*
77K Sulfided-Mo/Al_2O_3, reduced in H_2 (473 K) (Muller et al. 1993, 9028-9033)	*2190, 2154, 2110, 2060*		
373 K Sulfided Mo/Al_2O_3 (Sarbak 2005, 263-270)	*2174, 2105, 2072, 2051*		
613 K sulfided-Mo/Al_2O_3 under CO hydrogenation (Koizumi et al. 2004, 173-182)	*2095, 2065, 2010*		
Adsorbed on MoS_2 prepared from Phophomolybdic acid	*2070, 2052*	*2362, 2330*	*2052, 833?*
MoS_2 prepared in DRIFTS cell from ATTM at 300 °C	*2070, 2052*		

represent coordination to Mo in various reduced states; Scheme 4.6.2.1 illustrates possible adsorption scenarioes to explain the observed vibrational spectrum. MoS_2 reduction under CO produces similar sulfur vacancies as reduction under H_2 as seen by the similarity of

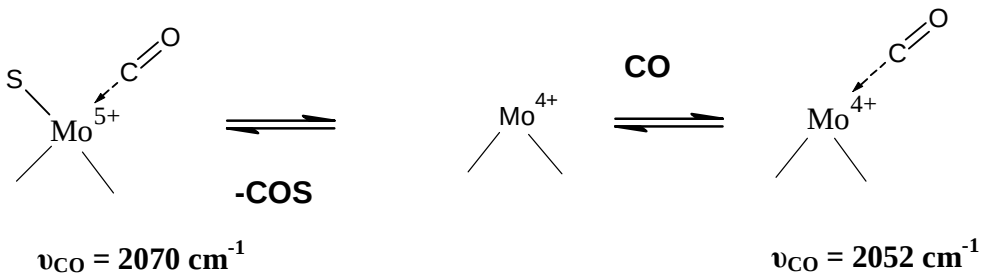

Scheme 4.6.2. 1: Possible multiple adsorption scenario for CO on MoS_2

the adsorbed CO vibrational bands (Mauge et al. 2001; Sarbak 2005). Although the band at 2052 cm^{-1} is near one of the vibrational bands of gas phase COS (2062 cm^{-1}), it is likely due to an adsorbed species since,

i) no corresponding C-S vibrational absorption is at 859 cm^{-1} is observed, and

ii) the vibration band at high temperature is rather sharp and well-resolved unlike gas phase molecular vibrations (cf. gas phase CO at 2170 cm^{-1} and 2143 cm^{-1}).

iii) although COS is present in the system it occurs at a small concentration not justified by the intensity of the 2052 cm^{-1} vibrational band

The intensity of the 2070 cm^{-1} band is greater than that for the band at 2052 cm^{-1}.

After activation at 300 °C, a gas sample was collected from the DRIFTS chamber and analyzed via GC-TCD to determine the composition of the gas mixture. The compositions are reported in Table 4.6.2.2. As can be noted, COS is present in minor amounts with no detectable H_2S. This suggests that a surface reaction occurs with CO analogous to that with H_2, for instance,

$$* S + CO \Leftrightarrow COS + *$$

From DRIFTS, υ_{CO} at 340 °C under CO is similar to υ_{CO} reported in literature observed during low-temperature FT-IR of unsupported MoS_2 activated under H_2 (Mauge et al. 2001). Reduction of MoS_2 under CO produces COS and sulfur vacancies, which from CO adsorption studies have similar characteristics as sulfur vacancies formed under H_2.

Table 4.6.2. 2: Gas Analysis from DRIFTS Experiments, CO reduction of MoS_2 prepared from ATTM

Molecular Species	Mol %, External Standard, 240 °C	Mol %, External Standard, 300 °C
He	77.88	77.78
H_2	0	0
O_2	1.62482	2.17463
N_2	13.3502	14.31849
CH_4	0	0
CO	5.69671	1.96038
CO_2	0	0
COS	1.43966	3.76344
H_2S	0	0
Total	100	100

Using TPR, Jacobsen et al. measured the temperature of H_2 evolution from sulfided catalysts and suggested this method could be utilized to determine metal-sulfur bond strength (Jacobsen et al. 1999). Activity tests of HDS, HDN and HYD correlated with the order of metal-sulfur bond strength proposed earlier by Pecoraro and Chianelli (Pecoraro 1981),

$$RuS_2 < ReS_2 < MoS_2 < NbS_2 \sim Co_9S_8$$

Sulfur-oxygen exchange involving Mo vacancies on sulfided-Mo/Al_2O_3 have also been suggested to be important in the WGS reaction (Hou et al. 1983). In the case of WGS, the metal-oxygen bond strength in addition to the metal-sulfur bond strength may be important; this may explain why molybdenum sulfides show appreciable water gas shift activity. Comparison of the metal-oxygen bond strength perhaps using temperature-programmed sulfidation for the metal series above may highlight which metal sulfides would be suitable as WGS catalysts.

Under conditions of WGS, water is present as a reagent on the catalyst surface. Water was exposed to MoS_2 prepared from thermal decomposition of ATTM which was then exposed to (9.94 vol% CO)/He and heated from room temperature to 340 °C. Adsorption of CO similar to a dry catalyst occurs, with some formation of CO_2 possibly from WGS. For WGS to occur, CO must liberate surface S and form COS to produce sulfur vacancies allowing another CO molecule to adsorb. The sulfur vacancies or coordinatively unsaturated sites are similar regardless of the reductant. If WGS is activity is desired, CO can substitute for H_2 during catalyst activation to form sulfur vacancies.

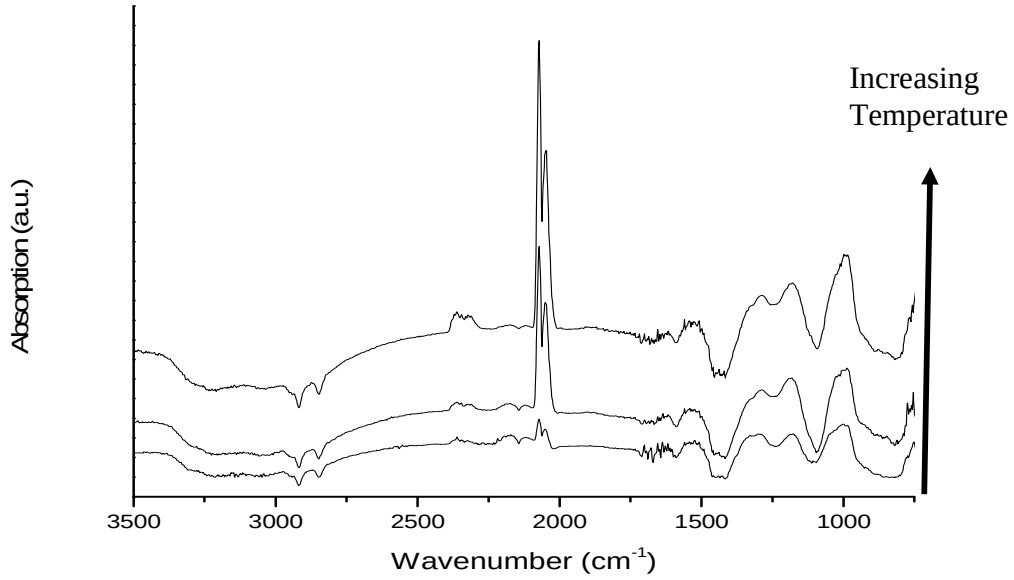

Figure 4.6.2.2: CO adsorption on MoS_2 from ATTM exposed to H_2O before treatment (240 °C, 280 °C, 340 °C)

4.6. 3 CO adsorption onto MoS_2 prepared from sulfided-PMA under $CO/H_2O/H_2S$

The spectrum of MoS_2 prepared from WGS and reduced under CO displays some notable features (Figure 4.6.3.1). Upon heating significant changes are seen between 750 – 1800 cm^{-1}. The growth of bands in this region may be due to changes of surface species such as carbon sulfides or carbon oxysulfides such as xanthates (-OC(S)S-) which absorb strongly in the 1000 – 1200 cm^{-1} region (Little 1966). The catalyst prepared in-situ during reaction

likely contain residual adsorbed surface species. XPS data from an earlier study of a catalyst sample prepared under similar conditions indicate that in addition to

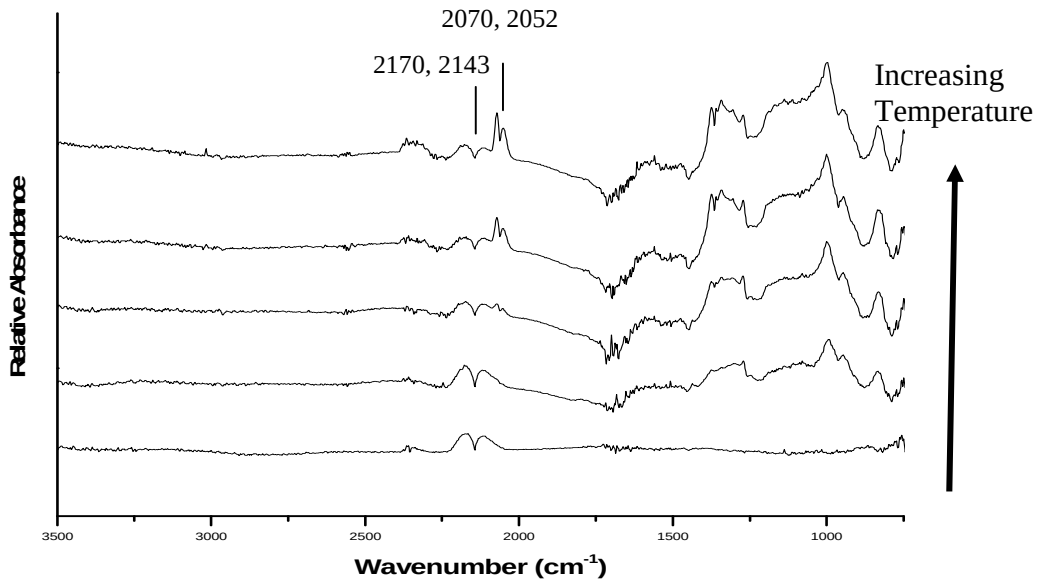

Figure 4.6.3.1: DRIFTS Spectrum – Reduction of MoS_2 (9.94% CO/He) at increasing temperature(80-240 °C, ΔT = 40 °C) on MoS_2 prepared ex-situ from PMA; PMA preparation conditions: 600 psig, 180 psi H_2S, 4.0°C/min, 340 °C for 2 hrs, 25 ml Water, 100 ml toluene, 4.09 g hydrated PMA, 1500 rpm impeller speed

Mo, S and O, appreciable amounts of C exist on the surface (Lee 2004). A sharp absorption occurring at 834 cm^{-1} occurs in the region for C-S or C-O stretching or surface carbonate. A series of broad vibrational absorptions occurring between 1250 – 1400 cm^{-1} could be due to various O-C-O vibrations on the catalyst surface. The DRIFTS spectrum for MoS_2 formed ex-situ from PMA may be more complex than for MoS_2 formed from ATTM due to residual surface contamination of C and O from reaction conditions.

Upon heating above 160 °C, gas phase CO bands (2170 cm^{-1} and 2143 cm^{-1}) decrease and new bands appear at 2070 and 2052 cm^{-1} (Figure 4.6.3.2), ascribed to adsorbed CO on unsupported MoS_2 (Mauge et al. 2001). Appearance of minor amounts of CO_2 (2352, 2330 cm^{-1}) may be due to strong adsorption of residual CO_2. The adsorbed CO is stable at room temperature under a sealed atmosphere as seen from the IR spectrum recorded after cooling (Figure 4.6.3.2). Upon flushing with N_2 to remove gas phase and weakly adsorbed species, CO_2 (2352, 2330 cm^{-1}), gas phase CO (2170, 2143 cm^{-1}) and adsorbed CO (2070, 2052 cm^{-1}) disappear. Adsorbed CO is not very stable under flow conditions at room temperature and is markedly reduced even after 5 minutes of flushing. The inverted CO_2 band after 20 minutes flushing may be due to desorption of CO_2 initially present and adsorbed on the MoS_2 surface. Gas phase CH_4 can be seen from the low intensity vibrational absorption at 3020 cm^{-1} (Figure 4.6.3.2). CO adsorption to sulfur vacancies begins at 160 °C with adsorption relatively stable under non-flow conditions when cooled to room temperature.

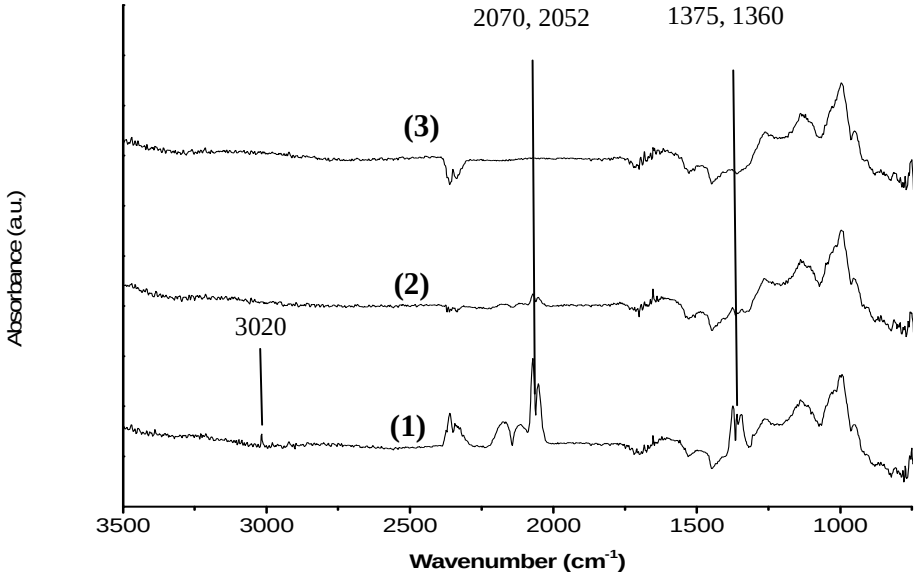

Figure 4.6.3.2: DRIFTS Spectrum after MoS_2 reduction in CO/He Adsorbed CO at 22 °C (1); flushing with N_2 for 5 minutes (2); flushing with N_2 for 20 minutes (3) on MoS_2 prepared ex-situ from PMA*; *(600 psig, 180 psi H_2S, 4.0°C/min, 340 °C for 2 hrs, 25 ml Water, 100 ml toluene, 4.09 g hydrated PMA, 1500 rpm impeller speed)

4. 7 Comparison of Experimentally adsorbed CO to Theoretical Studies

The heterogeneity of the MoS_xO_y surface of MoS_2 sulfided from PMA under reaction conditions complicates the spectroscopic interpretation due to residual reaction species.

Recent DFT studies have calculated theoretical vibrational frequencies for CO adsorbed to different MoS_2 vacancies. The vibrational bands at 2070 and 2052 cm^{-1} may represent CO adsorption on different sites of the MoS_2 particles. Theoretical calculations for υ_{CO} adsorption on triangular and hexagonal MoS_2 nanoclusters were performed by Zeng et al. (Zeng et al. 2005; Zeng et al. 2005) For triangular and hexagonal clusters, υ_{CO}

on Mo corner sites was 2049 and 2045 cm^{-1}, respectively. υ_{CO} on edge sites was 2075 cm^{-1} for triangular clusters and 2080 cm^{-1} for hexagonal clusters, which are quite close to our observed bands at 2070 and 2052 cm^{-1}. MoS_2 particles produced in-situ from PMA match literature dimension for hexagonal clusters as measured by HR-TEM (Liu 2008). However, the DFT calculations were performed for single clusters of pure MoS_2; an unsupported catalyst that has undergone WGS is likely slightly oxidized with surface carbon and oxygen. Actual unsupported catalysts consist of stacked layers of MoS_2 as revealed by HR-TEM (Eijsbouts et al. 2007). Comparison between theoretical calculations and the experimental results though not conclusive suggest our υ_{CO} experimental assignments are reasonable. If these vibrational bands are indicative of CO adsorption to corner and edge sites, this may allow a rough semi-quantitative estimate of the ratio of sulfur vacancies on edge Mo to corner Mo by comparison with diffuse reflectance signal intensities. In addition, the ratio of absorbance intensity of CO at 2070 compared with 2052 cm^{-1} appears constant, indicating an equilibrium type relationship between these sites, which could be due to MoS_2 cluster morphology. Whether MoS_2 is reduced under H_2 or CO, the wavenumber of adsorbed CO does not change indicating that similar coordinatively unsaturated sites (cus) are formed (Mauge et al. 2001; Sarbak 2005).

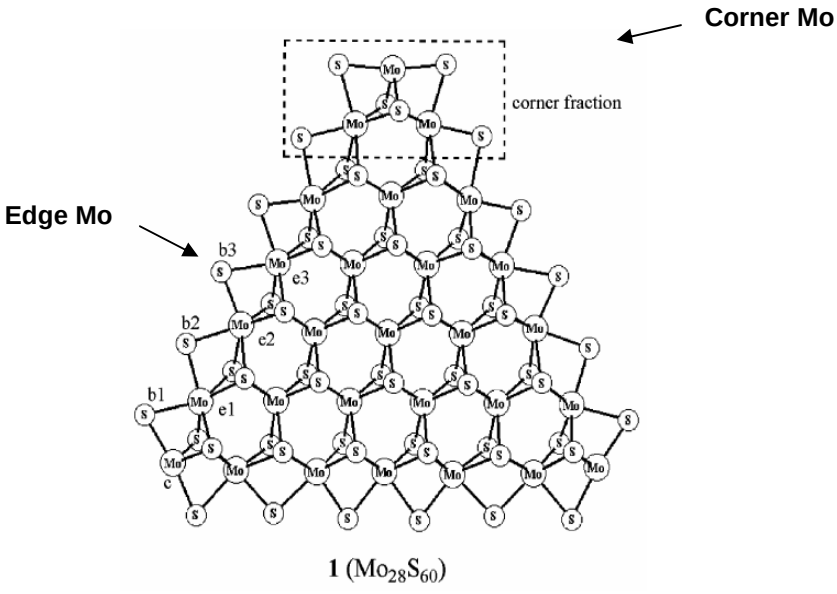

Figure 4.7.1: Triangular Nano-cluster of MoS_2. Reprinted with permission from Zeng et al. (Zeng et al. 2005) . Copyright 2005 American Chemical Society.

4. 8 Conclusion

Exchange of protons between aromatic species and water is accelerated in reducing (CO, H_2) atmospheres versus N_2 where sites of exchange may be related to sulfur vacancies on Mo. Comparison of the hydrogenation and exchange indices (HI and EI) for $CO/D_2O/H_2S$ indicates that exchange reactions incorporate deuterium to a greater extent than hydrogenation. The exchange mechanism may involve dissociation of H_2O and aromatic hydrogen; this dissociated hydrogen may help prevent coke formation during bitumen upgrading by terminating organic radicals and preventing condensation into solids.

The water gas shift rate was not inhibited by aromatic species (toluene) but rather was faster compared to n-octane/water. Under n-octane, the highest rate of hydrogenation occurred with H_2/H_2O, in contrast to results reported under toluene/water (Abusaido 1999). Comparing the WGS rate in H_2O versus D_2O, the measured apparent normal

kinetic isotope effect of 1.58 is similar to a quasi-equilibrium thermodynamic isotope effect reported for hydroxyl group dissociation. KIE for C-H bond activations are closer to 2.5-4.0. This suggests under batch conditions the kinetic rate determining step may be masked by side reactions or a change in the kinetically limiting step due to transient reactant concentrations. Naphthalene hydrogenation is favoured over CO hydrogenation as observed by the significant conversion to tetralin relative to the trace concentrations of CH_4 detected from TCD-GC analysis during batch autoclave experiments. Fu et al. observed a similar occurrence during hydrogenation of phenanthrene via water gas shift (Fu et al. 1995).

Adsorption of CO on the MoS_2 catalyst begins at 160 °C. Whether the formation of sulfur vacancies or the adsorption of CO is the key step may be probed using temperature-programmed catalyst studies. CO can substitute for H_2 as a reducing agent by forming COS and producing sulfur vacancies which are believed to be active sites for hydrodesulfurization and hydrogenation. The substitution of CO for H_2 would be preferred to remove water from bitumen emulsions while producing hydrogen via the WGS.

4. 9 Recommendations

Temperature Programmed Reduction (TPR) and desorption (TPD) with CO could be performed to determine surface coverage and bond strength of adsorbed CO or COS. This may allow comparison of the bond strengths (TPR temperature) between not only CO and H_2 adsorption, but also between different CO adsorptive modes. Quantification of the υ_{CO}

vibrational bands at 2070 cm^{-1} and 2052 cm^{-1} during temperature programmed DRIFTS studies may elucidate further details about the nature of each adsorption mode. The degree of sulfidation of catalyst may also affect CO adsorption. Comparison of D_2O and H_2O in DRIFTS studies of WGS over MoS_2 may also help identify possible surface intermediates, but this should be performed in a flow type DRIFTS reaction cell to avoid masking of kinetically relevant steps during batch reaction conditions.

Chapter 5: Ruthenium, Iron and Vanadium with MoS_2

5. 1 Introduction

One of the main goals in developing better upgrading catalysts is to increase the hydrogenation activity of catalysts in oil/water emulsions, especially to improve their activity in water. An alternative to this theme could be to improve and exploit a high WGS activity which would rapidly decrease the water concentration while increasing the availability of hydrogen.

Ru from two precursors, ruthenium (III) acetylacetonate ($Ru(C_5H_7O_2)_3$, where $C_5H_7O_2$ = acac) and ruthenium (0) carbonyl ($Ru_3(CO)_{12}$) were sulfided in-situ and tested for their water gas shift and hydrogenation activity with naphthalene in a toluene/water emulsion. Additional experiments were performed to determine the promoting ability of Ru on Mo. In these experiments the total molar concentration (Ru + Mo) was held constant while the Ru atomic fraction, r ,was varied where r,

$$r = \frac{Ru}{Mo + Ru}$$

Fe and V with Mo and V with NiMo were tested to determine their activity for water gas shift and in-situ hydrogenation of naphthalene using $FeSO_4$ and $VO(acac)_2$ as precursors in toluene/water. $FeSO_4$ was chosen because it is cheap while an organic soluble VO precursor was chosen to model chelated vanadyl porphyrins found in bitumen (Semple et al. 1990). The results are compared to reactions using only Mo from PMA.

The concentration of Mo (1.16 mmole) remained the same in all experiments while the total metal concentration was varied by addition of Fe, Ni or V precursors (0.70 mmole each). The additive concentrations were chosen according to the optimal Ni:Mo ratio of 0.6 determined for an unsupported, dispersed Mo catalyst (Zhang 2005). This was done to determine the feasibility of metals deposition from asphaltenes during bitumen upgrading versus comparison to the base case of Mo catalyst only.

5. 2 Activity of $Ru_3(CO)_{12}$ and $Ru(C_5H_{10}O_2)_3$ in Water Gas Shift and Naphthalene Hydrogenation

5.2. 1 Water Gas Shift and Conversion of CO under Ru

Comparison of $Ru_3(CO)_{12}$ and phosphomolybdic acid (PMA) under $CO/H_2O/H_2S$ indicates conversion of CO at similar reaction times is higher for Mo than Ru (Figure 5.2.1.1). $Ru_3(CO)_{12}$ is known to catalyze the water gas shift very rapidly , therefore the presence of sulfur might be inhibiting. The pseudo-first order rate constant for $Ru_3(CO)_{12}$ (2.71×10^{-3} min^{-1}) is lower than for MoS_2 (5.58×10^{-3} min^{-1}, sulfided from PMA) at 340 °C. In addition, it is quite evident that the initial CO mol% for PMA is much lower than for $Ru_3(CO)_{12}$, 33.5 mol% versus 76.9 mol% respectively. For reference, the blank "wall effect" rate constants are reported in Table D.2, Appendix D (Experiment #30). The wall effect is considered constant and therefore any difference in kinetics between Ru and Mo would reflect differences in catalyst activity.

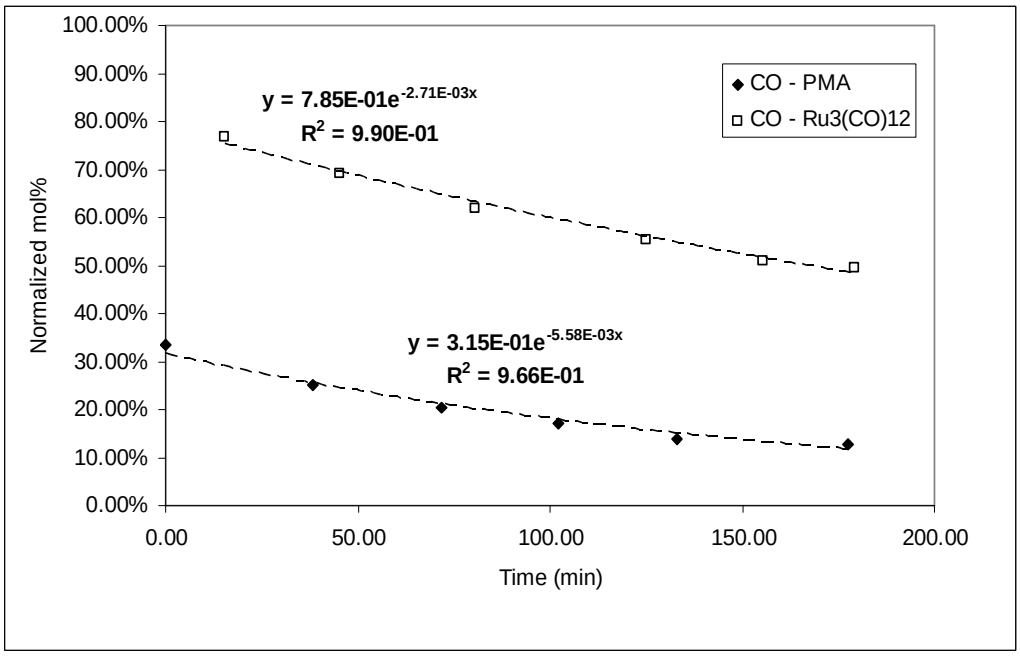

Figure 5.2.1. 1: Mol% of CO under $Ru_3(CO)_{12}$ (Experiment #33) and Phosphomolybdic Acid (Experiment #32) ($CO/H_2O/H_2S$, 600 psig, 15 psi H_2S, 3.0°C/min, 340 °C for 3 hrs, 10 ml H_2O, 100 ml toluene, 35.1 mmol NAPH, 0.47 mmole Mo, 1500 rpm impeller speed)

5.2. 2 Naphthalene Hydrogenation to Tetralin catalyzed by Ru3(CO)12 and Ru(acac)3 under CO/H2O/H2S

Plots of naphthalene concentration versus reaction time at 340 °C are shown in Figure 5.2.2.1. Note that hydrogenation conditions for PMA and $Ru_3(CO)_{12}$ are for initial loading of $CO/H_2O/H_2S$. $Ru(acac)_3$ showed negligible WGS activity, therefore naphthalene hydrogenation was tested separately under $H_2/H_2O/H_2S$. PMA under $CO/H_2O/H_2S$ displays the best rate of conversion for naphthalene. $Ru_3(CO)_{12}$ displays no activity for hydrogenation, while $Ru(acac)_3$ under molecular hydrogen does have some catalytic behaviour but still lags the activity of in-situ hydrogen catalyzed by PMA (Figure

5.2.2.1.). This is surprising since Ru sulfided in N_2/H_2S at 400 °C is known to have a higher activity than Mo for hydrogenation (Geantet et al. 1991). The poor hydrogenation performance observed with the Ru unsupported catalyst prepared from both the Ru^0 carbonyl and Ru^{3+} acetylacetonate precursors (red toluene solutions) may be due to incomplete sulfidation of Ru at 340 °C (613 K) as indicated by the reddish hue of collected liquid samples. The reddish colour did not disappear until after 90 minutes of reaction time. The low H_2S concentration (15 psi), low temperature (340 °C) and presence of hydrogen formed during WGS may favour reduction of Ru rather than formation of active RuS_2 phases. The absence of orange ($Ru_3(CO)_{12}$) or red-brown

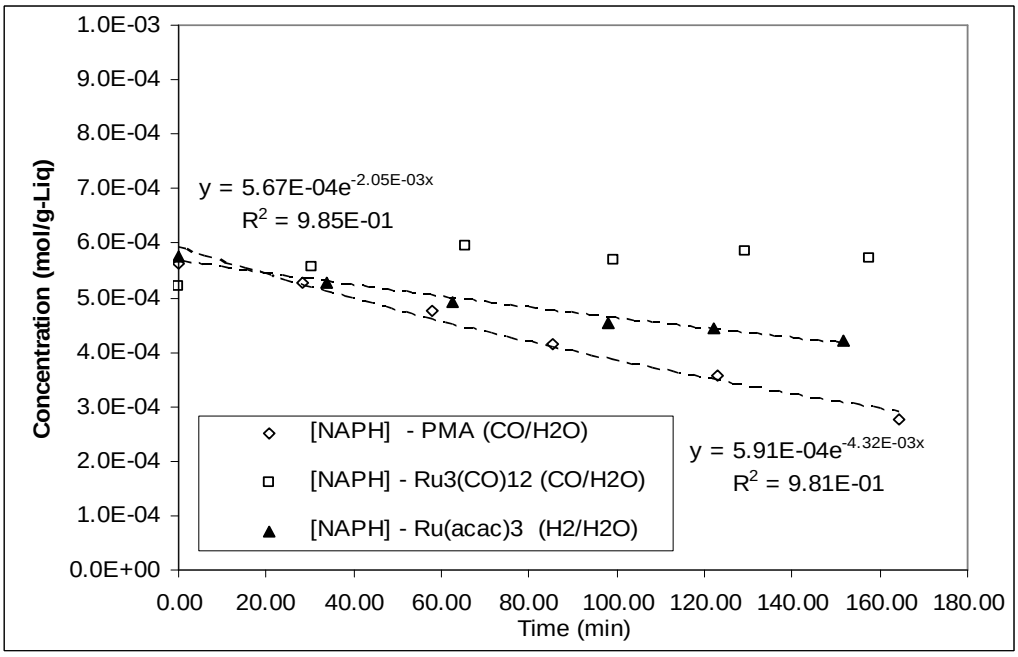

Figure 5.2.2. 1: Naphthalene Concentration during Hydrogenation with $Ru_3(CO)_{12}$ (Experiment #33), $Ru(acac)_3$ (Experiment #34) and PMA (Experiment #32) (600 psig, 15 psi H_2S, 3.0°C/min, 340 °C for 3 hrs, 10 ml H_2O, 100 ml toluene, 35.1 mmol NAPH, 0.47 mmole Mo, 1500 rpm impeller speed)

($Ru(acac)_3$) colour in the collected end product (120 minutes) and the presence of black solids may indicate transformation to sulfides or oxysulfides by the end of reaction; nonetheless the WGS and hydrogenation activity of Ru prepared from $Ru_3(CO)_{12}$ and $Ru(acac)_3$ precursors is negligible compared to PMA.

5. 3 Activity of $Ru(C_5H_{10}O_2)_3$ with Phosphomolybdic Acid for water gas shift and naphthalene hydrogenation in toluene/water emulsions

5.3. 1 Introduction

Following the poor ability of $Ru_3(CO)_{12}$ and $Ru(acac)_3$ to independently catalyze water gas shift and naphthalene hydrogenation compared to PMA (possibly due to difficulty in forming active RuS_2), it was decided to test the activity of RuMo sulfides by utilizing $Ru(acac)_3$ and PMA simultaneously. An r value of 0.25 was chosen as this ratio exhibited the highest hydrogenation activity for RuMo when sulfided in N_2/H_2S (Geantet et al. 1991), where r,

$$r = \frac{Ru}{Mo + Ru}$$

5.3. 2 Water Gas Shift for Ru-doped Mo sulfide catalysts

Gas phase compositions for the reference experiment performed using PMA at 1500 ppm Mo (1.16 mmole) are shown in Figure 5.3.2.1, while the run with Ru promotion at r = 0.25 is shown in Figure 5.3.2.2. It can be seen that the conversion of CO via water gas shift is much faster in the Mo system (Figure 5.3.2.1) than the binary RuMo system (Figure 5.3.2.2) at 340 °C. At the beginning of reaction time, the CO concentration is less than 10 mol% for Mo while for RuMo the CO concentration is 36 mol%. Irreversible pseudo-first order rate constants for CO conversion are shown in Table 5.3.2.1. k_{CO} for RuMo is 1.47 x 10^{-4} s^{-1} compared to 2.05 x 10^{-4} s^{-1} for Mo. Ru added to PMA does not appear to promote WGS.

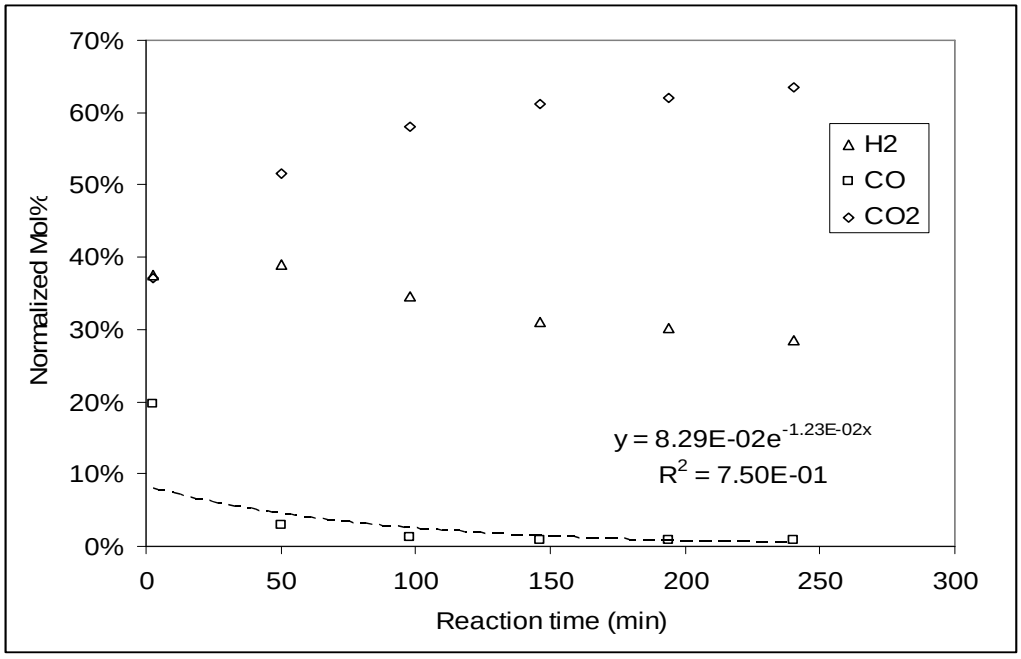

Figure 5.3.2. 1: Gas-phase compositions for Mo (Experiment #10) ($CO/H_2O/H_2S$, 600 psig, 15 psi H_2S, 3.0°C/min, 340 °C for 2 hrs, 18 ml H_2O, 52 ml toluene, 87.1 mmol NAPH, 1.16 mmole Mo, 1500 rpm impeller speed)

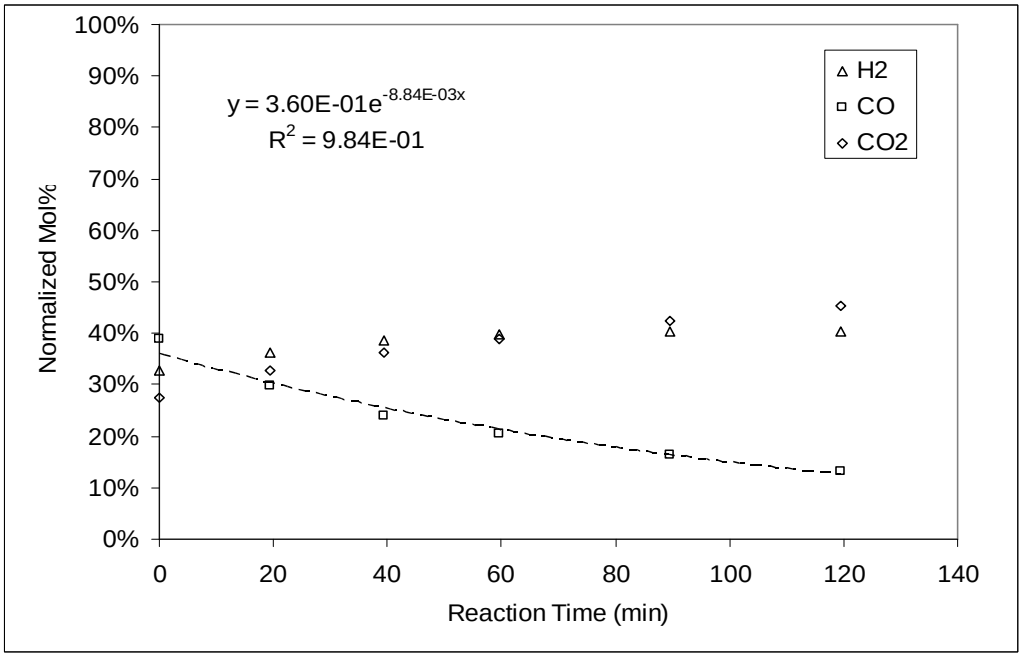

Figure 5.3.2. 2: Gas-phase compositions for RuMo (Experiment #36) ($CO/H_2O/H_2S$, 600 psig, 15 psi H_2S, 3.0°C/min, 340 °C for 2 hrs, 18 ml H_2O, 52 ml toluene, 87.1 mmol NAPH, 0.87 mmole Mo, 0.29 mmole Ru, 1500 rpm impeller speed)

Table 5.3.2. 1: Pseudo-first order Rate Constants for MoS_2 and $RuMoS_2$ catalysts

	Mo (1500 ppm) 4.486 mmol Mo	[B]Experiment #10 Mo (1500 ppm) 1.16 mmol Mo	[A,B] Experiment #36 RuMo (r=0.25) 0.87 mmol Mo 0.29 mmole Ru
k_{CO} (10^{-4} s^{-1})	*3.03 **2.0	2.05 (irrev.) 4.19 (rev.)	1.47
k_{NAPH} (10^{-5} s^{-1})	*8.5 **6.7	11.1	5.47

* (Abusaido 1999)
**(Zhang 2005)
[A] *Ruthenium precursor = Ru(acac)$_3$*

[B]($CO/H_2O/H_2S$, 600 psig, 15 psi H_2S, 3.0°C/min, 340 °C for 2 hrs, 18 ml H_2O, 52 ml toluene, 87.1 mmol NAPH, 1500 rpm impeller speed)

5.3. 3 Naphthalene Hydrogenation to Tetralin for Ru-doped Mo sulfide catalysts

The plot of naphthalene and tetralin concentration versus reaction time at 340 °C is shown in Figures 5.3.3.1 and 5.3.3.2 for Mo and RuMo respectively. Values of k_{NAPH} were shown in Table 5.3.2.1. Clearly the unpromoted Mo system hydrogenates much faster than when the $Ru(acac)_3$ precursor is added to PMA. The slow rate of hydrogenation for the promoted RuMo system may be due to slow sulfidation and reduction of the $Ru(acac)_3$ precursor. The Ru precursor dissolves in the toluene solvent to give a deep red solution; liquid samples did not shed their reddish tinge until approximately 90 minutes of reaction time. Geantet et al. reported that whether a synergistic effect of Ru promotion on Mo is observed depends upon the preparation method such as calcination, balance gas used

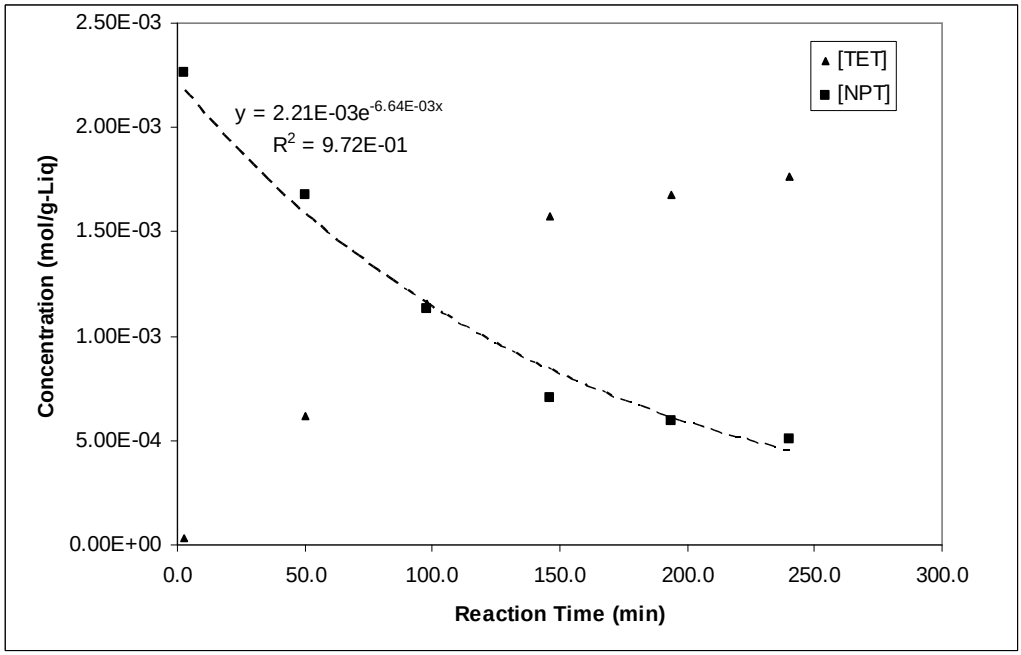

Figure 5.3.3. 1: Organic-Phase Concentrations for Mo catalyst (Experiment #10) ($CO/H_2O/H_2S$, 600 psig, 15 psi H_2S, 3.0°C/min, 340 °C for 2 hrs, 18 ml H_2O, 52 ml toluene, 87.1 mmol NAPH, 1.16 mmole Mo, 1500 rpm impeller speed)

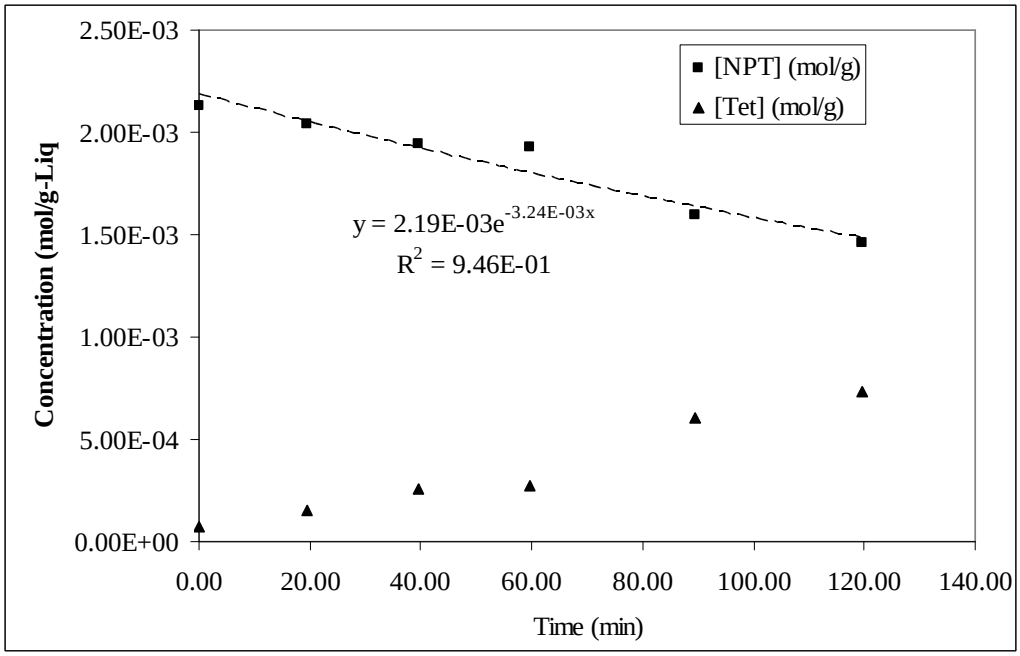

Figure 5.3.3. 2: Organic-Phase Concentrations for RuMo catalyst (Experiment #36) ($CO/H_2O/H_2S$, 600 psig, 15 psi H_2S, 3.0°C/min, 340 °C at 2 hrs, 18 ml H_2O, 52 ml toluene, 87.1 mmol NAPH, 0.87 mmole Mo; 0.29 mmole Ru, 1500 rpm impeller speed)

during catalyst sulfidation (H_2/H_2S versus N_2/H_2S), and sulfidation temperature (Geantet et al. 1991). Impregnation of Mo/Al_2O_3 with Ru (III) acetate yielded poor hydrotreatment performance compared with unpromoted Mo/Al_2O_3 when calcined, but did provide a synergistic effect with no calcination (Mitchell et al. 1987). Geantet et al.studied hydrogenation of biphenyl on $RuMo/Al_2O_3$ (Geantet et al. 1991) and found that the highest activity occurred after sulfidation in N_2/H_2S (15% H_2S) at 673 K. HR-TEM revealed RuS_2 particles were dispersed in close proximity with MoS_2 particles. In contrast to hydrogenation, the hydrodesulfurization activity of RuMo is maximum at higher sulfidation temperatures (873 – 973 K) in N_2/H_2S (15% H_2S), where the sulfide crystallites were more distinctly heterogeneous (Castillo-Villalon et al. 2008). The sulfidation of RuMo catalysts in H_2/H_2S did not give activities as high as those prepared

under N_2/H_2S. Ru sulfided at 673 K forms amorphous RuS_2 with Ru sites that can be reduced and has excellent activity for naphthalene hydrogenation but is not as active for hydrodesulfurization as MoS_2 (Castillo-Villalon et al. 2008). It was reported that sulfidation of Ru precursors at temperatures of 873 - 973 K (15% H_2S) gave a very stable pyrite form of ruthenium sulfide that has excellent hydrodesulfurization capabilities with reduced hydrogenation activity (Castillo-Villalon et al. 2008). Ru is an excellent example where different forms of the metal sulfide are active for different reactions.

MoS_2 may be formed rapidly since at the start of reaction, substantial WGS and some hydrogenation has already occurred. The red hue of the recovered liquid samples remains until approximately 90 minutes reaction time. Active MoS_2 is formed at temperatures below 340 °C as inferred by the significant CO conversion at 340 °C. Since $Ru(acac)_3$ is red in solution, if the disappearance of red indicates sulfidation/reduction of $Ru(acac)_3$ and does not occur until 90 minutes at 340 °C, ruthenium sulfides may deposit as crystallites, possibly covering some active MoS_2 sites. Under the studied conditions (2.5% H_2S, 613 K, CO/H_2O), Ru is not an attractive catalyst or promoter for Mo due to the expense and negligible activity of Ru alone or in conjunction with Mo.

5. 4 FeMo, VMo, NiMo and VNiMo-sulfide unsupported, dispersed catalysts

The promotion effect of Ni for both HDS and hydrogenation has been extensively studied previously and gives a significant increase in catalytic activity with in-situ generated hydrogen compared with unpromoted MoS_2 (Zhang 2005). From an economic perspective, the cost of using Fe is attractive since it could be used in a once-through

process. In addition to Ni, large quantities of V are present in bitumen asphaltenes (Dunn et al. 2003; Miller 1999). If vanadium can be demetallized and sulfided into an active form for hydrogenation and HDS, the active residue could be recycled as catalyst. Bulk vanadium sulfides and Mo-promoted vanadium sulfides have been shown to have good hydrogenation activity but low hydrodesulfurization ability (Lacroix et al. 1992; Hubaut 2007). A water gas shift catalyst such as molybdenum sulfide would be required for in-situ generation of hydrogen. As mentioned previously, Ni is an excellent promoter for hydrogenation when used in conjunction with Mo. Ni is also found in substantial amounts in Athabasca bitumen (Dunn et al. 2003). Under conditions of in-situ upgrading, it may be expected that metals deposition of Ni and V onto dispersed, unsupported catalyst may occur, similar to deposition onto supported hydroprocessing catalysts (Yumoto et al. 1996). However, if sulfidation of PMA occurs simultaneously with Ni and V sulfide formation, this may alter the structure of the final catalyst such that it behaves closer to promoted vanadium sulfide catalysts. Previous work utilizing hydrogen generated in-situ to upgrade bitumen emulsions with an unsupported, dispersed catalyst found that the upgraded liquid had significantly reduced metal concentrations (Moll 1999). It was suggested that the metals were deposited onto the residual solid fraction recovered from the upgrading experiments. Therefore, it is important to determine what effect Ni and V deposition may have on the MoS_2 catalyzed water gas shift and subsequent in-situ hydrogenation of model bitumen compounds. Experiments with Fe, Ni and V as additives to Mo were performed and compared to the base-case of pure Mo (1.16 mmol). In all experiments the concentration of Mo was held constant while the total metal concentration

was varied by addition of Fe, Ni or V precursors. This was performed in order to model the effect of metals deposition from asphaltenes onto the MoS_2 catalyst.

5.4. 1 Naphthalene Hydrogenation activity for sulfided Mo, FeMo, VMo, NiMo and NiVMo Catalysts

The pseudo-first order irreversible rate constants for naphthalene hydrogenation and water gas shift are listed in Table 5.4.1.1 and shown in Figure 5.4.1.1. Blank kinetic reactor "wall effects" are shown in Table D.2, Appendix D (Experiment #12) for comparison.

Table 5.4.1. 1: Pseudo-first order rate constants for NAPH hydrogenation and water gas shift over Mo and Mixed-metal Mo catalysts ($CO/H_2O/H_2S$, 600 psig, 15 psi H_2S, 3.0°C/min, 340 °C for 2 hrs, 18 ml H_2O, 52 ml toluene, 87.1 mmol NAPH, 1.16 mmole Mo, 0.70 mmole each (Fe, V, Ni), 1500 rpm impeller speed)

Binary Catalyst (Run Order)	**k_{NAPH} (x 10^{-5} s^{-1})**	**Irrev. k_{CO} (x 10^{-4} s^{-1})**	**Rev. k_{CO} (x 10^{-4} s^{-1})**
Mo (#40)	18.8	2.05	4.02
MoFe (#37)	6.83	1.41	2.25
MoV (#38)	6.08	2.36	3.03
MoNi (#39)	21.0	1.35	1.61
MoNiV (#41)	13.7	1.73	2.19

The MoS_2 catalyst prepared from PMA gives k_{NAPH} of 18.8 x 10^{-5} s^{-1}. Both Fe and V, each in combination with Mo, inhibit hydrogenation when added to PMA. The Ni promoted catalyst, NiMo sulfide gives the highest hydrogenation activity of 21.0 x 10^{-5} s^{-1} as expected. Mo yields a rate constant of 18.8 x 10^{-5} s^{-1}. The ternary VNiMo-sulfided catalyst activity is impaired (13.7 x 10^{-5} s^{-1}) compared to pure Mo and Ni. The presence of vanadium in VNiMo sulfide decreases naphthalene hydrogenation compared to NiMo

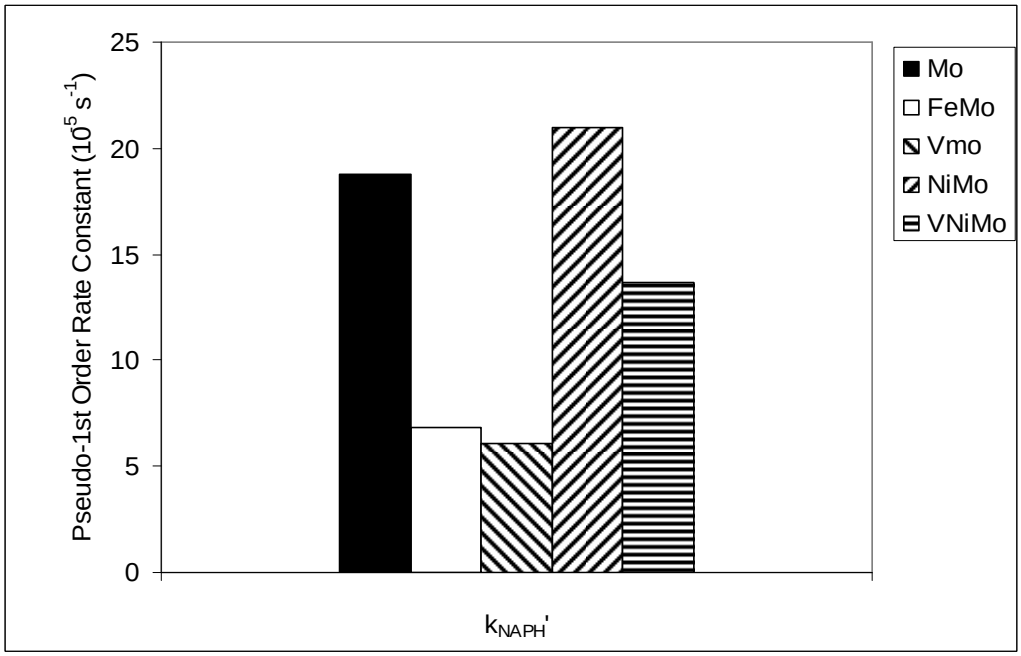

Figure 5.4.1. 1: Pseudo-First Order Rate Constants for Naphthalene Hydrogenation over Mo and Mixed-metal Mo catalysts ($CO/H_2O/H_2S$, 600 psig, 15 psi H_2S, 3.0°C/min, 340 °C for 2 hrs, 18 ml H_2O, 52 ml toluene, 87.1 mmol NAPH, 1.16 mmole Mo, 0.70 mmole each (Fe, V, Ni), 1500 rpm impeller speed)

and the base-case Mo, but the activity is still high relative to Fe and V. The order of the calculated pseudo-first order irreversible hydrogenation rate constants is, k_{NAPH}:

NiMo > Mo > VNiMo > FeMo > VMo

The graph of H_2 mol% supports the high activity of NiMo (Figure 5.4.1.2). The mol% of H_2 is lowest at all reaction times for NiMo which indicates consumption of hydrogen in naphthalene hydrogenation. Table 5.4.1.2 lists the conversion of naphthalene as a function of isothermal reaction time at 340 °C. The order for naphthalene conversion at 120 minutes is

NiMo > Mo > VNiMo > FeMo > VMo

Figure 5.4.1.3 shows the naphthalene conversions for various doped-MoS_2 over the reaction time. NiMo displays the highest activity in hydrogenation in agreement with previous studies (Zhang 2005).

In the hydrogenation of toluene over alumina-supported catalysts, the effect of V was studied by depositing vanadyl octaethylporphyrin onto Mo/Al_2O_3 and $NiMo/Al_2O_3$ (Hubaut 2007). As the percentage of V deposits increased, the activity for a Mo/Al_2O_3

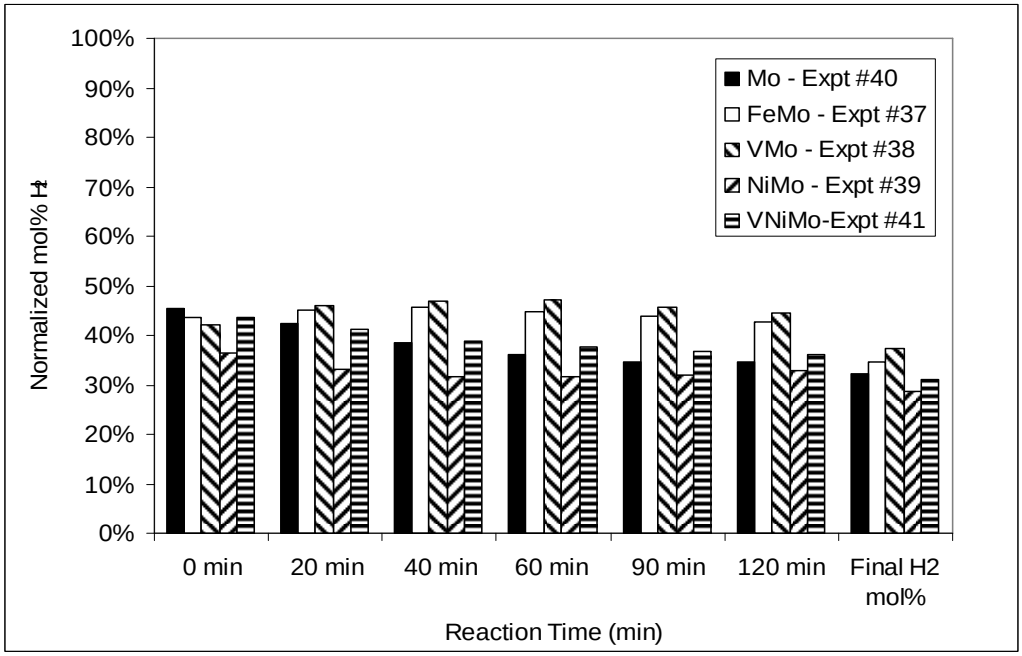

Figure 5.4.1. 2: Normalized H_2 mol% during reaction for various doped-Mo catalysts ($CO/H_2O/H_2S$, 600 psig, 15 psi H_2S, 3.0°C/min, 340 °C for 2 hrs, 18 ml H_2O, 52 ml toluene, 87.1 mmol NAPH, 1.16 mmole Mo, 0.70 mmole each (Fe, V, Ni), 1500 rpm impeller speed)

Table 5.4.1. 2: Naphthalene Conversion at 120 minutes ($CO/H_2O/H_2S$, 600 psig, 15 psi H_2S, 3.0°C/min, 340 °C for 2 hrs, 18 ml H_2O, 52 ml toluene, 87.1 mmol NAPH, 1.16 mmole Mo, 0.70 mmole each (Fe, V, Ni), 1500 rpm impeller speed)

Binary Catalyst	**Naphthalene Conversion at 120 minutes (%)**	**Normalized mol% CO at 120 minutes**
Mo	76.22%	1.97%
MoFe	45.80%	6.09%
MoV	40.10%	3.77%
MoNi	81.3%	5.72%
MoNiV	66.30%	2.85%

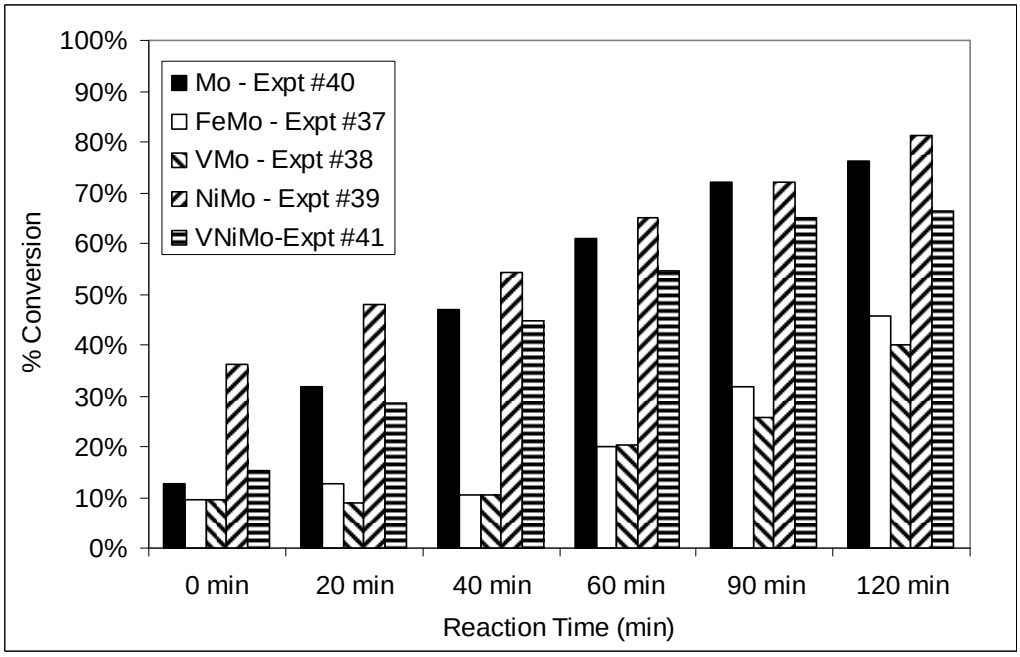

Figure 5.4.1.3: Naphthalene Conversion for FeMo, VMo, NiMo and VNiMo unsupported, dispersed catalysts ($CO/H_2O/H_2S$, 600 psig, 15 psi H_2S, 3.0°C/min, 340 °C for 2 hrs, 18 ml H_2O, 52 ml toluene, 87.1 mmol NAPH, 1.16 mmole Mo, 0.70 mmole each (Fe, V, Ni), 1500 rpm impeller speed)

catalyst increased; the opposite trend was observed for V deposited on $NiMo/Al_2O_3$ (Hubaut 2007). In contrast, catalysts prepared hydrothermally in-situ from sulfided-PMA

displayed inhibited hydrogenation when vanadium was incorporated. Yumoto et al. studied Ni and V deposition onto a sulfided $NiMo/Al_2O_3$ catalyst and found that while nickel did not affect activity, vanadium inhibited hydrogenation of naphthalene, but enhanced the hydrogenative desulfurization pathway in dibenzothiophene HDS (Yumoto et al. 1996). Kim and Massoth compared deposition of a vanadium salt and vanadium tetraphenylporphyrin onto a sulfided $NiMo/Al_2O_3$ catalyst and found that while vanadium deactivated the catalyst, the vanadium salt impaired activity to a greater degree than the vanadium tetraphenylporphyrin (Kim 1993). Lacroix et al. (Lacroix et al. 1992) prepared bulk vanadium and molybdenum-promoted vanadium sulfides from thermal decomposition of ammonium thiosalt precursors and tested their hydrogenation and cracking activity with biphenyl. An atomic ratio, r, of 0.35 yielded the higest rate, where,

$$r = Mo / (Mo+V)$$

XPS, XRD and STEM analysis indicated that V_5S_8 and MoS_2 species were present, where V_5S_8 acts as a support to the highly-dispersed layered MoS_2-phase. The presence of benzene and cyclohexane indicated cracking of biphenyl over these catalysts. Pure vanadium sulfide was found to be more active in hydrogenation than molybdenum sulfide but is less active than nickel-promoted molybdenum sulfide (Lacroix et al. 1992); the highest activity occurred at r = 0.35 (Table 5.4.1.3). The decrease in activity observed when V is deposited on $NiMo/Al_2O_3$ has been ascribed to substitution of the Ni by V in promotion sites in catalytic clusters (Ledoux et al. 1987).

The ternary sulfide VNiMo prepared from $VO(acac)_2$, $NiSO_4$ and PMA with an atomic ratio of Ni:V:Mo of 0.6:0.6:1 {r_{Mo} = (Mo / (Mo + V + Ni)) = 0.45 and r_{Ni} = 0.27} qualitatively behaves similarly to vanadium-deactivated MoS_2 catalysts rather than molybdenum-promoted vanadium sulfides since hydrogenation is inhibited compared to NiMo and Mo. However, the presence of Ni somewhat offsets the inhibiting effect of V.

Table 5.4.1. 3: Characteristics of Promoted-Vanadium Sulfides (Lacroix et al. 1992)

r = Mo / (Mo + V)	**BET Area ($m^2 g^{-1}$)**	**A_s (10^{-8} mol s^{-1} g^{-1})**	**A_i (10^{-8} mol s^{-1} m^{-2})**	**Selectivity to Cracking (%)**
0	26	6.2	0.24	3
0.35	17	9.5	0.56	43
1	7	0.3	0.04	19

5.4. 2 Water Gas Shift Reaction over FeMo, VMo, NiMo and VNiMo-sulfided unsupported, dispersed catalysts

The other reaction of importance is the water gas shift reaction. The water gas shift rate is important since it supplies hydrogen for the upgrading reactions; a fast water gas shift rate compared to hydrogenation/hydrodesulfurization is necessary to ensure a sufficient hydrogen concentration for upgrading.

Figure 5.4.2.1 displays the normalized mol% of CO versus reaction time. The calculated irreversible pseudo-first order rate constants for CO, calculated from the derivation by Milad (Milad 1994) are shown in Table 5.4.1.1. Although the calculated equilibrium values are close to 98% conversion, the normalized mol% of CO is very low

(5-15 mol%) therefore the reversible pseudo-first order rate constants are reported. Irreversible pseudo-first order rate constants are shown in Figure 5.4.2.2. Substantial conversion of CO has occurred at 0 minutes, indicating that the rate of water gas shift begins at a temperature lower than 340 °C (Section 4.6.3). The reversible rate constants ranked in decreasing order are,

$$Mo > VMo > FeMo \sim VNiMo > NiMo$$

The role of vanadium in the water gas shift has been studied for a supported Fe and a Pt/CeO_2 catalyst (Duarte de Farias et al. 2008; Lima Junior et al. 2005). Lima

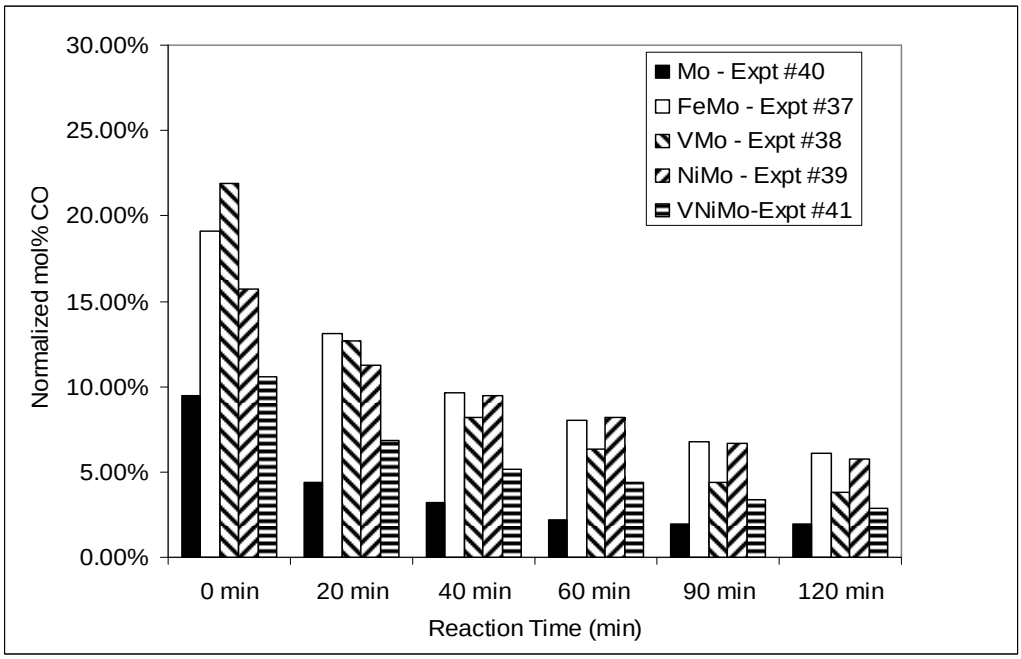

Figure 5.4.2. 1: Normalized mol% CO for FeMo, VMo, NiMo and VNiMo-sulfided dispersed, unsupported catalysts ($CO/H_2O/H_2S$, 600 psig, 15 psi H_2S, 3.0°C/min, 340 °C for 2 hrs, 18 ml H_2O, 52 ml toluene, 87.1 mmol NAPH, 1.16 mmole Mo, 0.70 mmole each (Fe, V, Ni), 1500 rpm impeller speed)

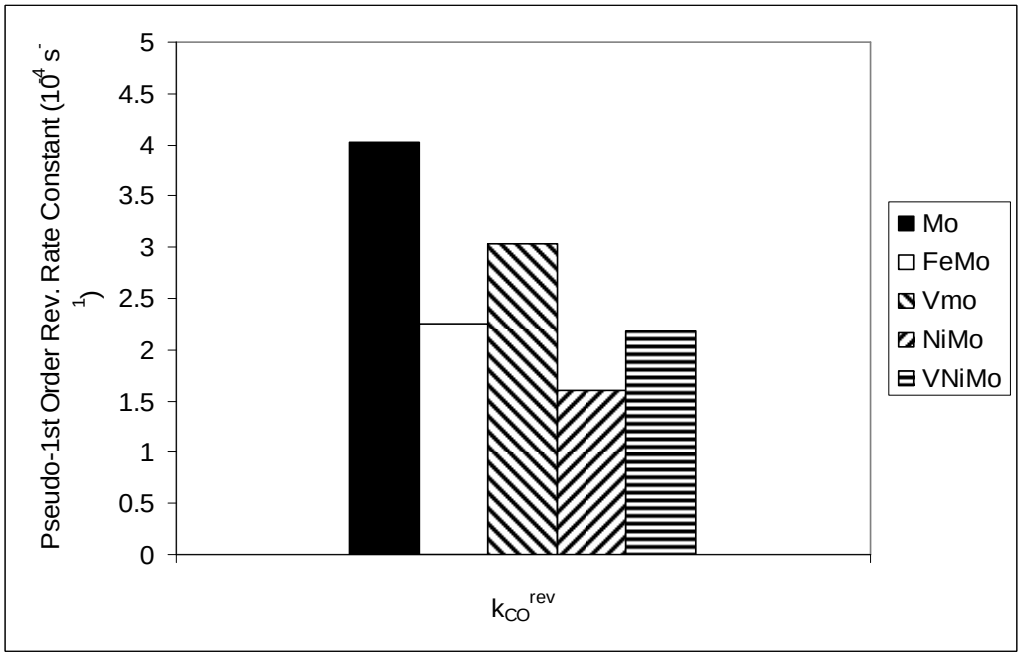

Figure 5.4.2. 2: Pseudo-First Order Reversible WGS Rate Constant($CO/H_2O/H_2S$, 600 psig, 15 psi H_2S, 3.0°C/min, 340 °C for 2 hrs, 18 ml H_2O, 52 ml toluene, 87.1 mmol NAPH, 1.16 mmole Mo, 0.70 mmole each (Fe, V, Ni), 1500 rpm impeller speed)

Junior et al. utilized a fixed-bed reactor to compare vanadium promoted iron high-temperature shift (HTS) catalyst with a commercial chromium-doped iron HTS catalyst. They found the vanadium-promoted catalysts to be more active than the commercial chromium-promoted HTS catalyst. From HR-TEM, Mossbauer and BET studies they attributed this to a structural effect of incorporated vanadium which prevented sintering during the reaction as well as to a chemical effect where vanadium was proposed to stabilize Fe(III) in the catalyst, enhancing the redox cycle and preventing reduction to metallic iron (Lima Junior et al. 2005). Vanadium was suggested to have a dual role,

i. as a structural promoter preventing sintering during reaction, and

ii. to electronically stabilize Fe(III) in an oxidized state preventing reduction to metallic iron

From their spectroscopic analysis, of a V-promoted Pt/CeO_2 catalyst, Duarte de Farais concluded that the presence of V-O-Ce bonds were responsible for the increased activity, while V-O-V bonds with tridimensional structure decreased the activity (Duarte de Farias et al. 2008).

The apparent higher WGS activity of VMo compared to FeMo, NiMo and VNiMo may be due to an electronic effect of V or VS_x on Mo in MoS_2. Vanadium may facilitate oxidation of Mo atoms which has been suggested as a key step in the proposed redox mechanism of WGS over MoS_2 (Hou et al. 1983). This may enhance WGS, while the ability of vanadium to keep Mo oxidized would adversely affect the reduced coordinatively unsaturated state of Mo, where the coordinatively unsaturated sites (CUS) of Mo have been suggested to be an active site in the hydrogenation and HDS reaction on MoS_2.

5. 5 Conclusion

5.5. 1 $Ru_3(CO)_{12}$ and $Ru(acac)_3$ compared to Phosphomolybdic Acid

PMA was more active for water gas shift and naphthalene hydrogenation than $Ru_3(CO)_{12}$ and $Ru(acac)_3$ prepared under similar conditions. The poor activity of Ru in hydrogenation may be due to incomplete sulfidation of the Ru precursors. The incomplete sulfidation may be due to too low of a temperature (613 K) as compared to literature (673

K) (Castillo-Villalon et al. 2008), low concentration of H_2S in the sulfiding gas mixture and the presence of H_2O.

5.5. 2 RuMo unsupported, dispersed catalysts

MoS_2 appears necessary for appreciable water gas shift activity when sulfur (H_2S) is present. Comparing a system of RuMo catalyst prepared from $Ru(acac)_3$ and PMA (r = 0.25) with a catalyst from pure PMA, the highest activity at 340 °C occurs for Mo; Ru does not enhance catalytic activity and displays a decreased activity for hydrogenation and water gas shift. Addition of $Ru_3(CO)_{12}$ and $Ru(acac)_3$ to PMA to generate catalyst in-situ at 340 °C and 15 psi H_2S would not be beneficial since in addition to the high cost of ruthenium, a much lower activity for water gas shift and hydrogenation is observed.

5.5. 3 FeMo, VMo, NiMo and VNiMo sulfide unsupported, dispersed catalysts

$FeSO_4$ and $VO(acac)_2$, when added to PMA to form a mixed metal catalyst (1.16 mmol Mo, 0.70 mmol each of Me), inhibit the hydrogenation of naphthalene via in-situ generated hydrogen. When vanadyl acetate, nickel sulfate and phosphomolybdic acid were sulfided in-situ with H_2S, the rate of naphthalene hydrogenation compared with NiMo and base-case Mo (1.16 mmol Mo) was impaired but still higher than VMo or FeMo. The pseudo-first order naphthalene rate constants, k_{NAPH} occur in the order,

$$NiMo > Mo > VNiMo > FeMo > VMo$$

This suggests the enhanced activity with Ni to some degree can offset the inhibiting effect of V in VNiMo.

Both water gas shift and naphthalene hydrogenation are slightly inhibited by Fe. VMo has the highest activity for water gas shift reaction among the binary catalysts. The ternary VNiMo system displays a similar water gas shift rate to FeMo. The pseudo-first order reversible rate constant for the water gas shift, k_{CO}, occurs in the order,

$$Mo > VMo > FeMo \sim VNiMo > NiMo$$

The presence of V inhibits hydrogenation compared with NiMo but appears to enhance the water gas shift activity.

5. 6 Recommendations

XRD, XPS, HRTEM and EDX analysis of the recovered catalytic solids may reveal the nature (decorated or isolated crystallites) and confirm the formation of mixed metal sulfides prepared in-situ. DRIFTS using CO may indicate the nature of sulfur vacant active sites; the relative metal-sulfur bond energies (Me-S) may be studied using TPR and may be relevant in determining the formation energies of coordinatively unsaturated sites.

WGS and HYD activity should be tested after complete sulfidation and confirmation of Ru precursors to RuS_2 crystallites. Ru and RuMo candidates should be sulfided in the absence of water before reaction or sulfided at higher H_2S concentrations and temperatures to ensure complete transformation to RuS_2.

Chapter 6: The Effect of Temperature, P_{H2S} and CO on VNiMo Catalyst Activity

6. 1 Introduction

Research into hydrodesulfurization and hydrogenation with metal sulfides has shown that not only the type of metal is significant, but also that different forms of sulfides with the same metal species drastically alters the catalytic behaviour regarding hydrodesulfurization and hydrogenation (Castillo-Villalon et al. 2008; Hubaut 2007). Altering the preparation conditions for metal sulfides is most easily achieved by varying several factors. Two important factors affecting activity are the sulfidation/reduction temperature and composition of the sulfidation/reduction gas (Jacobsen et al. 1999; Geantet et al. 1991). Temperature affects the degree of sulfidation of the metal species in addition to affecting hydrogenation/hydrodesulfurization rate. The type of sulfidation/reduction atmosphere has similar affects. Specifically, the percentage of H_2S can increase the degree of surface sulfidation, but if present during reaction may reduce the rate of hydrodesulfurization due to the equilibrium between active sites and H_2S (Jacobsen et al. 1999).

6. 2 Experimental Design of 2^3 Factorial Experiment for VNiMo catalysts

A three-factor two-level experiment was performed in order to determine the effect of temperature, H_2S pressure and type of reduction gas (H_2 or CO) on the hydrogenation of naphthalene with simultaneous water gas shift using dispersed, unsupported $VNiMoS_2$. The full 2^3 factorial experiment includes 3 replicates performed at the centrepoint conditions to estimate experimental error (Figure 6.2.1). Centre-point replicates were

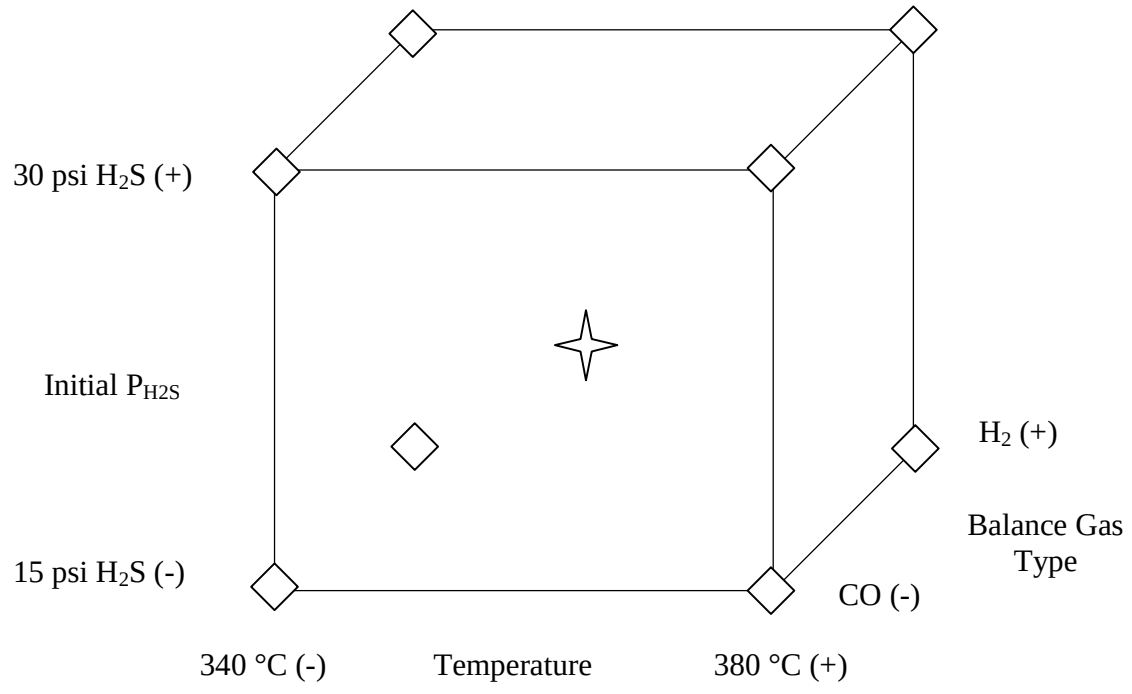

Figure 6.2. 1: Multifactorial Experiment with centrepoint replicates for Temperature, Balance Gas Type and Initial H_2S Pressure

distributed evenly in the reaction sequence to account for experimental drift such as reactor memory effects. A plot of the error versus experiment number indicates error appears to be randomly distributed (Figure 6.2.2). The experimental order was randomized by selecting paper labels out of a box. Experiment #53 does not belong to the factorial experiment but was performed at a reduced catalyst concentration of 500 ppmw Mo (0.50 mmol Mo, 0.30 mmol each Ni,V) to determine the effect of catalyst concentration on the rate of naphthalene hydrogenation and water gas shift. Rate constants for the blank reactor "wall effect" experiment are shown in Table D.2, Appendix D (Experiment #30). Since the experimental error appears randomly distributed (Figure

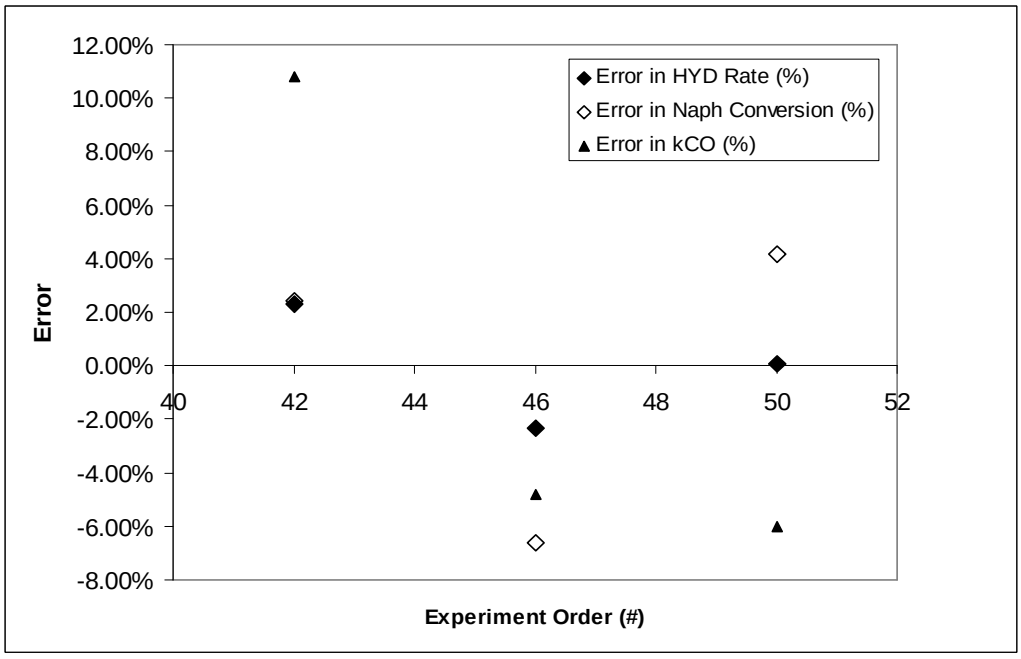

Figure 6.2. 2: Experimental Error as a function of Reaction Sequence to check for Experimental Drift((1:1 molar CO/H_2)/H_2O/H_2S, 600 psig, 22.5 psi H_2S, 4.0°C/min, 360 °C for 2 hrs, 10 ml H_2O, 100 ml toluene, 78.0 mmol NAPH, 1.50 mmole Mo; 0.91 mmole each (V, Ni), 1500 rpm impeller speed)

6.2.2), the “wall effect” can be considered constant with no cumulative increase due to “wall memory” where the wall activity varies depending upon experimental conditions in the preceding reaction.

6. 3 Analysis of Effects (ANOVA) on Naphthalene Conversion to Tetralin

Table 6.3.1 shows the results of temperature, initial H_2S pressure and gas type on pseudo-first order rate constant for HYD and naphthalene conversion. Tetralin was the major product with trace amounts of cis and trans-decalins observed. Additional products detected with GC retention times below decalins may be cracking products, as vanadium was reported to impart some cracking activity due to its acidity (Yumoto et al. 1996). It should be noted that due to the longer heat-up time required to reach 380 °C versus 340 °C (heating temperature ramp of 4.0 °C/min) total naphthalene conversion is not a suitable variable for comparison on the factors in this study. Therefore the isothermal naphthalene conversion was used, defined as the conversion at 180 minutes minus the conversion at 0 minutes sample (reaction) time,

$$X_{iso} = X_{t180} - X_{t0}$$

The results were analyzed using Analysis of Variance (ANOVA) techniques to determine significant effects at the 95% confidence level. $F_{experimental}$ values greater than

$F_{critical}$ are deemed significant effects. From Table 6.3.2 the only significant effect is temperature which has an apparent negative impact on the isothermal conversion.

Table 6.3. 1: Calculated Pseudo-first order naphthalene rate constant and conversion (600 psig, 4.0°C/min, 2 hrs, 10 ml H_2O, 100 ml toluene, 78.0 mmol NAPH, 1.50 mmole Mo; 0.91 mmole each (V, Ni), 1500 rpm impeller speed)

Run Order	***Temperature (°C)***	***H_2S Pressure (psi)***	***Gas Type (CO or H_2)***	***Pseudo-First Order Naphthalene Rate Constant, k_{NAPH} (10^{-5} s^{-1})***	***Isothermal Naphthalene Conversion, $X_{t180} - X_{t0}$ (mol %)***
45	380	15	CO	13.03	33.49%
44	340	15	CO	10.1	36.93%
48	380	30	CO	12.2	46.09%
47	340	30	CO	8.93	24.23%
49	380	15	H_2	10.1	26.01%
52	340	15	H_2	8.5	37.60%
51	380	30	H_2	14.27	10.04%
43	340	30	H_2	7.5	17.14%
46	360	22.5	CO/H_2	6.93	32.17%
50	360	22.5	CO/H_2	7.1	9.68%
42	360	22.5	CO/H_2	7.26	33.85%
53	340	15	CO	6.43	28.55%

Table 6.3. 2: ANOVA Analysis of Isothermal Naphthalene Conversion (600 psig, 4.0°C/min, 2 hrs, 10 ml H_2O, 100 ml toluene, 78.0 mmol NAPH, 1.50 mmole Mo; 0.91 mmole each (V, Ni), 1500 rpm impeller speed)

Source	**Effect on $X_{t180} - X_{t0}$**	**SS (10^{-3})**	**DF**	**MS (10^{-3})**	**$F_{experimental}$**
Main Effect					
Temperature	-0.2334	109	1	109	68.4612
Initial H_2S Pressure	-0.0676	9.15	1	9.15	5.7484
Gas Type (CO or H_2)	-0.0509	5.19	1	5.19	3.2572
Interaction Effects					
T x P_{H2S}	0.0137	0.374	1	0.374	2.0711
T x Gas	0.0457	4.18	1	4.18	0.2350
P_{H2S} x Gas	0.0972	18.9	1	18.9	2.6275
T x P_{H2S} x Gas	-0.0406	3.30	1	3.30	11.8737
Error			2	1.59E-03	
$F_{critical}$					18.5128

6.3. 1 Effect of Temperature on Naphthalene Conversion

At increased temperature an increase in reaction rate (Arrhenius) should occur, however because hydrogenation is exothermic the equilibrium conversion will decrease. In line with industrial practice, for $NiMo/Al_2O_3$ catalysts deactivated with vanadium salt and vanadium-TPP, Kim and Massoth found that in a fixed-bed reactor at 35 atm H_2 under

vapour phase conditions with no water, as temperature was increased from 300 °C to 400 °C naphthalene conversion to tetralin increased concomitantly (Kim 1993). Zhang examined naphthalene hydrogenation using a NiMo unsupported, dispersed catalyst with in-situ hydrogen and concluded that conversion was not significantly higher at 370 °C compared to 340 °C (Zhang 2005). A naphthalene hydrogenation equilibrium conversion correlation developed by Frye and Weitkamp (Frye 1969) was used to calculate the theoretical equilibrium conversion (X_{eq}) under reaction conditions. The experimental conversions compared to the theoretical conversions (180 minutes) are shown in Table 6.3.1.1. For the reactions at 380 °C the equilibrium conversion is less than the measured experimental conversion. Figure 6.3.1.1 displays the typical comparison of experimental conversion versus equilibrium conversion over reaction time at 380 °C under H_2. This particular experiment should give the highest "best-case" X_{eq} due to the apparent high concentration of hydrogen. It can be observed that even at 20 minutes the experimental conversion exceeds the theoretical value. This would explain the decrease in conversion with respect to increasing temperature as calculated by the ANOVA analysis. In addition, the consumption of hydrogen will decrease the hydrogen concentration in the batch autoclave further decreasing the X_{eq}. Therefore, comparing conversions when temperature is a variable is not accurate under our conditions in a batch autoclave. Considering Figure 6.3.1.2, which displays a typical reaction performed at 340 °C indicates that equilibrium is not achieved until near the end of reaction.

Table 6.3.1. 1: Experimental Naphthalene Conversions and Calculated Equilibrium Conversions (600 psig, 4.0°C/min, 2 hrs, 10 ml H_2O, 100 ml toluene, 78.0 mmol NAPH, 1.50 mmole Mo; 0.91 mmole each (V, Ni), 1500 rpm impeller speed)

Run Order / Experiment Number	***Temper-ature***	***H_2S***	***CO/H_2***	***Final Naph Conversion (%)***	***Naph Conversion, Heating (%)***	***Tet Yield (%)***	***Final [H_2] (mol/g)***	***Equilibrium Conversion, X_{eq}***
CL45	+	-	-	54.25%	30.02%	43.49%	0.00095	39.91%
CL44	-	-	-	55.68%	9.59%	52.76%	0.00102	75.42%
CL48	+	+	-	48.35%	38.31%	47.76%	0.00111	48.17%
CL47	-	+	-	55.77%	18.16%	53.35%	0.00095	73.34%
CL49	+	-	+	50.77%	33.63%	46.96%	0.00075	29.92%
CL52	-	-	+	53.86%	20.01%	53.47%	0.00102	76.34%
CL51	+	+	+	48.19%	38.51%	43.83%	0.00076	29.42%
CL43	-	+	+	56.56%	19.63%	59.30%	0.00083	70.55%
CL46	0	0	0	49.61%	23.60%	53.61%	0.00094	55.79%
CL50	0	0	0	49.99%	17.83%	48.23%	0.00104	59.81%
CL42	0	0	0	56.80%	23.31%	50.71%	0.00114	65.74%
CL53	-			37.66%	9.11%	42.99%	0.00114	78.75%

* [H_2] calculated from pressure, volume, temperature and GC mol% analysis of gas flashed from liquid sample

** Equilibrium calculation from (Frye 1969)

$$Log\, K_{eq} = \frac{6460}{T(K)} - 12.4; \quad K_P = \frac{N_{TET}}{N_{NAPH} * (P_{H2} + 0.00033 P_{H2}{}^2)^2}; \quad X_{eq} = 1 - [1 + \frac{N_{TET}}{N_{NAPH}}]^{-1}$$

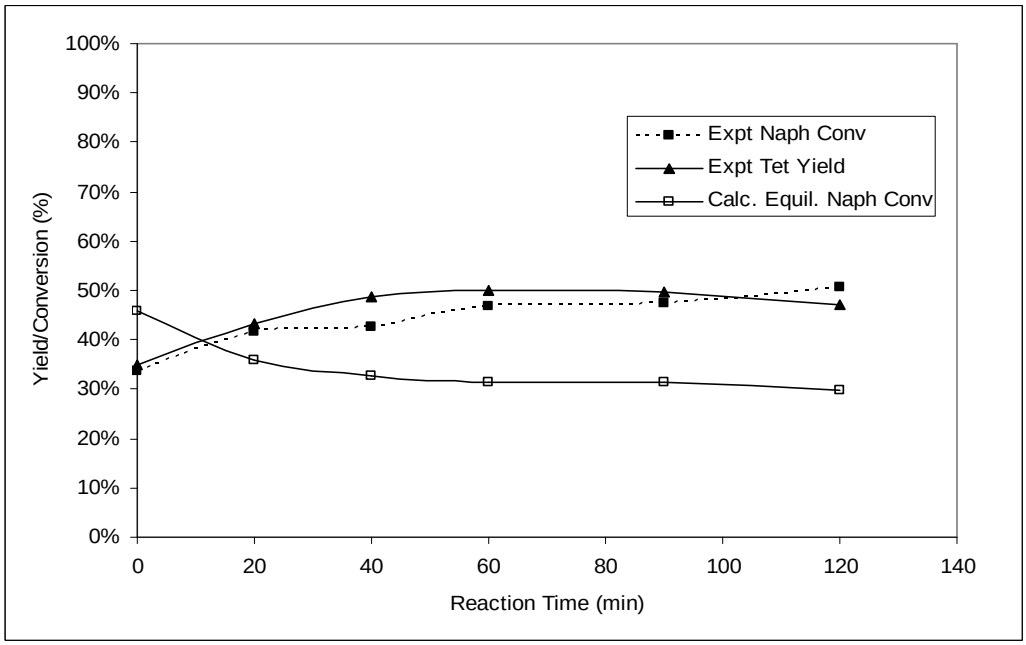

Figure 6.3.1. 1: Experimental and Equilibrium Naphthalene Conversions, Experiment #49 ($H_2/H_2O/H_2S$, 15 psig H_2S, 585 psig CO, 4.0°C/min, 380 °C, 2 hrs, 10 ml H_2O, 100 ml toluene, 10.0 g NAPH, 1.50 mmole Mo; 0.91 mmoles $NiSO_4$; 0.91 mmoles $VO(acac)_2$, 1500 RPM Impeller Speed)

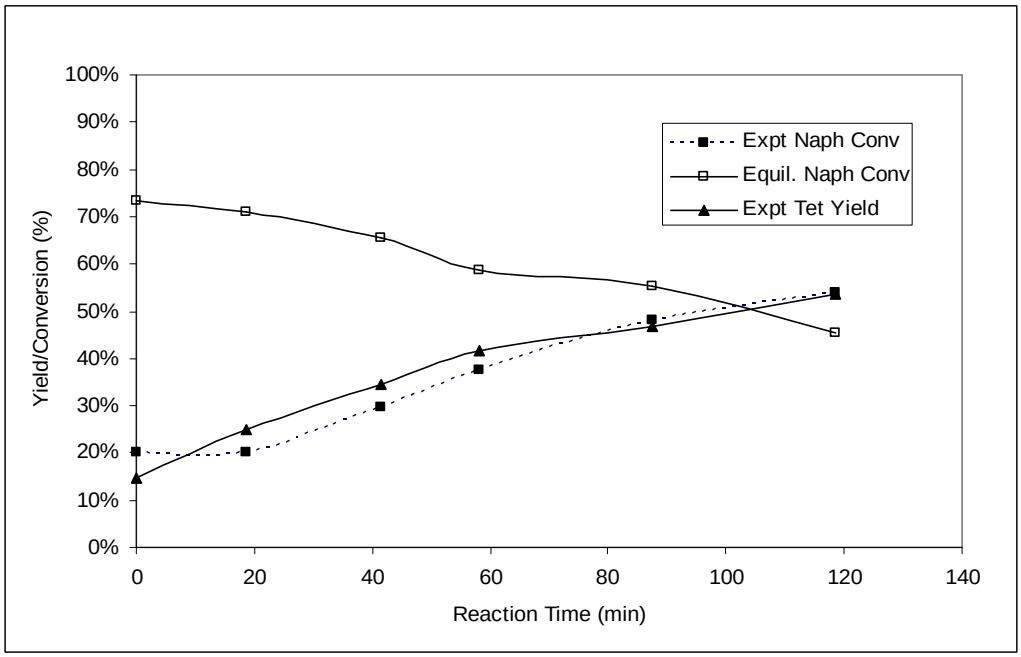

Figure 6.3.1. 2: Experimental and Equilibrium Naphthalene, Experiment #52 ($H_2/H_2O/H_2S$, 15 psig H_2S, 585 psig CO, 4.0°C/min, 340 °C, 2 hrs, 10 ml H_2O, 100 ml toluene, 10.0 g NAPH, 1.50 mmole Mo; 0.91 mmoles $NiSO_4$; 0.91 mmoles $VO(acac)_2$, 1500 RPM Impeller Speed)

6.3. 2 ANOVA Analysis of the Pseudo-First Order Hydrogenation Rate, k_{NAPH}

An ANOVA analysis of the pseudo-first order naphthalene rate constant is shown in Table 6.3.2.1. As can be seen, the main effects of temperature and gas type are significantly larger than the experimental error. In addition, the 2-factor interactions

Table 6.3.2. 1: ANOVA Table for pseudo-first order rate constant, k_{NAPH} (Temperature, Initial H_2S Pressure, Gas Type) (600 psig, 4.0°C/min, 2 hrs, 10 ml H_2O, 100 ml toluene, 78.0 mmol NAPH, 1.50 mmole Mo; 0.91 mmole each (V, Ni), 1500 rpm impeller speed)

Source	***Effect on k_{NAPH} (10^{-5})***	***SS***	***DF***	***MS (10^{-10})***	***$F_{experimental}$***
Main Effect					
Temperature	3.6425	2.65E-09	1	26.5	**974.3799**
Initial H_2S			1		
Pressure	0.2925	1.71E-11		0.171	6.283201
Gas Type			1		
(CO or H_2)	-0.9725	1.89E-10		1.89	**69.45578**
Interaction					
Effects					
T x P_{H2S}	1.3775	3.8E-10	1	3.87	**139.3517**
T x Gas	0.5425	5.89E-11	1	0.589	**21.61368**
P_{H2S} x Gas	1.2925	3.34E-10	1	3.34	**122.6847**
T x P_{H2S} x			1		
Gas	-0.2575	1.33E-11		0.133	4.869492
Error			2	.0272	
$F_{critical}$					18.5128

* Method of initial rates was used to calculated k_{NAPH} at 380 °C due to equilibrium conversions

between temperature and H_2S pressure, temperature and gas type and H_2S pressure and gas type are also significant.

6.3. 3 Effect of Temperature on Naphthalene Hydrogenation Rate, k_{NAPH}

An increase in temperature increases the reaction rate; from 340 °C to 380 °C k_{NAPH} increases by 3.64 x 10^{-5} s^{-1} (Table 6.3.2.1).

.

6.3. 4 Lack of Effect of H_2S Partial Pressure on Naphthalene Hydrogenation Rate, k_{NAPH}

An increase from 15 psi to 30 psi H_2S has no significant effect on k_{NAPH}. The concentration of H_2S is known to influence not only catalyst preparation but the reactivity during operation. The mol% H_2S in the recovered gas phase after reaction is listed for various conditions (Table 6.3.4.1). Considering Table 6.3.6.1 the final mol% H_2S varies not only with initial P_{H2S} but also with gas type (CO or H_2). P_{H2S} is higher under H_2 since during hydrogenation H_2 is consumed and total gas pressure decreases, while during WGS although water and CO are consumed CO_2 is produced in addition to H_2.

Insufficient H_2S during catalyst sulfidation may form a greater fraction of reduced metallic sites, which may aid hydrogenation such as with RuS_2 (Castillo-Villalon et al. 2008). However, H_2S during reaction conditions may be detrimental to hydrogenation activity. Jacobsen et al. studied the metal-sulfur bond strengths of various metal sulfides using TPR, and determined that H_2S exists in equilibrium with surface sulfur, H_2 and

Table 6.3.4. 1: Final H_2S mol% (600 psig, 4.0°C/min, 2 hrs, 10 ml H_2O, 100 ml toluene, 78.0 mmol NAPH, 1.50 mmole Mo; 0.91 mmole each (V, Ni), 1500 rpm impeller speed)

Run Order / Experiment Number	***Temperature (°C)***	***H_2S Pressure (psi)***	***Gas Type (CO or H_2)***	***Final mol% H_2S***
45	380	15	CO	0.54
44	340	15	CO	0.55
48	380	30	CO	1.38
47	340	30	CO	1.37
49	380	15	H_2	0.7
52	340	15	H_2	0.85
51	380	30	H_2	1.51
43	340	30	H_2	2.01
46	360	22.5	CO/H_2	1.11
50	360	22.5	CO/H_2	0.62
42	360	22.5	CO/H_2	1.07
53	340	15	CO	0.48

surface vacancies (Jacobsen et al. 1999),

$$\mathbf{S^* + H_2 \leftrightarrow H_2S + *}$$

Higher P_{H2S} may therefore shift equilibrium to a higher concentration of surface sulfur sites, lowering the number of vacant sites. Because these sulfur vacancies are believed to be active sites for hydrogenation, hydrodesulfurization and hydrodenitrogenation, a decrease in the number of sulfur vacancies would inhibit activity. Under conditions where

water is present, the situation becomes even more complex due to the occurrence of water gas shift and exchange of surface oxygen with sulfur, which has been suggested as necessary in giving MoS_2 water gas shift activity (Hou et al. 1983). In hydrogenation of tetralin over $NiMo/Al_2O_3$, Yasuda et al. reported that increasing P_{H2S} an order of magnitude from 0.1% to 1.0% only decreased the hydrogenation rate by 20% (Yasuda et al. 1997). Zhang studied naphthalene hydrogenation under CO/H_2O with a dispersed, unsupported NiMo catalyst and found that increasing the S:Mo atomic ratio (constant Mo concentration) from 8.1 to 24.8 resulted in a 5% decrease in the pseudo-first order rate constant (Zhang 2005). From experimental results reported in this work, no significant effect due to varying P_{H2S} was observed likely because over the studied P_{H2S} interval (15 to 30 psi, S:Mo atomic ratio from 4 to 8) any change in rate was small enough to fall within experimental variability.

6.3. 5 Effect of CO or H_2 on Naphthalene Hydrogenation Rate, k_{NAPH}

Water has been shown to inhibit hydrodesulfurization, and its consumption in the WGS may be one factor in the higher HDS activity of in-situ generated hydrogen over molecular hydrogen (Moll 1999; Lee 2006). The mass of water recovered in the liquid phase for each multifactorial experiment is displayed in Table 6.3.5.1. Water contents for in-situ conditions are lower than those for molecular H_2. Under molecular H_2 no consumption of water is expected; the apparent difference between the water recovered and water initially charged may be due to the water lost during sampling, which may also hold true for the water gas shift runs under CO. Although for in-situ runs the molar

fraction of H_2 (related to mol% of H_2) is lower than for molecular H_2, the total moles of dissolved gas in oil is higher for in-situ conditions due to the WGS occurring (Appendix B). This is indicated by the higher gas phase pressure of in-situ gas samples flashed from recovered liquid samples. This results in similar H_2 liquid concentrations for in-situ and molecular H_2 runs, where dividing by the pseudo-steady state H_2 concentration gives a pseudo-second order rate constant, k''_{NAPH}, for comparison (Table 6.3.5.2). The ANOVA

Table 6.3.5. 1: Mass of Recovered Water from Reactions (600 psig, 4.0°C/min, 2 hrs, 10 ml H_2O, 100 ml toluene, 78.0 mmol NAPH, 1.50 mmole Mo; 0.91 mmole each (V, Ni), 1500 rpm impeller speed)

Run Order/ Experiment Number	***Temperature (°C)***	***H_2S Pressure (psi)***	***Gas Type (CO or H_2)***	***Mass of Recovered Water (g)***	***Pseudo-First Order Naphthalene Rate Constant, k_{NAPH} (10^{-5} s^{-1})***
45	380	15	CO	3.75	13.03
44	340	15	CO	0	10.1
48	380	30	CO	3.2	12.2
47	340	30	CO	1.72	8.93
49	380	15	H_2	5.06	10.1
52	340	15	H_2	5.68	8.5
51	380	30	H_2	4.84	14.27
43	340	30	H_2	5.88	7.5
46	360	22.5	CO/H_2	4.61	6.93
50	360	22.5	CO/H_2	4.31	7.1
42	360	22.5	CO/H_2	3.95	7.26
53	340	15	CO	3.18	6.43

results (95% significance level) for this pseudo-second order rate constant are shown in Table 6.3.5.3. The ANOVA analysis of $k"_{NAPH}$ indicates that using CO or H_2 does not have a significant effect. Comparison of molecular H_2 and in-situ generated hydrogen in naphthalene hydrogenation (Zhang 2005) and diesel hydrodesulfurization (Siewe 1998) indicated comparable activities in hydrogenation and sulfur removal. If water noticeably

Table 6.3.5. 2: Table for pseudo-second order rate constant, $k"_{NAPH}$ (Temperature, Initial H_2S Pressure, Gas Type) (600 psig, 4.0°C/min, 2 hrs, 10 ml H_2O, 100 ml toluene, 78.0 mmol NAPH, 1.50 mmole Mo; 0.91 mmole each (V, Ni), 1500 rpm impeller speed)

Run Order	***Temperature (°C)***	***H_2S Pressure (psi)***	***Gas Type (CO or H_2)***	***Pseudo-First Order Naphthalene Rate Constant, k_{NAPH} (10^{-5} s^{-1})***	****Pseudo-Steady Sate Dissolved Hydrogen Concentration (mol/g-oil)***	***Pseudo-Second Order Rate Constant, ($k"_{NAPH}$ ($g\text{-}mol^{-1}\text{-}s^{-1}$)***
45	380	15	CO	13.03	0.00096	0.1357
44	340	15	CO	10.1	0.001188	0.0849
48	380	30	CO	12.2	0.001058	0.1151
47	340	30	CO	8.93	0.001050	0.0850
49	380	15	H_2	10.1	0.000751	0.1347
52	340	15	H_2	8.5	0.001303	0.0654
51	380	30	H_2	14.27	0.000753	0.1903
43	340	30	H_2	7.5	0.001017	0.0735
46	360	22.5	CO/H_2	6.93	0.001042	0.0666
50	360	22.5	CO/H_2	7.1	0.001159	0.0612
42	360	22.5	CO/H_2	7.26	0.001302	0.0558
53(500 ppmw Mo)	340	15	CO	6.43	0.001075	0.0595

* Calculated from the average of measured [H_2] over 120 minute reaction time

Table 6.3.5. 3: ANOVA Table for Change in Pseudo-second Order Rate Constant, $k"_{NAPH}$ (Temperature, Initial H2S Pressure, Gas Type) (600 psig, 4.0°C/min, 2 hrs, 10 ml H_2O, 100 ml toluene, 78.0 mmol NAPH, 1.50 mmole Mo; 0.91 mmole each (V, Ni), 1500 rpm impeller speed)

Source	**Effect on k_{NAPH}" (10^{-2} g/(mol-s))**	**SS (10^{-4})**	**DF**	**MS (10^{-5})**	**$F_{experimental}$ = MS / MS_{error}**
Main Effect					
Temperature	6.673	89.06	1	89.06	306.06
Initial H_2S			1		
Pressure	1.082	2.342		2.342	8.05
Gas Type			1		
(CO or H_2)	1.078	2.322		2.322	7.98
Interaction					
Effects					
T x P_{H2S}	0.662	0.888	1	0.888	3.05
T x Gas	2.628	13.81	1	13.81	47.47
P_{H2S} x Gas	2.105	8.863	1	8.863	30.46
T x P_{H2S} x			1		
Gas	-0.836	1.398		1.398	4.81
Error			2	2.91	
$F_{critical}$ =					18.5128
$F_{1,2,\ 0.05}$					

inhibits hydrogenation then the consumption of water to form in-situ hydrogen via WGS should increase hydrogenation activity unless it is masked by the presence of CO_2. The effect of water on hydrogenation rate may also not be apparent over the measured difference in water content recovered from the CO and H_2 experiments (Table 6.3.5.1).

The insensitivity of the pseudo-second order rate constant to either initial CO or initial H_2 reinforces the dependence of hydrogenation rate on the hydrogen concentration. One may expect under an $H_2/H_2O/H_2S$ atmosphere to have a higher concentration of hydrogen than under $CO/H_2O/H_2S$. However, water gas shift and hydrogenation occur in the same reacting phase where the catalyst is located and a fast WGS rate may increase the local hydrogen availability. The concentration of H_2 (flashed from recovered liquid samples) generated in-situ via WGS may approach or exceed the concentration of H_2 under $H_2/H_2O/H_2S$ as observed from the experimental results (Table 6.3.5.2). A higher "liquid" H_2 concentration under $CO/H_2O/H_2S$ may be due to consumption of water by WGS and/or the production of molecular hydrogen in the catalytic "liquid" phase. Under $H_2/H_2O/H_2S$ the batch autoclave pressure decreases as H_2 is consumed. The autoclave pressure decreases much more slowly under $CO/H_2O/H_2S$ due to the production of H_2 and CO_2. The partial pressure of CO_2 and its solubility in the liquid phase under these conditions does not appear to inhibit hydrogenation activity compared to when no CO_2 is present ($H_2/H_2O/H_2S$). While no significant effect was observed for k_{NAPH}", the positive effect observed for CO on the pseudo-first order rate constant is likely due to a higher hydrogen concentration during the water gas shift reaction.

In the recovered products from experiments performed under initial H_2, the aqueous phase takes on a milky appearance which may indicate some form of fine solids species is present. The recovered aqueous phase for experiments performed under CO are noticeably more transparent (Figure 6.3.5.1). An elemental analysis of the aqueous phase may indicate what type of inorganic species, if any, are present.

Figure 6.3.5. 1: Recovered Aqueous Phase (600 psig, 4.0°C/min, 2 hrs, 10 ml H_2O, 100 ml toluene, 78.0 mmol NAPH, 1.50 mmole Mo; 0.91 mmole each (V, Ni), 1500 rpm impeller speed)

6.3. 6 Interaction Effect of Temperature x P_{H2S} on Naphthalene Hydrogenation Rate Constant, k_{NAPH}

The interaction between T x P_{H2S} significantly positively affects the pseudo-first order rate constant (k_{NAPH}) but not the pseudo-second order rate constant (k_{NAPH}"), which may indicate the effect is dependent upon hydrogen concentration. At low temperature, low P_{H2S} gives a higher rate while at high temperature increasing P_{H2S} enhances k_{NAPH}. At

higher temperature a higher H_2S partial pressure may be required to maintain active MoS_2 sites.

6.3. 7 Interaction Effect of T x Gas on Naphthalene Hydrogenation Rate Constant, k_{NAPH}

The interaction effect of T x Gas indicates significant but minor enhancement of both k_{NAPH} and k_{NAPH}". In a toluene/water emulsion, the use of CO at lower temperatures will increase the naphthalene hydrogenation activity. Conversely, using H_2 at higher temperature will increase activity slightly. Since WGS is fast compared to hydrogenation, higher equilibrium WGS conversions at lower temperatures may increase the H_2 concentration which increases the pseudo-first order rate constant, k_{NAPH}.

6.3. 8 Interaction Effect of P_{H2S} x Gas on Naphthalene Hydrogenation Rate Constant, k_{NAPH}

The two-factor interaction between P_{H2S} x Gas on naphthalene hydrogenation is minor in comparison to the temperature main-effect but significant for both k_{NAPH} and k_{NAPH}". At low P_{H2S}, the use of CO will increase the hydrogenation activity while at high P_{H2S} the use of H_2 will yield higher activity. A chemical equilibrium between active sulfur vacancies and adsorbed H_2S was observed for MoS_2 and other chalcogenides active for HDS and HYD (Jacobsen et al. 1999). At low P_{H2S} over-reduction of MoS_2 can occur to metallic Mo. These results may indicate a lower propensity for CO to over-reduce MoS_2 compared to H_2 under these conditions.

6. 4 Effects of Temperature, P_{H2S} and CO or H_2 on WGS Rate

At 380 °C the water gas shift has attained equilibrium as seen by the constant concentration of CO from the gas phase concentration-time figures (Appendix B). The measured pseudo-first order irreversible and reversible rate constants for water gas shift (k_{CO}) are shown in Table 6.4.1. Since the reaction is close to equilibrium at 0 minutes, ANOVA analysis of the kinetic rate data was not performed since kinetic analysis performed on these results may be inaccurate.

6. 5 Effect of Total Metal Concentration (Constant atomic ratio, Me:Mo = 0.6 each of Ni and V)

Although the effect of catalyst concentrations cannot be analyzed with ANOVA, nonetheless some preliminary conclusions can be drawn from the data. The pseudo-second order rate constant was calculated for direct comparison. While maintaining the same atomic ratio (0.6) of Ni:Mo and V:Mo, increasing the total metal concentration from 1.10 mmoles to 3.32 mmoles increases k_{NAPH}" from 0.060 g-mol^{-1}-s^{-1} to 0.072 g-mol^{-1}-s^{-1}, while k_{CO} increases from 27.7x10^{-4} s^{-1} to 41.2x10^{-4} s^{-1}(Table 6.5.1). This corresponds to an increase of k_{CO} by 0.608 s^{-1}/ (mol total metal) and for an increase of k_{NAPH} by 5.41 g-mol^{-1} s^{-1} / (mol total metal). Since only two experimental points were measured, a rate constant with respect to total metal content could not be accurately calculated. Abusaido studied the effect of changing Mo concentration on the water gas shift and naphthalene hydrogenation rate at an H_2O:CO molar ratio of 3:1 (Abusaido 1999) and observed for the WGS an overall pseudo-second order dependence (first order in Mo concentration) of

Table 6.4. 1: Pseudo-first order irreversible water gas shift rate constant (600 psig, 4.0°C/min, 2 hrs, 10 ml H_2O, 100 ml toluene, 78.0 mmol NAPH, 1.50 mmole Mo; 0.91 mmole each (V, Ni), 1500 rpm impeller speed)

Run Order	***Temp***	***H_2S Pressure (psi)***	***Gas Type (CO or H_2)***	***Pseudo-First Order Irreversible WGS Rate Constant, k_{CO} (10^{-4} s^{-1})***	***Pseudo-First Order Reversible WGS Rate Constant, k_{CO} (10^{-4} s^{-1})***
45	380	15	CO	1.39	1.22
44	340	15	CO	2.25	2.49
48	380	30	CO	0.580	0.495*
47	340	30	CO	1.88	3.07
46	360	22.5	CO/H_2	1.60	
50	360	22.5	CO/H_2	1.58	
42	360	22.5	CO/H_2	1.87	
53	340	15	CO	1.90	

*reaction may have reached equilibrium

Table 6.5. 1: Effect of Total Metal Concentration on Reaction Rates (600 psig, 4.0°C/min, 2 hrs, 10 ml H_2O, 100 ml toluene, 78.0 mmol NAPH, 1.50 mmole Mo; 0.91 mmole each (V, Ni), 1500 rpm impeller speed)

Mo Concentration (ppmw wrt total hydrocarbon)	***Pseudo-First Order WGS Rate Constant, k_{CO} (10^{-5} s^{-1})***	***Pseudo-Second Order Rate Constant, $\{k_{NAPH}/[H_2]\} = k_{NAPH}$" (g-$mol^{-1}$-$s^{-1}$)***	***Pseudo-First Order WGS Rate Constant increase (s^{-1}/ mol total Me)***	***Pseudo-Second Order Naph Rate Constant, k_{NAPH}" (g-mol^{-1} s^{-1} / mol total Me)***
1500 (3.32 mmole metal)*	41.2	0.072	0.608	5.41
500 (1.10 mmole metal)**	27.7	0.06		

*1.5 mmole Mo, 0.91 mmole Ni, 0.91 mmole V

**0.5 mmole Mo, 0.30 mmole Ni, 0.30 mmole V

2.0 x 10^{-7} (s-ppmw Mo)$^{-1}$. For naphthalene hydrogenation, a pseudo-second order dependence of 5.0 x 10^{-7} (s-ppmw Mo)$^{-1}$ was calculated (Abusaido 1999). Since only two metal concentrations were measured, extrapolation beyond the measured metal concentration may not be accurate.

Although catalytic effects due to the reactor wall were not explicitly corrected for in the reported rate constants, future work should account for the catalytic effect of the reactor internals in the experimental design.

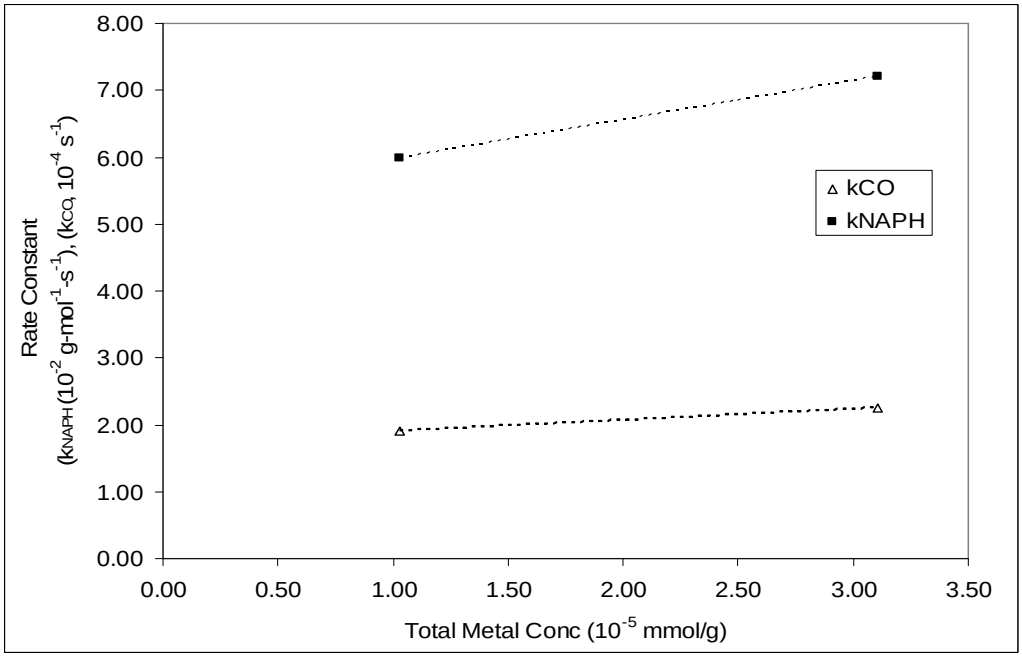

Figure 6.5. 1: Effect of Total Metal Concentration on Reaction Rates (600 psig, 4.0°C/min, 2 hrs, 10 ml H_2O, 100 ml toluene, 78.0 mmol NAPH, 1.50 mmole Mo; 0.91 mmole each (V, Ni), 1500 rpm impeller speed)

6. 6 Conclusion

Conversion is not an accurate measure for comparing the effect of temperature on naphthalene hydrogenation since nearly equilibrium conversion was attained at 380 °C early in the reaction in a batch autoclave. However, HYD rate constants at higher temperature could be measured using the method of initial rate analysis. Higher temperature increases the pseudo-first order naphthalene hydrogenation rate constant (k_{NAPH}). CO also had a positive effect on k_{NAPH}. Two-factor interaction effects also had a positive effect on k_{NAPH}", the magnitude of the effects in decreasing order,

$$\text{Temp} >> (\text{Temp x Gas}) > (P_{H2S} \text{ x Gas}) > (\text{Temp x Gas})$$

Dividing by the "liquid-phase" H_2 concentration (mol/g-liquid) yields a pseudo-second order rate constant, $k"_{NAPH}$, where the ANOVA analysis indicates the effect of gas type (CO or H_2) is not large enough to be considered significant. Significant differences are due to the concentration of hydrogen in the reacting phase, which may differ under CO due to in-situ hydrogen generation versus H_2. A small two-factor interaction effect suggests the activity is higher when CO is used at low temperature and H_2 is used at high temperature. Hydrogenation activity is slightly enhanced at low P_{H2S} under CO or when using H_2 at higher P_{H2S}

6. 7 Recommendations

Future study on the relative atomic amounts of Ni and V, to determine the independent and combined effect of each species on water gas shift, hydrogenation and hydrodesulfurization is recommended. Another important factor would be to determine effects due to water content, as water inhibits hydrodesulfurization, hydrodenitrogenation and hydrogenation. Determining interaction effects between temperature and water content may indicate whether H_2O content affects the hydrogenation rate constant. In addition, calculation of the rate constant with respect to the total metals or Mo concentration would be important to elucidate the optimum amount of catalyst required. A plot of the catalyst concentration versus pseudo-second order reaction rate would also allow determination of the catalytic effects from the reactor wall, allowing a more accurate rate constant determination. Characterization of the solids (XRD, XPS, EDX and HR-TEM) and elemental analysis of the aqueous phase would indicate what type of inorganic species are present.

Phosphorus has been found to enhance demetallation (Panariti 2000) in addition to CCR conversion (Bearden 1981). For actual bitumen feed, phosphoric acid addition to PMA and H_2S should be tested in order to determine whether enhanced demetallation occurs which could lead to greater deposition or incorporation of Ni and V into MoS_2.

Chapter 7: Conclusions and Recommendations

7. 1 Conclusion

H-exchange between D_2O and aromatics was accelerated under CO or H_2 compared to N_2 when using MoS_2. For $CO/D_2O/H_2S$, the deuterium incorporation into naphthalene and tetralin through exchange was greater than through hydrogenation as measured by hydrogenation and exchange Indices. Dissociated H^+ from H_2O produced via exchange may reduce condensation reactions that form coke solids/asphaltenes.

In n-octane/water molecular hydrogen gave the highest hydrogenation activity compared to in-situ hydrogen generated from CO and H_2O. The activity of molecular hydrogen was dependent upon the $[H_2]$ in the liquid phase. In n-octane the second-order rate (with respect to naphthalene and hydrogen) under CO/H_2 was lower than in N_2/H_2 which may suggest competitive adsorption between CO and H_2 for sulfur vacancies on the MoS_2 surface.

Isotopic labeling using D_2O resulted in an apparent isotope effect of 1.58 for the WGS rate, similar to a quasi-equilibrium thermodynamic isotope effect reported for hydroxyl group dissociation in CH_xO-H.

Adsorption of CO onto MoS_2 begins at 160 °C and produces COS, analogous to the reduction of MoS_2 under H_2 producing H_2S. Interpretation of the υ_{CO} vibrational absorptions suggests the character of the Mo coordinatively unsaturated sites formed is similar whether MoS_2 is treated with H_2 or CO by comparison with the reported literature. υ_{CO} was observed at 2070 cm^{-1} and 2052 cm^{-1} on activated, unsupported dispersed MoS_2

which indicates two states of reduced active sites. These two υ_{CO} bands may relate to CO adsorption on edge and corner sites of hexagonal MoS_2 clusters. Comparison with theoretical calculations from literature indicates reasonable agreement with our experimental data.

Ru(0) and Ru(III) precursors did not display high WGS and HYD activity when sulfided in-situ under toluene/water emulsions at 340 °C. Incomplete sulfidation due to low temperature or H_2S pressure (15 psi) may have led to the low activity. The low activity of a RuMo catalyst was also attributed to incomplete sulfidation of the Ru precursor.

$FeSO_4$ or $VO(acac)_2$ sulfided with PMA inhibited naphthalene hydrogenation in toluene/water emulsions compared to sulfided PMA, but VMo exhibited good activity in WGS. V and Ni addition to Mo reduced naphthalene hydrogenation compared to NiMo and Mo, but VNiMo still retained higher activity than FeMo or VMo, suggesting Ni may offset the inhibition caused by V. As such, recycle of residues rich in Ni, V and Mo from a catalytic slurry upgrading process may be feasible.

Finally, a multifactorial study including temperature, H_2S and gas type (CO or H_2) of the ternary VNiMo-sulfide unsupported catalyst was conducted. Significant effects are shown in decreasing order for naphthalene hydrogenation (pseudo-second order rate constant, k_{NAPH}",

$$\text{Temperature} > \text{Temperature x Gas Type} > P_{H2S} \text{ x Gas Type}$$

ANOVA analysis of the WGS could not be performed since equilibrium conversions were observed at the beginning of the reaction. An increase in the total metal concentration from 1.10 mmol to 3.32 mmol (Mo:Ni:V = 1:0.6:0.6) increased the WGS rate by 48% and increased k_{NAPH}" by 20%.

7. 2 Recommendations

In-situ DRIFTS of the WGS should be performed on MoS_2 prepared from ATTM since the intensity of the reflected signal is greater than for MoS_2 prepared by sulfiding PMA. MoS_2 decomposed from ATTM should present less surface impurities as well. Integration of the υ_{CO} absorbances at 2070 cm^{-1} and 2052 cm^{-1} could be performed in conjunction with HR-TEM studies of the solids samples to determine whether IR intensities correlate with the MoS_2 nano-cluster morphology. TPR of MoS_2 under H_2 and CO should be compared to determine which is a stronger reductant. DRIFTS studies of CO adsorption could also be performed for the sulfides of RuMo, VMo and VNiMo.

Although Ru is expensive for a commercial slurry upgrading process, the high intrinsic activity for HDS and HYD reported in the literature makes further studies appealing. Characterization of the recovered solids by XRD, elemental analysis and TEM may indicate the type of sulfided species formed. Preparation of RuS_2 (supported or unsupported) ex-situ could be carried out under N_2/H_2S at 673 K (HYD catalyst) and 873 K(HDS catalyst). The fully sulfided catalysts could then be tested for WGS activity and in HYD and HDS with simultaneous WGS in oil/water emulsions.

The parametric study of VNiMo could be expanded to include effects due to the relative ratios of Ni:V:Mo on HYD and HDS. Additionally, star points conducted for the 2^3 factorial experiment would yield a Central Composite Design (CCD) for modeling the effects of temperature, H_2S and CO/H_2. The effect of different water contents on naphthalene hydrogenation, both under CO and H_2, should be addressed. Catalytic wall effects should be accounted for when calculating conversions and rate constants for WGS and hydrogenation. Characterization of the VNiMo and RuMo solids formed under $CO/H_2O/H_2S$ using XRD, CO adsorption ,TPR and HR-TEM should be completed to determine the degree of sulfidation and catalyst particle morphology.

Actual bitumen emulsion upgrading should be performed to determine the incorporation of Ni/V metal into produced solids. Parameters such as initial H_2S, CO/H_2 ratios, H_2O content and temperature could be varied. The Conradson Carbon Residue, HDS conversion and metals incorporation into coke/asphaltene solids could be measured to determine optimal conditions for operation.

References

Abusaido, F. S. 1999. Aromatic hydrogenation and sulfur removal via the water gas shift reaction using dispersed catalysts. M.A.Sc., University of Waterloo.

Bearden, R., and C. L. Aldridge. 1981. Novel catalyst and process to upgrade heavy oils. *Energy Progress* 1, (1), 44-8.

Breysse, M., M. Kougionas Cattenot V., J. C. Lavalley, F. Mauge, J. L. Portefaix, and J. L. Zotin. 1997. Hydrogenation properties of ruthenium sulfide clusters in acidic zeolites. *Journal of Catalysis,* 168, 143-153.

Bunluesin, T., R. J. Gorte, and G. W. Graham. 1998. Studies of the water-gas-shift reaction on ceria-supported pt, pd, and rh: Implications for oxygen-storage properties. *Applied Catalysis B: Environmenta,l* 15, 107-114.

California Air Resources Board. The california diesel fuel regulations. [cited 02/01 2009]. Available from www.arb.ca.gov/fuels/diesel/081404dlsregs.pdf.

Castillo-Villalon, P., J. Ramirez, C. Louis, and P. Massiani. 2008. Characterization and catalytic performance of ruthenium sulfide catalysts supported on H-BEA, na- and cs-H-BEA zeolites. *Applied Catalysis A: General,* 343, 1-9.

Castillo-Villalon, P., J. Ramirez, and F. Mauge. 2008. Structure, stability and activity of RuS_2 supported on alumina. *Journal of Catalysis,* 260, 65-74.

Chinchen, G. C., and M. S. Spencer. 1988. A comparison of the water-gas shift reaction on chromia-promoted magnetite and on supported copper catalysts. *Journal of Catalysis,*112, 325-327.

Cooper, B. H., and B. B. L. Donnis. 1996. Aromatic saturation of distillates: An overview. *Applied Catalysis A: General,* 137, 203-223.

Cotton, F. A., and G. Wilkinson. 1988. *Advanced inorganic chemistry*. 5th ed. New York: Wiley and Sons.

Duarte de Farias, A. M., P. Bargiela, M. da Graca, and M. A. Fraga. 2008. Vanadium-promoted Pt/CeO_2 catalyst for water-gas shift reaction. *Journal of Catalysis,* 260, 93-102.

Dunn, J. A., J. B. MacLeod, R. D. Myers, and R. Jr Bearden. 2003. Recycle of vanadium and nickel-based catalysts in a hydroconversion process. *Energy & Fuels,* 17, 38-45.

Eijsbouts, S., S. W. Mayo, and K. Fujita. 2007. Unsupported transition metal sulfide catalysts: From fundamentals to industrial application. *Applied Catalysis A: General,* 322, 58-66.

Environment Canada. Cold lake bitumen. [cited 02/05 2009]. Available from www.etc-cte.ec.gc.ca/databases/OilProperties/pdf/WEB_Cold_Lake_Bitumen.pdf.

Fachinetti, G., T. Funaioli, L. Lecci, and F. Marchetti. 1996. Ru3(CO)12 in acidic media. intermediates of the acid-cocatalyzed water-gas shift reaction (WGSR). *Inorganic Chemistry,* 35, 7217-7224.

Frye, C. G., and A. W. Weitkamp. 1969. Equilibrium hydrogenations of multi-ring aromatics. *Journal of Chemical Engineering Data* 14, (3): 372.

Fu, Y. C., K. Ishikuro, T. Fueta, and M. Akiyoshi. 1995. Hydrogenation of model compounds in syngas-D_2O systems. *Energy and Fuels,* 9, 406-12.

Garnett, J. L., and W. A. Sollich-Baumgartner. 1966. Pi complex adsorption in hydrogen exchange. *Advances in Catalysis,* 16, 95.

Geantet, C., S. Gobolos, J. A. De Los Reyes, M. Cattenot, M. Vrinat, and M. Breysse. 1991. Ruthenium molybdenum sulfide catalysts: Physicochemical characterization and catalytic properties in HDS, hydrogenation and HDN reactions. *Catalysis Today,* 10, 661-680.

Gines, M. J. L., A. J. Marchi, and C. R. Apesteguia. 1997. Kinetic study of the reverse water-gas shift reaction over CuO/ZnO/Al_2O_3 catalysts. *Applied Catalysis A: General,* 154, 155-171.

Ho, T. C. 2004. Deep HDS of diesel fuel: Chemistry and catalysis. *Catalysis Today,* 98, 3-18.

———. 1994. Hydrogenation of mononuclear aromatics over a sulfided-NiMo/Al_2O_3 catalyst. *Energy & Fuels,* 8, (6), 1149-1151.

Hochhauser, A. M. 2008. Gasoline and other motor fuels. In *Kirk-othmer encyclopedia of chemical technology.* Vol. 12.

Hook, B. D., and A. Akgerman. 1986. Desulfurization of dibenzothiophene by in situ hydrogen generation through a water gas shift reaction. *Industrial Engineering and Chemistry Process Design and Development,* 25, 278-284.

Hou, P., D. Meeker, and H. Wise. 1983. Kinetic studies with a sulfur-tolerant water gas shift catalyst. *Journal of Catalysis,* 80, 280-5.

Hubaut, R. 2007. Vanadium-based sulfides as hydrotreating catalysts. *Applied Catalysis A: General,* 322, 121-128.

Jacobs, G., S. Khalid, P. M. Patterson, D. E. Sparks, and B. H. Davis. 2004. Water-gas shift catalysis: Kinetic isotope effect identifies surface formates in rate limiting step for Pt/ceria catalysts. *Applied Catalysis A: General,* 268, 255-66.

Jacobsen, C. J. H., E. Tornqvist, and H. Topsoe. 1999. HDS, HDN and HYD activities and temperature-programmed reduction of unsupported transition metal sulfides. *Catalysis Letters,* 63, 179-183.

Kerby, M. C., T. F. Degnan Jr., D. O. Marler, and J. S. Beck. 2005. Advanced catalyst technologies and applications for high quality fuels and lubricants. *Catalysis Today,* 104, 55-63.

Kim, C. S., and F. E. Massoth. 1993. Deactivation of a Ni/Mo hydrotreating catalyst by vanadium deposits. *Fuel Processing Technology,* 35, 289-302.

Kim, D. K., and E. Iglesia. 2008. Isotopic and kinetic assessment of the mechanism of CH_3OH-H_2O catalysis on supported copper clusters. *Journal of Physical Chemistry C,* 112, 17235-17243.

Koizumi, N., G. Bian, K. Murai, T. Ozaki, and M. Yamada. 2004. In situ DRIFT studies of sulfided K-mo/γ-Al_2O_3 catalysts. *Journal of Molecular Catalysis A: Chemical,* 207, 173-182.

Lacroix, M., N. Boutarfa, C. Guillard, M. Vrinat, and M. Breysse. 1989. Hydrogenating properties of unsupported transition metal sulphides. *Journal of Catalysis,* 120, 473-477.

Lacroix, M., M. Guillard, M. Breysse, and M. Vrinat. 1992. Preparation characterization and catalyitc properties of unsupported and molybdenum-promoted vanadium sulfides. *Journal of Catalysis,* 135, 304-309.

Laine, R. M., and E. J. Crawford. 1988. Homogeneous catalysis of the water-gas shift reaction. *Journal of Molecular Catalysis,* 44, 357-387.

Lauritsen, J. V., M. Nyberg, J. K. Norskov, B. S. Clausen, H. Topsoe, E. Laegsgaard, and F. Besenbacher. 2004. Hydrodesulfurization pathways on MoS2 nanoclusters revealed by surface tunneling microscopy. *Journal of Catalysis,* 224, 94-106.

Ledoux, M. J., O. Michaux, S. Hantzer, P. Panissod, P. Petit, J. J. Andre, and H. J. Callot. 1987. Hydrodesulfurization (HDS) poisoning by vanadium compounds: EPR and metal solid NMR analysis. *Journal of Catalysis,* 106, 525.

Lee, R. Z., and F. T. T. Ng. 2006. Effect of water on HDS of DBT over a dispersed mo catalyst using in situ generated hydrogen. *Catalysis Today,* 116, 505-511.

Lee, Z. 2004. Investigation of hydrodesulfurization of dibenzothiophene and hydrodenitrogenation of qunioline using *in-situ* H_2 Generated via water gas shift reaction over dispersed mo-based catalysts. Ph.D., University of Waterloo.

Lima Junior, I., J. M. Millet, M. Aouine, and M. do Carmo Rangel. 2005. The role of vanadium on the properties of iron based catalysts for the water gas shift reaction. *Applied Catalysis A: General,* 283, (91-98).

Little, L. H. 1966. *Infrared spectra of adsorbed species*.

Liu, K. 2008. Unpublished results.

Liu, K., C. Choy, and F. T. T. Ng. 2007. Hydrotreating synthetic crude with in-situ hydrogen and nano-dispersed mo catalyst.

Liu, K., and F. T. T. Ng. 2008. Use of nano-dispersed molybdenum based catalysts for upgrading heavy oils. Paper presented at Canadian Symposium on Catalysis, Kingston, ON.

Liu, Y., W. Shen, Y. Song, and J. Cheng. 2006. The mechanism of diesel hydrogenation using supercritical water-syngas. *Petroleum Science and Technology,* 24, (11), 1283-1289.

Lund, C. R. F. 1996. Microkinetics of water-gas shift over sulfided Mo/Al_2O_3 catalysts. *Industrial Engineering and Chemistry Research,* 35, 2531-2538.

Madix, R., and S. G. Telford. 1992. The kinetic isotope effect for C-H bond activation on cu(110): The effects of tunneling. *Surface Science,* 277, 246-252.

Maegawa, T., A. Akashi, and H. Sajiki. 2006. A mild and facile method for complete hydrogenation of aromatic nuclei in water. *Synthesis Letters,* 9, 1440-1442.

Marzin, R., Pereira, P., Zacarias, L., Rivas, L., McGrath, M. and Thompson, G. J. Resid conversion through the aquaconversion technology - an economical and environmental solution. 1986 [cited 02/28 2009]. Available from www.oildrop.org/Info/Centre/Lib/7thConf/19980086.pdf.

Mauge, F., J. Lamotte, N. S. Nesterenko, O. Manioilova, and A. A. Tsyganenko. 2001. FT-IR study of surface properties of unsupported MoS2. *Catalysis Today,* 70, 271-84.

Mauge, F., and J. C. Lavalley. 1992. FT-IR study of CO adsorption on sulfided Mo/Al_2O_3 unpromoted or promoted by metal carbonyls: Titration of sites. *Journal of Catalysis,* 137, 69-76.

McVicker, G. B., M. Daage, M. S. Touvelle, C. W. Hudson, D. P. Klein, W. C. Baird Jr., B. R. Cook, et al. 2002. Selective ring opening of naphthenic molecules. *Journal of Catalysis,* 210, 137-148.

Meunier, F. C., D. Reid, A. Goguet, S. Shekhtman, C. Hardacre, R. Burch, W. Deng, and M. Flytzani-Stephanopoulos. 2007. Quantitative analysis of the reactivity of formate species seen over a Au/Ce(la)O_2 water-gas shift catalyst: First unambiguous evidence of the minority role of formates as reaction intermediates. *Journal of Catalysis,* 247, 277-287.

Milad, I. K. 1994. Kinetic study of catalytic desulphurization in an emulsion via in-situ generated H_2. M.A.Sc., University of Waterloo.

Miller, J. T., and R. B. Fisher. 1999. Structural determination by XAFS spectroscopy of non-porphyrin nickel and vanadium in maya residuum, hydrocracked residuum and toluene-insoluble solid. *Energy & Fuels,* 13, 719-727.

Mitchell, P. C. H., C. E. Scott, J. P. Bonnelle, and J. Grimblot. 1987. Ru/Alumina and ru-Mo/Alumina catalysts: An XPS study. *Journal of Catalysis,* 107, 482-489.

Moe, J. M. 1962. Design of water-gas shfit reactors. *Chemical Engineering Progress,* 58, (3), 33.

Moll, Jennifer. 1999. Feasibility study on desulphurization of bitumen emulsion using hydrogen from the water gas shift reaction. M.A.Sc., University of Waterloo.

Monteiro-Gezork, A. C. A., R. Natividad, and J. M. Winterbottom. 2008. Hydrogenation of naphthalene on NiMo- ni- and Ru/Al_2O_3 catalysts: Langmuir-hinshelwood kinetic modelling. *Catalysis Today,* 130, 471-485.

Muller, B., A. D. van Langeveld, J. A. Moulijn, and H. Knozinger. 1993. Characterization of sulfided Mo/Al_2O_3 catalysts by temperature-programmed reduction and low-temperature fourier transform infrared spectroscopy of adsorbed carbon monoxide. *Journal of Physical Chemistry,* 97, 9028-9033.

Ng, F. T. T., and S. K. Tsakiri. 1993. Homogeneous catlysis of water-gas shift reaction in emulsions. *Fuel,* 72, 211-215.

———. 1992. Activation of water in emulsion for catalytic desulphurization of benzothiophene. *Fuel,* 71, 1309-14.

———. 1989. *Upgrading crude oil emulsions.* Patent 5055175, filed 1989, and issued July 14, 1989.

Osada, M., N. Hiyoshi, O. Sato, K. Arai, and M. Shirai. 2008. Subcritical water regeneration of supported ruthenium catalyst poisoned by sulfur. *Energy & Fuels,* 22, (2), 845-849.

Panariti, N., A. Del Bianco, and Del Piero, G. Marchionna, M. 2000. Petroleum residue upgrading with dispersed catalysts part 1. catalysts activity and selectivity. *Applied Catalysis A: General,* 204, 203-213.

Payne, M., D. L. Leussing, and S. G. Shore. 1991. Kinetics of ^{13}CO exchange with ^{12}CO in $[HM_3(CO)_{11}]^-$ and $[DM_3(CO)_{11}]^-$ (M = ru, ox): Study of the effects of ion pairing and deuterium labeling on the exchange process and hydride activation. *Organometallics,* 10, 574-580.

Pecoraro, T. A., and R. R. Chianelli. 1981. Hydrodesulfurization catalysis by transition metal sulfides. *Journal of Catalysis,* 67, 430-445.

Rana, M. S., V. Samano, J. Ancheyta, and J. A. I. Diaz. 2007. A review of recent advances on process technologies for upgrading of heavy oils and residua. *Fuel,* 86, 1216-31.

Ratnasamy, P., and J. Fripiat. 1970. Surface chemistry of sulfides. part I. - infra-red study of molybdenum and germanium sulfides and of their reaction with H_2, H_2O, thiophene, and ethanethiol. *Transactions of the Faraday Society,* 66, 2897.

Rintjema, R. 1992. Hydrodesulphurization of benzothiophene emulsions through in situ hydrogen generation. M.A.Sc., University of Waterloo.

Roland, T. F., J. Borysow, and M. Fink. 2006. Surface mediated isotope exchange reactions between water and gaseous deuterium. *Journal of Nuclear Materials,* 353, 193-201.

Roof, J. G. 1970. Three-phase critical point in hydrocarbon-water systems. *Journal of Chemical and Engineering Data,* 15, 301-303.

Sapre, A., and B. Gates. 1981. Hydrogenation of aromatic hydrocarbons catalyzed by sulfided $CoO\text{-}MoO_3/Al_2O_3$. reactivities and reaction networks. *Industrial Engineering and Chemistry Process Design and Development,* 20, 68-73.

Sarbak, Z. 2005. FT-IR studies on coke formation over low loaded mo catalyst supported on Al_2O_3. *Reaction Kinetics and Catalysis Letters,* 84, (2), 263-270.

Schweighardt, F. K., B. C. Bockrath, R. A. Friedel, and H. L. Retcofsky. 1976. Deuterium magnetic resonance spectrometry as a tracer tool in coal liquefaction processes. *Analytical Chemistry,* 48, (8), 1254-5.

Semple, K., N. Cyr, P. M. Fedorak, and D. W. S. Westlake. 1990. Characterization of asphaltenes from cold lake heavy oil: Variations in chemical structure and composition with molecular size. *Canadian Journal of Chemistry,* 68, 1092-1099.

Shido, T., and Y. Iwasawa. 1993. Reactant-promoted reaction mechanism for water-gas shift reaction on rh-doped CeO_2. *Journal of Catalysis,* 141, 71.

Siewe, C. N., and F. T. T. Ng. 1998. Hydrodesulfurization of cold lake diesel fraction using dispersed catalysts: Influence of hydroprocessing medium and sources of H_2. *Energy & Fuels,* 12, 598-606.

Skowronski, R. P., J. J. Ratto, I. B. Goldberg, and L. A. Heredy. 1984. Hydrogen incorporation during coal liquefaction. *Fuel,* 63, 441.

Song, Tao, Zisheng Zhang, Jinwen Chen, Zbigniew Ring, Hong Yang, and Ying Zheng. 2006. Effect of aromatics on deep hydrodesulfurization of dibenzothiophene and 4,6-dimethyldibenzothiophene over $NiMo/Al_2O_3$ catalyst. *Energy and Fuels,* 20, 2344-2349.

Speight, J. G. 2006. Petroleum refinery processes. In *Kirk-othmer encyclopedia of technology.* Online ed. Vol. 18. Wiley Interscience.

Takemura, Y., H. Itoh, and K. Ouchi. 1981. Catalytic hydrodesulfurization of residual oil by a mixture of carbon monoxide and water. *Journal of the Japanese Petroleum Institute* 24, (6), 357-362.

Travert, A., C. Dujardin, F. Mauge, S. Cristol, J. F. Paul, E. Payen, and D. Bougeard. 2001. Parallel between infrared characterization and ab initio calculations of CO adsorption on sulphided mo catalysts. *Catalysis Today* 70, (255), 269.

Tsyganenko, A. A., F. Can, A. Travert, and F. Mauge. 2004. FTIR study of unsupported molybdenum sulfide-in situ synthesis and surface properties characterization. *Applied Catalysis A: General,* 268, 189-197.

Vernon, L. W. 1980. Free radical chemistry of coal liquefaction: Role of molecular hydrogen. *Fuel,* 59, 102-106.

Yasuda, H., Higo, M., Yoshitomi, S., Sato, T., Imamura, M., Matsubayashi, H., Shimada, H., Nishijima, A., Yoshimura, Y. 1997. Hydrogenation of Tetralin over sulfided nickel-tungstate/alumina and nickel-molybdate/alumina catalyst. *Catalysis Today*. 39, 77-87.

Young, D. C., R. I. McNeil, D. C. Cronauer, R. G. Ruberto, and L. G. Galya. 1984. Characterization of isotopically labeled coal liquefaction solvents and products by deuterium and carbon-13 nuclear magnetic resonance spectrometry. *Analytical Chemistry,* 56, 557-62.

Yu, J., F. J. Tian, and C-Z Li. 2007. Novel water-gas shift reaction catalyst from iron-loaded victorian brown coal. *Energy & Fuels,* 21, 395-398.

Yumoto, M., S. G. Kukes, M. T. Klein, and B. C. Gates. 1996. Catalytic hydroprocessing of aromatic compounds: Effects of nickel and vanadium sulfide deposits on reactivities and reaction networks. *Industrial Engineering and Chemistry Research,* 35, 3203-3209.

Zeng, T., X. D. Wen, Y. W. Li, and H. Jiao. 2005. Density functional theory study of triangular molybdenum sulfide nanocluster and CO adsorption on it. *Journal of Physical Chemistry B,* 109, 13704-13710.

———. 2005. Removal of surface sulfur from MoSx cluster under CO adsorption. *Journal of Molecular Catalysis A: Chemical,* 241, 219-226.

Zeng, T., X. D. Wen, G. S. Wu, Y. W. Li, and H. Jiao. 2005. Density functional theory study of CO adsorption on molybdenum sulfide. *Journal of Physical Chemistry B,* 109, 2846-2854.

Zhang, A. 2005. Aromatics hydrogenation via water gas shift reaction over unsupported catalysts. M.A.Sc., University of Waterloo.

Zhang, S., D. Liu, W. Deng, and G. Que. 2007. A review of slurry-phase hydrocracking heavy oil technology. *Energy & Fuels,* 21, (6), 3057-3062.

APPENDICES

Appendix A: Analytical Methods

Liquid Phase Analysis

The organic liquid product was analyzed on a Varian CP-3800 GC-FID with a 30 m x 0.32 mm VF-5MS column. The temperature program is listed below (Table A1).

Table A. 1: Temperature Ramp for Varian CP-3800 Liquid Product Analysis

Rate (°C / min)	**Temperature (°C)**	**Time at Temperature (min)**	**Total Time (min)**
	80		
5.0	120	0	8.00
2	134	0	15.00

He Flow: 23.0 ml/min

Table A. 2: Varian CP-3800 Operating Temperatures

Rate (°C / min)	**Temperature (°C)**	**Time at Temperature (min)**	**Total Time (min)**
Sample Inlet Temp. (°C)			
Injector Temperature (°C)	300		
Detector Temperature (°C)	134	0	15.00

Table A. 3: Retention Times of Naphthalene and Hydrogenated Products

Retention Time (min)	**Compound name**
7.25	Trans-decalin
8.37	Cis-decalin
10.08	Tetralin
10.99	Naphthalene

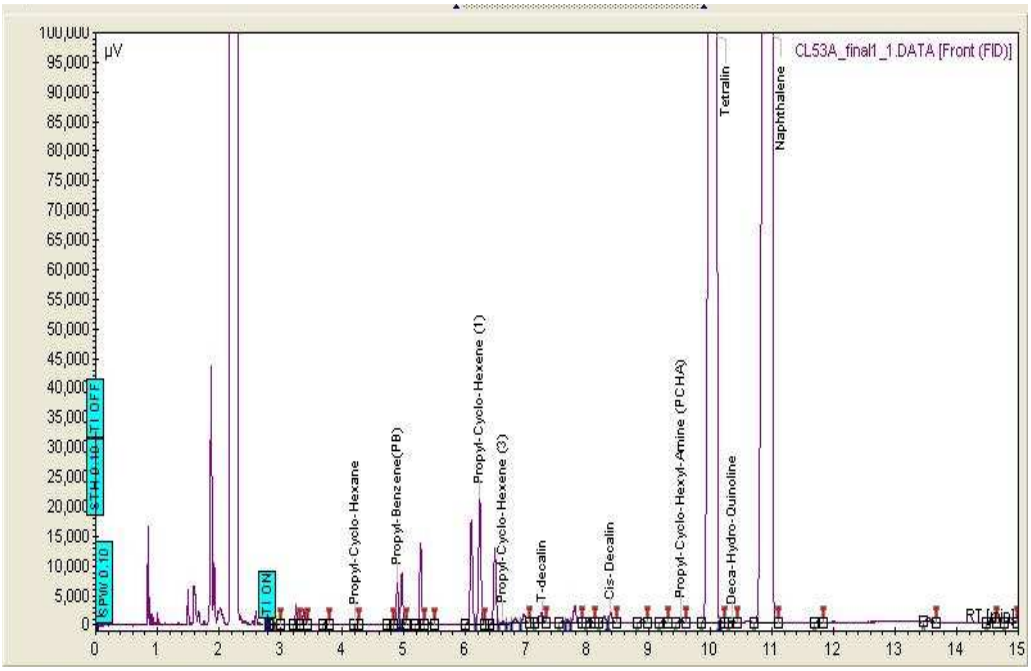

Figure A. 1: Representative GC-FID Chromatogram of Liquid Organic products from Naphthalene Hydrogenation

Gas Phase Analysis

Gas phase samples were collected in a 5 mL gas-tight syringe with valve. An Agilent 3000A MicroGC was used for analysis. The conditions are listed in Table A4. H_2, N_2, O_2, CO were analyzed on a Mol. Sieve 5A column using argon for sensitivity to H_2. CO_2, methane, propane, propylene, H_2S and COS were analyzed using a PLOT U column running helium. A standard RGA calibration mixture supplied by Agilent was used to calibrate the MicroGC bi-weekly. H_2S and COS were calibrated using a Certified Standard supplied by Praxair of 2.54 vol% H_2S and 5.02 vol% COS.

Table A. 4: Agilent 3000A MicroGC Operating Conditions

3000A GC Setpoints	***Column A***	***Column B***	***Column C***	***Column D***
Sample Inlet Temp. (°C)	100	Same as A	Same as A	Same as A
Injector Temperature (°C)	100	100	100	100
Column Temperature (°C)	110	100	140	90
Sampling Time (s)	30	30	Same as B	Same as B
Inject Time (ms)	200	20	20	20
Run Time (min)	120	120	120	120
Post Run Time (min)	10	10	10	10
Pressure Equilibration Time (s)	20	20	20	20
Column Pressure (psi)	40.00	36.00	36.00	36.00
Post Run Pressure (psi)	40.00	36.00	36.00	36.00
Detector Sensitivity	Standard	Standard	Standard	Standard
Detector Data Rate (Hz)	50	50	50	50
Baseline Offset (mV)	0	0	0	0
Backflush Time (s)	11.0	6.5	8.0	n/a
Injector Type	Backflush	Backflush	Backflush	Fixed Volume
Carrier Gas	Argon	Helium	Helium	Helium
Column Type	Mol. Sieve 5A	PLOT U	Alumina	OV-1
Detector Type	TCD	TCD	TCD	TCD
Inlet Type	Heated	Heated	Heated	Heated
Column Dimension	10 m x 0.32 mm x 30 μm	8 m x 0.32 mm x 30 μm	10 m x 0.32 mm x 8 μm	10 m x 0.15 mm x 2 μm
Precolumn Type	PLOT U	PLOT Q	Alumina	n/a
Precolumn Dimensions	3 m x 0.32 m x 30 μm	1 m x 0.32 mm x 10 μm	1 m x 0.32 mm x 3 μm	10 m x 0.15 mm x 2 μm
Injector Volume (μl)	1.0 backflush	1.0 backflush	0.4 backflush	1.6 backflush

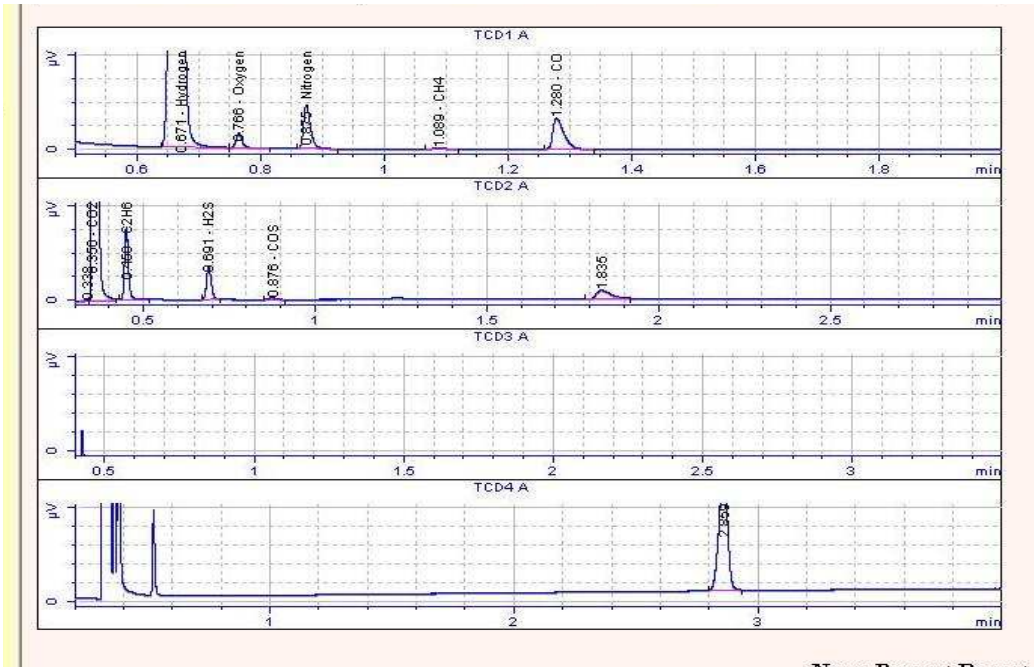

Figure A. 2: Representative GC-TCD Chromatogram of Gas Phase species

Appendix B: Experimental Data

Sample Data including Figures:

Experimental Conditions for #46: ($CO//H_2/H_2O/H_2S$, 22.5 psig H_2S, 577.5 psig (1:1 = $CO:H_2$), 4.0°C/min, 360 °C, 2 hrs, 10 ml H_2O, 100 ml toluene, 10.0 g NAPH, 1.50 mmole Mo; 0.91 mmoles $NiSO_4$; 0.91 mmoles $VO(acac)_2$)

Table B.46. 1: Mass of Samples, Experiment #46

Sample #	Reaction Time (min)	Mass of Empty Vial (g)	Mass of sample + vial (g)	mass of liquid sample (g)
Purge		16.42	19.015	2.5946
1	0	16.587	18.739	2.1516
2		16.492	17.883	1.3911
2B	20.25	16.391	18.701	2.3093
3		16.371	17.454	1.0833
3B	39.75	16.51	18.8	2.2903
4		16.452	17.564	1.1126
4B	62.75	16.487	18.822	2.3343
5		16.492	17.967	1.4746
5B	104.75	16.45	18.694	2.2437
6		16.58	17.49	0.914
6B	119.75	16.4	18.771	2.3707

Table B.46. 2: GC Analysis, Experiment #46

Reaction Time (min)	0	20.25	39.75	62.75	104.75	119.75	Final
[NPT] (mol/g-liq)	0.000917	0.000805	0.000759	0.000695	0.000626	0.000605	0.000479
[TET] (mol/g-liq)	0.000284	0.000379	0.000478	0.000563	0.000623	0.000644	0.000533
[c-DEC] (mol/g-liq)	1.69E-07	2.89E-07	4.82E-07	7.84E-07	1.08E-06	1.21E-06	9.89E-07
[t-DEC] (mol/g-liq)	3.13E-07	5.79E-07	8.92E-07	1.57E-06	1.88E-06	2.21E-06	3.18E-06
$[NPT] = [NPT]_0 - [TET]-[DEC]$	0.000916	0.00082	0.000721	0.000635	0.000575	0.000553	0.000664

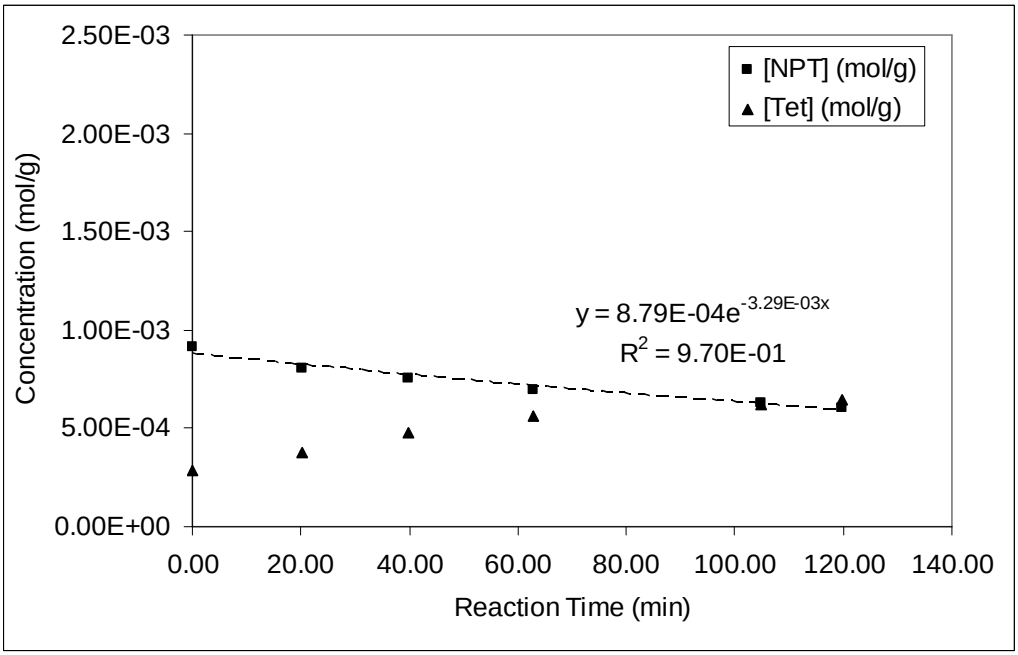

Figure B.46. 1: Liquid Concentrations, Experiment #46

Table B.46. 3: GC Analysis, ESTD mol%, Experiment #46

Reaction Time (min)	0	20.25	39.75	62.75	104.75	119.75	Final
H2	30.07429	27.84524	26.4261	25.43746	24.28098	24.16692	50.30766
O2	9.83826	9.64063	9.91633	9.967585	10.15451	10.13501	2.42214
N2 Total	37.9341	37.05327	37.91671	38.1216	38.79734	38.73345	9.758667
CH4	0.07729	0.09033	0.099635	0.109334	0.116715	0.11857	0.162667
CO	3.43802	2.083535	1.46754	1.184365	0.90609	0.944935	13.54203
CO2	16.50438	18.61863	19.61847	20.6667	21.19443	21.43949	23.8155
C2H4	0	0	0	0	0	0	0
C2H6	0.15326	0.161515	0.164705	0.17026	0.16973	0.169715	0.165677
C2H2	0	0	0	0	0	0	0
H2S	1.349165	1.42875	1.428025	1.46343	1.473405	1.473365	0.993283
COS	0	0	0	0	0	0	0.06518
1,2-Prop=	0	0	0	0	0	0.012005	0
Water	0.40971	0	0	0	0	0	0
Prop	0	0	0	0	0	0	0
C3	0	0	0	0	0	0	0
n-C4	0	0	0	0	0	0	0
i-C4	0	0	0	0	0	0	0
n-C6	0	0	0	0	0	0	0
n-C8	0	0	0	0	0	0	0

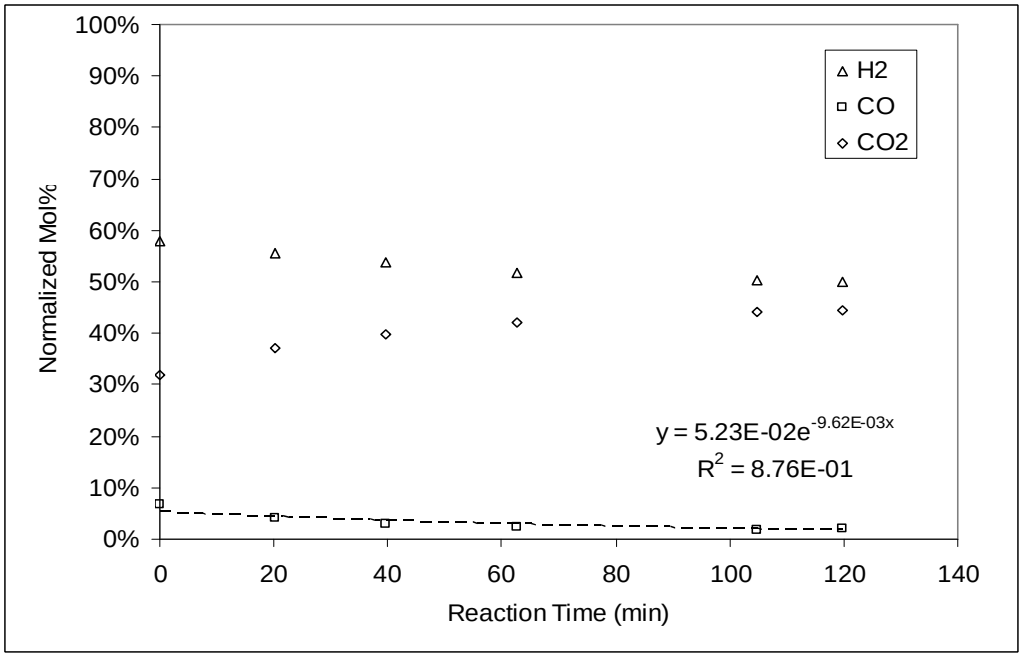

Figure B.46. 2 Normalized Gas Composition, Experiment #46

Table B.46. 4: GC Analysis, Experiment #46

Reaction Time (min)	0	20.25	39.75	62.75	104.75	119.75
Total calculated moles of gas in sampling bomb (moles)	0.008718	0.008577	0.008463	0.008406	0.008421	0.008348
[H2] (mol/g-liq)	0.001219	0.00111	0.001039	0.000994	0.00095	0.000938
[CO] (mol/g-liq)	0.000139	8.31E-05	5.77E-05	4.63E-05	3.55E-05	3.67E-05
[CO2] (mol/g-liq)	0.000669	0.000742	0.000772	0.000807	0.00083	0.000832

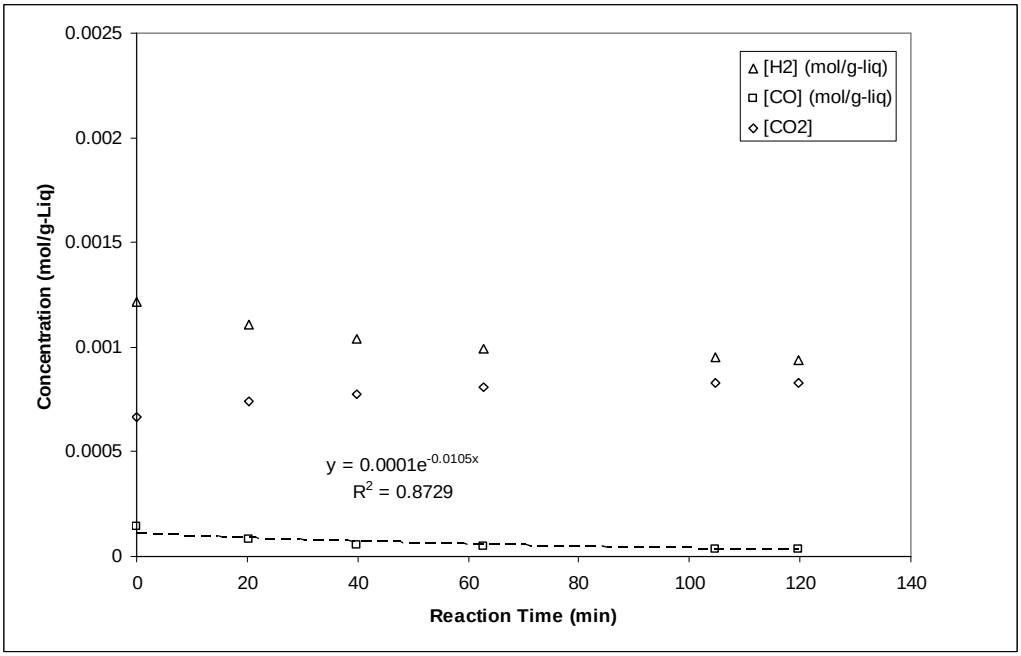

Figure B.46.3: Gas Concentration, Experiment #46

B 1. Deuterium Labeling and NMR Experiments

Experiment conditions for #2R1: $H_2/D_2O/H_2S$, 15 psig H_2S, 585 psig H_2, 4.0°C/min, 340 °C, 3 hrs, 10 ml D_2O, 100 ml n-octane, 3.7 g NAPH, 0.39 mmoles Mo, 1500 RPM Impeller Speed

Table B.2.2. 1: Mass of Samples, Experiment #2R1

Reaction Time (min)	4.67	40.67	81.17	116.17	152.17	180
Mass of Empty Vial	16.8256	16.9281	16.7142	16.7145	16.7682	16.7874
Mass of sample + vial	17.9359	19.0405	18.3061	18.6766	18.7312	18.0182
mass of liquid sample	1.1103	2.1124	1.5919	1.9621	1.963	1.2308

Table B.2.2. 2: GC Liquid Analysis, Experiment #2R1

Reaction Time (min)	4.67	40.67	81.17	116.17	152.17	180	Final
[NPT] (mol/g-liq)	0.000461	0.000328	0.000218	0.00014	9.13E-05	5.52E-05	0.000102
[Tet] (mol/g-liq)	2.5E-05	0.000158	0.000268	0.000346	0.000395	0.000431	0.000497

Table B.2.2. 3: GC Gas Analysis, ESTD mol%, Experiment #2R1

Reaction Time (min)	4.67	40.67	81.17	116.17	152.17	180
H2	30.18806	34.57954	33.09117	32.32426	31.89249	48.18291
O2	14.61807	13.86178	14.16013	14.3369	14.43238	10.432
N2	50.66164	47.93423	49.01484	49.59892	49.90676	36.46792
CH4		0	0	0	0	0
CO	1.011228	0	0	0	0	0
CO2	0	0	0	0	0	0
C2H6	0	0.055044	0.059363	0.059042	0.062815	0.109502
C2H2						
H2S	1.094662	1.289045	1.357886	1.354321	1.43379	2.576758
COS	0	0	0	0	0	0
n-C4					0	0.011011
i-C4	0.03166		0	0	0	0.025328
n-C6	0.006609	0.004699	0.009555	0.010036	0.010373	0.011079
n-C8	2.348634	2.285669	2.307055	2.316523	2.261387	2.168703

Table B.2.2. 4: Calculated Concentrations of Deuterated Organics from NMR

Reaction Time (min)	0.166667	36.16667	76.66667	111.6667	147.6667	180
mass of empty vial (g)	2.4377	2.4421	2.449	2.4358	2.4474	2.4602
m2 = mass of vial + NMR sample	2.84344	2.7788	2.7994	2.8571	2.8328	2.8573
m3 = m2 + n-C8 diluent (GC sample)	3.0856	3.0497	3.0582	3.1316	3.1126	3.1304
[NAPH] NMR sample (g/g)	0.014643	0.01878	0.006108	0.006265	0.002624	0.001204
[NAPH] diluted-GC sample (mol/g)	7.15E-05	8.12E-05	2.74E-05	2.96E-05	1.19E-05	5.57E-06
[NAPH] (mol/g) NMR sample	0.000114	0.000147	4.77E-05	4.89E-05	2.05E-05	9.39E-06
[TET] NMR Sample (g/g)	0.001086	0.00945	0.00871	0.017672	0.012301	0.011297
[TET] GC sample (mol/g)	5.14E-06	3.96E-05	3.79E-05	8.09E-05	5.39E-05	5.06E-05
[t-DEC] NMR Sample (g/g)	0	3.61E-05	5.22E-05	0.000165	0.000161	0.000231
[c-DEC] NMR Sample (g/g)	0	0	1.74E-05	0.000121	0.000104	0.000152
[d6-Acetone] GC sample (mol/g)	9.35E-05	4.07E-05	4.24E-05	4.31E-05	2.69E-05	4.03E-05
[d6-acetone] in NMR sample (g/g)	0.009565	0.004704	0.004723	0.004553	0.002969	0.00436
mol of total Naph/mol of n-C8 (from GC)						
Total NAPH mol / mol n-C8	0.013387	0.017305	0.005552	0.005748	0.002381	0.001092
Total Tetralin mol / mol n-C8	0.000962	0.008443	0.007676	0.01572	0.010824	0.009931
[NAPH] reactor sample (mol/g)						
[TET] reactor sample (mol/g)						
molar ratios from ^{1}H-NMR Integration						
MOL I / MOL n-Octane] (calculated from n-Octane $-CH_3$ NMR resonance)						
Naphthalene A	0.005522	0.005969	0.001952	0.001945	0.000785	0.000351
Naphthalene B	0.007345	0.006745	0.001952	0.001945	0.000785	0.000351
Tetralin Ar	0.000331	0.002686	0.002733	0.005251	0.003689	0.003401
Tetralin B	0.000442	0.003164	0.003319	0.006029	0.00416	0.003787
% ^{1}H-Incorporation						
Reaction Time (min)	0.17	36.17	76.67	111.67	147.67	180.00
NAPH A mol%	41.25%	34.50%	35.16%	33.83%	32.96%	32.12%
NAPH B mol%	54.86%	38.98%	35.16%	33.83%	32.96%	32.12%
TET Aromatic mol%	34.43%	31.82%	35.60%	33.40%	34.08%	34.25%
Tet Sat mol%	45.90%	37.47%	43.23%	38.35%	38.43%	38.13%

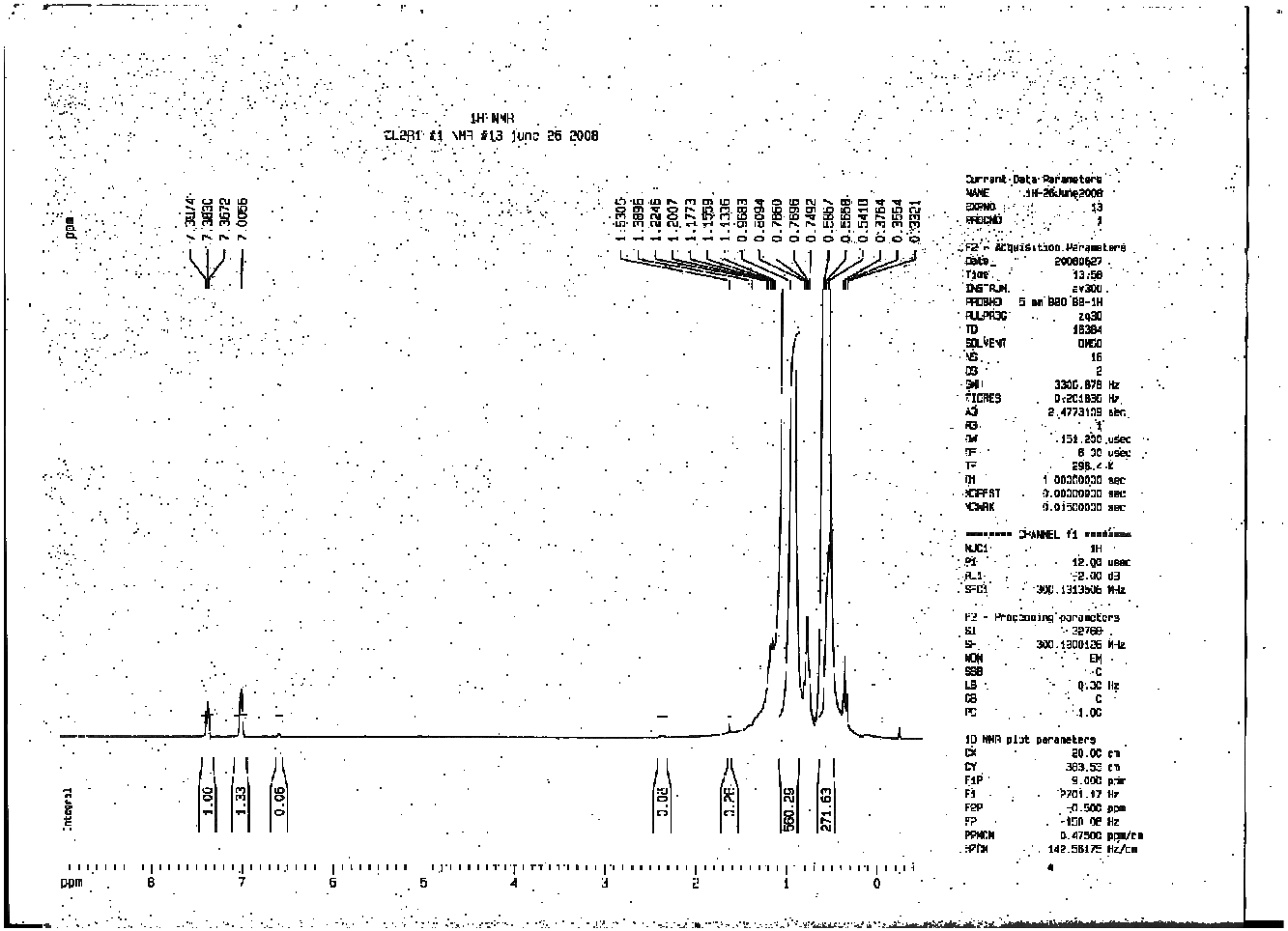

Figure B.2.2. 1: ^{1}H-NMR Spectrum of naphthalene and tetralin in n-octane, sample #1, Experiment #2R1

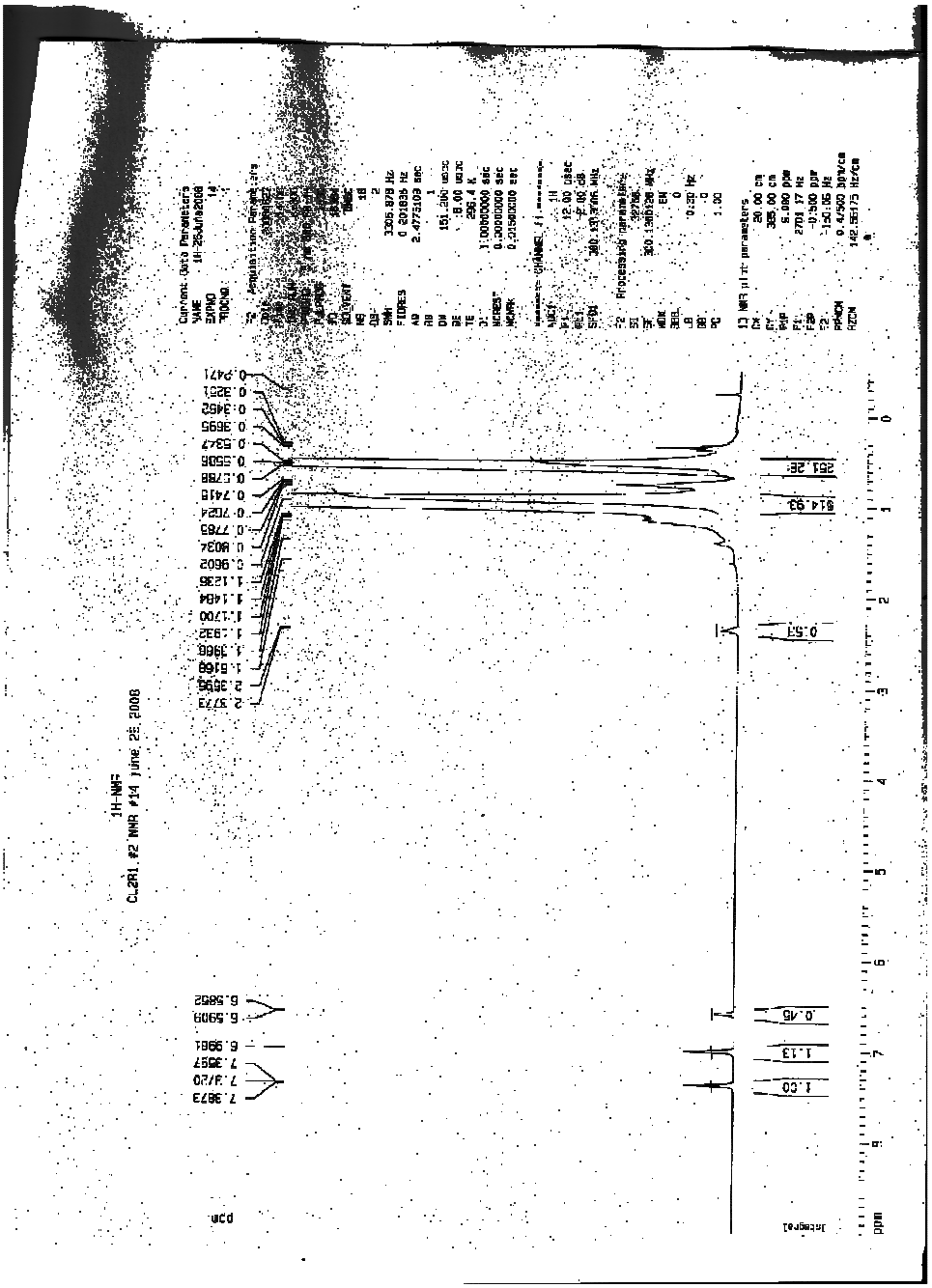

Figure B2.2. 2: ^{1}H-NMR Spectrum of naphthalene and tetralin in n-octane, sample #2, Experiment #2R1

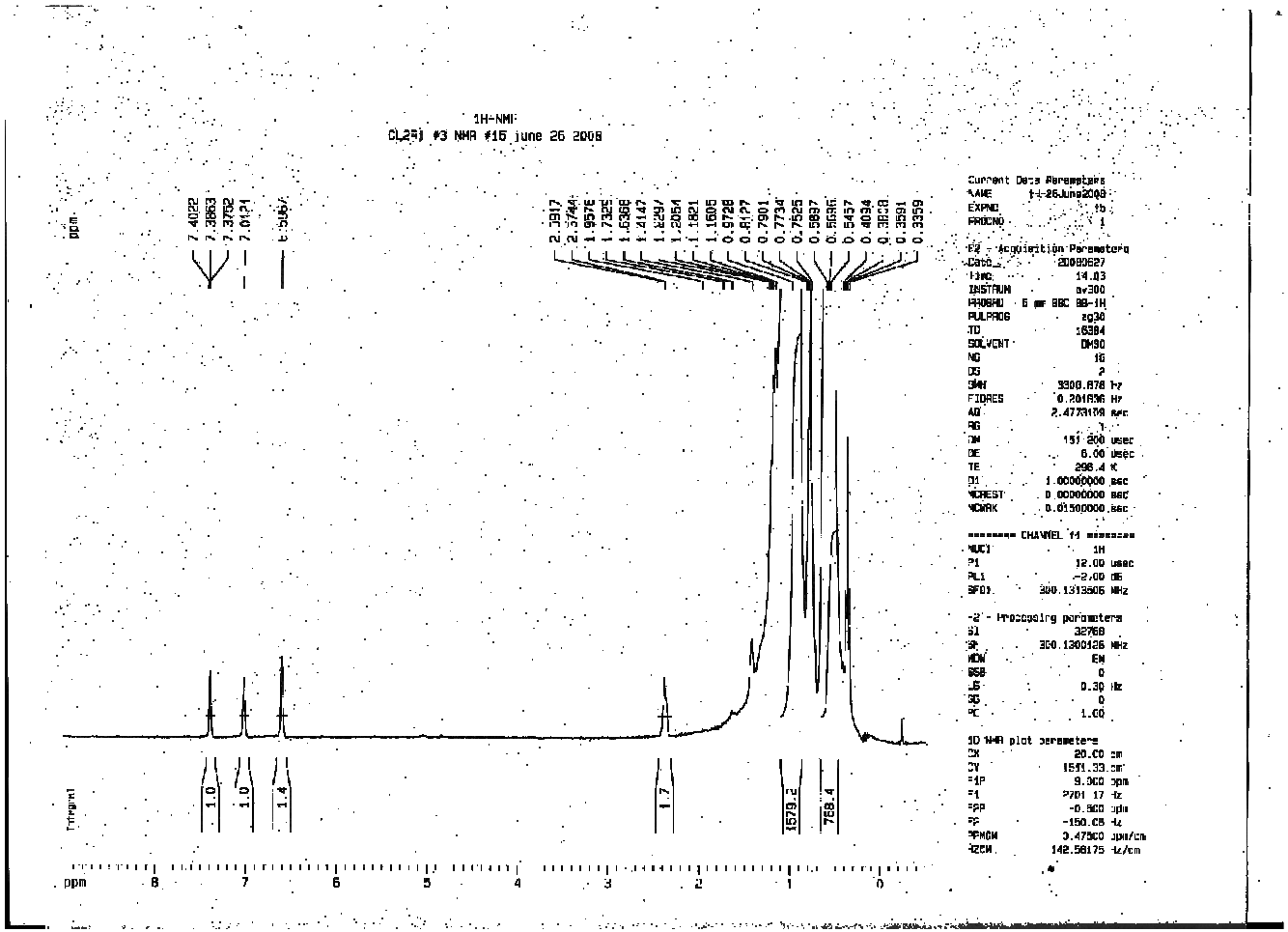

Figure B2.2. 3: [1]H-NMR Spectrum of naphthalene and tetralin in n-octane, sample #3 , Experiment #2R1

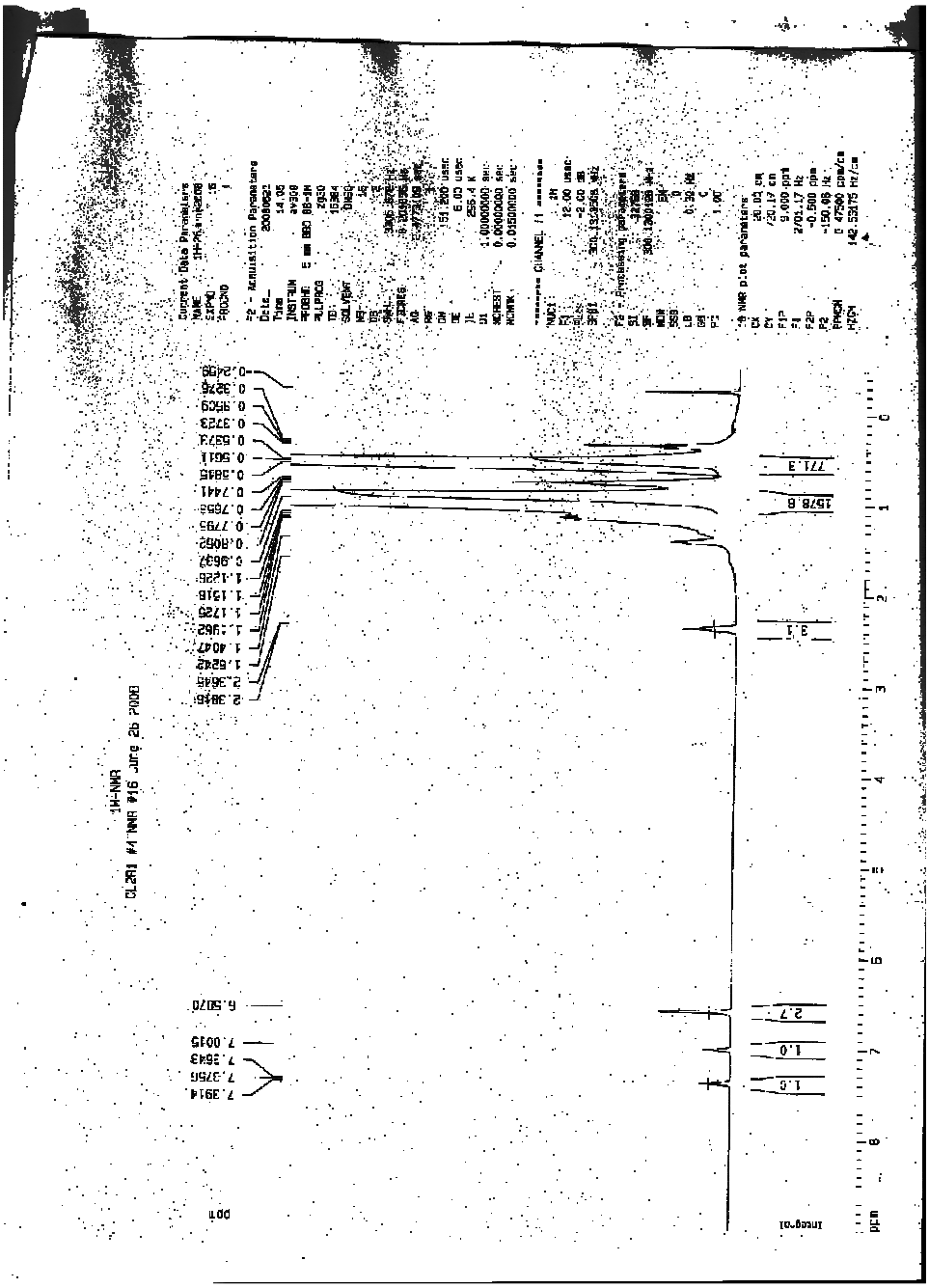

Figure B2.2. 4: ^{1}H-NMR Spectrum of naphthalene and tetralin in n-octane, sample #4, Experiment #2R1

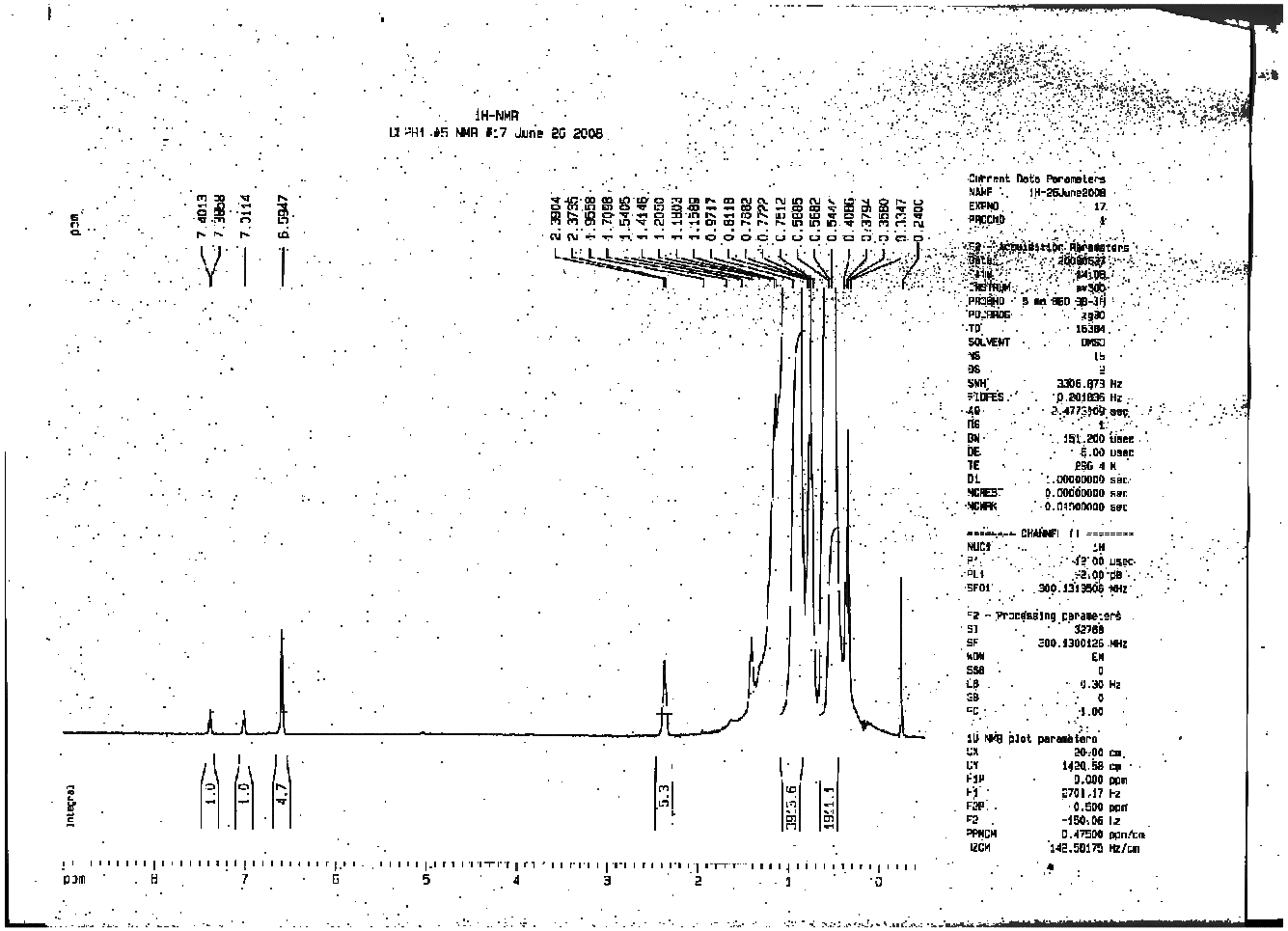

Figure B2.2. 5: ^{1}H-NMR Spectrum of naphthalene and tetralin in n-octane, sample #, Experiment #2R1

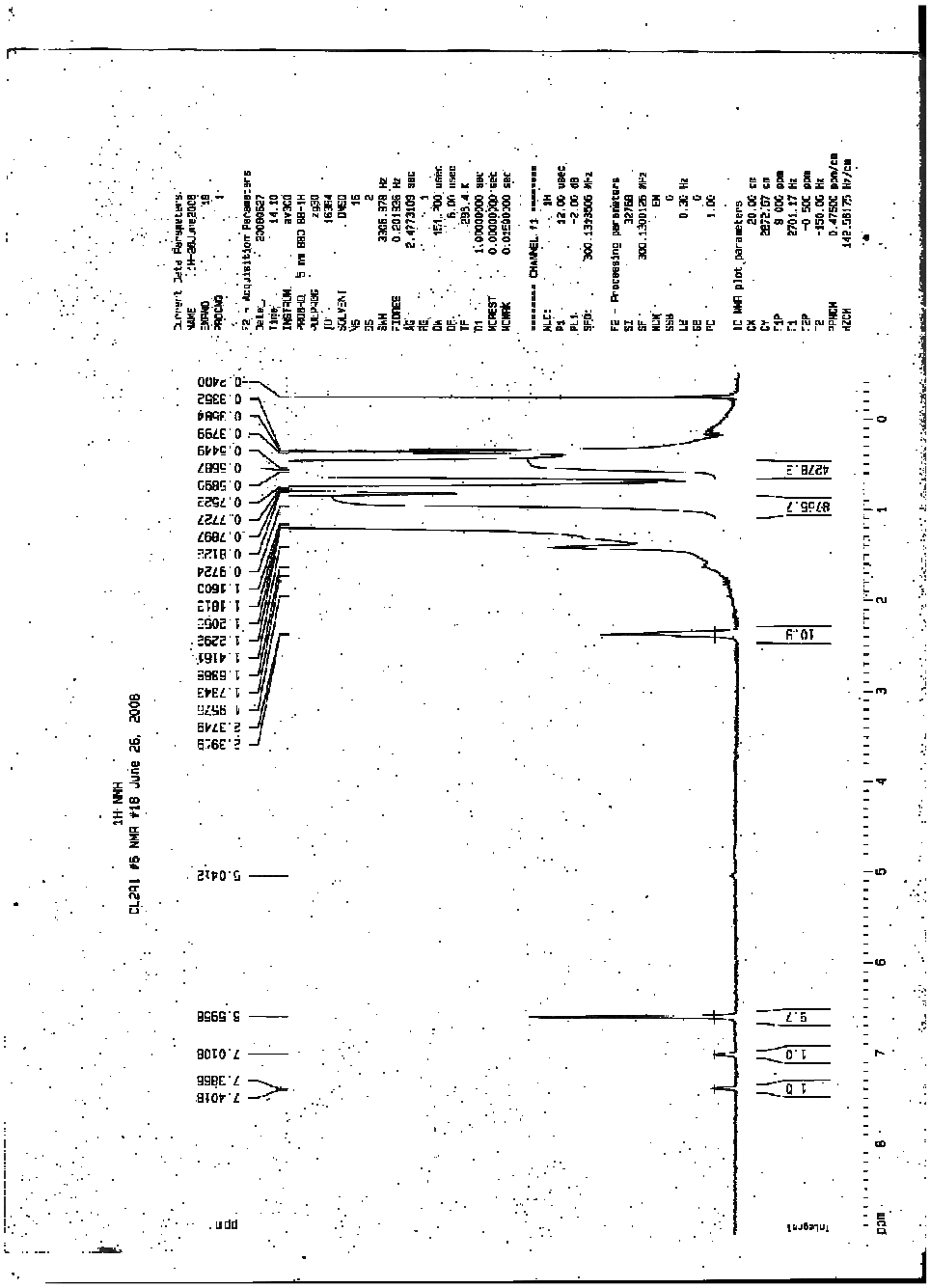

Figure B2.2. 6: ^{1}H-NMR Spectrum of naphthalene and tetralin in n-octane, sample #6 , Experiment #2R1

Experimental Conditions for #5R1: $CO/D_2O/H_2S$, 15 psig H_2S, 585 psig H_2, 4.0°C/min, 340 °C, 3 hrs, 10 ml D_2O, 100 ml n-octane, 3.7 g NAPH, 0.39 mmoles Mo, 1500 RPM Impeller Speed

Table B.5.2. 1: Mass of Samples, Experiment #5R1

Reaction Time (min)	5.58	46.18	81.58	126.33	159.67	180
Mass of Empty Vial	16.7407	16.6286	16.6202	16.6489	16.6112	16.8046
Mass of sample + vial	18.3233	17.9446	18.2862	19.364	17.5427	17.0859
mass of liquid sample	1.5826	1.316	1.666	2.7151	0.9315	0.2813

Table B.5.2. 2: GC Liquid Analysis, Experiment #5R1

Reaction Time (min)	5.58	46.18	81.58	126.33	159.67	180
[NPT] (mol/g-liq)	0.000452	0.000387	0.000321	0.000248	0.000222	0.000211
[Tet] (mol/g-liq)	1.17E-05	5.85E-05	0.000122	0.000182	0.000208	0.000301

Table B.5.2. 3: GC Gas Mol % Analysis, Experiment #5R1

Reaction Time (min)	4.3	39.3	75.3	110.3	151.3	180
ESTD mol%						
H2	9.066576	10.87217	12.23117	13.19319	18.62307	19.43325
O2	9.020861	10.20158	10.04462	9.459652	4.857653	4.265845
N2	31.43043	35.32372	34.79603	32.83021	17.23422	15.2685
CH4		0.023439	0.047952	0.071517	0.125653	0.149419
CO	33.1404	24.46693	19.9542	17.96471	21.77468	19.84595
CO2	13.52281	15.97547	19.9941	23.45097	34.09645	37.71986
C2H4						
C2H6	0.016677	0.020013	0.026988	0.073767	0.110603	0.116426
C2H2						
H2S	0.829949	0.787151	0.814428	0.864189	1.214569	1.256804
COS	0.127044	0.074523	0.053924	0.04995	0.058616	0.056518
n-C4					0.010377	0.012537
i-C4	0.036874		0.016753	0.02227	0.024799	0.025427
n-C6	0.006763	0.008286	0.006895	0.007362	0.008583	0.008481
n-C8	2.801617	2.246724	2.021308	2.012219	1.860733	1.840982

Table B.5.2.4: Calculated Deuterated Organic Concentrations from NMR Data

Reaction Time (min)	39.3	75.3	110.3	151.3	180
mass of empty vial (g)	2.4526	2.4421	2.4639	2.4569	2.4428
m2 = mass of vial + NMR sample	2.8647	2.7959	2.8515	2.85	2.865
m3 = m2 + n-C8 diluent (GC sample)	3.1332	3.0661	3.1277	3.1269	3.1414
[NAPH] NMR sample (g/g)	0.018673	0.018989	0.014517	0.011999	0.005775
[NAPH] diluted-GC sample (mol/g)	8.82E-05	8.4E-05	6.61E-05	5.49E-05	2.72E-05
[NAPH] (mol/g) NMR sample	0.000146	0.000148	0.000113	9.36E-05	4.51E-05
[TET] NMR Sample (g/g)	0.000639	0.003069	0.005903	0.009476	0.00583
[TET] GC sample (mol/g)	2.92E-06	1.32E-05	2.61E-05	4.21E-05	2.67E-05
[t-DEC] NMR Sample (g/g)	0	0	0	3.41E-05	1.65E-05
[c-DEC] NMR Sample (g/g)	0	0	0	1.7E-05	1.65E-05
[d6-Acetone] GC sample (mol/g)	3.84E-05	3.64E-05	3.51E-05	8.24E-05	8.24E-05
[d6-acetone] in NMR sample (g/g)	0.004057	0.004115	0.003848	0.008994	0.008731
mol of total Naph/mol of n-C8 (from GC)					
Total NAPH mol / mol n-C8	0.017038	0.017376	0.013258	0.011029	0.005253
Total Tetralin mol / mol n-C8	0.000565	0.002723	0.005227	0.008445	0.005142
[NAPH] reactor sample (mol/g)					
[TET] reactor sample (mol/g)					
molar ratios from ^{1}H-NMR Integration					
MOL I / MOL n-Octane] (calculated from n-Octane $-CH_3$ NMR resonance)					
Naphthalene A	0.003911	0.003095	0.002237	0.001856	0.00088
Naphthalene B	0.00571	0.003745	0.002237	0.001856	0.00088
Tetralin Ar	7.82E-05	0.000402	0.000895	0.0013	0.000792
Tetralin B	0.000196	0.000557	0.000895	0.001671	0.001057
% ^{1}H-Incorporation					
Reaction Time (min)	39.30	75.30	110.30	151.30	180.00
NAPH A mol%	22.95%	17.81%	16.88%	16.83%	16.76%
NAPH B mol%	33.51%	21.55%	16.88%	16.83%	16.76%
TET Aromatic mol%	13.85%	14.78%	17.12%	15.39%	15.41%
Tet Sat mol%	34.61%	20.46%	17.12%	19.78%	20.55%

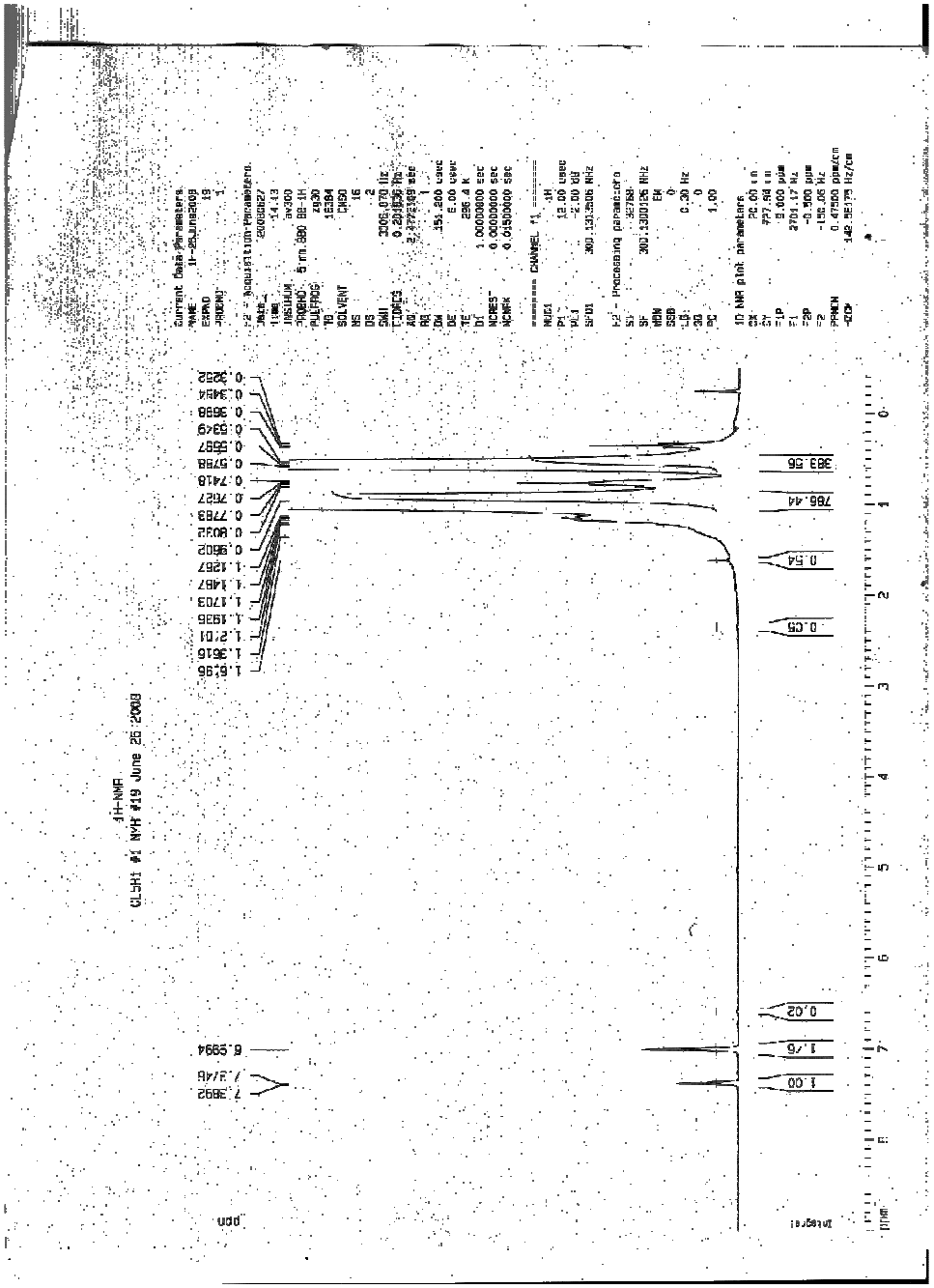

Figure B.5.2. 1: ^{1}H-NMR Spectrum of naphthalene and tetralin in n-octane, sample #1

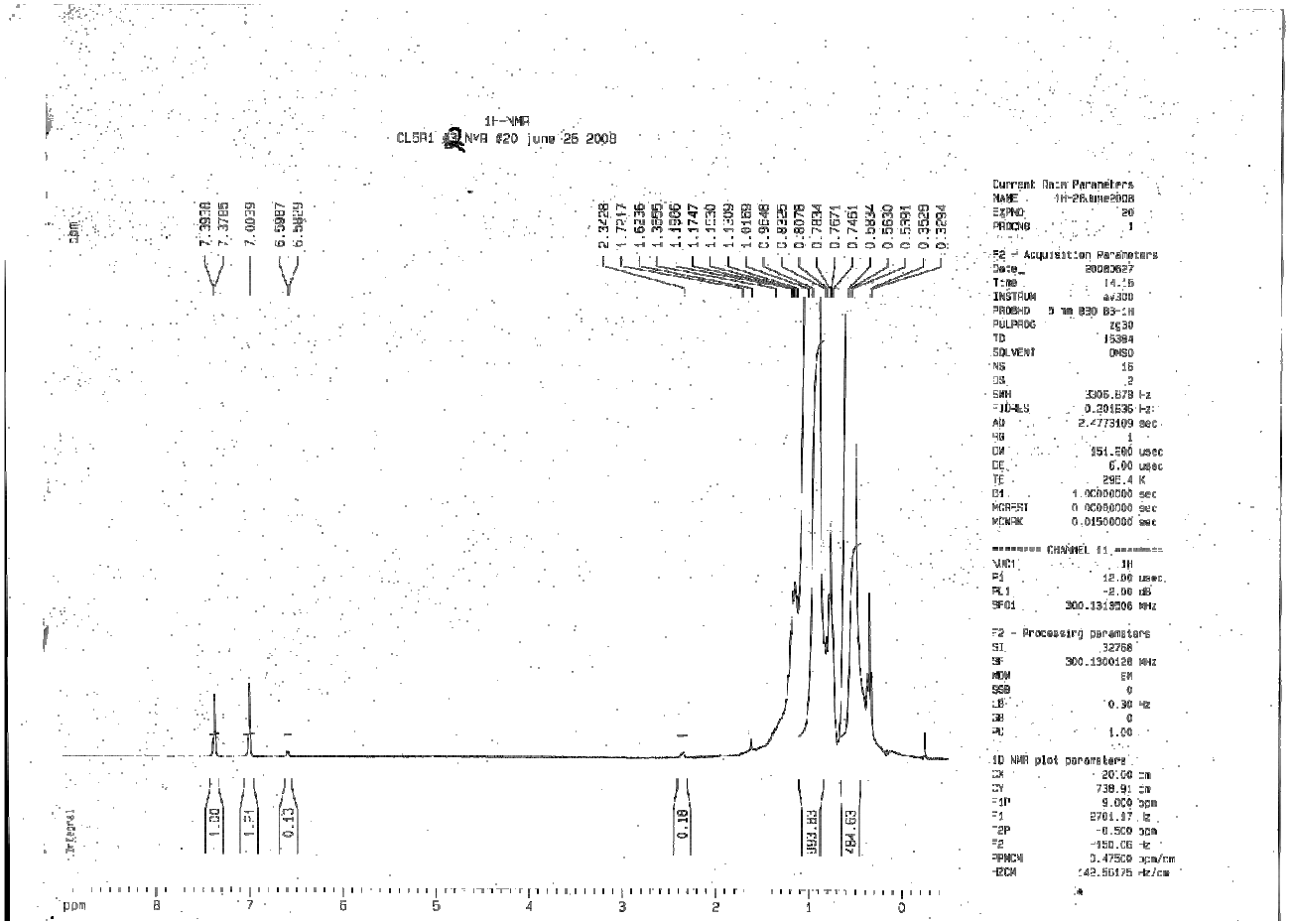

Figure B.5.2. 2: ^{1}H-NMR Spectrum of naphthalene and tetralin in n-octane, sample #2

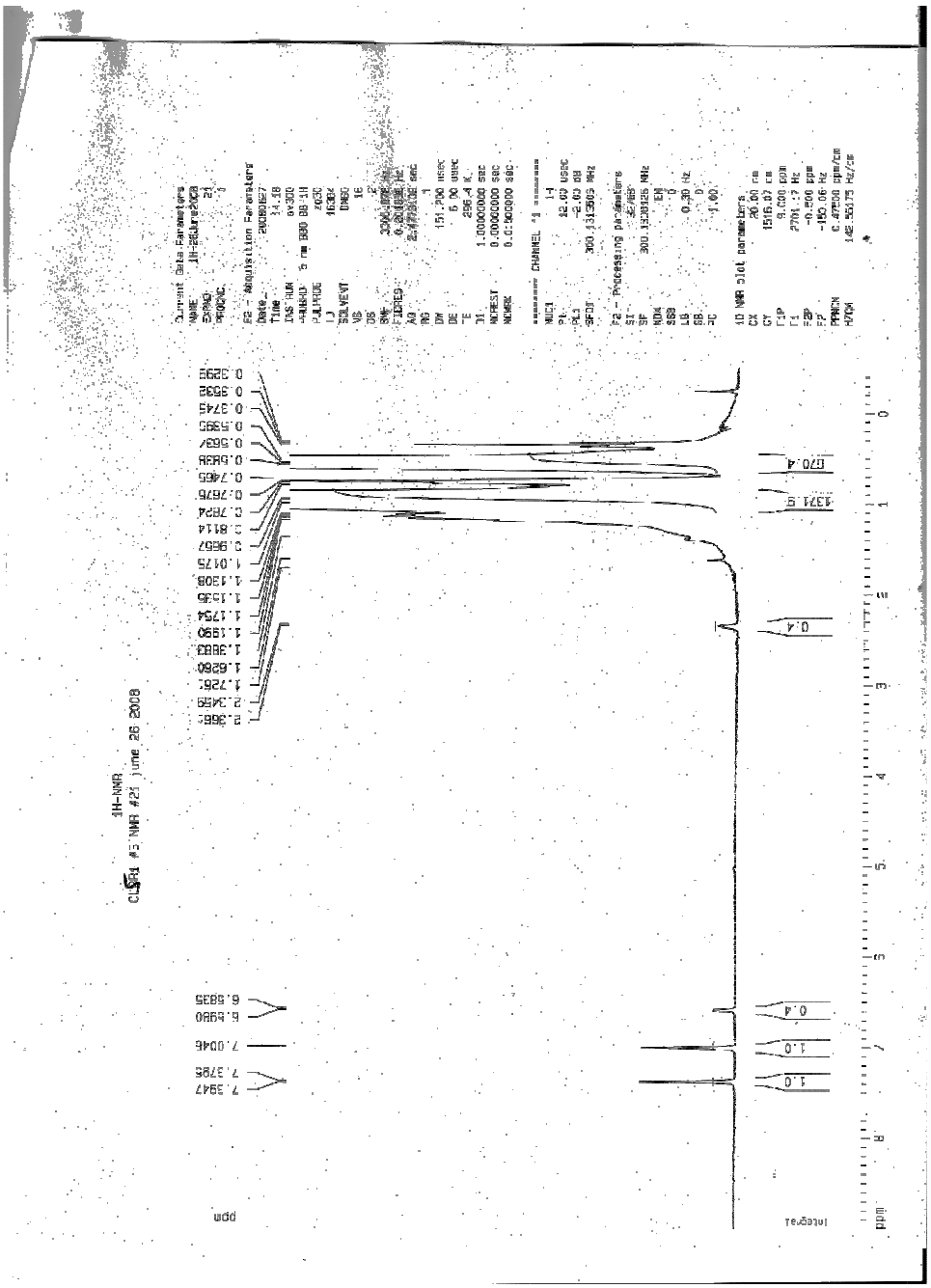

Figure B.5.2. 3: ^{1}H-NMR Spectrum of naphthalene and tetralin in n-octane, sample #3

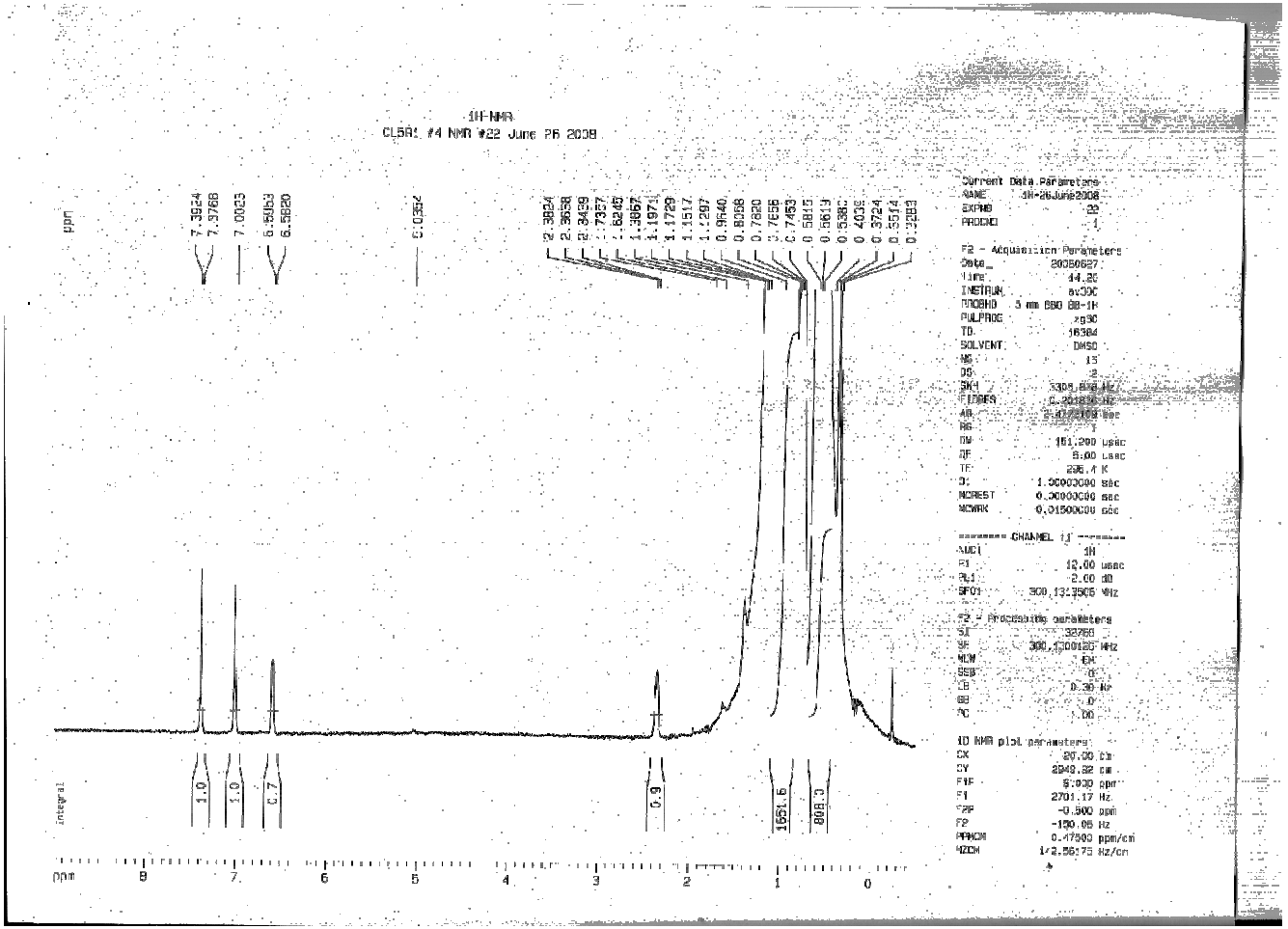

Figure B.5.2. 4: ^{1}H-NMR Spectrum of naphthalene and tetralin in n-octane, sample #4

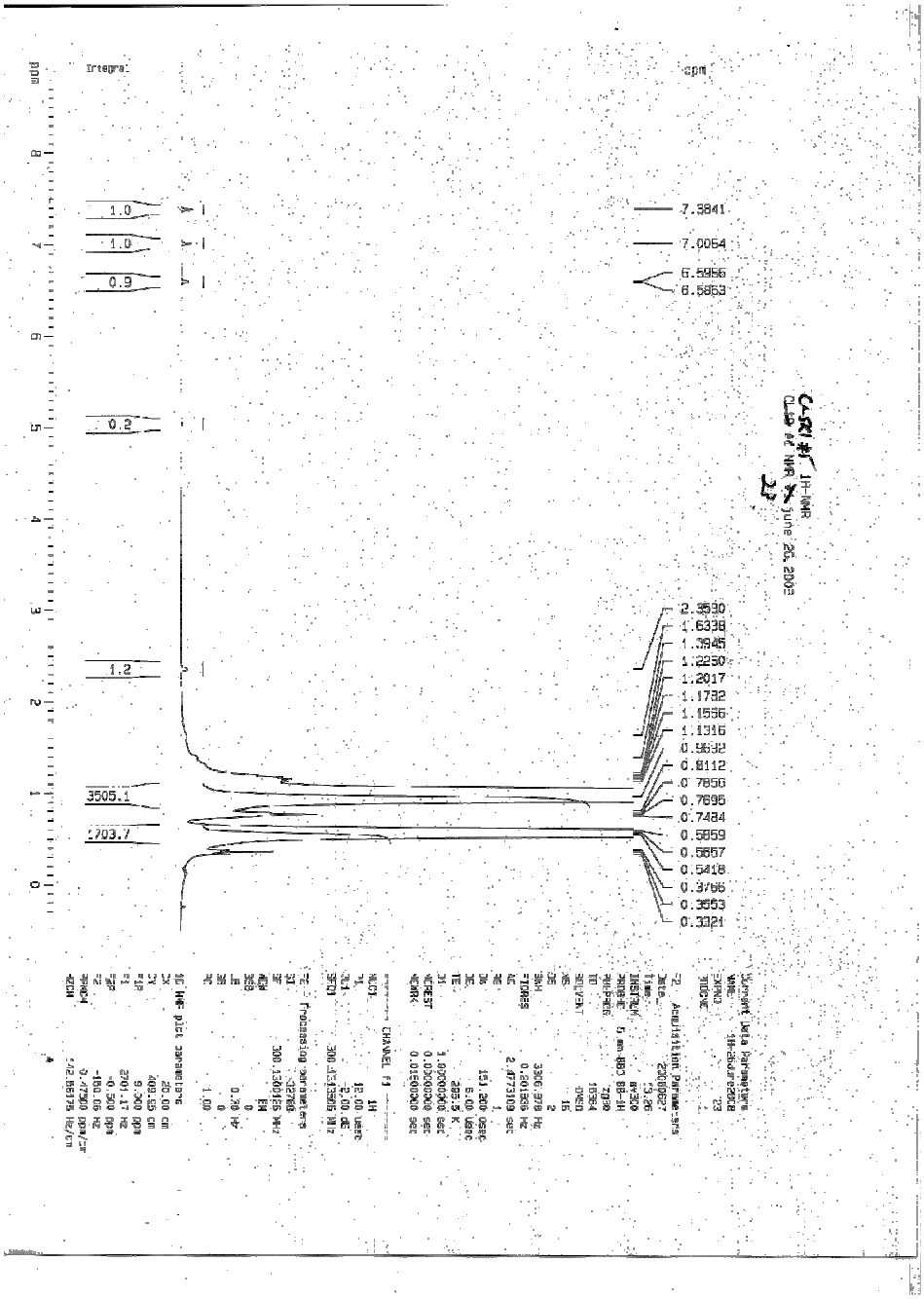

Figure B.5.2. 5: ^{1}H-NMR Spectrum of naphthalene and tetralin in n-octane, sample #5

Experimental Conditions for #14: $CO/H_2/D_2O/H_2S$, 15 psig H_2S, 585 psig (1:1 = $CO:H_2$), 4.0°C/min, 340 °C, 3 hrs, 10 ml D_2O, 100 ml n-octane, 3.7 g NAPH, 0.39 mmoles Mo, 1500 RPM Impeller Speed

Table B.14. 1: Mass of Samples, Experiment #14

Reaction Time (min)	1.25	37.08333	73.08333	108.0833	147.5833	180
Mass of Empty Vial	16.6623	16.4647	16.8075	16.6797	16.7532	16.507
Mass of sample + vial	17.2249	17.5961	17.7457	17.7758	17.8268	18.2836
mass of liquid sample	0.5626	1.1314	0.9382	1.0961	1.0736	1.7766

Table B.14. 2: GC Liquid Analysis, Experiment #14

Reaction Time (min)	1.25	37.08	73.08	108.08	147.58	180
[NPT] (mol/g-liq)	0.000495	0.000435	0.000385	0.000317	0.000264	0.000198
[TET] (mol/g-liq)	5.29E-06	5.29E-05	0.000123	0.000178	0.000245	0.000275
[c-DEC] (mol/g-liq)	0	0	0	0	0	7.23E-07
[t-DEC] (mol/g-liq)	0	0	0	7.23E-07	7.23E-07	1.45E-06
[NPT] = [NPT]0 - [TET]-[DEC]	0.00049	0.000442	0.000372	0.000316	0.00025	0.000218

Table B.14. 3: GC Gas Analysis, Experiment #14

Reaction Time (min)	1.25	37.08333	73.08333	108.0833	147.5833	180	Final
Average ESTD mol%							
H2	7.84353	17.52007	17.75634	18.60356	18.73798	26.9496	43.16259
O2	16.0348	11.33972	11.7306	11.67012	11.42967	7.6879	1.925095
N2	60.5116	45.78424	44.42618	44.13592	43.31006	29.26967	7.53834
CH4		0.03887	0.07131	0.098665	0.132145	0.21813	0.251115
CO	7.14568	10.20143	7.659775	6.24928	5.22558	6.51478	16.94407
CO2	6.59588	6.581995	8.35314	9.87061	11.54707	17.74149	18.33649
C2H4							0
C2H6	0	0.0464	0.057215	0.063995	0.073935	0.12295	0.086155
C2H2							0
H2S	0.96144	1.284615	1.26168	1.285815	1.346245	1.88834	1.31172
COS	0.03429	0.043315	0.032265	0.025995	0.023035	0.02525	0.07747
1,2-Prop=	0	0	0	0	0	0	0
Water	3.6901	3.192914	3.901535	3.22995	3.82105	3.8767	3.57522
Prop	0	0	0	0	0	0	0
C3	0	0	0	0	0	0	0
n-C4	0	0	0	0	0	0.00768	0
i-C4	0		0	0	0	0	0
n-C6	0	0	0	0	0	0.003775	0
n-C8	0.76544	1.889685	2.274685	1.939705	2.178005	2.119445	0.643065

Table B.14. 4: Calculated Deuterated Organic Concentrations from NMR

Reaction Time (min)	1.25	37.08333	73.08333	108.0833	147.5833	180
mass of empty vial (g)	2.458	2.4917	2.4844	2.4714	2.4568	2.4631
m2 = mass of vial + NMR sample	2.8625	2.9308	2.9302	2.8719	2.8138	2.8099
m3 = m2 + n-C8 diluent (GC sample)	3.2935	3.2088	3.2079	3.1443	3.091	3.0865
[NAPH] NMR sample (g/g)	0.008283	0.022341	0.020373	0.018185	0.024136	0.009264
[NAPH] diluted-GC sample (mol/g)	3.13E-05	0.000107	9.79E-05	8.44E-05	0.000106	4.02E-05
[NAPH] (mol/g) NMR sample	6.46E-05	0.000174	0.000159	0.000142	0.000188	7.23E-05
[TET] NMR Sample (g/g)	0.000131	0.002869	0.006854	0.010798	0.02374	0.013835
[TET] GC sample (mol/g)	4.79E-07	1.33E-05	3.19E-05	4.86E-05	0.000101	5.82E-05
[t-DEC] NMR Sample (g/g)	0	0	0	1.68E-05	7.7E-05	6.59E-05
[c-DEC] NMR Sample (g/g)	0	0	0	0	5.33E-05	5.39E-05
[d6-Acetone] GC sample (mol/g)	4.2E-05	5.43E-05	6.72E-05	5.24E-05	5.58E-05	7.51E-05
[d6-acetone] in NMR sample (g/g)	0.005549	0.005683	0.006984	0.00564	0.006348	0.008646
mol of total Naph/mol of n-C8 (from GC)						
Total NAPH mol / mol n-C8	0.007485	0.020542	0.018797	0.016786	0.022744	0.008526
Total Tetralin mol / mol n-C8	0.000115	0.002558	0.006131	0.009664	0.021689	0.012347
[NAPH] reactor sample (mol/g)	0.000495	0.000435	0.000385	0.000317	0.000264	0.000198
[TET] reactor sample (mol/g)	5.29E-06	5.29E-05	0.000123	0.000178	0.000245	0.000275
molar ratios from ^{1}H-NMR Integration						
MOL I / MOL n-Octane] (calculated from n-Octane –CH_3 NMR resonance)						
Naphthalene A	0.004241	0.00553	0.00511	0.004507	0.003834	0.002233
Naphthalene B	0.004962	0.006194	0.00511	0.004462	0.003834	0.002233
Tetralin Ar	0	0.000608	0.001584	0.002524	0.003566	0.003127
Tetralin B	0	0.000719	0.001789	0.00302	0.0051	0.003574
% ^{1}H-Incorporation						
Reaction Time (min)	1.25	37.08	73.08	108.08	147.58	180.00
NAPH A mol%	56.66%	26.92%	27.19%	26.85%	16.86%	26.20%
NAPH B mol%	66.29%	30.15%	27.19%	26.58%	16.86%	26.20%
TET Aromatic mol%	0.00%	23.78%	25.84%	26.12%	16.44%	25.33%
Tet Sat mol%	0.00%	28.11%	29.17%	31.25%	23.51%	28.94%
[1H-NAPH]-A (mol/g)						
[NAPH]-[1H-NAPH]-A						
[1H-NAPH]	0.000328	0.000131	0.000105	8.43E-05	4.46E-05	5.2E-05
[NAPH]	0.000167	0.000304	0.00028	0.000233	0.00022	0.000146

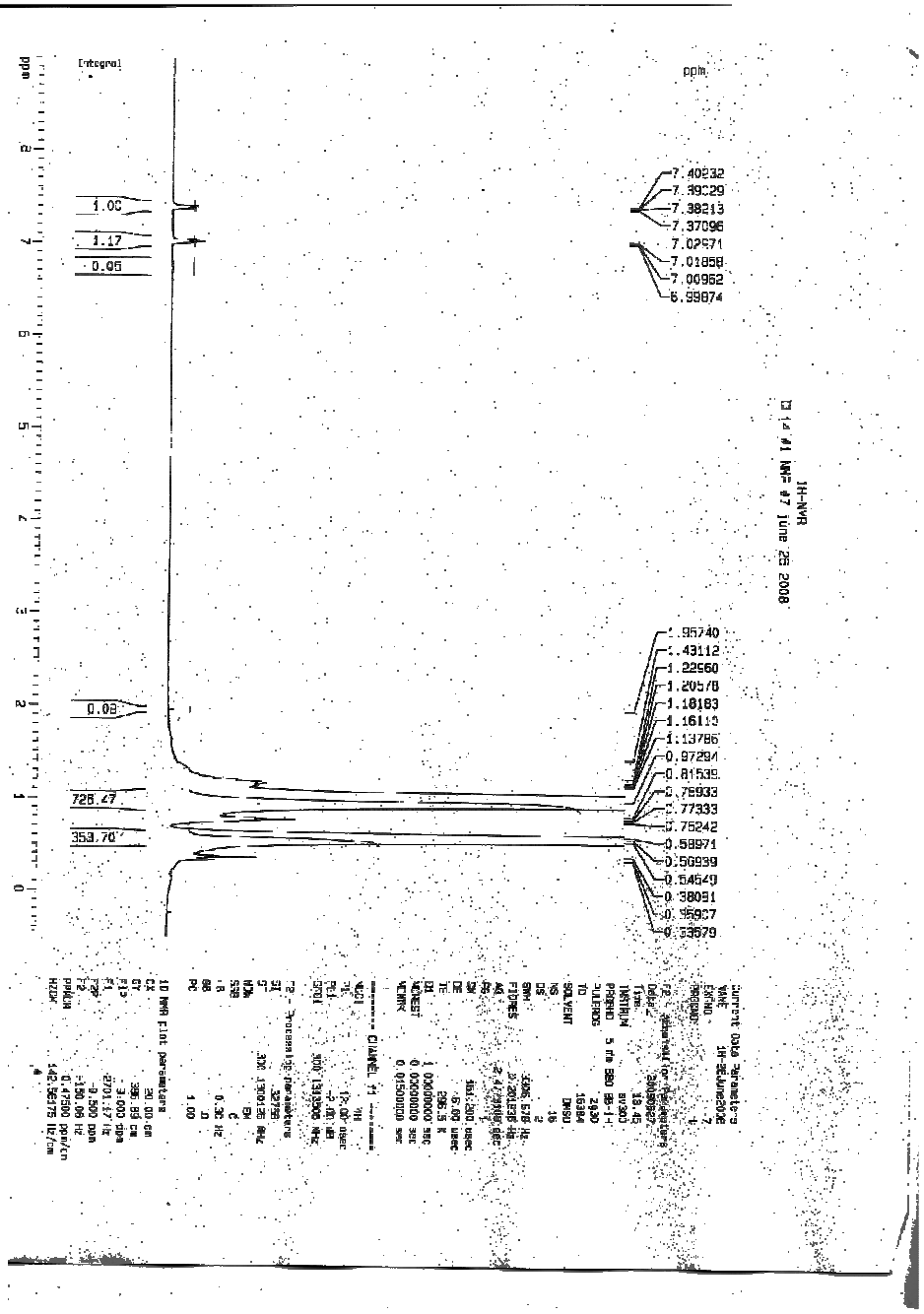

Figure B.14. 1: ^{1}H-NMR Spectrum of naphthalene and tetralin in n-octane, sample #1

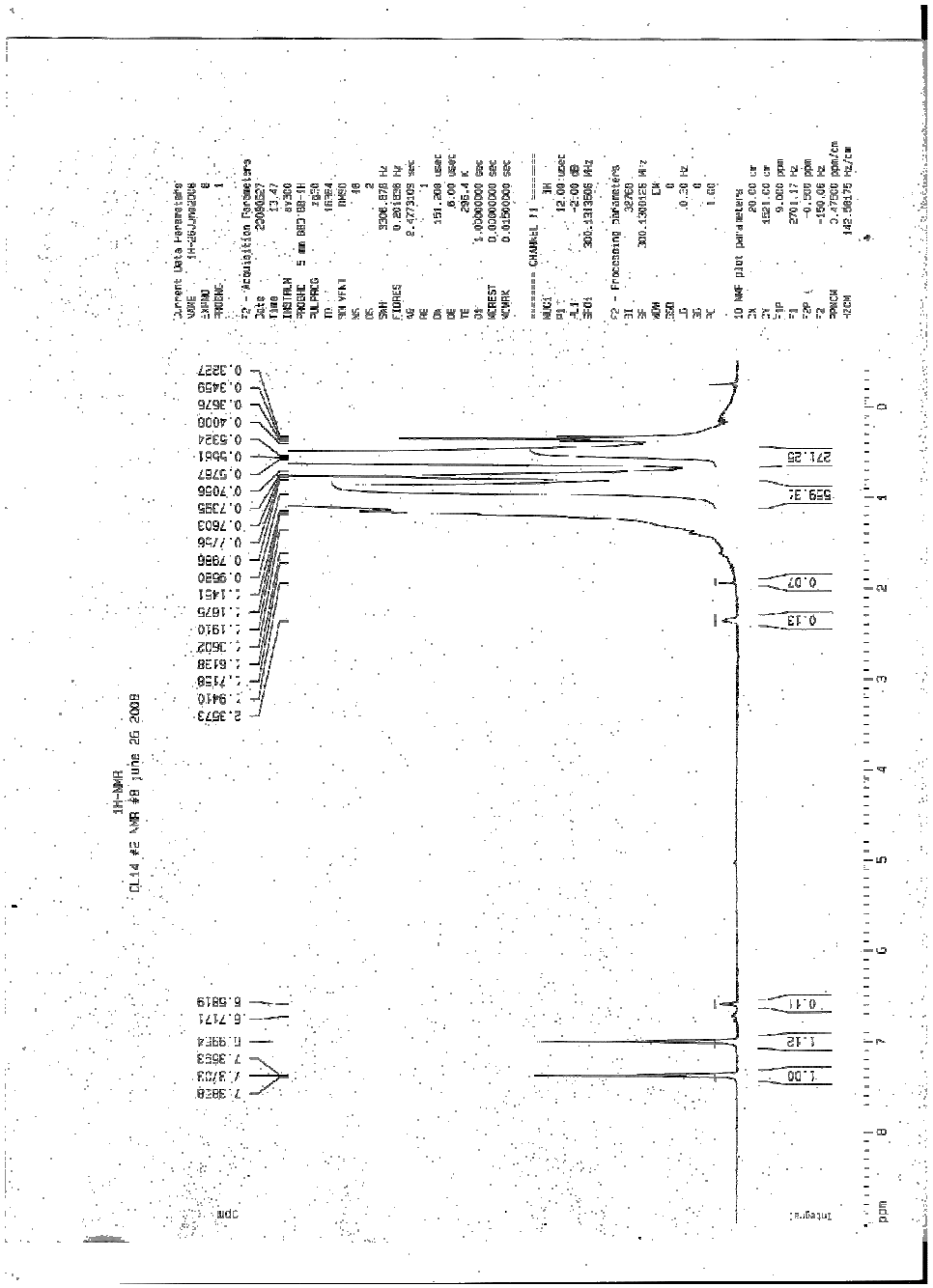

Figure B.14. 2: ^{1}H-NMR Spectrum of naphthalene and tetralin in n-octane, sample #2

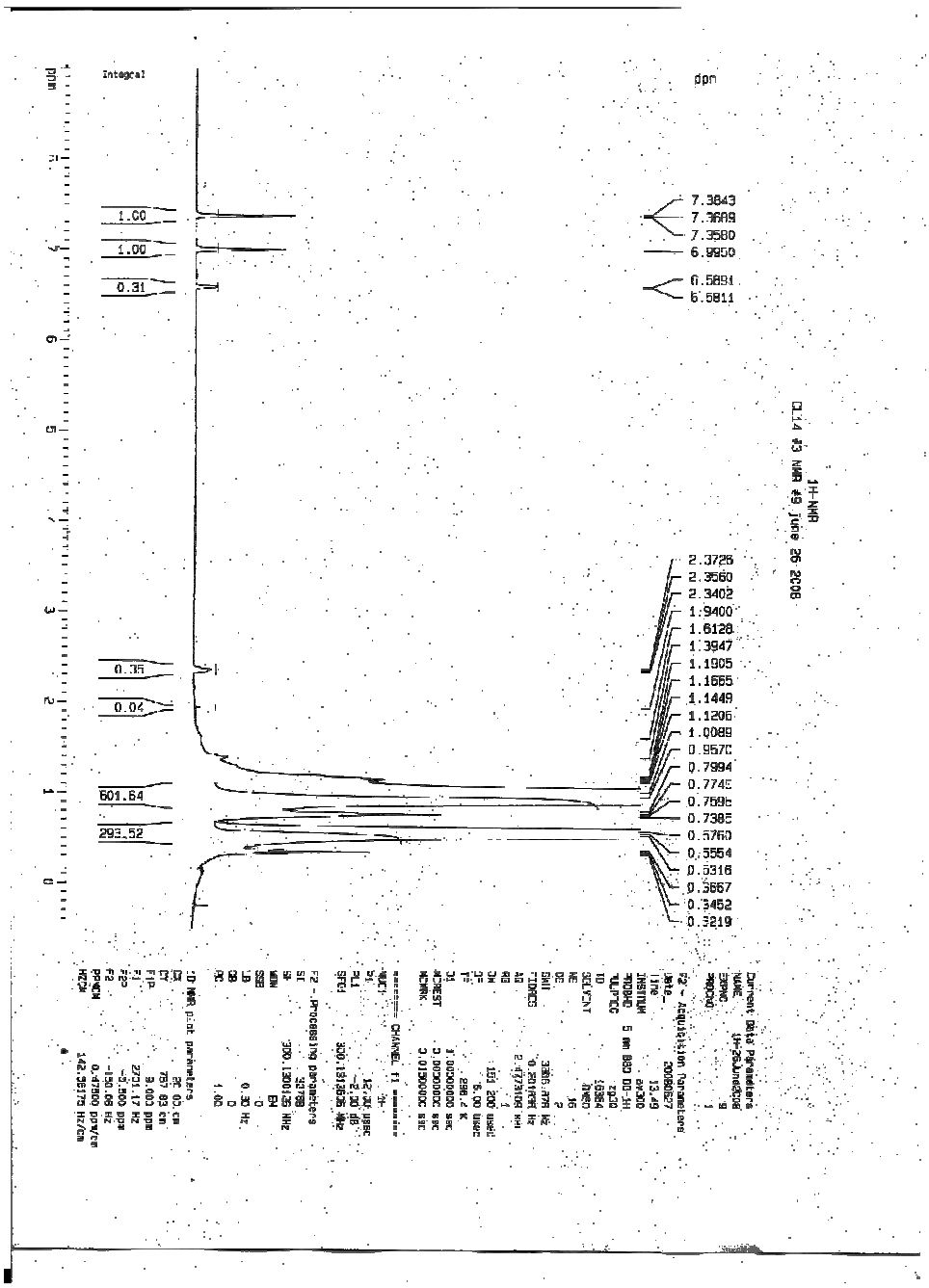

Figure B.14. 3: ^{1}H-NMR Spectrum of naphthalene and tetralin in n-octane, sample #3

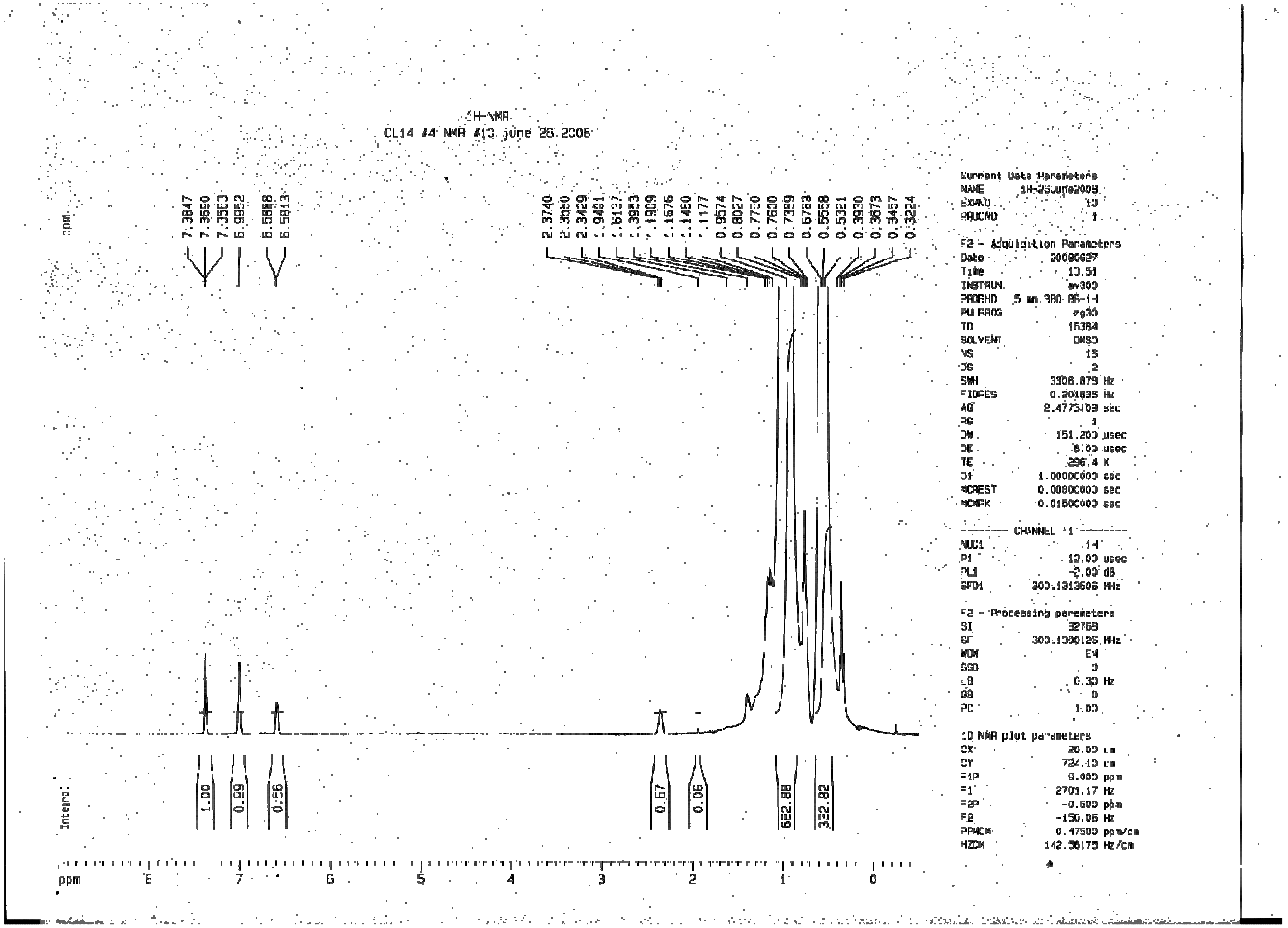

Figure B.14. 4: ^{1}H-NMR Spectrum of naphthalene and tetralin in n-octane, sample #4

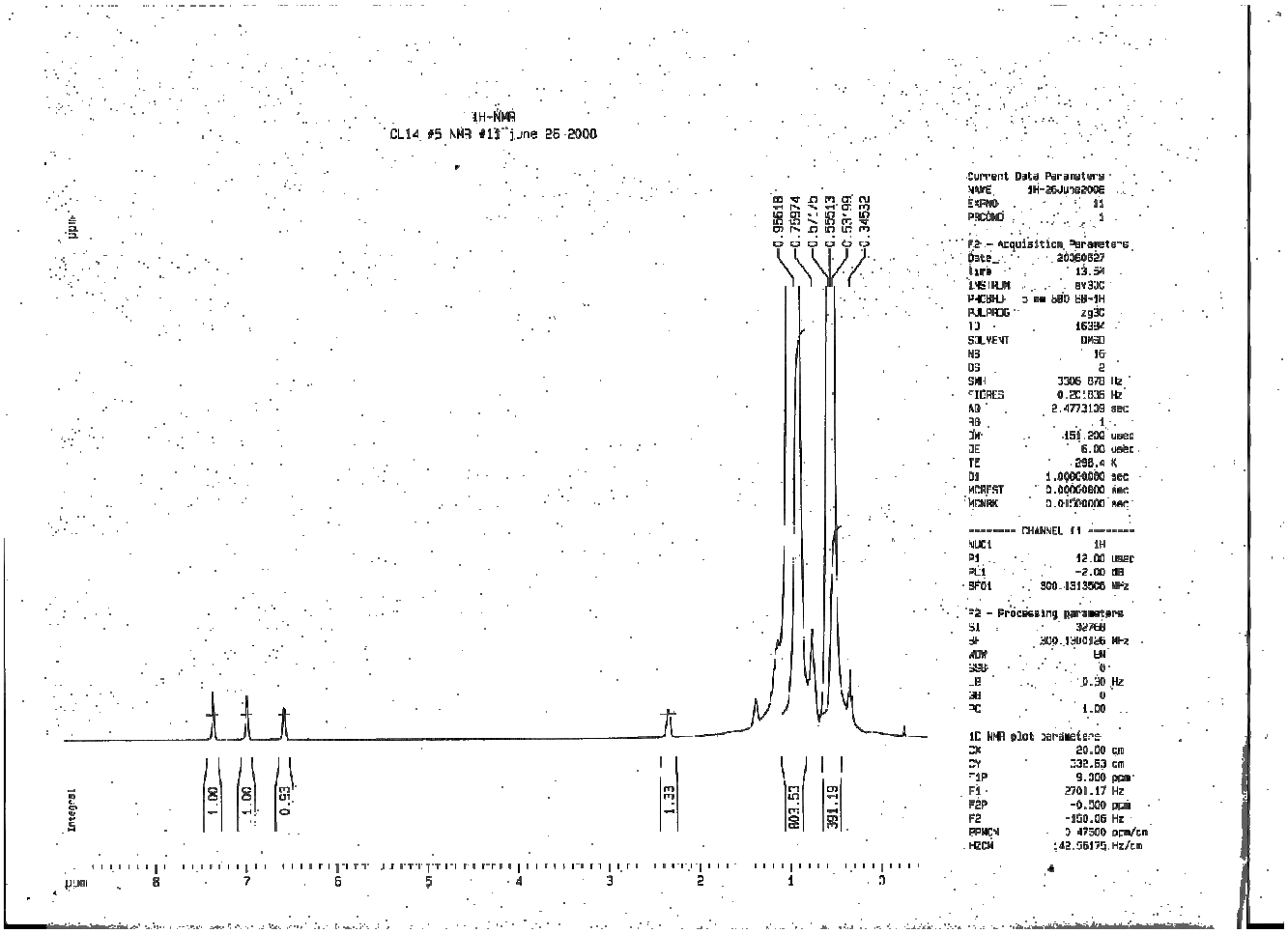

Figure B.14. 5: ^{1}H-NMR Spectrum of naphthalene and tetralin in n-octane, sample #5

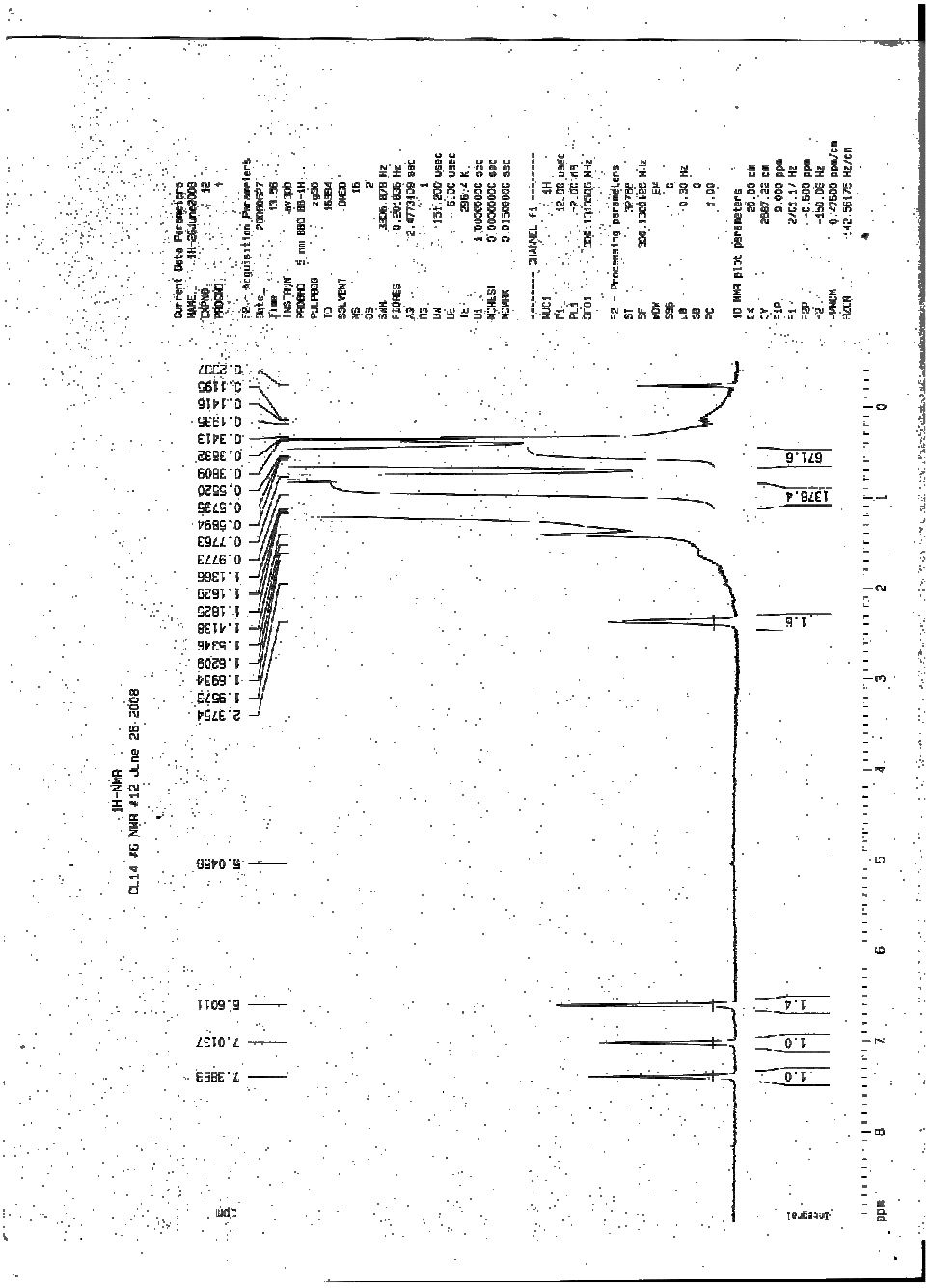

Figure B.14. 6: ^{1}H-NMR Spectrum of naphthalene and tetralin in n-octane, sample #6

Experimental Conditions for #19: $N_2/D_2O/H_2S$, 15 psig H_2S, 585 psig N_2, 4.0°C/min, 340 °C, 3 hrs, 10 ml D_2O, 100 ml n-octane, 3.7 g NAPH, 0.39 mmoles Mo, 1500 RPM Impeller Speed

Table B.19. 1: Mass of Samples, Experiment #19

Reaction Time (min)	1.23	38.23	72.73	110.23	143.73	180.00
Mass of Empty Vial (g)	16.4928	16.4251	16.5274	16.5447	16.4664	16.467
Mass of sample + vial (g)	17.0721	16.7305	16.986	16.9297	18.5875	18.5052
mass of liquid sample (g)	0.5793	0.3054	0.4586	0.385	2.1211	2.0382

Table B.19. 2: GC Liquid Analysis, Experiment #19

Reaction Time (min)	1.23	38.23	72.73	110.23	143.73	180.00
[NPT] (mol/g-liq)	0.000405	0.000425	0.000387	0.000402	0.000401	0.000403
[TET] (mol/g-liq)	0	0	2.27E-07	7.24E-07	1.36E-06	1.64E-06
[c-DEC] (mol/g-liq)	0	3.34E-08	0	0	0	0
[t-DEC] (mol/g-liq)	0	1E-07	1.09E-07	9.9E-08	1.21E-07	1.21E-07
$[NPT] = [NPT]_0 - [TET]-[DEC]$	0.000405	0.000405	0.000404	0.000404	0.000403	0.000403

Table B.19. 3: GC Gas Analysis, Experiment #19

Reaction Time (min)	1.23	38.23	72.73	110.23	143.73	180.00	Final
Average ESTD mol%							
H2	0.00074	0.08545	0.16486	0.2171	0.221735	0.47056	0.492143
O2	11.51899	11.31558	11.23607	10.95648	12.62915	7.56984	1.847
N2	88.016	87.3915	87.3991	87.4266	85.956	91.8825	99.66393
CH4		0	0	0	0	0	0
CO	0	0	0	0	0	0	0
CO2	0.04237	0.04683	0.04777	0.04955	0.05042	0.05667	0.08712
C2H4							0
C2H6	0	0	0.00711	0.01008	0.01072	0.01814	0.01214
C2H2							0
H2S	0.1642	0.32195	0.40812	0.48130	0.45653	0.83631	0.75487
COS	0	0	0	0	0	0	0
1,2-Prop=	0	0	0	0	0	0	0
Water	0.356425	0.41574	0.43306	0.480025	0.44566	0.433015	0.365043
Prop	0	0	0	0	0	0	0
C3	0	0	0	0	0	0	0
n-C4	0	0	0	0.003925	0	0.003185	0
i-C4	0.02764		0.030865	0.030295	0.02697	0.014215	0
n-C6	0.004555	0.004025	0.00383	0.003715	0.00325	0.00412	0
n-C8	1.25644	1.39675	1.39794	1.46176	1.367015	1.29084	0.107533

Table B.19. 4: Calculated Deuterated Organic Concentrations from NMR, Experiment #19

Reaction Time (min)	1.23	38.23	72.73	110.23	143.73	180.00
mass of empty vial (g)	2.4903	2.4471	2.4432	2.4667	2.4766	2.4442
m2 = mass of vial + NMR sample	2.9198	2.8823	2.8992	2.9014	2.912	2.9444
m3 = m2 + n-C8 diluent (GC sample)	3.1968	3.1618	3.1794	3.1794	3.191	3.222
[NAPH] NMR sample (g/g)	0.011361	0.019307	0.018626	0.019805	0.029042	0.031493
[NAPH] diluted-GC sample (mol/g)	5.39E-05	9.17E-05	9E-05	9.43E-05	0.000138	0.000158
[NAPH] (mol/g) NMR sample	8.86E-05	0.000151	0.000145	0.000155	0.000227	0.000246
[TET] NMR Sample (g/g)	0	0	0	0	0	0
[TET] GC sample (mol/g)	0	0	0	0	0	0
[t-DEC] NMR Sample (g/g)	0	0	0	0	0	0
[c-DEC] NMR Sample (g/g)	0	0	0	0	0	0
[d6-Acetone] GC sample (mol/g)	6.21E-05	5.93E-05	6.82E-05	5.1E-05	5.85E-05	5.39E-05
[d6-acetone] in NMR sample (g/g)	0.006536	0.006235	0.00705	0.00535	0.006142	0.00537
Mole Ratios of Molecules from GC						
Total NAPH mol / mol n-C8	0.010308	0.017655	0.017034	0.018104	0.026823	0.029137
Total Tetralin mol / mol n-C8	0	0	0	0	0	0
[NAPH] reactor sample (mol/g)	0.000405	0.000425	0.000388	0.000403	0.000402	0.000405
[TET] reactor sample (mol/g)						
Mole Ratios from ^{1}H-NMR Integration						
MOL I / MOL n-Octane] (calculated from n-Octane $-CH_3$ NMR resonance)						
Naphthalene A	0.00804	0.008849	0.004565	0.004189	0.005644	0.006804
Naphthalene B	0.008523	0.011857	0.007944	0.006702	0.007225	0.00796
Tetralin Ar	0	0	0	0	0	0
Tetralin B	0	0	0	0	0	0
% ^{1}H-Incorporation						
NAPH A mol%	78.00%	50.12%	26.80%	23.14%	21.04%	23.35%
NAPH B mol%	82.68%	67.16%	46.63%	37.02%	26.94%	27.32%

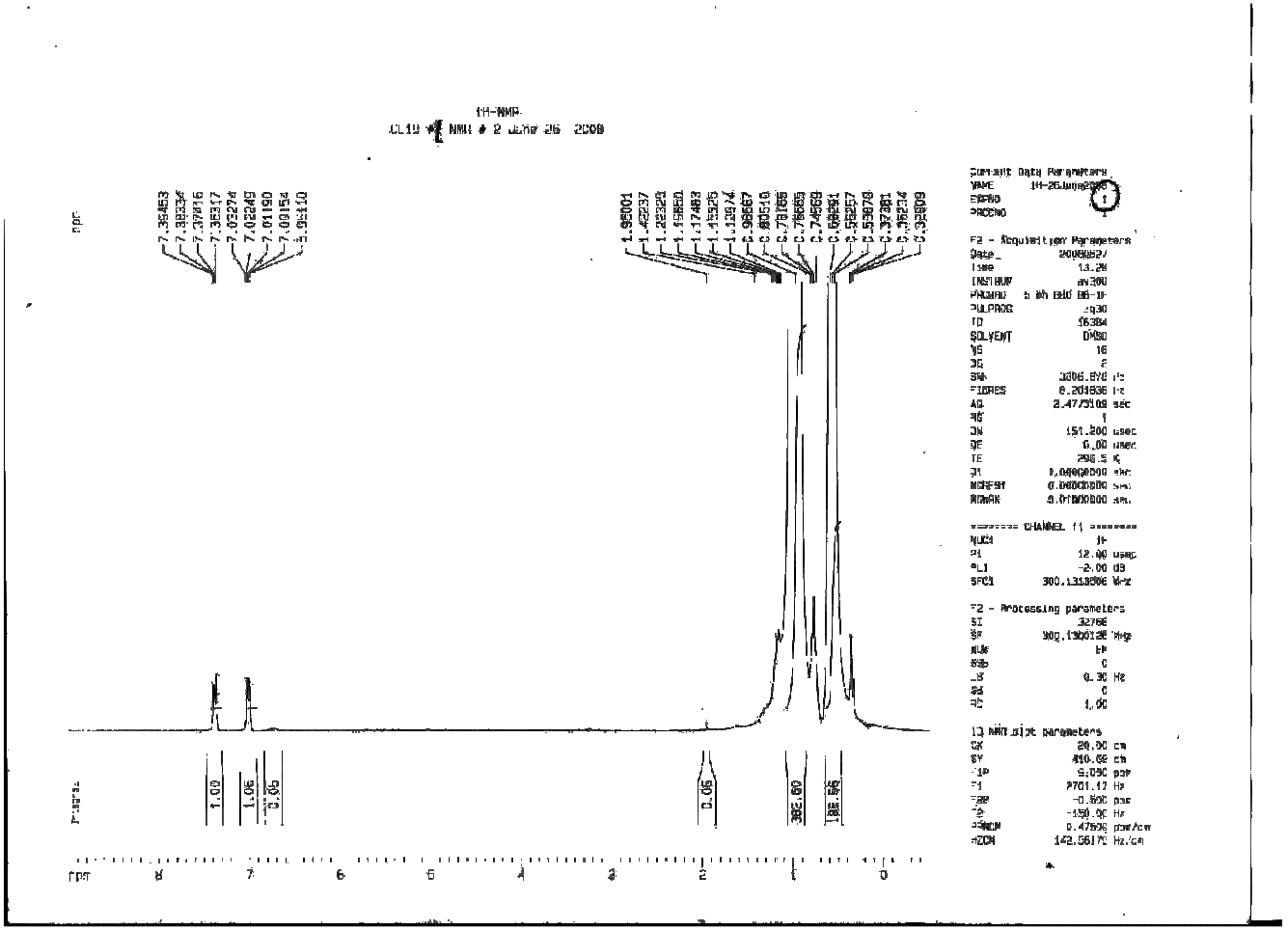

Figure B.19. 1: ^{1}H-NMR Spectrum of naphthalene and tetralin in n-octane, sample #1

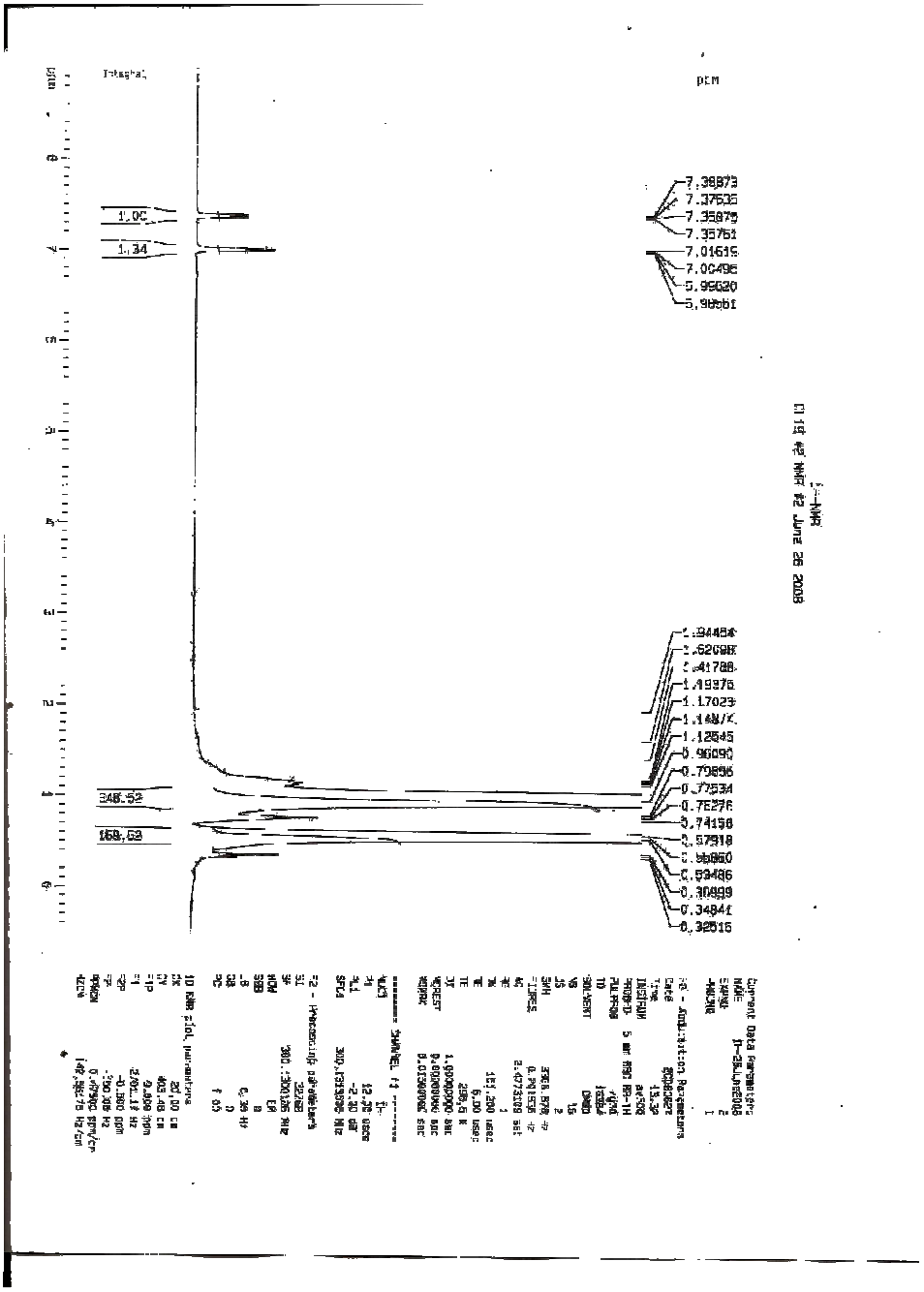

Figure B.19. 2: ^{1}H-NMR Spectrum of naphthalene and tetralin in n-octane, sample #2

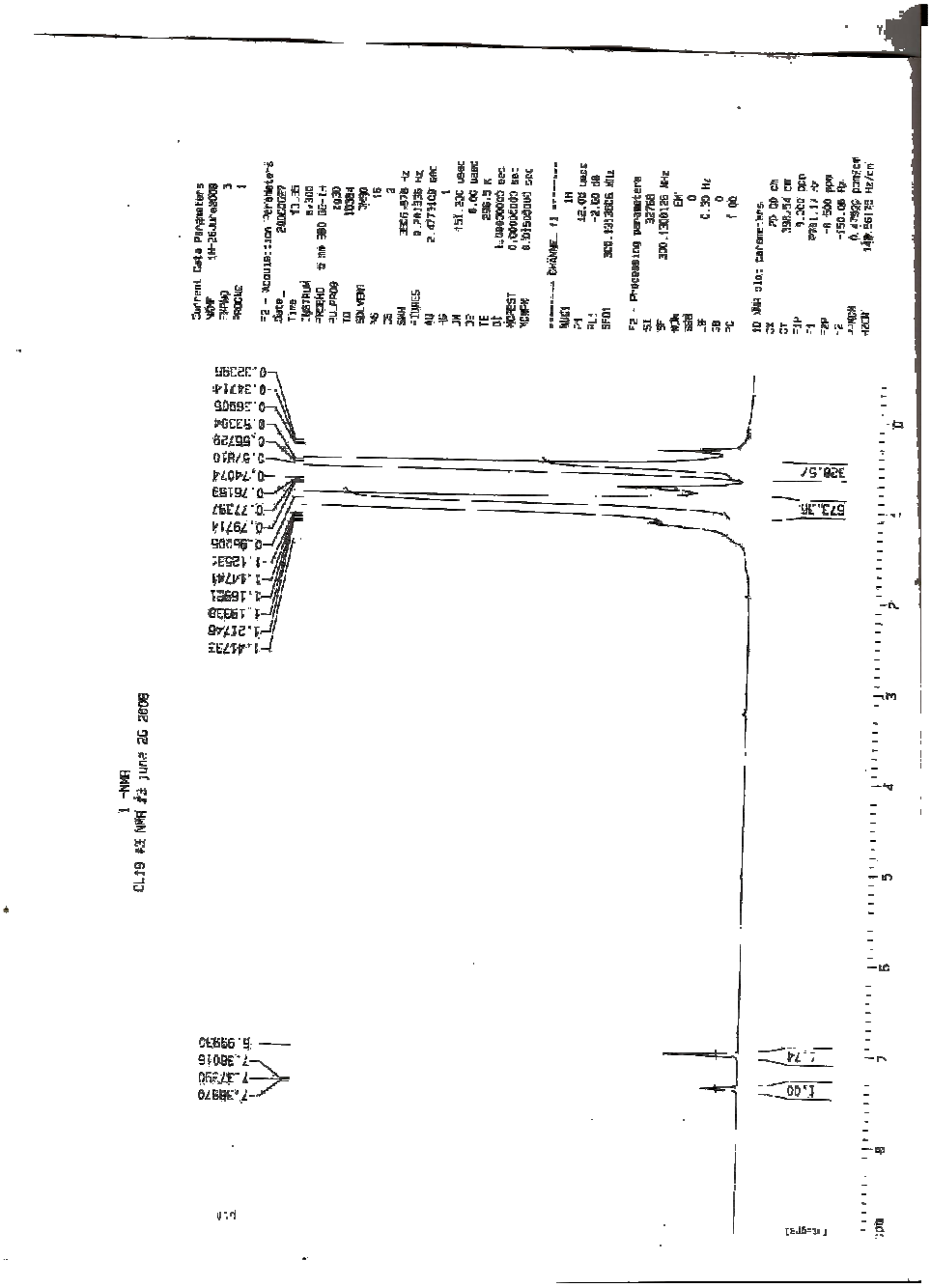

Figure B.19. 3: ^{1}H-NMR Spectrum of naphthalene and tetralin in n-octane, sample #3

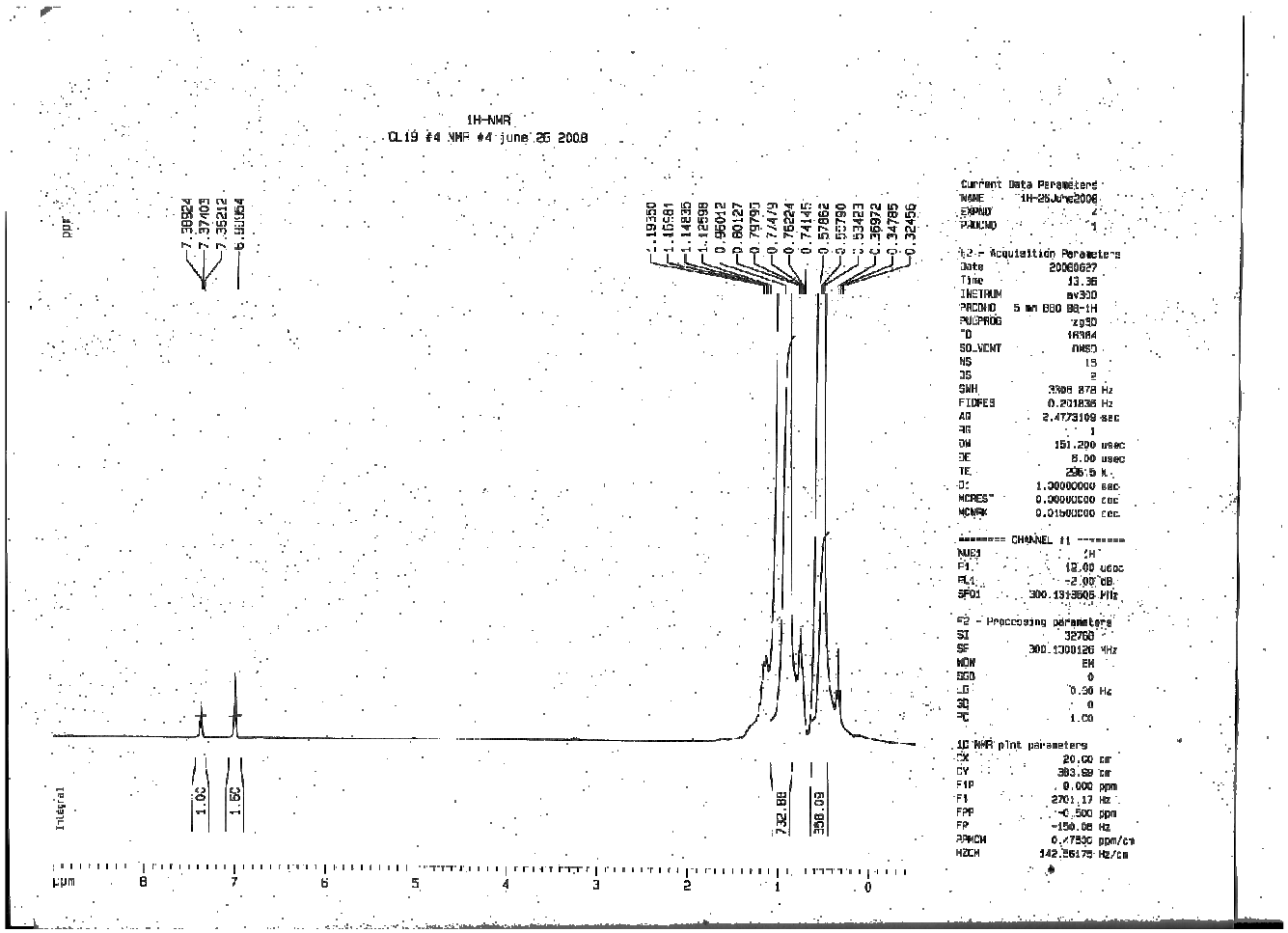

Figure B.19. 4: ^{1}H-NMR Spectrum of naphthalene and tetralin in n-octane, sample #4

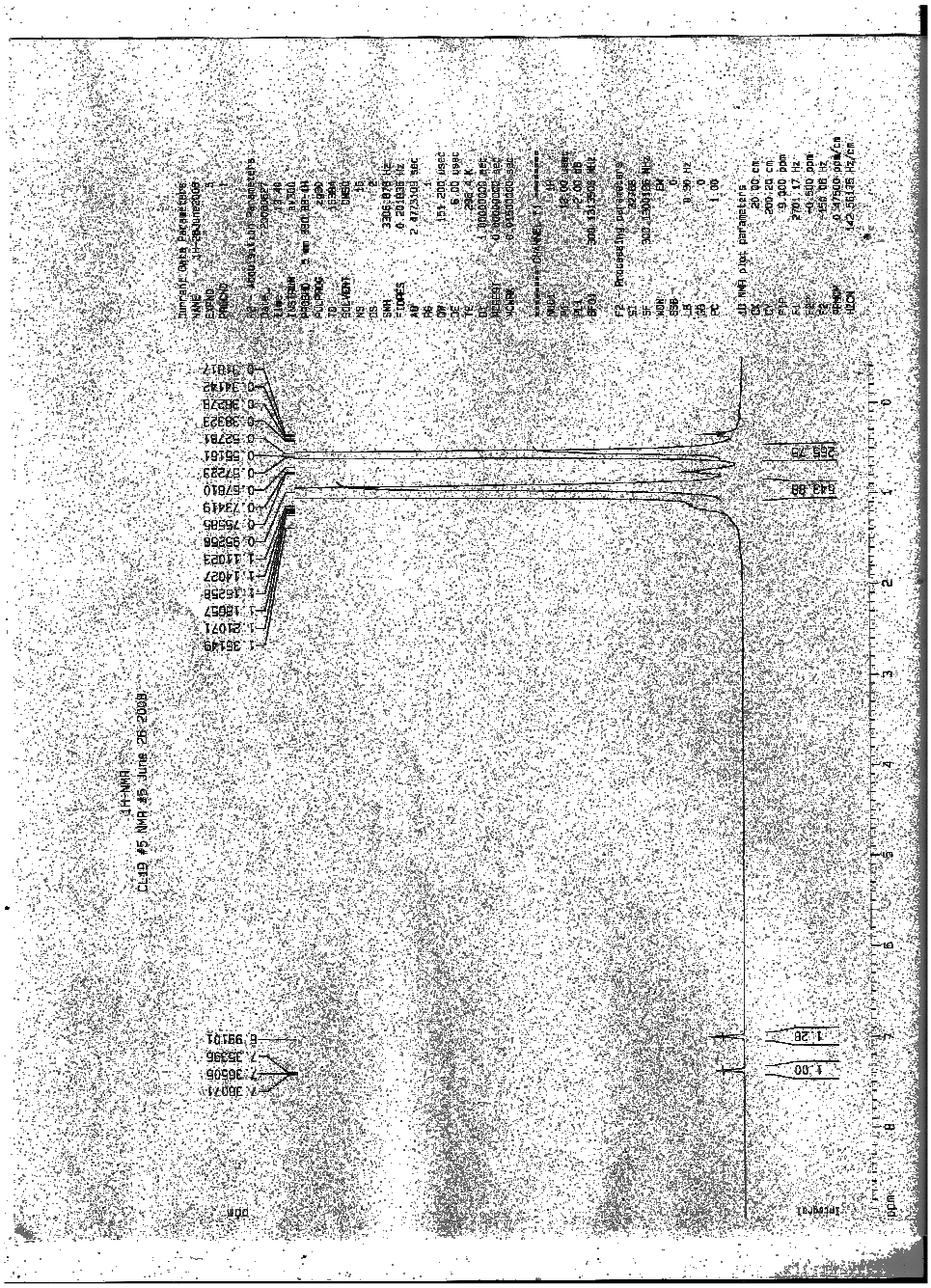

Figure B.19. 5: ^{1}H-NMR Spectrum of naphthalene and tetralin in n-octane, sample #5

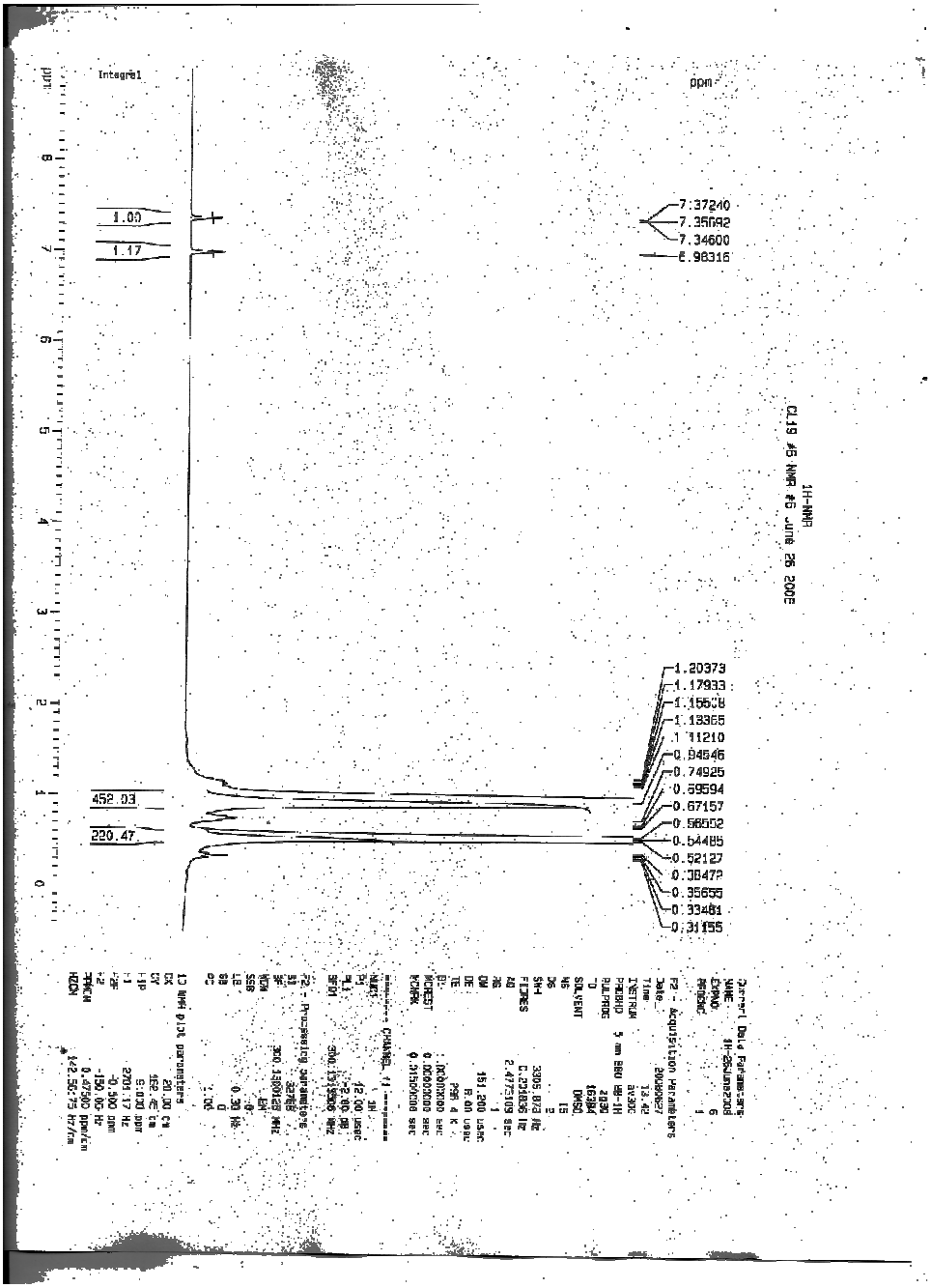

Figure B.19. 6: ^{1}H-NMR Spectrum of naphthalene and tetralin in n-octane, sample #6

B 2. Kinetic Isotope Labeling Experiments

Experimental Conditions for #1: $CO/H_2/D_2O/H_2S$, 15 psig H_2S, 585 psig (1:1 = $CO:H_2$), 4.0°C/min, 340 °C, 3 hrs, 10 ml D_2O, 100 ml n-octane, 3.7 g NAPH, 0.39 mmoles Mo, 1500 RPM Impeller Speed

Table B.1.1. 1: Sample Masses, Experiment #1

Reaction Time (min)	2.17	40.92	76.92	112.92	148.92	180.08
Mass of Empty Vial	16.6795	16.7661	16.7501	16.6811	16.6294	16.8317
Mass of sample + vial	17.7095	17.921	17.5964	17.9676	17.7716	17.8319
mass of liquid sample	1.03	1.1549	0.8463	1.2865	1.1422	1.0002

Table B.1.1. 2: GC Liquid Analysis, Experiment #1

Reaction Time (min)	2.17	40.92	76.92	112.92	148.92	180.08	Final
[NPT] (mol/g-liq)	0.000307	0.000201	0.000149	8.79E-05	5.8E-05	3.85E-05	2.68E-05
[Tet] (mol/g-liq)	3.4E-06	5.7E-05	0.000159	0.000216	0.000255	0.000266	0.000282

Table B.1.1. 3: GC Gas Mol % Fraction Analysis, Experiment #1

Reaction Time (min)	2.17	40.92	76.92	112.92	148.92	180.08
Normalized Mol Fraction						
H2	0.236208	0.318903	0.375825	0.384299	0.396676	0.404356
CO	0.463339	0.307961	0.248351	0.181194	0.161131	0.146641
CO2	0.236208	0.318903	0.375825	0.384299	0.396676	0.404356
H2S	0.064244	0.054233	0	0.050208	0.045516	0.044648

Experimental Conditions for #1R1: $CO/H_2/D_2O/H_2S$, 15 psig H_2S, 585 psig (1:1 = $CO:H_2$), 4.0°C/min, 340 °C, 3 hrs, 10 ml D_2O, 100 ml n-octane, 3.7 g NAPH, 0.39 mmoles Mo, 1500 RPM Impeller Speed

Table B.1.2. 1: Mass of Samples, Experiment #1R1

Reaction Time (min)	3.25	42.25	78.25	114.25	150.25	180.00
Mass of Empty Vial	16.6856	16.5874	16.6365	16.7241	16.6546	16.6008
Mass of sample + vial	17.4551	19.199	19.1499	19.0276	18.842	18.478
mass of liquid sample	0.7695	2.6116	2.5134	2.3035	2.1874	1.8772

Table B.1.2. 2: GC Liquid Analysis, Experiment #1R1

Reaction Time (min)	3.25	42.25	78.25	114.25	150.25	180.00	Final
[NPT] (mol/g-liq)	0.000376	0.00035	0.000327	0.000284	0.000258	0.000211	0.00023
[Tet] (mol/g-liq)	4.92E-06	2.82E-05	7.14E-05	0.000111	0.000152	0.000167	0.000224

Table B.1.2. 3: GC Gas Analysis, ESTD mol%, Experiment #1R1

Reaction Time (min)	3.25	42.25	78.25	114.25	150.25	180.00	Final
H2	19.38814	31.13855	36.73953	40.36954	41.8974	43.39267	42.53408
O2	9.514835	4.43307	2.28463	1.25915	0.76097	0.49852	1.82926
N2	33.79096	16.02376	8.259585	4.526985	2.689905	1.77751	6.179627
CH4			0.07952	0.12891	0.17384	0.215335	0.19715
CO	20.17789	26.71712	25.88908	23.30827	20.34387	18.16531	21.61134
CO2	2.99182	7.79635	12.83702	16.9388	20.54243	22.59611	17.52267
C2H4		0.03293					
C2H6	0.029865	0.04593	0.05689	0.074865	0.11491	0.11914	0.05805
C2H2							
H2S	0.82312	1.36903	1.645095	1.727095	1.81761	1.779125	0.900127
COS	0.04049	0.05419	0.051435	0.0446	0.03882	0.03614	0.057863
1,2 prop=							
Water		2.85213	3.126225	3.12047	3.355315	3.056865	1.649717
C3							
n-C4					0.010255	0.011345	
i-C4			0.01458	0.01658	0.018335	0.01811	

n-C6	0.00244	0.00327	0.003585	0.003455	0.003625	0.00366	

Experimental Conditions for #2: $H_2/D_2O/H_2S$, 15 psig H_2S, 585 psig H_2, 4.0°C/min, 340 °C, 3 hrs, 10 ml D_2O, 100 ml n-octane, 3.7 g NAPH, 0.39 mmoles Mo, 1500 RPM Impeller Speed

Table B.2.1. 1: Sample Masses, Experiment #2

Reaction Time (min)	1.88	38.08	73.58	112.58	145.58	177.58
Mass of Empty Vial	16.8458	16.7053	16.7473	16.8522	16.8152	16.8717
Mass of sample + vial	17.2895	17.8966	17.9841	17.9036	17.7806	17.9773
mass of liquid sample	0.4437	1.1913	1.2368	1.0514	0.9654	1.1056

Table B.2.1. 2: GC Liquid Analysis, Experiment #2

Reaction Time (min)	1.88	38.08	73.58	112.58	145.58	177.58	Final
[NPT] (mol/g-liq)		0.000182	0.000115	6.87E-05	4.37E-05	3.25E-05	2.52E-05
[Tet] (mol/g-liq)	1.44E-05	0.000107	0.00017	0.000224	0.000228	0.000289	0.000306
[NPT] = [NPT0] – [TET]	0.000284	0.000191	0.000128	7.48E-05	7.08E-05	9.52E-06	-7.1E-06

Experimental Conditions for #5: $CO/D_2O/H_2S$, 15 psig H_2S, 585 psig H_2, 4.0°C/min, 340 °C, 3 hrs, 10 ml D_2O, 100 ml n-octane, 3.7 g NAPH, 0.39 mmoles Mo, 1500 RPM Impeller Speed

Table B.5.1. 1: Mass of Samples, Experiment #5

Reaction Time (min)	3.5	39.5	75.5	111.667	147.5	180
Mass of Empty Vial	16.7074	16.5252	16.7941	16.8342	16.6296	16.7431
Mass of sample + vial	18.941	18.2452	18.5283	18.3647	18.7368	18.401
mass of liquid sample	2.2336	1.72	1.7342	1.5305	2.1072	1.6579

Table B.5.1. 2: GC Liquid Analysis, Experiment #5

Reaction Time (min)	3.5	39.5	75.5	111.667	147.5	180
[NPT] (mol/g-liq)	0.000311	0.000276	0.000247	0.000205	0.000159	0.000129
[Tet] (mol/g-liq)	5.3E-06	2.93E-05	6.91E-05	0.000109	0.000149	0.00018
[NPT] = $[NPT]_0$ -	0.000305	0.000281	0.000241	0.000202	0.000162	0.000131

[TET]						

Experimental Conditions for #5R2: ($CO/D_2O/H_2S$, 15 psig H_2S, 585 psig H_2, 4.0°C/min, 340 °C, 3 hrs, 10 ml D_2O, 100 ml n-octane, 3.7 g NAPH, 0.39 mmoles Mo, 1500 RPM Impeller Speed)

Table B.5.3. 1: Mass of Samples, Experiment #5R2

Reaction Time (min)	5.58	46.18	81.58	126.33	159.67	180
Mass of Empty Vial	17.0891	16.7705	16.8136	16.8494	16.8024	16.9147
Mass of sample + vial	18.2402	18.5611	18.2402	18.3443	18.2537	18.2857
mass of liquid sample	1.1511	1.7906	1.4266	1.4949	1.4513	1.371

Table B.5.3. 2: GC Liquid Analysis, Experiment #5R2

Reaction Time (min)	5.58	46.18	81.58	126.33	159.67	180
[NPT] (mol/g-liq)		0.000243	0.000229	0.000185	0.000147	0.000144
[Tet] (mol/g-liq)	1.51E-06	1.36E-05	4.34E-05	7.26E-05	9.56E-05	0.000133
$[NPT] = [NPT]_0 - [TET]$	0.00026	0.000248	0.000218	0.000189	0.000166	0.000128

Table B.5.3. 3: GC Gas Mol % Analysis, Experiment #5R2

Reaction Time (min)	5.58	46.18	81.58	126.33	159.67	180
Normalized Mol%						
H_2	0.146636	0.150284	0.150284	0.175684	0.113459	0.145363
CO	0.675384	0.619797	0.520476	0.440647	0.412599	0.3592
CO_2	0.17798	0.253393	0.318078	0.36729	0.456613	0.457342
H_2S		0.011161	0	0.017329	0.018619	0.017744

Experimental Conditions for #6: $CO/D_2O/H_2S$, 15 psig H_2S, 585 psig H_2, 4.0°C/min, 340 °C, 3 hrs, 10 ml D_2O, 100 ml n-octane, 3.7 g NAPH, 0 mmoles Mo, 1500 RPM Impeller Speed

Table B.6. 1: Mass of Samples, Experiment #6

Reaction Time (min)	4.50	41.00	85.00	122.00	158.00	182
Mass of Empty Vial (g)	17.0753	16.5784	16.6568	16.6009	16.49	16.53
Mass of sample + vial (g)	18.5782	17.3924	18.1736	17.7797	17.225	17.3266
mass of liquid sample (g)	1.5029	0.814	1.5168	1.1788	0.735	0.7966

Table B.6. 2: GC Liquid Analysis, Experiment #6

Time (min)	4.50E+00	3.95E+01	4.10E+01	8.20E+01	8.50E+01	1.18E+02	1.22E+02	1.58E+02	1.80E+02	182
Average [NPT] (mol/g)	4.10E-04	4.39E-04	4.28E-04	4.05E-04	3.83E-04	3.89E-04	3.66E-04	3.51E-04	3.43E-04	0.000326
Average [Tet] (mol/g)	0.00000416	0.00000983	0.0000217	0.0000277	0.0000456	0.0000615	0.0000754	0.0000963	0.000106	0.000117

Table B.6. 3: GC Gas Mol % Analysis, Experiment #6

Reaction Time (min)	4.50	39.5	41.0	82.0	85.0	118.	122.0	153.5	158.0	180.0	182	Final
mol%												
H2	20.69124	24.9819	37.57694	32.40777	34.93157	36.16861	37.57111	38.41682	38.90 08	38.61666	39.68133	41.91776
O2	2.1342	1.90372	1.052581	0.991645	0.823 64	0.910305	0.853895	0.936 62	1.013 68	1.175 94	1.029465	1.680055
N2	38.37341	27.42673	7.435521	13.87449	10.20 522	7.985 13	6.419365	5.746	5.383 515	5.546 15	4.600505	6.314 56
CH4			0.089022	0.032645	0.047 68	0.064 96	0.081675	0.096	0.111 26	0.122 295	0.135 99	0.112 18
CO	24.93 35	29.31783	29.82277	33.23359	33.14705	31.91019	30.79753	29.16239	27.89451	26.24699	25.74412	29.93 84
CO2	1.293835	2.344 06	10.86117	5.365955	7.136575	8.964915	10.45868	12.05291	13.44543	14.56238	15.50671	10.85286
C2H4		0.031 08	0.025943	0.026435	0.025 45							
C2H6	0.016677	0.026 42	0.066802	0.043925	0.058 05	0.057515	0.066185	0.074 29	0.081 99	0.087 57	0.092305	0.043 13
C2H2												
H2S	1.366 12	1.680 02	2.255486	2.155 21	2.295495	2.377 46	2.418 22	2.471 08	2.511 78	2.516 36	2.524 02	1.137 55
COS	0.066325	0.081285	0.091284	0.101 51	0.100515	0.096 89	0.092 33	0.088 5	0.084 52	0.079 43	0.076515	0.099 95
1,2 prop=												
Water		3.442 42	2.792224	3.093625	2.737 3	3.135 15	3.102	3.148 67	3.337 22	3.235775	2.918 73	0.599772
C3			0.010 76		0.008 7	0.010 2	0.012145	0	0.014 4		0.015555	
n-C4			0.010 84				0.006 37	0.010 9	0.010625	0.014145	0.009955	
i-C4	0	0	0.017479	0.014025	0.014 75	0.017 55	0.016805	0.016 61	0.018 82	0.021225	0.019 61	
n-C6	0.004 98	0.005 16	0.005917	0.005 65	0.005475	0.005885	0.005 86	0.006 15	0.006155	0.006 28	0.005995	
n-C8	1.990 88	2.258 53	1.704659	1.971495	1.788665	1.996 67	1.895 39	1.919 26	1.939925	1.914 45	1.798 36	0.225015

Experimental Conditions for #7: $CO/H_2O/H_2S$, 15 psig H_2S, 585 psig H_2, 4.0°C/min, 340 °C, 3 hrs, 10 ml D_2O, 100 ml n-octane, 3.7 g NAPH, 0.39 mmoles Mo, 1500 RPM Impeller Speed

Table B.7.1: Mass of Samples, Experiment #7

Reaction Time (min)	5.5	37.5	76.5	109.5	142.5	180
Mass of Empty Vial	16.6681	16.6094	16.7357	16.6511	16.8674	16.6669
Mass of sample + vial	19.2175	18.9172	18.1973	19.2986	19.0684	18.4452
mass of liquid sample	2.5494	2.3078	1.4616	2.6475	2.201	1.7783

Table B.7. 2: GC Liquid Analysis, Experiment #7

Reaction Time (min)	5.5	37.5	76.5	109.5	142.5	180
[NPT] (mol/g-liq)	0.000409	0.000375	0.000328	0.000283	0.000231	0.000181
[Tet] (mol/g-liq)	6.43E-06	3.15E-05	7.49E-05	0.000128	0.000186	0.000226
$[NPT] = [NPT]_0 - [TET]$	0.000402	0.000377	0.000334	0.000281	0.000222	0.000183

Table B.7. 3: GC Gas Analysis, ESTD mol%, Experiment #7

Reaction Time (min)	5.5	37.5	76.5	109.5	142.5	180	Final
H2	10.23121	19.51655	27.13614	31.24715	34.01994	35.64341	27.04866
O2	8.01412	3.43116	1.47417	0.63503	0.310295	0.1114	1.959717
N2	31.26973	14.2776	6.9002	3.60615	2.333235	1.796585	9.431377
CH4			0.019065	0.03168	0.04543	0.059695	0.05133
CO	32.7435	38.68886	33.40004	27.18789	22.33753	18.48655	31.28957
CO2	10.01717	19.35892	26.87526	33.54757	37.87991	41.15709	32.72063
C2H4							
C2H6	0.010505	0.02126	0.07457	0.07823	0.083055	0.095525	0.05081
C2H2		0					
H2S	0.12275	0.18369	0.212975	0.24542	0.25762	0.26751	0.101913
COS	0.02534	0.02561	0.019905	0.01515	0.01235		0.04187
Water		2.81466	3.029175	3.02817	3.02408	3.24378	0.641963
C3		0.01555	0.00809				
n-C4			0.004385		0.007795	0.00847	
i-C4			0.0025	0.0172	0.017975	0.019715	
n-C8	2.01209	1.74105	1.761085	1.79384	1.74269	1.852175	0.19877

Experimental Conditions for #17: $H_2/H_2O/H_2S$, 15 psig H_2S, 585 psig H_2, 4.0°C/min, 340 °C, 3 hrs, 10 ml H_2O, 100 ml n-octane, 3.7 g NAPH, 0.39 mmoles Mo, 1500 RPM Impeller Speed

Table B.17. 1: Mass of Samples, Experiment #17

Reaction Time (min)	1.75	39	76.75	113	146.75	180
Mass of Empty Vial (g)	16.4928	16.4251	16.5274	16.5447	16.4664	16.467
Mass of sample + vial (g)	17.0721	16.7305	16.986	16.9297	18.5875	18.5052
mass of liquid sample (g)	0.5793	0.3054	0.4586	0.385	2.1211	2.0382

Table B.17. 2: GC Analysis, Experiment #17

Reaction Time (min)	1.75	39	76.75	113	146.75	180	Final
[NPT] (mol/g-liq)	0.000517	0.000407	0.000231	0.000141	6.52E-05	4.75E-05	0.00047052
[TET] (mol/g-liq)	3.02E-05	0.000159	0.000305	0.000419	0.000388	0.000385	0
[c-DEC] (mol/g-liq)	0	3.69E-07	1.11E-06	2.81E-06	4.32E-06	5.47E-06	1.13462E-05
[t-DEC] (mol/g-liq)	0	3.69E-07	1.85E-06	4.45E-06	7.14E-06	8.97E-06	1.91626E-05
$[NPT] = [NPT]_0 - [TET]-[DEC]$	0.000517	0.000566	0.000539	0.000568	0.000464	0.000447	0.000501

Table B.17. 3: Gas Analysis, ESTD mol%, Experiment #17

Experiment #17						
Reaction Time (min)	1.75	39	76.75	113	146.75	180
Average ESTD mol%						
H2	30.54748	30.97922	31.50314	28.92085	48.86165	50.77078
O2	12.88293	13.64099	13.7689	14.28802	10.34075	9.95006
N2	50.972	51.61658	51.92845	53.90311	38.77356	37.28057
CH4		0	0	0	0	0
CO	0	0	0	0	0	0
CO2	0.111335	0.07188	0.07052	0.07499	0.09133	0.09322
C2H4						
C2H6	0.12585	0.07735	0.08402	0.08244	0.129935	0.13356
C2H2						
H2S	0.764225	1.00744	1.05781	1.020235	1.607785	1.64965
COS	0	0	0	0	0	0
1,2-Prop=	0	0	0	0	0	0
Water	0	0	0	0	0	0
Prop	0	0	0	0	0	0
C3	0	0	0	0	0	0
n-C4	0	0	0	0	0.00234	0.00501
i-C4	0		0.003665	0.0037	0.004535	0.004705
n-C6	0	0.00237	0.003295	0.003145	0.00372	0.004275
n-C8	2.234765	2.125045	1.98877	2.06194	1.90478	1.941105

Table B.17. 4: Calculated Gas Concentrations, Experiment #17

Reaction Time (min)	1.75	39	76.75	113	146.75	180
Total calculated moles of gas in sampling bomb (moles)	0.006665	0.006333	0.006265	0.00602	0.007917	0.007302
n H2 (mols) from gas sampling PT data	0.002036	0.001962	0.001974	0.001741	0.003868	0.003707
[H2] (mol/g-Liq)	0.003515	0.006424	0.004304	0.004522	0.001824	0.001819

Experimental Conditions for #28: $H_2/H_2O/H_2S$, 15 psig H_2S, 585 psig CO, 4.0°C/min, 340 °C, 3 hrs, 10 ml H_2O, 100 ml n-octane, 3.7 g NAPH, 0.39 mmoles Mo, 1500 RPM Impeller Speed

Table B.28. 1: Mass of Samples, Experiment #28

Sample #	*Purge*	1	2	2B	3	3B	4	4B	5	5B	6	6B
Reaction Time (min)		0		36		76.5		113.5		153.5		179.3
Mass of Empty Vial (g)	16.782	16.4334	16.6457	16.4187	16.4406	16.4696	16.4939	16.9483	16.9435	16.5416	16.5142	16.728
Mass of sample + vial (g)	18.7742	18.5138	17.377	18.3391	17.1728	18.4145	17.1378	18.7062	17.266	18.1335	17.1559	18.3445
mass of liquid sample (g)	1.9922	2.0804	0.7313	1.9204	0.7322	1.9449	0.6439	1.7579	0.3225	1.5919	0.6417	1.6165

Table B.28. 2: GC Analysis, Experiment #28

Reaction Time (min)	0	36	76.5	113.5	153.5	179.3167
[NPT] (mol/g-liq)	0.000403	0.000244	0.000128	7.46E-05	5.15E-05	4.69E-05
[TET] (mol/g-liq)	4.89E-05	0.000224	0.000315	0.000343	0.00036	0.000386
[c-DEC] (mol/g-liq)	1.45E-07	5.55E-07	1.83E-06	3.22E-06	5.06E-06	6.53E-06
[t-DEC] (mol/g-liq)	2.41E-07	1.08E-06	3.23E-06	5.64E-06	8.5E-06	1.09E-05
$[NPT] = [NPT]_0 - [TET]-[DEC]$	0.000395	0.000218	0.000124	9.26E-05	7.04E-05	4.01E-05

Table B.28. 3: GC Analysis, ESTD mol%, Experiment #28

Reaction Time (min)	0	36	76.5	113.5	153.5	179.3167
H2	48.52133	49.01566	47.66606	50.66847	48.56587	37.70443
O2	10.07084	9.869535	10.16225	9.566325	9.93073	12.20178
N2	37.9991	37.30546	38.35841	36.11552	37.48964	46.31809
CH4	0	0	0	0	0	0
CO	0	0	0	0	0	0
CO2	0.122825	0.15088	0.11811	0.187145	0.124185	0.11421
C2H4	0.09247	0	0	0	0	0
C2H6	0.44287	0.70153	0.715225	0.80451	0.710995	0.52571
C2H2	0	0	0	0	0	0
H2S	0.94378	1.162985	1.21971	1.37202	1.24392	0.868675
COS	0	0	0	0	0	0
1,2-Prop=	0	0	0	0	0	0
Water	0.46768	0.53217	0.511125	0.507465	0.596225	0.432165
Prop	0	0	0	0	0	0
C3	0	0	0	0	0	0
n-C4	0	0	0	0	0	0
i-C4	0.02807	0.02748	0.02693	0.02633	0.02681	0.02239
n-C6	0	0	0	0.002175	0	0.00432
n-C8	1.41547	1.36672	1.312615	1.306785	1.449605	1.14064

Table B.28. 4: Calculated Gas Analysis, Experiment #28

Reaction Time (min)	0	36	76.5	113.5	153.5	179.3167
Total calculated moles of gas in sampling bomb (moles)	0.008541	0.008293	0.008135	0.00806	0.008095	0.00971
[H2] (mol / g-Liq)	0.001992	0.002117	0.001994	0.002323	0.00247	0.002265

B 3 Effect of Solvent on WGS and and naphthalene hydrogenation in emulsions

Experimental Conditions for #15: $CO/H_2/H_2O/H_2S$, 15 psig H_2S, 585 psig (1:1 = $CO:H_2$), 4.0°C/min, 340 °C, 3 hrs, 10 ml H_2O, 100 ml n-octane, 3.7 g NAPH, 0.39 mmoles Mo, 1500 RPM Impeller

Table B.15. 1: Mass of Samples, Experiment #15

Reaction Time (min)	2.55	37.21667	73.55	108.05	144.05	180
Mass of Empty Vial	16.4732	16.4952	16.6002	16.909	16.9691	16.5493
Mass of sample + vial	17.457	17.5397	17.561	18.1449	18.0785	18.6634
mass of liquid sample	0.9838	1.0445	0.9608	1.2359	1.1094	2.1141

Table B.15. 2: GC Liquid Analysis, Experiment #15

Reaction Time (min)	2.55	37.21667	73.55	108.05	144.05	180	Final
[NPT] (mol/g-liq)	0.000474	0.000392	0.000316	0.000277	0.000216	0.00016	0.000471
[TET] (mol/g-liq)	1.71E-05	8.35E-05	0.000154	0.000216	0.00026	0.000287	0.000718
[c-DEC] (mol/g-liq)	0	0	0	7.23E-07	7.23E-07	1.28E-06	4.65E-06
[t-DEC] (mol/g-liq)	0	0	0	7.23E-07	1.21E-06	1.74E-06	7.48E-06
[NPT] = [NPT]0 - [TET]-[DEC]	0.000456	0.00039	0.00032	0.000256	0.000212	0.000183	-0.00026

Table B.15. 3: GC Analysis, ESTD mol%, Experiment #15

Reaction Time (min)	2.55	37.21667	73.55	108.05	144.05	180	Final
H2	20.91247	22.72481	26.06571	25.32719	23.66655	35.26026	47.81594
O2	12.26851	11.96504	10.88215	11.12995	11.59396	7.6117	2.938305
N2	46.5536	45.29375	41.24555	42.1874	43.88056	28.88559	11.05437
CH4		0.02626	0.04959	0.066125	0.074375	0.13007	0.150635
CO	11.16778	8.27789	7.177445	5.606535	4.271755	5.31705	14.10342
CO2	4.905645	7.798445	10.68041	12.19014	12.58895	19.56075	21.75184
C2H4							0
C2H6	0.068065	0.065535	0.078095	0.08364	0.082145	0.119965	0.09832
C2H2							0
H2S	0.64779	0.72693	0.83206	0.86192	0.81677	1.16475	0.90427
COS	0.030815	0.02415	0.02052	0.0169	0.013205	0.01494	0.04956
1,2-Prop=	0	0	0	0	0	0	0
Water	2.981325	2.750725	2.75679	2.308315	3.1754	2.89593	3.211485
Prop	0	0	0	0	0	0	0
C3	0	0	0	0.00818	0.00766	0.01054	0
n-C4	0	0	0	0.004355	0.00409	0.00653	0
i-C4	0		0.003715	0.004305	0.00357	0.00515	0
n-C6	0.00263	0.00267	0.002475	0.002725	0.00261	0.004205	0
n-C8	1.15778	1.64834	1.71474	1.532615	1.802065	1.762575	0.66002

Table B.15. 4: GC Gas Concentrations, Experiment #15

Reaction Time (min)	2.55	37.21667	73.55	108.05	144.05	180
Total calculated moles of gas in sampling bomb (moles)	0.006887	0.006974	0.00716	0.007075	0.007184	0.009768
[H2] (mol/g liq)	0.001464	0.001517	0.001942	0.00145	0.001532	0.001629
[CO] (mol/g liq)	0.000782	0.000553	0.000535	0.000321	0.000277	0.000246
[CO2] (mol/g liq)	0.000343	0.000521	0.000796	0.000698	0.000815	0.000904

Experimental Conditions for #25: $CO/H_2O/H_2S$, 15 psig H_2S, 585 psig CO, 4.0°C/min, 340 °C, 3 hrs, 10 ml H_2O, 100 ml toluene, 3.7 g NAPH, 0.39 mmoles Mo, 1500 RPM Impeller Speed

Table B.25. 1: Mass of Samples, Experiment #25

Sample #	Purge	1	2	2B	3	3B	4	4B	5	5B	6	6B
Reaction Time (min)		1		37.5		72.5		108		144.5		180
Mass of Empty Vial (g)	16.5378	16.6988	16.6032	16.5188	16.5156	16.5835	16.626	16.5135	16.5344	16.5766	16.4163	16.5174
Mass of sample + vial (g)	18.5412	19.179	18.8047	18.3452	18.2046	18.5627	17.8922	18.7028	17.6812	18.7988	17.5367	18.7888
mass of liquid sample (g)	2.0034	2.4802	2.2015	1.8264	1.689	1.9792	1.2662	2.1893	1.1468	2.2222	1.1204	2.2714

Table B.25. 2: GC Liquid Analysis, Experiment #25

Reaction Time (min)	1	37.5	72.5	108	144.5	180
[NPT] (mol/g-liq)	0.000431	0.000368	0.00026	0.000177	0.000138	0.000118
[TET] (mol/g-liq)	2.95E-05	0.00013	0.000238	0.00029	0.000335	0.000356
[c-DEC] (mol/g-liq)	1.45E-07	1.69E-07	4.34E-07	8.44E-07	1.66E-06	2.22E-06
[t-DEC] (mol/g-liq)	2.89E-07	3.62E-07	6.99E-07	1.66E-06	3.42E-06	4.12E-06
$[NPT] = [NPT]_0 - [TET]-[DEC]$	0.000455	0.000355	0.000246	0.000192	0.000145	0.000122

Table B.25. 3: GC Analysis, ESTD mol%, Experiment #25

Reaction Time (min)	1	37.5	72.5	108	144.5	180
H2	18.83904	23.66447	23.639	23.319	23.34695	22.92294
O2	6.4901	6.148	6.06356	5.93037	5.754895	5.794815
N2	24.87588	23.53149	23.0773	22.57958	21.91093	22.04533
CH4		0	0	0	0	0
CO	26.00336	15.14023	10.33037	7.81876	6.75008	5.855175
CO2	17.3898	28.16114	30.05821	32.99538	35.06144	36.13704
C2H4						
C2H6	0.052405	0.08503	0.130465	0.134835	0.136855	0.138305
C2H2						
H2S	0.71693	0.90719	0.915495	0.913825	0.953515	0.936135
COS	0.091275	0.04655	0.03095	0.022765	0.02079	0.01815
1,2-Prop=	0	0	0	0	0	0
Water	0.51425	0.58673	0.565115	0.620775	0.55662	0.58188
Prop	0	0	0	0	0	0
C3	0	0	0	0	0	0
n-C4	0	0	0	0	0	0
i-C4	0.020185		0.01242	0.018575	0.012575	0.0123
n-C6	0	0	0	0	0	0
n-C8	0	0	0	0	0	0

Table B.25. 4: GC Gas Concentrations, Experiment #25

Reaction Time (min)	1	37.5	72.5	108	144.5	180
Total calculated moles of gas in sampling bomb (moles)	0.009774	0.010281	0.010522	0.010621	0.010458	0.010547
[H2] (mol/g liq)	0.001025	0.000628	0.000438	0.000335	0.000285	0.000249
[CO] (mol/g liq)	0.000742	0.000981	0.001003	0.000999	0.000984	0.000975
[CO2] (mol/g liq)	0.000685	0.001167	0.001275	0.001413	0.001478	0.001537

.

Experimental Conditions for #29: $N_2/H_2/H_2O/H_2S$, 15 psig H_2S, 585 psig (1:1 = CO/H_2), 4.0°C/min, 340 °C, 3 hrs, 10 ml H_2O, 100 ml n-octane, 3.7 g NAPH, 0.39 mmoles Mo, 1500 RPM Impeller Speed

Table B.29. 1: Mass of Samples, Experiment #29

Sample #	*Purge*	1	2	2B	3	3B	4	4B	5	5B	6	6B
Reaction Time (min)		0.5		36.5		70		106.3		143		179.9
Mass of Empty Vial (g)	16.3807	16.5295	16.9221	16.6963	16.2579	16.3339	16.5873	16.49	16.6556	16.6351	16.3269	16.6421
Mass of sample + vial (g)	17.8903	18.6163	17.9339	18.4526	17.3333	18.3495	17.4166	18.3583	17.2891	18.57	17.0985	18.92
mass of liquid sample (g)	1.5096	2.0868	1.0118	1.7563	1.0754	2.0156	0.8293	1.8683	0.6335	1.9349	0.7716	2.2779

Table B.29. 2: GC Analysis, Experiment #29

Reaction Time (min)	0.5	36.5	70	106.3	143	179.9167
[NPT] (mol/g-liq)	0.0004	0.000304	0.00024	0.000201	0.000172	0.000155
[TET] (mol/g-liq)	3.37E-05	0.000123	0.000186	0.000235	0.000254	0.000266
[c-DEC] (mol/g-liq)	2.17E-07	1.45E-07	2.89E-07	5.79E-07	7.59E-07	9.76E-07
[t-DEC] (mol/g-liq)	2.89E-07	2.89E-07	5.79E-07	1.01E-06	1.41E-06	1.88E-06
$[NPT] = [NPT]_0 - [TET]-[DEC]$	0.000396	0.000307	0.000243	0.000193	0.000174	0.000161

Table B.29. 3: GC Analysis, ESTD mol%, Experiment #29

Reaction Time (min)	0.5	36.5	70	106.3	143	179.9167	Final
H2	24.89579	22.7451	20.65091	18.07557	18.73282	20.77378	0.388953
O2	8.711115	8.40815	8.784355	9.552125	9.12212	8.21031	0.022468
N2 (air) – calculated from O2 mol%	34.84446	33.6326	35.13742	38.2085	36.48848	32.84124	0.089873
N2 (system)	26.53447	29.11421	29.36834	27.46538	29.28675	32.68608	0.59238
N2 (total) – measured by GC	61.37893	62.74681	64.50576	65.67388	65.77523	65.52732	
CH4	0	0	0	0	0	0	0
CO	0	0	0	0	0	0	0
CO2	0.11581	0.11739	0.099285	0.09602	0.10034	0.09627	0.001115
C2H4	0.126105	0.05708	0	0	0	0	0
C2H6	0.4693	0.8973	0.900975	0.85895	0.894155	0.948665	0.00289
C2H2	0	0	0	0	0	0	0
H2S	0.779745	0.914835	0.85168	0.89081	0.93179	0.98934	0.007428
COS	0	0	0	0	0	0	0
1,2-Prop=	0	0	0	0	0	0	0
Water	0.44091	0.58215	0.592375	0.72193	0.70723	0.6436	0.004128
Prop	0	0	0	0	0	0	0
C3	0	0	0	0	0	0	0
n-C4	0	0	0	0	0	0	0
i-C4	0.00776	0.01027	0.0198	0.00695	0.0149	0.01504	0
n-C6	0	0	0	0	0	0	0
n-C8	1.429975	1.600115	1.56493	1.696655	1.733405	1.557555	0.003106

Table B.29. 4: GC Analysis, Experiment #29

Reaction Time (min)	0.5	36.5	70	106.3	143	179.9167
Total calculated moles of gas in sampling bomb (moles)	0.008669	0.008618	0.00891	0.008887	0.008421	0.008747
[H2] (mol/g-liq)	0.001034	0.001116	0.000913	0.00086	0.000815	0.000798
[N2] (mol/g-liq)	0.001102	0.001429	0.001298	0.001306	0.001275	0.001255

Table B.24. 1: Mass of Samples, Experiment #24

Experimental Conditions for #24: $CO/H_2O/H_2S$, 15 psig H_2S, 585 psig CO, 4.0°C/min, 340 °C, 3 hrs, 10 ml H_2O, 100 ml toluene, 4.5 g NAPH, 0.47 mmoles Mo, 1500 RPM Impeller Speed

Sample #	Purge	1	2	2B	3	3B	4	4B	5	5B	6	6B
Reaction Time (min)		1.75		39		76.75		113		146.75		180
Mass of Empty Vial (g)	16.6108	16.5568	16.573	16.4738	16.5838	16.5821	16.5907	16.4891	16.5599	16.6097	16.5407	16.5743
Mass of sample + vial (g)	18.9427	19.2505	17.8019	19.0021	17.9428	18.9716	18.1643	17.6402	17.6239	17.8998	17.4802	18.8461
mass of liquid sample (g)	2.3319	2.6937	1.2289	2.5283	1.359	2.3895	1.5736	1.1511	1.064	1.2901	0.9395	2.2718

Table B.24. 2: GC Liquid Analysis, Experiment #24

Time (min)	1.00	37.5	72.5	108	144.5	180
[NPT] (mol/g-liq)	0.000465	0.000405	0.000288	0.000218	0.000156	0.000128
[TET] (mol/g-liq)	2.4E-05	0.000146	0.00025	0.000351	0.00036	0.000343
[c-DEC] (mol/g-liq)	3.62E-07	3.86E-07	7.23E-07	1.06E-06	1.45E-06	1.93E-06
[t-DEC] (mol/g-liq)	6.03E-07	6.75E-07	1.01E-06	1.93E-06	3.06E-06	3.18E-06
$[NPT] = [NPT]_0 - [TET]-[DEC]$	0.000507	0.000385	0.00028	0.000178	0.000168	0.000184

Table B.24. 3: GC Gas Analysis, ESTD mol%, Experiment #24

Reaction Time (min)	1	37.5	72.5	108	144.5	180	Final
Average ESTD mol%							
H2	17.42496	21.94358	22.72219	15.79708	14.46455	20.71866	24.83501
O2	6.582735	5.788025	5.570615	9.903865	9.759925	6.07343	0.87273
N2	25.53505	22.42639	21.60324	37.71162	38.05975	23.3895	3.795143
CH4		0	0	0	0	0	0
CO	27.34936	16.95907	11.81247	6.30105	4.83709	5.700205	26.02378
CO2	17.08484	26.29272	30.57282	23.63066	26.47778	35.8348	40.88964
C2H4							0
C2H6	0.12805	0.18652	0.193325	0.117575	0.145235	0.196735	0.19122
C2H2							0
H2S	0.57216	0.77065	0.793165	0.61622	0.21827	0.85157	1.030533
COS	0.09774	0.05339	0.035765	0.022995	0.02055	0.019135	0.14232
1,2-Prop=	0	0	0	0	#DIV/0!	0	0
Water	0.43713	0.461325	0.551325	0.45408	0.58906	0.563905	0.39412
Prop	0.0121	0	0	0	0	0	0
C3	0	0	0	0	0	0	0
n-C4	0	0	0	0	0	0	0
i-C4	0.01542		0.020325	0.024785	0.03647	0.02535	0
n-C6	0	0.0021	0	0	0	0	0
n-C8	0.049825	0.036755	0.029825	0.0271	0.039065	0.02774	0.01497

Table B.24. 4: GC Gas Concentrations, Experiment #24

Reaction Time (min)	1	37.5	72.5	108	144.5	180
Total calculated moles of gas in sampling bomb (moles)	0.009486	0.010307	0.010216	0.007024	0.007063	0.010415
[H2] (mol/g liq)	0.000963	0.000649	0.000448	0.000164	0.000127	0.00022
[CO] (mol/g liq)	0.000614	0.00084	0.000862	0.000412	0.000379	0.000801
[CO2] (mol/g liq)	0.000602	0.001006	0.001159	0.000616	0.000694	0.001385

B4 Mixed-metal Catalysts for WGS and Naphthalene Hydrogenation

Experimental Conditions for #10: $CO/H_2O/H_2S$, 15 psig H_2S, 585 psig CO, 4.0°C/min, 340 °C, 4 hrs, 18 ml D_2O, 52 ml toluene, 11.17 g NAPH, 1.16 mmoles Mo, 1500 RPM Impeller Speed

Table B.10. 1: Mass of Samples, Experiment #10

Reaction Time (min)	2.333333	50	98	146	194	240
Mass of Empty Vial	16.7094	16.5821	16.8526	16.6112	16.7102	16.3757
Mass of sample + vial	18.3507	17.6686	17.9454	17.5919	17.618	17.1968
mass of liquid sample	1.6413	1.0865	1.0928	0.9807	0.9078	0.8211

Table B.10. 2: GC Analysis, Experiment #10

Reaction Time (min)	2.333333	50	98	146	194	240	
[NPT] (mol/g-liq)	0.002297	0.001658	0.000976	0.000801	0.000619	0.00056	0.000471
[TET] (mol/g-liq)	3.18E-05	0.000619	0.001158	0.001577	0.001681	0.001763	0.001583
[c-DEC] (mol/g-liq)	0	9.27E-07	2.89E-06	6.21E-06	7.65E-06	1.04E-05	1.13E-05
[t-DEC] (mol/g-liq)	0	1.39E-06	4.34E-06	8.79E-06	1.34E-05	1.77E-05	1.92E-05
$[NPT] = [NPT]_0 - [TET]-[DEC]$	0.002265	0.001676	0.001132	0.000705	0.000595	0.000506	0.000684

Table B.10. 3: GC Gas Analysis, ESTD mol%, Experiment #10

Reaction Time (min)	2.333333	50	98	146	194	240
H2	20.51126	23.13192	21.26485	19.60065	18.10106	17.34976
O2	8.5417	7.74653	7.333535	6.99561	7.54379	7.282195
N2	32.459	29.35316	27.81058	26.54217	28.58188	27.5672
CH4		0.06065	0.084525	0.09971	0.102275	0.10974
CO	10.81996	1.796275	0.73883	0.58182	0.47927	0.474445
CO2	20.30867	30.56363	35.68412	38.5065	37.2428	38.71705
C2H4						
C2H6	0.20065	0.248545	0.28295	0.30604	0.29274	0.305265
C2H2						
H2S	0.583855	0.705075	0.84204	0.908015	0.867715	0.91729
COS	0.024485	0	0	0	0	0
1,2-Prop=						
Water						
Prop						
C3						
n-C4						0.005805
i-C4	0		0.00745	0.008065	0.00799	0.008245
n-C6	0	0	0	0	0	0
n-C8	0.1932	0.17396	0.1349	0.52114	0.056615	0.042135

Table B.10. 4: GC Gas Concentration, Experiment #10

Reaction Time (min)	2.333333	50	98	146	194	240
Total calculated moles of gas in sampling bomb (moles)	0.00897	0.01041	0.010262	0.01015	0.010186	0.009798
[H2] (mol/g liq)	0.001121	0.002216	0.001997	0.002029	0.002031	0.00207
[CO] (mol/g liq)	0.000591	0.000172	6.94E-05	6.02E-05	5.38E-05	5.66E-05
[CO2] (mol/g liq)	0.00111	0.002928	0.003351	0.003985	0.004179	0.00462

Experimental Conditions for #12: $CO/H_2O/H_2S$, 15 psig H_2S, 585 psig CO, 4.0°C/min, 340 °C, 4 hrs, 18 ml H_2O, 52 ml toluene, 11.17 g NAPH, 0 mmoles Mo, 1500 RPM Impeller Speed

Table B.12. 1: Sample of Masses, Experiment #12

Reaction Time (min)	2.75	47.25	95.75	142.24	189.75	240
Mass of Empty Vial	16.4932	16.4647	16.3275	16.5898	16.4082	16.4798
Mass of sample + vial	17.955	17.515	17.3706	17.6336	17.3678	18.1438
mass of liquid sample	1.4618	1.0503	1.0431	1.0438	0.9596	1.664

Table B.12. 2: GC Analysis, Experiment #12

Reaction Time (min)	2.75	47.25	95.75	142.24	189.75	240	Final
[NPT] (mol/g-liq)	.001963	0.001966	0.001951	0.001864	0.001766	0.001243	0.000471
[TET] (mol/g-liq)	0	4.21e-05	0.000107	0.000186	0.000283	0.000316	0.001583
[c-DEC] (mol/g-liq)	0	0	0	0	0	0	0
[t-DEC] (mol/g-liq)	0	0	0	0	0	0	0

Table B.12. 3: GC Analysis, Experiment #12

Reaction Time (min)	2.75	47.25	95.75	142.25	189.75	240
Average ESTD mol%						
H2	8.44547	16.42401	20.62474	22.04905	22.22162	28.05889
O2	9.557655	8.07252	7.26574	7.08282	7.540775	4.629415
N2	36.25177	30.49896	27.49574	26.85425	28.4217	17.56415
CH4		0.019795	0.03847	0.05472	0.066085	0.10242
CO	30.04017	20.72653	16.40921	12.76979	9.854625	10.02895
CO2	7.76776	15.7986	20.25204	23.38165	24.43037	33.69321
C2H4						
C2H6	0.039895	0.13082	0.19608	0.247945	0.269875	0.36749
C2H2						
H2S	0.63896	0.802855	0.837405	0.834635	0.79491	0.936965
COS	0.14117	0.08219	0.054935	0.039995	0.027655	0.027495
1,2-Prop=						
Water						
Prop						
C3						
n-C4						0.006165
i-C4	0		0	0.003985	0.004435	0.005485
n-C6	0	0	0	0	0	0
n-C8	0.08095	0.06965	0.03404	0.019445	0.012785	0

Experimental Conditions for #30: ($CO/H_2O/H_2S$, 15 psig H_2S, 585 psig CO, 4.0°C/min, 340 °C, 3 hrs, 10 ml H_2O, 100 ml toluene, 3.7 g NAPH, 0 mmoles Mo)

Table B.30. 1: Mass of Samples, Experiment #30

Sample #	Purge	1	2	2B	3	3B	4	4B	5	5B	6	6B
Reaction Time (min)		0		28.5		72		102		133		177.8
Mass of Empty Vial (g)	16.562	16.609	16.465	16.629	15.86	16.695	16.4	16.516	16.779	16.386	16.576	16.477
Mass of + sample vial (g)	18.374	18.338	17.495	18.462	16.615	17.409	18.192	18.151	17.884	18.018	17.661	17.8
mass of liquid sample (g)	1.8126	1.7287	1.0307	1.8332	0.7551	0.7144	1.7923	1.635	1.1055	1.6318	1.0851	1.3232

Table B.30. 2: GC Analysis, Experiment #30

Reaction Time (min)	0	38.5	72	102	133	177.75
[NPT] (mol/g-liq)	0.000556	0.000545	0.000519	0.000436	0.000441	0.00042
[TET] (mol/g-liq)	2.02E-05	3.58E-05	4.9E-05	6.66E-05	9.08E-05	0.000123
[c-DEC] (mol/g-liq)	1.45E-07	1.45E-07	4.82E-08	7.61E-08	7.23E-08	7.23E-08
[t-DEC] (mol/g-liq)	2.17E-07	2.17E-07	4.82E-08	7.61E-08	7.23E-08	1.45E-07
$[NPT] = [NPT]_0 - [TET]-[DEC]$	0.000536	0.00052	0.000507	0.00049	0.000465	0.000433

Table B.30. 3: GC Analysis, Experiment #30

Reaction Time (min)	0	38.5	72	102	133	177.75
Average ESTD mol%						
H2	10.56892	16.3314		19.26483	19.68537	20.19802
O2	9.13483	7.84206		7.56177	7.555205	7.459035
N2 Total	34.55176	29.95559		28.70335	28.67492	28.35941
CH4	0	0		0.03041	0.03849	0.048985
CO	31.27573	25.4229		20.59983	19.00374	17.44838
CO2	9.988	15.95281		19.88774	20.99054	22.25722
C2H4	0.0422	0		0	0	0
C2H6	0.027265	0.026425		0.03364	0.03583	0.0386
C2H2	0	0		0	0	0
H2S	0.44398	0.453085		0.553505	0.542735	0.520035
COS	0.155355	0.097665		0.07054	0.062325	0.056265
1,2-Prop=	0	0		0	0	0
Water	0.484705	0.503455		0.456375	0.49758	0.517685
Prop	0	0		0	0	0
C3	0	0		0	0	0
n-C4	0	0		0	0	0
i-C4	0.018515	0.00516		0	0	0
n-C6	0	0		0	0	0
n-C8	0.03119	0.01759		0	0	0

Experimental Conditions for #32: $CO/H_2O/H_2S$, 15 psig H_2S, 585 psig CO, 4.0°C/min, 340 °C, 3 hrs, 10 ml H_2O, 100 ml toluene, 3.7 g NAPH, 0.47 mmoles Mo, 1500 RPM Impeller Speed

Table B.32. 1: Mass of Samples, Experiment #32

Sample #	Purge	1	2	2B	3	3B	4	4B	5	5B	6	6B
Reaction Time (min)		0		28.5		58		85.5		123		164.5
Mass of Empty Vial (g)	16.601	16.426	16.604	16.501	16.469	16.489	16.518	16.574	16.559	16.469	16.476	16.417
Mass of + sample vial (g)	18.341	17.917	17.827	18.243	17.4		17.795	18.143	17.757	18.154	17.614	18.234
mass of liquid sample (g)	1.74	1.4914	1.2225	1.7425	0.9313		1.2776	1.5689	1.1981	1.6849	1.1377	1.8168

Table B.32. 2: GC Analysis, Experiment #32

Reaction Time (min)	0	28.5	58	85.5	123	164.5
[NPT] (mol/g-liq)	0.000564	0.000527	0.000476	0.000416	0.000358	0.000277
[TET] (mol/g-liq)	2.96E-05	7.7E-05	0.000133	0.000197	0.00025	0.0003
[c-DEC] (mol/g-liq)	0	7.23E-08	1.45E-07	2.28E-07	3.38E-07	5.79E-07
[t-DEC] (mol/g-liq)	0	0	1.45E-07	2.28E-07	4.82E-07	7.59E-07
$[NPT] = [NPT]_0 - [TET]-[DEC]$	0.000573	0.000526	0.000469	0.000406	0.000352	0.000301

Table B.32. 3: GC Analysis, Experiment #32

Reaction Time (min)	0	28.5	58	85.5	123	164.5
H2	19.41251	22.12124	23.00018	22.59082	22.83067	21.98403
O2	7.26638	7.20756	7.146255	7.15926	6.86144	7.11771
N2 Total	27.88216	27.62378	27.37499	27.39449	26.30607	27.24875
CH4	0.02422	0.04887	0.06605	0.08153	0.1013	0.105
CO	20.10525	15.42438	12.55929	10.58658	8.563515	7.852905
CO2	19.21731	22.74794	25.08062	26.79698	29.15283	29.43669
C2H4	0	0	0	0	0	0
C2H6	0.11253	0.124715	0.15853	0.191475	0.19882	0.196345
C2H2	0	0	0	0	0	0
H2S	0.44449	0.64059		0.69862	0.71526	0.69758
COS	0.073375	0.04781		0.0311	0.02542	0.023875
1,2-Prop=	0	0	0	0	0	0
Water	0.52152	0.470865	0.43578	0.520185	0.62613	0.716795
Prop	0	0	0	0	0	0
C3	0	0	0	0	0	0
n-C4	0	0	0	0	0	0
i-C4	0	0	0	0	0	0
n-C6	0	0	0	0	0	0
n-C8	0	0	0	0	0	0

Experimental Conditions for #33: $CO/H_2O/H_2S$, 15 psig H_2S, 585 psig CO, 4.0°C/min, 340 °C, 3 hrs, 10 ml H_2O, 100 ml toluene, 3.7 g NAPH, 0.47 mmoles Ru ($Ru_3(CO_{12}$, 1500 RPM Impeller Speed

Table B.33. 1: Mass of Samples, Experiment #33

Sample #	Purge	1	2	2B	3	3B	4	4B	5	5B	6	6B
Reaction Time (min)		0		28.5		58		85.5		123		164.5
Mass of Empty Vial (g)	16.546	16.447	16.648	16.477	16.446	16.459	16.544	16.639	16.569	16.434	16.479	16.529
Mass of + sample vial (g)	18.538	18.399	17.9	18.423	17.715	18.601	17.65	18.603	17.727	18.432	17.523	18.534
mass of liquid sample (g)	1.9917	1.9512	1.2515	1.9461	1.2682	2.1417	1.106	1.9645	1.1574	1.9983	1.0437	2.0046

Table B.33. 2: GC Analysis, Experiment #33

Reaction Time (min)	0	28.5	58	85.5	123	164.5
[NPT] (mol/g-liq)	0.000521	0.000558	0.000595	0.000571	0.000585	0.000574
[TET] (mol/g-liq)	8.14E-06	5.27E-06	7.89E-06	9.06E-06	1.25E-05	1.5E-05
[c-DEC] (mol/g-liq)	0	0	0	0	0	0
[t-DEC] (mol/g-liq)	0	0	7.23E-08	0	7.23E-08	7.23E-08
$[NPT] = [NPT]_0 - [TET]-[DEC]$	0.00058	0.000583	0.00058	0.000579	0.000575	0.000573

Table B.33. 3: GC Analysis, Experiment #33

Reaction Time (min)	15.25	45.5	80.5	125	155.5	179.2833
H2	5.606175	8.268888	10.71512	12.65042	14.06458	14.14804
O2	8.97056	8.58566	8.20197	8.107045	8.03633	8.02602
N2 Total	34.57495	32.67987	31.25922	30.94626	30.66457	30.61359
CH4	0	0	0	0	0	0
CO	39.31039	38.27881	35.64102	32.12815	30.46162	29.33169
CO2	4.618045	7.258685	9.638525	11.56268	12.92263	13.64798
C2H4	0.396605	0.36834	0.392535	0.4066	0.384355	0.3725
C2H6	0.0245	0.04436	0.04411	0.061355	0.073155	0.08016
C2H2	0	0	0	0	0	0
H2S	0.774885	0.92256	0.99606	1.01821	1.027695	1.02044
COS	0.386465	0.27227	0.21474	0.170945	0.152915	0.14714
1,2-Prop=	0	0	0	0	0	0
Water	0	0	0	0	0.55179	0.59719
Prop	0	0	0	0	0	0
C3	0	0	0	0	0	0
n-C4	0	0	0	0	0	0
i-C4	0	0	0	0	0	0
n-C6	0	0	0	0	0	0
n-C8	0	0	0	0	0	0

Experimental Conditions for #34: $CO/H_2O/H_2S$, 15 psig H_2S, 585 psig CO, 4.0°C/min, 340 °C, 3 hrs, 10 ml H_2O, 100 ml toluene, 3.7 g NAPH, 0.47 mmoles $Ru(acac)_3$, 1500 RPM Impeller Speed

Table B.34. 1: Mass of Samples, Experiment #34

mass of liquid sample (g)	1.8482	1.974	1.0606	2.0276	0.9636	2.0202	0.9892	1.9371	1.0246	2.0049	0.6682	1.9752
Mass of sample + vial (g)	18.307	18.544	17.515	18.607	17.43	18.525	17.546	18.353	17.748	18.364	17.189	18.367
Mass of Empty Vial (g)	16.458	16.57	16.455	16.579	16.466	16.504	16.557	16.416	16.724	16.36	16.521	16.392
Reaction Time (min)		0		34		62.5		98		122		151.5
Sample #	Purge	1	2	2B	3	3B	4	4B	5	5B	6	6B

Table B.34. 2: GC Liquid Analysis, Experiment #34

Reaction Time (min)	0	34	62.5	98	122	151.5
[NPT] (mol/g-liq)	0.000575	0.000529	0.000492	0.000454	0.000443	0.000422
[TET] (mol/g-liq)	2.31E-05	5.26E-05	7.75E-05	0.00011	0.000132	0.000163
[c-DEC] (mol/g-liq)	0	0	0	7.61E-08	7.23E-08	1.45E-07
[t-DEC] (mol/g-liq)	0	0	7.23E-08	1.52E-07	1.69E-07	2.53E-07
$[NPT] = [NPT]_0 - [TET]-[DEC]$	0.000552	0.000523	0.000498	0.000464	0.000443	0.000412

Table B.34. 3: GC Analysis, ESTD mol%, Experiment #34

Reaction Time (min)	0	34	62.5	98	122	151.5
H2	5.49802					
O2	1.406005					
N2 Total	6.034055					
CH4	0					
CO	81.72848					
CO2	3.357705					
C2H4	0.285865					
C2H6	0.03851					
C2H2	0					
H2S	0.35542					
COS	0.05303					
1,2-Prop=	0					
Water	0.303435					
Prop	0					
C3	0					
n-C4	0					
i-C4	0					
n-C6	0					
n-C8	0					

Experimental Conditions for #36: $CO/H_2O/H_2S$, 15 psig H_2S, 585 psig CO, 4.0°C/min, 340 °C, 4 hrs, 18 ml H_2O, 52 ml toluene, 11.17 g NAPH, 1.16 mmoles Mo; 0.7 mmole $Ru(acac)_3$, 1500 RPM Impeller Speed

Table B.36. 1: Mass of Samples, Experiment #36

Sample #	Purge	1	2	2B	3	3B	4	4B	5	5B	6	6B
Reaction Time (min)		0		19.5		39.5		59.5		89.5		119.5
Mass of Empty Vial (g)	16.6678	16.6473	16.8497	16.5515	16.5481	16.596	16.5632	16.6636	16.6449	16.7039	16.6354	16.811
Mass of sample + vial (g)	18.8602	17.9896	17.7072	17.9918	17.3862	18.1706	17.3089	18.3028	17.5055	18.4664	17.296	18.47
mass of liquid sample (g)	2.1924	1.3423	0.8575	1.4403	0.8381	1.5746	0.7457	1.6392	0.8606	1.7625	0.6606	1.659

Table B.36. 2: GC Analysis, Experiment #36

Reaction Time (min)	0.00	19.50	39.50	59.50	89.50	119.50
[NPT] (mol/g-liq)	0.002198	0.002142	0.001806		0.001711	0.001379
[TET] (mol/g-liq)	7.28E-05	0.000156	0.000258	0.000274	0.000602	0.000737
[c-DEC] (mol/g-liq)	0	0	0	8.52E-08	2.23E-07	4.44E-07
[t-DEC] (mol/g-liq)	0	0	4.71E-08	1.7E-07	4.02E-07	7.41E-07
$[NPT] = [NPT]_0 - [TET]-[DEC]$	0.002125	0.002042	0.00194	0.001923	0.001595	0.00146

Table B.36. 3: GC Gas Analysis, ESTD mol%, Experiment #36

Reaction Time (min)	0.00	19.50	39.50	59.50	89.50	119.50	Final
H2	21.61203	24.60084	26.54063	27.1485	27.55704	27.33566	31.3899
O2	5.510625	5.131565	4.856475	4.84554	4.68334	4.789505	1.53187
N2 Total	21.05513	19.67583	18.63441	18.61563	17.98258	18.38055	6.103523
CH4	0	0.019055	0.02589	0.032495	0.040185	0.04748	0.05332
CO	25.70463	20.24663	16.58459	13.94418	11.09918	8.866325	23.37887
CO2	18.17618	22.31261	25.0169	26.60906	28.97455	30.54275	33.16078
C2H4	0.015895	0	0	0	0	0	0
C2H6	0.10683	0.122665	0.12756	0.13007	0.153685	0.1543	0.162537
C2H2	0	0	0	0	0	0	0
H2S	0.54783	0.564395	0.56445	0.547445	0.545485	0.542775	0.57402
COS	0.037375	0.02907	0.023575	0.020445	0.016045	0.013135	0.042203
1,2-Prop=	0	0	0	0	0	0	0
Water	0	0	0	0	0	0	0
Prop	0.01419	0	0	0	0	0	0
C3	0	0	0	0	0	0	0
n-C4	0	0	0	0	0	0	0
i-C4	0	0	0	0	0	0	0
n-C6	0	0	0	0	0	0	0
n-C8	0	0	0	0	0	0	0

B5. Fe, V and Ni-promoted Molybenum catalysts

Experimental Conditions for #37: ($CO/H_2O/H_2S$, 15 psig H_2S, 585 psig CO, 4.0°C/min, 340 °C, 4 hrs, 18 ml H_2O, 52 ml toluene, 11.17 g NAPH, 1.16 mmole Mo; 0.47 mmoles $FeSO_4$)

Table B.37. 1: Mass of Samples, Experiment #37

Sample #	Purge	1	2	3	2B	3B	4	4B	5	5B	6	6B
Reaction Time (min)		0			19.5	39.5		59.5		89.5		119.5
Mass of Empty Vial (g)	16.6678	16.6473	16.8497	16.5481	16.5515	16.596	16.5632	16.6636	16.6449	16.7039	16.6354	16.811
Mass of sample + vial (g)	18.8602	17.9896	17.7072	17.3862	17.9918	18.1706	17.3089	18.3028	17.5055	18.4664	17.296	18.47
mass of liquid sample (g)	2.1924	1.3423	0.8575	0.8381	1.4403	1.5746	0.7457	1.6392	0.8606	1.7625	0.6606	1.659

Table B.37. 2: GC Liquid Analysis, Experiment #37

Reaction Time (min)	0	19.5	39.5	59.5	89.5	119.5
[NPT] (mol/g-liq)	0.002579	0.002248	0.002306	0.002065	0.001756	0.001399
[TET] (mol/g-liq)	0.000122	0.000245	0.00044	0.00063	0.00088	0.001038
[c-DEC] (mol/g-liq)	0	7.23E-08	1.45E-07	2.8E-07	6.51E-07	1.21E-06
[t-DEC] (mol/g-liq)	2.41E-08	1.45E-07	2.17E-07	3.81E-07	9.16E-07	1.71E-06
$[NPT] = [NPT]_0 - [TET]-[DEC]$	0.002457	0.002334	0.002139	0.001948	0.001698	0.001538

Table B.37. 3: GC Analysis, ESTD mol%, Experiment #37

Reaction Time (min)	0	19.5	39.5	59.5	89.5	119.5	Final
H2	29.02572	30.16229	30.59468	29.79058	29.04537	28.12419	29.99602
O2	5.346095	5.007545	4.923065	4.915365	4.940405	4.953145	1.470163
N2 Total	20.38092	19.00656	18.71403	18.7106	18.80008	18.8679	5.827253
CH4	0.018465	0.031225	0.04219	0.051505	0.06384	0.071785	0.04926
CO	12.66594	8.78712	6.4612	5.347645	4.44765	4.018745	21.31095
CO2	23.87859	27.18775	29.13855	30.59855	31.78375	32.86302	35.88772
C2H4	0	0	0	0	0	0	0
C2H6	0.25477	0.26117	0.26437	0.265695	0.270385	0.27505	0.288753
C2H2	0	0	0	0	0	0	0
H2S	0.596015	0.618405	0.6147	0.605455	0.609675	0.61768	0.635347
COS	0.019605	0.013195	0	0	0	0	0.052137
1,2-Prop=	0	0	0	0	0	0	0
Water	0	0	0	0	0	0	0
Prop	0	0	0	0	0	0	0
C3	0	0	0	0	0	0	0
n-C4	0	0	0	0	0	0	0
i-C4	0	0	0	0	0	0	0
n-C6	0	0	0	0	0	0	0
n-C8	0	0	0	0	0	0	0

Experimental Conditions for #38: $CO/H_2O/H_2S$, 15 psig H_2S, 585 psig CO, 4.0°C/min, 340 °C, 4 hrs, 18 ml H_2O, 52 ml toluene, 11.17 g NAPH, 1.16 mmole Mo; 0.47 mmoles $VO(acac)_2$, 1500 RPM Impeller Speed

Table B.38. 1: Mass of Samples, Experiment #38

Sample #	Purge	1	2	2B	3	3B	4	4B	5	5B	6	6B
Reaction Time (min)		0		19		39		58		89		119
Mass of Empty Vial (g)	16.6678	16.6473	16.8497	16.5515	16.5481	16.596	16.5632	16.6636	16.6449	16.7039	16.6354	16.811
Mass of sample + vial (g)	18.8602	17.9896	17.7072	17.9918	17.3862	18.1706	17.3089	18.3028	17.5055	18.4664	17.296	18.47
mass of liquid sample (g)	2.1924	1.3423	0.8575	1.4403	0.8381	1.5746	0.7457	1.6392	0.8606	1.7625	0.6606	1.659

Table B.38. 2: GC Analysis, Experiment #38

Reaction Time (min)	0	19	39	58	89	119
[NPT] (mol/g-liq)	0.002313	0.002108	0.002067	0.001846	0.001721	0.001385
[TET] (mol/g-liq)	8.34E-05	0.000167	0.000292	0.000435	0.000658	0.000851
[c-DEC] (mol/g-liq)	0	0	7.71E-08	1.54E-07	2.92E-07	6.41E-07
[t-DEC] (mol/g-liq)	0	0	2.31E-07	3.08E-07	6.82E-07	1.11E-06
$[NPT] = [NPT]_0 - [TET]-[DEC]$	0.002229	0.002146	0.002021	0.001877	0.001654	0.00146

Table B.38. 3: GC Analysis, ESTD mol%, Experiment #38

Reaction Time (min)	0	19	39	58	89	119	Final
H2	27.78295	30.83965	31.42804	31.74592	30.29152	29.43155	32.64154
O2	5.312175	4.960765	4.95615	4.99298	4.958805	4.95649	1.173777
N2 Total	20.16909	18.80698	18.76554	18.90694	18.81862	18.8578	4.597137
CH4	0.008035	0.011695	0.01734	0.042185	0.05152	0.05635	0
CO	14.39192	8.477195	5.47497	4.22553	2.94739	2.500355	20.95384
CO2	22.62186	26.667	28.96119	30.0343	32.148	33.20338	34.46132
C2H4	0.02502	0	0	0	0	0	0
C2H6	0.341365	0.376575	0.424775	0.430535	0.442415	0.439445	0.41761
C2H2	0	0	0	0	0	0	0
H2S	0.57288	0.605775	0.59733	0.594785	0.604835	0.600271	0.467357
COS	0.019075	0.011295	0	0	0	0	0.037237
1,2-Prop=	0.027605	0.031335	0.032525	0.03293	0.033935	0.03367	0.007557
Water	0	0	0	0	0	0	0
Prop	0.03532	0.014685	0	0	0	0	0
C3	0	0	0	0	0	0	0
n-C4	0	0	0	0	0	0	0
i-C4	0	0	0	0	0	0	0
n-C6	0	0	0	0	0	0	0
n-C8	0	0	0	0	0	0	0

Experimental Conditions for #39: $CO/H_2O/H_2S$, 15 psig H_2S, 585 psig CO, 4.0°C/min, 340 °C, 4 hrs, 18 ml H_2O, 52 ml toluene, 11.17 g NAPH, 1.16 mmole Mo; 0.47 mmoles $NiSO_4$, 1500 RPM Impeller Speed

Table B.39. 1: Mass of Samples, Experiment #39

Sample #	Purge	1	2	2B	3	3B	4	4B	5	5B	6	6B
Reaction Time (min)		0		21.5		39.5		59.5		90		118.5
Mass of Empty Vial (g)	16.6678	16.6473	16.8497	16.5515	16.5481	16.596	16.5632	16.6636	16.6449	16.7039	16.6354	16.811
Mass of sample + vial (g)	18.8602	17.9896	17.7072	17.9918	17.3862	18.1706	17.3089	18.3028	17.5055	18.4664	17.296	18.47
mass of liquid sample (g)	2.1924	1.3423	0.8575	1.4403	0.8381	1.5746	0.7457	1.6392	0.8606	1.7625	0.6606	1.659

Table B.39. 2: GC Analysis, Experiment #39

Reaction Time (min)	0	21.5	39.5	59.5	90	118.5
[NPT] (mol/g-liq)	0.001361	0.001113	0.000976	0.000747	0.000596	0.00061
[TET] (mol/g-liq)	0.000655	0.001039	0.001326	0.001406	0.00136	0.001444
[c-DEC] (mol/g-liq)	4.41E-07	1.71E-06	3.17E-06	4.71E-06	5.85E-06	5.16E-06
[t-DEC] (mol/g-liq)	5.29E-07	2.1E-06	3.99E-06	6.36E-06	8.95E-06	1.24E-05
$[NPT] = [NPT]_0 - [TET]-[DEC]$	0.001479	0.001091	0.000801	0.000717	0.00076	0.000673

Table B.39. 3: GC Analysis, ESTD mol%, Experiment #39

Reaction Time (min)	0	21.5	39.5	59.5	90	118.5	
H2	23.21004	20.54814	19.42989	19.46511	19.74885	20.26856	24.26024
O2	5.418475	5.48124	5.547	5.53677	5.49159	5.46603	1.47174
N2 Total	20.70286	20.92147	21.15656	21.13834	20.98122	20.8727	5.996073
CH4	0	0	0.040925	0.046565	0.05167	0.05539	0.060333
CO	9.98744	6.945845	5.790535	5.03428	4.14066	3.5317	21.2907
CO2	29.4351	33.28446	34.87877	35.86465	36.73487	36.91289	39.63121
C2H4	0	0	0	0	0	0	0
C2H6	0.165115	0.198885	0.204675	0.21366	0.21743	0.21561	0.218143
C2H2	0	0	0	0	0	0	0
H2S	0.720685	0.786685	0.78541	0.777165	0.77198	0.76149	0.671493
COS	0.02369	0.020145	0.017355	0.015	0.01222	0	0.080407
1,2-Prop=	0	0	0	0	0	0	0
Water	0	0	0	0	0	0	0
Prop	0	0	0	0	0	0	0
C3	0	0	0	0	0	0	0
n-C4	0	0	0	0	0	0	0
i-C4	0	0	0	0	0	0	0
n-C6	0	0	0	0	0	0	0
n-C8	0	0	0	0	0	0	0

Experimental Conditions for #40: $CO/H_2O/H_2S$, 15 psig H_2S, 585 psig CO, 4.0°C/min, 340 °C, 4 hrs, 18 ml H_2O, 52 ml toluene, 11.17 g NAPH, 1.16 mmole Mo, 1500 RPM Impeller Speed

Table B40. 1: Mass of Samples, Experiment #40

Sample #	Purge	1	2	2B	3	3B	4	4B	5	5B	6	6B
Reaction Time (min)		0.00		20.00		40.00		60.00		90.00		120.00
Mass of Empty Vial	16.6678	16.6473	16.8497	16.5515	16.5481	16.596	16.5632	16.6636	16.6449	16.7039	16.6354	16.811
Mass of sample + vial	18.8602	17.9896	17.7072	17.9918	17.3862	18.1706	17.3089	18.3028	17.5055	18.4664	17.296	18.47
mass of 1st liquid sample	2.1924	1.3423	0.8575	1.4403	0.8381	1.5746	0.7457	1.6392	0.8606	1.7625	0.6606	1.659

Table B40. 2: GC Analysis, Experiment #40

Reaction Time (min)	0	20	40	60	89.5	120
[NPT] (mol/g-liq)	0.001785558	0.00140007	0.001086123	0.000797044	0.000573	0.00048716
[TET] (mol/g-liq)	0.000413419	0.00075261	0.001078052	0.001243362	0.00133	0.001445197
[c-DEC] (mol/g-liq)	2.14065E-07	7.3475E-07	1.99268E-06	3.50517E-06	5.54E-06	7.91652E-06
[t-DEC] (mol/g-liq)	3.85316E-07	1.2399E-06	3.10858E-06	5.29776E-06	8.08E-06	1.22903E-05
$[NPT] = [NPT]_0 - [TET]-[DEC]$	0.001634362	0.00129379	0.000965226	0.000796215	0.000705	0.000582976

Table B40. 3: Gas Analysis, ESTD mol%, Experiment #40

Reaction Time (min)	0	20	40	60	89.5	120	
H2	29.07346	27.14499	25.39397	24.46187	23.57037	23.48459	4.732082
O2	5.17174	5.098315	5.098505	5.123725	5.211975	5.10862	3.599278
N2 Total	19.58152	19.4266	19.41973	19.46664	19.8503	19.44866	8.495335
CH4	0.040425	0.06259	0.076225	0.083675	0.089075	0.092285	8.587816
CO	7.04598	4.494975	3.360375	2.879365	2.178475	1.847755	9.124555
CO2	29.75816	33.3084	35.44299	36.57465	37.37213	38.32921	8.587286
C2H4	0	0	0	0	0	0	6.487703
C2H6	0.120415	0.13586	0.15389	0.16344	0.173725	0.17602	6.986757
C2H2	0	0	0	0	0	0	7.556236
H2S	0.774895	0.827665	0.84127	0.834635	0.8369	0.824335	8.243167
COS	0.01406	0	0	0	0	0	8.998351
1,2-Prop=	0	0	0	0	0	0	9.989951
Water	0	0	0	0	0	0	11.2387
Prop	0	0	0	0	0	0	12.84422
C3	0	0	0	0	0	0	14.98493
n-C4	0	0	0	0	0	0	17.98191
i-C4	0	0	0	0	0	0	22.47739
n-C6	0	0	0	0	0	0	29.96985
n-C8	0	0	0	0	0	0	44.95478

Experimental Conditions for #41: $CO/H_2O/H_2S$, 15 psig H_2S, 585 psig CO, 4.0°C/min, 340 °C, 4 hrs, 18 ml H_2O, 52 ml toluene, 11.17 g NAPH, 1.16 mmole Mo; 0.47 mmoles $NiSO_4$; 0.47 mmoles $VO(acac)_2$, 1500 RPM Impeller Speed

Table B.41. 1: Mass of Samples, Experiment #41

Sample #	Purge	1	2	2B	3	3B	4	4B	5	5B	6	6B
Reaction Time (min)		0		20		40		60		89.5		120
Mass of Empty Vial (g)	16.6678	16.6473	16.8497	16.5515	16.5481	16.596	16.5632	16.6636	16.6449	16.7039	16.6354	16.811
Mass of sample + vial (g)	18.8602	17.9896	17.7072	17.9918	17.3862	18.1706	17.3089	18.3028	17.5055	18.4664	17.296	18.47
mass of liquid sample (g)	2.1924	1.3423	0.8575	1.4403	0.8381	1.5746	0.7457	1.6392	0.8606	1.7625	0.6606	1.659

Table B.41. 2: GC Analysis, Experiment #41

Reaction Time (min)	0	20	40	60	89.5	120
[NPT] (mol/g-liq)	0.001858	0.001565	0.001211	0.000998	0.000765	0.000738
[TET] (mol/g-liq)	0.000416	0.00076	0.000996	0.001187	0.001276	0.001426
[c-DEC] (mol/g-liq)	2.84E-07	7.52E-07	1.62E-06	2.72E-06	3.92E-06	5.37E-06
[t-DEC] (mol/g-liq)	2.84E-07	8.36E-07	1.84E-06	3.28E-06	5.23E-06	6.95E-06
$[NPT] = [NPT]_0 - [TET]-[DEC]$	0.001774	0.001429	0.001191	0.000998	0.000906	0.000752

Table B.41. 3: GC Analysis, ESTD mol%, Experiment #41

Reaction Time (min)	0	20	40	60	89.5	120	
H2	29.07346	27.14499	25.39397	24.46187	23.57037	23.48459	4.732082
O2	5.17174	5.098315	5.098505	5.123725	5.211975	5.10862	3.599278
N2 Total	19.58152	19.4266	19.41973	19.46664	19.8503	19.44866	8.495335
CH4	0.040425	0.06259	0.076225	0.083675	0.089075	0.092285	8.587816
CO	7.04598	4.494975	3.360375	2.879365	2.178475	1.847755	9.124555
CO2	29.75816	33.3084	35.44299	36.57465	37.37213	38.32921	8.587286
C2H4	0	0	0	0	0	0	6.487703
C2H6	0.120415	0.13586	0.15389	0.16344	0.173725	0.17602	6.986757
C2H2	0	0	0	0	0	0	7.556236
H2S	0.774895	0.827665	0.84127	0.834635	0.8369	0.824335	8.243167
COS	0.01406	0	0	0	0	0	8.998351
1,2-Prop=	0	0	0	0	0	0	9.989951
Water	0	0	0	0	0	0	11.2387
Prop	0	0	0	0	0	0	12.84422
C3	0	0	0	0	0	0	14.98493
n-C4	0	0	0	0	0	0	17.98191
i-C4	0	0	0	0	0	0	22.47739
n-C6	0	0	0	0	0	0	29.96985
n-C8	0	0	0	0	0	0	44.95478

B 6. Effect of Temperature, P_{H2S} and type of reducing gas on WGS and Naphthalene Hydrogenation

Experimental Conditions for #42: $CO/H_2/H_2O/H_2S$, 22.5 psig H_2S, 577.5 psig (1:1 = CO/H_2), 4.0°C/min, 360 °C, 2 hrs, 10 ml H_2O, 100 ml toluene, 10.0 g NAPH, 1.50 mmole Mo; 0.98 mmoles $NiSO_4$; 0.97 mmoles $VO(acac)_2$, 1500 RPM Impeller Speed

Table B.42. 1: Mass of Samples, Experiment #42

Sample #	Purge	1	2	2B	3	3B	4	4B	5	5B	6	6B
Reaction Time (min)		0		18.5		38.5		58.5		88.5		118.5
Mass of Empty Vial (g)	16.3653	16.6143	16.5324	16.7043	16.8098	16.6309	16.5035	16.6562	16.6058	16.6406	16.6309	16.7462
Mass of sample + vial (g)	18.5123	18.4621	17.8614	18.7209	18.2211	18.7354	17.8674	18.8929	17.9473	18.7952	18.1511	18.8769
mass of liquid sample (g)	2.147	1.8478	1.329	2.0166	1.4113	2.1045	1.3639	2.2367	1.3415	2.1546	1.5202	2.1307

Table B.42. 2: GC Analysis, Experiment #42

Reaction Time (min)	0	18.5	38.5	58.5	88.5	118.5	Final
[NPT] (mol/g-liq)	0.000953	0.000866	0.000745	0.000651	0.000597	0.000537	0.000457
[TET] (mol/g-liq)	0.000285	0.000423	0.000525	0.00059	0.000633	0.00063	0.000563
[c-DEC] (mol/g-liq)	1.93E-07	3.62E-07	5.79E-07	9.38E-07	1.13E-06	1.47E-06	1.33E-06
[t-DEC] (mol/g-liq)	3.13E-07	8.92E-07	9.89E-07	2.62E-06	4.7E-06	4.34E-06	3.57E-06
$[NPT] = [NPT]_0 - [TET]-[DEC]$	0.000958	0.000819	0.000716	0.000649	0.000604	0.000607	0.000675

Table B.42. 3: GC Analysis, ESTD mol%, Experiment #42

Reaction Time (min)	0	18.5	38.5	58.5	88.5	118.5	Final
H2	30.43808	29.50305	26.88104	26.2846	26.05975	24.76823	51.45206
O2	9.188425	9.24453	9.47494	9.52384	9.62075	9.796966	2.47313
N2 Total	35.00545	35.20906	36.07016	36.25488	36.63657	37.30018	9.615643
CH4	0.090965	0.108555	0.12012	0.12668	0.13357	0.137195	0.1922
CO	4.570485	2.899675	1.932655	1.535585	1.259015	1.069545	13.42159
CO2	15.90597	18.4688	19.56206	20.32495	21.14963	21.61823	23.57899
C2H4	0	0	0	0	0	0	0
C2H6	0.28358	0.301215	0.304055	0.308225	0.343585	0.318835	0.362707
C2H2	0	0	0	0	0	0	0
H2S	1.10282	1.19119	1.20702	1.20885	1.24449	1.24938	0.9678
COS	0.01247	0	0	0	0	0	0.038237
1,2-Prop=	0.02766	0.0304	0.03185	0.03334	0.035115	0.035715	0
Water	0	0	0	0	0	0	0
Prop	0	0	0	0	0	0	0
C3	0	0	0	0	0	0	0
n-C4	0	0	0	0	0	0	0
i-C4	0	0	0	0	0	0	0
n-C6	0	0	0	0	0	0	0
n-C8	0	0	0	0	0	0	0

Table B.42. 4: Gas Concentrations, Experiment #42

Reaction Time (min)	0	18.5	38.5	58.5	88.5	118.5
Total calculated moles of gas in sampling bomb (moles)	0.008969	0.009051	0.008843	0.008681	0.008702	0.008533
[H2] (mol/g-liq)	0.001477	0.001445	0.001286	0.001235	0.001227	0.001144
[CO] (mol/g-liq)	0.000222	0.000142	9.25E-05	7.21E-05	5.93E-05	4.94E-05
[CO2] (mol/g-liq)	0.000772	0.000905	0.000936	0.000955	0.000996	0.000998

Experimental Conditions for #43: $H_2/H_2O/H_2S$, 30 psig H_2S, 570 psig H_2, 4.0°C/min, 340 °C, 2 hrs, 10 ml H_2O, 100 ml toluene, 10.0 g NAPH, 1.50 mmole Mo; 0.91 mmoles $NiSO_4$; 0.91 mmoles $VO(acac)_2$, 1500 RPM Impeller Speed

Table B.43. 1: Mass of Samples, Experiment #43

Sample #	Reaction Time (min)	Mass of Empty Vial (g)	Mass of sample + vial (g)	mass of liquid sample (g)
Purge		16.6337	19.1875	2.5538
1	0	16.354	18.3799	2.0259
2		16.4686	16.5278	0.0592
2B	19.5	16.555	18.6212	2.0662
3		16.6488	16.9613	0.3125
3B	39.5	16.5529	18.2446	1.6917
4		16.4303	16.6212	0.1909
4B	59.5	16.5307	18.3879	1.8572
5		16.6404	17.0498	0.4094
5B	91.75	16.5386	18.4002	1.8616
6		16.4802	16.8281	0.3479
6B	120.5	16.3986	18.1638	1.7652

Table B.43. 2: GC Analysis, Experiment #43

Reaction Time (min)	0	19.5	39.5	59.5	91.75	120.5	Final
[NPT] (mol/g-liq)	0.000889	0.000652	0.000588	0.000631	0.000509	0.000481	0.000408
[TET] (mol/g-liq)	0.000363	0.000398	0.00048	0.000597	0.000611	0.000656	0.000606
[c-DEC] (mol/g-liq)	3.13E-07	3.86E-07	6.99E-07	1.04E-06	1.52E-06	1.74E-06	2.07E-06
[t-DEC] (mol/g-liq)	4.58E-07	6.27E-07	9.64E-07	1.87E-06	2.68E-06	2.89E-06	5.45E-06
$[NPT] = [NPT]_0 - [TET]-[DEC]$	0.000743	0.000708	0.000625	0.000507	0.000491	0.000446	0.000493

Table B.43. 3: GC Analysis, ESTD mol%, Experiment #43

Reaction Time (min)	0	19.5	39.5	59.5	91.75	120.5	Final
H2	37.19586	34.96836	33.69058	32.26195	31.0085	28.29482	86.49076
O2	12.64063	13.02541	13.42623	13.71191	13.99717	14.4785	4.431887
N2 Total	47.70812	49.32101	50.83021	51.9535	53.03314	54.84159	15.94335
CH4	0.036715	0.044135	0.046905	0.051875	0.05461	0.05524	0.083483
CO	0	0	0	0	0	0	0
CO2	0.118365	0.12135	0.104015	0.094395	0.09941	0.09915	0.21734
C2H4	0	0	0	0	0	0	0
C2H6	0.536905	0.550315	0.576675	0.590315	0.596585	0.578695	0.68433
C2H2	0	0	0	0	0	0	0
H2S	2.514535	2.52207	2.72008	2.758405	2.793665	2.720505	1.79569
COS	0	0	0	0	0	0	0
1,2-Prop=	0	0	0	0	0	0	0
Water	0	0	0	0	0	0	0
Prop	0	0	0	0	0	0	0
C3	0	0	0	0	0	0	0
n-C4	0	0	0	0	0	0	0
i-C4	0	0	0	0	0	0	0
n-C6	0	0	0	0	0	0	0
n-C8	0	0	0	0	0	0	0

Table B.43. 4: GC Analysis, Experiment #43

Reaction Time (min)	0	19.5	39.5	59.5	91.75	120.5
Total calculated moles of gas in sampling bomb (moles)	0.006607	0.0064	0.006264	0.006173	0.006064	0.005943
[H2] (mol/g-liq)	0.001213	0.001105	0.001042	0.000983	0.000928	0.00083

Experimental Conditions for #44: ($CO/H_2O/H_2S$, 15 psig H_2S, 585 psig CO, 4.0°C/min, 340 °C, 2 hrs, 10 ml H_2O, 100 ml toluene, 10.0 g NAPH, 1.50 mmole Mo; 0.91 mmoles $NiSO_4$; 0.91 mmoles $VO(acac)_2$)

Table B.44. 1: Mass of Samples, Experiment #44

Sample #	Purge	1	2	2B	3	3B	4	4B	5	5B	6	6B
Reaction Time (min)		0		19.75		39.75		60.25		90.75		119.75
Mass of Empty Vial (g)	16.529	16.468	16.708	16.645	16.41	16.55	16.475	16.538	16.43	16.58	16.5	16.283
Mass of sample + vial (g)	18.946	18.44	17.923	18.846	17.81	18.59	17.889	18.678	17.784	18.75	17.742	18.469
mass of liquid sample (g)	2.4166	1.972	1.2155	2.2006	1.401	2.038	1.4146	2.1398	1.3537	2.1698	1.2415	2.1855

Table B.44. 2: GC Analysis, Experiment #44

Reaction Time (min)	0	19.75	39.75	60.25	90.75	119.75	Finl
[NPT] (mol/g-liq)	0.001104	0.000987	0.000835	0.000769	0.00062	0.000541	0.00046
[TET] (mol/g-liq)	0.000165	0.000293	0.000421	0.00055	0.000597	0.000644	0.000591
[c-DEC] (mol/g-liq)	1.45E-07	2.65E-07	4.1E-07	6.87E-07	9.4E-07	1.37E-06	1.9E-06
[t-DEC] (mol/g-liq)	2.65E-07	2.89E-07	3.86E-07	1.31E-06	1.83E-06	3.35E-06	4.22E-06
[NPT] = $[NPT]_0$ – [TET]-[DEC]	0.001055	0.000928	0.000799	0.000669	0.000621	0.000572	0.000623

Table B.44. 3: GC Analysis, ESTD mol%, Experiment #44

Reaction Time (min)	0	19.75	39.75	60.25	90.75	119.75	Final
H2	24.55614	24.95199	22.97069	21.63969	20.16616	19.41919	26.91475
O2	7.70268	7.608975	7.68682	7.95952	7.847865	7.858635	1.839587
N2 Total	29.30873	28.95363	29.24273	30.25946	29.84227	29.90182	7.442167
CH4	0.04017	0.0577	0.06751	0.07375	0.081245	0.08749	0.108013
CO	7.6025	3.793175	2.78921	2.45836	1.935335	1.427395	22.86631
CO2	24.64168	28.21592	30.33065	31.17014	32.71652	34.13665	35.98512
C2H4	0	0	0	0	0	0	0
C2H6	0.342103	0.42425	0.435105	0.442725	0.44659	0.450845	0.38858
C2H2	0	0	0	0	0	0	0
H2S	0.61911	0.628265	0.657365	0.648205	0.65511	0.6643	0.47999
COS	0.014594	0	0	0	0	0	0.06879
1,2-Prop=	0.02559	0.02704	0.028995	0.0291	0.0304	0.031185	0
Water	0	0	0	0	0	0	0
Prop	0.00912	0	0	0	0	0	0
C3	0	0	0	0	0	0	0
n-C4	0	0	0	0	0	0	0
i-C4	0	0	0	0	0	0	0
n-C6	0	0	0	0	0	0	0
n-C8	0	0	0	0	0	0	0

Table B.44. 4: GC Analysis, Experiment #44

Reaction Time (min)	0	19.75	39.75	60.25	90.75	119.75
Total calculated moles of gas in sampling bomb (moles)	0.010448	0.010654	0.010652	0.01045	0.01045	0.010389
[H2] (mol/g-liq)	0.001301	0.001348	0.001241	0.001147	0.001069	0.001023
[CO] (mol/g-liq)	0.000403	0.000205	0.000151	0.00013	0.000103	7.52E-05
[CO2] (mol/g-liq)	0.001306	0.001524	0.001638	0.001652	0.001734	0.001798

Experimental Conditions for #45: $CO/H_2O/H_2S$, 15 psig H_2S, 585 psig CO, 4.0°C/min, 380 °C, 2 hrs, 10 ml H_2O, 100 ml toluene, 10.0 g NAPH, 1.50 mmole Mo; 0.91 mmoles $NiSO_4$; 0.91 mmoles $VO(acac)_2$, 1500 RPM Impeller Speed

Table B.45. 1: Mass of Samples, Experiment #45

Sample #	Purge	1	2	2B	3	3B	4	4B	5	5B	6	6B
Reaction Time (min)		0		17		39.83		56.82		93.33		118.83
Mass of Empty Vial (g)	16.436	16.5807	16.5229	16.4238	16.5767	16.4558	16.3451	16.4682	16.5627	16.41	16.5507	16.4386
Mass of sample + vial (g)	19.2375	18.764	17.8872	18.6968	17.9899	18.776	17.7162	18.7457	17.9216	18.7729	17.8683	18.6055
mass of liquid sample (g)	2.8015	2.1833	1.3643	2.273	1.4132	2.3202	1.3711	2.2775	1.3589	2.3629	1.3176	2.1669

Table B.45. 2: GC Analysis, Experiment #45

Reaction Time (min)	0	17	39.83333	56.83333	93.33333	118.8333	Final
[NPT] (mol/g-liq)	0.000794	0.000769	0.00066	0.000642	0.000526	0.000519	0.000509
[TET] (mol/g-liq)	0.00037	0.000483	0.000511	0.000556	0.000491	0.000493	0.000505
[c-DEC] (mol/g-liq)	1.18E-06	4.58E-07	7.96E-07	9.38E-07	8.92E-07	1.04E-06	1.16E-06
[t-DEC] (mol/g-liq)	4.58E-07	1.64E-06	4.51E-06	3.83E-06	1.76E-06	5.3E-06	3.42E-06
$[NPT] = [NPT]_0 - [TET]-[DEC]$	0.000762	0.000649	0.000618	0.000574	0.00064	0.000634	0.000624

Table B.45. 3: GC Analysis, ESTD mol%, Experiment #45

Reaction Time (min)	0	17	39.83333	56.83333	93.33333	118.8333	Final
H2	20.97208	20.37966	19.39538	18.95201	19.00868	19.1786	28.49905
O2	7.77083	7.68931	7.647315	7.694315	7.66471	7.826	1.868017
N2 Total	29.56156	29.22416	29.10385	29.25007	29.17263	29.77557	7.54385
CH4	0.10595	0.11798	0.13317	0.14077	0.160265	0.174705	0.20561
CO	4.09915	3.26741	2.672905	2.579445	2.092825	1.775025	21.75899
CO2	30.08463	32.37321	33.48159	33.8517	34.68679	34.60573	34.92959
C2H4	0	0	0	0	0	0	0
C2H6	0.43864	0.448635	0.456125	0.450355	0.45395	0.46489	0.419133
C2H2	0	0	0	0	0	0	0
H2S	0.75244	0.776745	0.784715	0.77348	0.775635	0.75223	0.463173
COS	0	0	0	0	0	0	0.06589
1,2-Prop=	0.026835	0.027895	0.02934	0.1641	0.03097	0.030445	0
Water	0	0	0	0	0	0	0
Prop	0	0	0	0	0	0	0
C3	0	0	0	0	0	0	0
n-C4	0	0	0	0	0	0	0
i-C4	0	0	0	0	0	0	0
n-C6	0	0	0	0	0	0	0
n-C8	0	0	0	0	0	0	0

Table B.45. 4: GC Analysis, Experiment #45

Reaction Time (min)	0	17	39.83333	56.83333	93.33333	118.8333
Total calculated moles of gas in sampling bomb (moles)	0.010423	0.010571	0.010581	0.010795	0.010833	0.010855
[H2] (mol/g-liq)	0.001001	0.000987	0.00094	0.000937	0.000943	0.000954
[CO] (mol/g-liq)	0.000196	0.000158	0.00013	0.000128	0.000104	8.82E-05
[CO2] (mol/g-liq)	0.001436	0.001567	0.001623	0.001674	0.001721	0.001721

Experimental Conditions for #46: ($CO//H_2/H_2O/H_2S$, 22.5 psig H_2S, 577.5 psig (1:1 = $CO:H_2$), 4.0°C/min, 360 °C, 2 hrs, 10 ml H_2O, 100 ml toluene, 10.0 g NAPH, 1.50 mmole Mo; 0.91 mmoles $NiSO_4$; 0.91 mmoles $VO(acac)_2$)

See Sample Data at beginning of Appendix B.

Experimental Conditions for #47: ($CO/H_2O/H_2S$, 30 psig H_2S, 570 psig CO, 4.0°C/min, 340 °C, 2 hrs, 10 ml H_2O, 100 ml toluene, 10.0 g NAPH, 1.50 mmole Mo; 0.91 mmoles $NiSO_4$; 0.91 mmoles $VO(acac)_2$)

Table B.47. 1: Mass of Samples, Experiment #47

Sample #	Purge	1	2	2B	3	3B	4	4B	5	5B	6	6B
Reaction Time (min)		0		21		48.5		69.5		90		119.5
Mass of Empty Vial (g)	16.4305	16.5241	16.4042	16.412	16.3845	16.4205	16.456	16.4998	16.4625	16.4976	16.3926	16.3325
Mass of sample + vial (g)	18.4762	18.7061	17.6564	18.6258	17.5985	18.6609	17.6899	18.7246	17.1568	18.8686	16.8323	18.5217
mass of liquid sample (g)	2.0457	2.182	1.2522	2.2138	1.214	2.2404	1.2339	2.2248	0.6943	2.371	0.4397	2.1892

Table B.47. 2: GC Analysis, Experiment #47

Reaction Time (min)	0.00	21.00	48.50	69.50	90.00	119.50	Final
[NPT] (mol/g-liq)	0.000983	0.000898	0.000763	0.000641	0.000593	0.000532	0.000438
[TET] (mol/g-liq)	0.000168	0.000316	0.000466	0.000544	0.0006	0.000641	0.000578
[c-DEC] (mol/g-liq)	7.23E-08	2.17E-07	4.82E-07	8.1E-07	1.01E-06	1.28E-06	1.23E-06
[t-DEC] (mol/g-liq)	1.69E-07	4.34E-07	1.83E-06	2.47E-06	3.35E-06	2.6E-06	4.95E-06
$[NPT] = [NPT]_0 - [TET]-[DEC]$	0.001034	0.000885	0.000733	0.000654	0.000597	0.000557	0.000618

Table B.47. 3: Gas Concentrations, Experiment #47

Reaction Time (min)	0.00	21.00	48.50	69.50	90.00	119.50
Total calculated moles of gas in sampling bomb (moles)	0.010548	0.010907	0.010665	0.010551	0.010617	0.010682
[H2] (mol/g-liq)	0.001192	0.001186	0.001038	0.000955	0.000983	0.000945
[CO] (mol/g-liq)	0.000285	0.000154	8.62E-05	7.64E-05	7.01E-05	6.69E-05
[CO2] (mol/g-liq)	0.001262	0.001444	0.001539	0.001556	0.001596	0.001609

Table B.47. 4: GC Analysis, ESTD mol%, Experiment #47

Reaction Time (min)	0.00	21.00	48.50	69.50	90.00	119.50	Final
H2	24.66112	23.72059	21.23526	19.75472	20.2061	19.31401	26.55071
O2	7.795025	7.807085	7.98117	8.08285	7.95938	8.03904	1.15954
N2 Total	29.71538	29.74176	30.37882	30.74604	30.32959	30.61311	4.94101
CH4	0.04187	0.062705	0.07802	0.08374	0.08974	0.09316	0.118203
CO	5.90118	3.09025	1.762865	1.579205	1.43988	1.366705	19.94448
CO2	26.0994	28.88692	31.48311	32.18875	32.80406	32.87307	39.11494
C2H4	0	0	0	0	0	0	0
C2H6	0.521085	0.535435	0.55446	0.586255	0.58215	0.575215	0.596153
C2H2	0	0	0	0	0	0	0
H2S	1.29262	1.304835	1.34617	1.3627	1.387175	1.374345	1.201787
COS	0.024165	0.0135	0	0	0	0	0.096773
1,2-Prop=	0	0	0	0	0	0.01245	0
Water	0	0	0	0	0	0	0.047603
Prop	0	0	0	0	0	0	0
C3	0	0	0	0	0	0	0
n-C4	0	0	0	0	0	0	0
i-C4	0	0	0	0	0	0	0
n-C6	0	0	0	0	0	0	0
n-C8	0	0	0	0	0	0	0

Experimental Conditions for #48: $CO/H_2O/H_2S$, 30 psig H_2S, 570 psig CO, 4.0°C/min, 380 °C, 2 hrs, 10 ml H_2O, 100 ml toluene, 10.0 g NAPH, 1.50 mmole Mo; 0.91 mmoles $NiSO_4$; 0.91 mmoles $VO(acac)_2$, 1500 RPM Impeller Speed

Table B.48. 1: Mass of Samples, Experiment #48

Sample #	Purge	1	2	2B	3	3B	4	4B	5	5B	6	6B
Reaction Time (min)		0		21		40		60		92		120
Mass of Empty Vial (g)	16.5	16.6	16.4	16.5	16.5	16.5	16.3	16.3	16.6	16.5	16.6	16.5
Mass of + sample vial (g)	18.4	18.6	17.5	18.9	17.8	18.9	17.2	18.7	18	18.7	18.4	18.8
mass of liquid sample (g)	1.97	2.01	1.09	2.33	1.28	2.37	0.98	2.36	1.45	2.22	1.85	2.26

Table B.48. 2: GC Analysis, Experiment #48

Reaction Time (min)	0	21	40	60	92	120	Final
[NPT] (mol/g-liq)	0.000722	0.00071	0.000672	0.000626	0.000604	0.000605	0.000521
[TET] (mol/g-liq)	0.000379	0.000509	0.000553	0.000563	0.000555	0.000559	0.000492
[c-DEC] (mol/g-liq)	4.1E-07	6.27E-07	7.96E-07	8.89E-07	1.08E-06	1.16E-06	1.25E-06
[t-DEC] (mol/g-liq)	2.19E-06	2.22E-06	2.96E-05	3.04E-06	5.18E-06	6.15E-06	5.06E-06
$[NPT] = [NPT]_0 - [TET]-[DEC]$	0.000789	0.000659	0.000587	0.000604	0.00061	0.000604	

Table B.48. 3: Calculated Gas Concentrations, Experiment #48

Reaction Time (min)	0	21	40	60	92	120
Total calculated moles of gas in sampling bomb (moles)	0.010754	0.010825	0.010534	0.010935	0.011138	0.011262
[H2] (mol/g-liq)	0.001109	0.001069	0.000998	0.001017	0.001044	0.001114
[CO] (mol/g-liq)	0.000131	0.00011	0.000103	0.000109	0.000102	9.72E-05
[CO2] (mol/g-liq)	0.001635	0.001767	0.001713	0.001833	0.001888	0.001929

Table B.48. 4: Gas Analysis, ESTD mol%, Experiment #48

Reaction Time (min)	0	21	40	60	92	120	Final
H2	20.73639	19.84033	19.04251	18.69025	18.84386	19.8843	28.63887
O2	8.009215	7.653615	8.01756	7.87848	7.706835	7.5023	1.312263
N2 Total	30.44117	29.09496	30.47921	29.95817	29.30793	28.56137	5.508387
CH4	0.10551	0.12953	0.1378	0.14828	0.16053	0.17189	0.208317
CO	2.45469	2.04121	1.956625	1.99973	1.84854	1.734035	23.13514
CO2	30.56909	32.81299	32.69266	33.69511	34.0665	34.43641	38.77527
C2H4	0	0	0	0	0	0	0
C2H6	0.457315	0.4785	0.50793	0.524275	0.52058	0.525755	0.52097
C2H2	0	0	0	0	0	0	0
H2S	1.425935	1.483755	1.482595	1.537355	1.522285	1.5279	1.28403
COS	0.01283	0	0	0	0	0	0.105883
1,2-Prop=	0	0.024485	0.024795	0.02635	0.026575	0.026885	0
Water	0	0	0	0	0	0	0.047793
Prop	0	0	0	0	0	0	0
C3	0	0	0	0	0	0	0
n-C4	0	0	0	0	0	0	0
i-C4	0	0	0	0	0	0	0
n-C6	0	0	0	0	0	0	0
n-C8	0	0	0	0	0	0	0

Experimental Conditions for #49: $H_2/H_2O/H_2S$, 15 psig H_2S, 585 psig CO, 4.0°C/min, 380 °C, 2 hrs, 10 ml H_2O, 100 ml toluene, 10.0 g NAPH, 1.50 mmole Mo; 0.91 mmoles $NiSO_4$; 0.91 mmoles $VO(acac)_2$, 1500 RPM Impeller Speed

Table B.49. 1: Mass of Samples, Experiment #49

Sample #	Reaction Time (min)	Mass of Empty Vial (g)	Mass of sample + vial (g)	mass of liquid sample (g)
Purge		16.54	18.74	2.2
1	0	16.37	19.05	2.68
2		16.53	19.07	2.54
2B	20	16.49	18.83	2.34
3		16.47	17.01	0.54
3B	40	16.46	18.83	2.37
4		16.49	17	0.51
4B	60	16.49	18.76	2.27
5		16.49	17.4	0.91
5B	90	16.48	19.01	2.53
6		16.51	17.52	1.01
6B	120	16.41	18.38	1.97

Table B.49. 2: GC Analysis, Experiment #49

Reaction Time (min)	0	20	40	60	90	120	Final
[NPT] (mol/g-liq)	0.000732	0.000645	0.000631	0.000587	0.00058	0.000543	0.000498
[TET] (mol/g-liq)	0.000386	0.000475	0.000538	0.000551	0.000546	0.000518	0.000477
[c-DEC] (mol/g-liq)	2.65E-07	4.82E-07	6.99E-07	8.91E-07	1.21E-06	1.23E-06	1.13E-06
[t-DEC] (mol/g-liq)	5.79E-07	9.16E-07	1.9E-06	4.42E-06	4.68E-06	3.93E-06	2.5E-06
[NPT] = $[NPT]_0$ - [TET]-[DEC]	0.000716	0.000625	0.000561	0.000546	0.00055	0.00058	0.000622

Table B.49. 3: Calculated Gas Concentrations, Experiment #49

Reaction Time (min)	0	20	40	60	90	120
Total calculated moles of gas in sampling bomb (moles)	0.006383	0.006039	0.006066	0.006042	0.006139	0.00621
[H2] (mol/g-liq)	0.000857	0.000737	0.000708	0.000711	0.000746	0.000748

Table B.49. 4: Gas Analysis, ESTD mol%, Experiment #49

Reaction Time (min)	0	20	40	60	90	120	Final
H2	35.99163	32.6944	31.28645	31.51985	32.57246	32.26696	96.48417
O2	13.29071	13.92122	14.01625	14.02568	13.97612	14.1713	4.048893
N2 Total	50.38837	52.8219	53.1115	53.18534	53.08027	53.7607	14.54227
CH4	0.06947	0.08245	0.086155	0.09304	0.108155	0.11443	0.155253
CO	0	0	0	0	0	0	0.124333
CO2	0.14795	0.127175	0.116685	0.11782	0.118045	0.119955	0.254547
C2H4	0	0	0	0	0	0	0
C2H6	0.68286	0.68284	0.67209	0.67152	0.72064	0.69172	0.824923
C2H2	0	0	0	0	0	0	0
H2S	0.75418	0.7097	0.74463	0.73596	0.78988	0.784275	0.693017
COS	0	0	0	0	0	0	0
1,2-Prop=	0	0	0	0	0	0	0
Water	0	0	0	0	0	0	0.09426
Prop	0	0	0	0	0	0	0
C3	0	0	0	0	0	0	0
n-C4	0	0	0	0	0	0	0
i-C4	0	0	0	0	0	0	0
n-C6	0	0	0	0	0	0	0
n-C8	0	0	0	0	0	0	0

Experimental Conditions for #50: CO//H_2/H_2O/H_2S, 22.5 psig H_2S, 577.5 psig (1:1 = CO:H_2), 4.0°C/min, 360 °C, 2 hrs, 10 ml H_2O, 100 ml toluene, 10.0 g NAPH, 1.50 mmole Mo; 0.91 mmoles $NiSO_4$; 0.91 mmoles $VO(acac)_2$, 1500 RPM Impeller Speed

Table B.50. 1: Mass of Samples, Experiment #50

Sample #	Purge	1	2	2B	3	3B	4	4B	5	5B	6	6B
Reaction Time (min)		0		20.3		40		60		88.5		120
Mass of Empty Vial (g)	16.4	16.5	16.5	16.5	16.5	16.5	16.6	16	16.3	16.4	16.5	16.4
Mass of sample + vial (g)	19.3	18.7	18	18.8	18.1	18.6	18.4	19	17.8	18.5	17.7	18.8
mass of liquid sample (g)	2.97	2.13	1.57	2.28	1.61	2.15	1.78	2.3	1.44	2.08	1.14	2.38

Table B.50. 2: GC Analysis, Experiment #50

Reaction Time (min)	0	20.25	40	60	88.5	120	Final
[NPT] (mol/g-liq)	0.000982	0.000973	0.000811	0.000693	0.000678	0.000598	0.000518
[TET] (mol/g-liq)	0.00019	0.000339	0.000409	0.000468	0.00056	0.000576	0.000531
[c-DEC] (mol/g-liq)	7.23E-08	2.17E-07	2.89E-07	3.81E-07	6.99E-07	8.44E-07	1.04E-06
[t-DEC] (mol/g-liq)	4.1E-07	4.82E-07	1.16E-06	1.16E-06	2.41E-06	2.53E-06	3.81E-06
$[NPT] = [NPT]_0 - [TET]-[DEC]$	0.001004	0.000855	0.000784	0.000725	0.000632	0.000615	0.000659

Table B.50. 3: Calculated Gas Concentrations, Experiment #50

Reaction Time (min)	0	20.25	40	60	88.5	120
Total calculated moles of gas in sampling bomb (moles)	0.009067	0.009006	0.008796	0.00855	0.008593	0.008671
[H2] (mol/g-liq)	0.001318	0.001258	0.001153	0.001107	0.001077	0.001043
[CO] (mol/g-liq)	0.00018	8.86E-05	5.97E-05	5.38E-05	4.95E-05	4.26E-05
[CO2] (mol/g-liq)	0.000651	0.00076	0.00077	0.000751	0.000809	0.000819

Table B.50. 4: Gas Analysis, ESTD mol%, Experiment #50

Reaction Time (min)	0	20.25	40	60	88.5	120	Final
H2	30.95419	29.74025	27.9247	27.56656	26.69075	25.61919	54.03875
O2	9.24615	9.29424	9.570375	9.896875	9.897495	10.11839	2.429957
N2 Total	35.17241	35.36696	36.42826	37.68643	37.68156	38.55033	9.624237
CH4	0.07377	0.09519	0.103455	0.10745	0.11517	0.115395	0.175787
CO	4.2326	2.0958	1.44645	1.339895	1.22803	1.04628	10.15649
CO2	15.29531	17.96858	18.64791	18.71342	20.05393	20.11251	24.14483
C2H4	0	0	0	0	0	0	0
C2H6	0.772155	0.82781	0.82827	0.80734	0.84348	0.80531	0.843727
C2H2	0	0	0	0	0	0	0
H2S	0.944675	1.00077	0.992445	0.99029	1.05757	1.02347	0.562327
COS	0	0	0	0	0	0	0.025947
1,2-Prop=	0.030975	0.03387	0.034375	0.03404	0.03712	0.036415	0
Water	0	0	0	0	0	0	0
Prop	0	0	0	0	0	0	0
C3	0	0	0	0	0	0	0
n-C4	0	0	0	0	0	0	0
i-C4	0	0	0	0	0	0	0
n-C6	0	0	0	0	0	0	0
n-C8	0	0	0	0	0	0	0

Experimental Conditions for #51: $H_2/H_2O/H_2S$, 30 psig H_2S, 570 psig CO, 4.0°C/min, 380 °C, 2 hrs, 10 ml H_2O, 100 ml toluene, 10.0 g NAPH, 1.50 mmole Mo; 0.91 mmoles $NiSO_4$; 0.91 mmoles $VO(acac)_2$, 1500 RPM Impeller Speed

Table B.51. 1: Mass of Samples, Experiment #51

Sample #	Purge	1	2	2B	3	3B	4	4B	5	5B	6	6B
Reaction Time (min)		0		20		40		60		89.5		120
Mass of Empty Vial (g)	16.51	16.49	16.48	16.39	16.47	16.47	16.5	16.59	16.45	14.69	16.5	14.71
Mass of sample + vial (g)	18.89	19.16	17.3	18.72	18.1	18.58	17.93	18.85	18.35	16.9	17.92	17.47
mass of liquid sample (g)	2.38	2.67	0.82	2.33	1.63	2.11	1.43	2.26	1.9	2.21	1.42	2.76

Table B.51. 2: GC Analysis, Experiment #51

Reaction Time (min)	0	20	40	60	89.5	120	Final
[NPT] (mol/g-liq)	0.000687	0.000698	0.000628	0.000606	0.000603	0.000579	0.000555
[TET] (mol/g-liq)	0.000403	0.000491	0.000513	0.000526	0.00052	0.00049	0.000468
[c-DEC] (mol/g-liq)	4.58E-07	5.55E-07	7.72E-07	9.66E-07	1.01E-06	9.89E-07	1.04E-06
[t-DEC] (mol/g-liq)	1.25E-06	2E-06	4.15E-06	3.99E-06	3.09E-06	4.24E-06	5.35E-06
$[NPT] = [NPT]_0 - [TET]-[DEC]$	0.000713	0.000624	0.0006	0.000587	0.000594	0.000623	0.000643

Table B.51. 3: Calculated Gas Concentrations, Experiment #51

Reaction Time (min)	0	20	40	60	89.5	120
Total calculated moles of gas in sampling bomb (moles)	0.006323	0.006377	0.006229	0.006108	0.006324	0.006275
[H2] (mol/g-liq)	0.000795	0.000726	0.000742	0.000726	0.000767	0.000762

Table B.51. 4: Gas Analysis, ESTD mol%, Experiment #51

Reaction Time (min)	0	20	40	60	89.5	120	Final
H2	33.59182	30.38989	31.78611	31.71854	32.36662	32.40268	78.11558
O2	13.46458	14.10937	14.00771	13.84023	13.76972	13.83507	6.251475
N2 Total	51.12759	53.51536	53.20115	52.61357	52.38145	52.5511	23.08126
CH4	0.08001	0.094425	0.10649	0.120645	0.132545	0.134835	0.153595
CO	0.026275	0.058215	0	0	0	0	0.071915
CO2	0.12644	0.12937	0.101935	0.108165	0.114555	0.100385	0.202525
C2H4	0	0	0	0	0	0	0
C2H6	0.737945	0.745405	0.73377	0.816315	0.80465	0.73339	0.735905
C2H2	0	0	0	0	0	0	0
H2S	2.150445	2.190295	2.17084	2.384125	2.32488	2.122935	1.236335
COS	0	0	0	0	0	0	0
1,2-Prop=	0	0	0	0	0	0	0
Water	0	0	0	0	0	0	0
Prop	0	0	0	0	0	0	0
C3	0	0	0	0	0	0	0
n-C5	0.0118	0.01282	0.01274	0.014985	0.01375	0	0
i-C4	0	0	0	0	0	0	0
n-C6	0	0	0	0	0	0	0
n-C8	0	0	0	0	0	0	0

Experimental Conditions for #52: $H_2/H_2O/H_2S$, 15 psig H_2S, 585 psig CO, 4.0°C/min, 340 °C, 2 hrs, 10 ml H_2O, 100 ml toluene, 10.0 g NAPH, 1.50 mmole Mo; 0.91 mmoles $NiSO_4$; 0.91 mmoles $VO(acac)_2$, 1500 RPM Impeller Speed

Table B.52. 1: Mass of Samples, Experiment #52

Sample #	Purge	1	2	2B	3	3B	4	4B	5	5B	6	6B
Reaction Time (min)		0		18.5		41.5		58.3		88		119
Mass of Empty Vial (g)	14.8	14.8	14.8	14.8	14.7	14.7	14.8	14.8	14.8	15	14.7	14.8
Mass of + sample vial (g)	16.8	16.6	15.7	17.4	15.5	16.5	16.4	16.3	15.7	17	16.1	17.2
mass of liquid sample (g)	1.97	1.88	0.99	2.62	0.78	1.75	1.67	1.55	0.95	2.2	1.42	2.41

Table B.52. 2: GC Analysis, Experiment #52

Reaction Time (min)	0	18.5	41.5	58.25	87.5	118.5	Final
[NPT] (mol/g-liq)	0.000911	0.000909	0.000799	0.00071	0.00059	0.000525	0.000438
[TET] (mol/g-liq)	0.000169	0.000284	0.000392	0.000476	0.000532	0.000609	0.000553
[c-DEC] (mol/g-liq)	7.23E-08	1.45E-07	2.89E-07	4.57E-07	6.75E-07	1.08E-06	1.21E-06
[t-DEC] (mol/g-liq)	4.82E-07	3.13E-07	5.06E-07	8.84E-07	1.64E-06	2.65E-06	4.29E-06
$[NPT] = [NPT]_0 - [TET]-[DEC]$	0.000969	0.000854	0.000746	0.000662	0.000605	0.000526	0.00058

Table B.52. 3: Calculated Gas Concentrations, Experiment #52

Reaction Time (min)	0	18.5	41.5	58.25	87.5	118.5
Total calculated moles of gas in sampling bomb (moles)	0.007077	0.006977	0.006706	0.006482	0.006342	0.006166
[H2] (mol/g-liq)	0.001526	0.001502	0.001357	0.001226	0.001188	0.001021

Table B.52. 4: Gas Analysis, ESTD mol%, Experiment #52

Reaction Time (min)	0	18.5	41.5	58.25	87.5	118.5	Final
Average ESTD mol%							
H2	40.53782	40.47078	38.03331	35.54247	35.20238	31.1358	95.01445
O2	12.46799	12.67503	13.22419	13.71282	13.81342	14.66773	4.092273
N2 Total	47.97388	47.92148	50.0705	52.0214	52.40861	55.57235	14.55314
CH4	0.02382	0.031105	0.032975	0.034995	0.037555	0.038455	0.061973
CO	0	0	0	0	0	0	0
CO2	0.071655	0.07185	0.07345	0.084065	0.083245	0.082015	0.133767
C2H4	0	0	0	0	0	0	0
C2H6	0.431495	0.459945	0.473995	0.49671	0.50102	0.47653	0.544067
C2H2	0	0	0	0	0	0	0
H2S	0.86574	0.87309	0.90872	0.929235	0.91855	0.82295	0.81755
COS	0	0	0	0	0	0	0
1,2-Prop=	0	0	0	0	0	0	0
Water	0	0	0	0	0	0	0
Prop	0	0	0	0	0	0	0
C3	0	0	0	0	0	0	0
n-C5	0.01261	0.01317	0.01265	0.01293	0.082205	0.006385	0
i-C4	0	0	0	0	0	0	0
n-C6	0	0	0	0	0	0	0
n-C8	0	0	0	0	0	0	0

Experimental Conditions for #53: ($CO/H_2O/H_2S$, 15 psig H_2S, 585 psig CO, 4.0°C/min, 340 °C, 2 hrs, 10 ml H_2O, 100 ml toluene, 10.0 g NAPH, 0.50 mmole Mo; 0.30 mmoles $NiSO_4$; 0.30 mmoles $VO(acac)_2$).

Table B.53. 1: Mass of Samples, Experiment #53

Sample #	Purge	1	2	2B	3	3B	4	4B	5	5B	6	6B
Reaction Time (min)		0		19		40		60		90		120
Mass of Empty Vial (g)	14.79	14.77	14.82	14.77	14.82	14.82	14.81	14.75	14.73	14.83	14.75	14.85
Mass of sample + vial (g)	17.12	16.82	16.17	17.03	16.36	17.08	16.26	17.11	16.07	17.38	16.25	17.19
mass of liquid sample (g)	2.33	2.05	1.35	2.26	1.54	2.26	1.45	2.36	1.34	2.55	1.5	2.34

Table B.53. 2: GC Analysis, Experiment #53

Reaction Time (min)	0	19	40	60	90	120	Final
[NPT] (mol/g-liq)	0.000994	0.00095	0.000909	0.000791	0.000828	0.000682	0.000588
[TET] (mol/g-liq)	5.91E-05	0.000122	0.000204	0.000278	0.000408	0.00047	0.000468
[c-DEC] (mol/g-liq)	7.23E-08	1.45E-07	2.17E-07	3.31E-07	6.51E-07	6.51E-07	8.2E-07
[t-DEC] (mol/g-liq)	1.45E-07	3.13E-07	5.3E-07	4.35E-07	9.64E-07	1.16E-06	1.74E-06
[NPT] = $[NPT]_0$ - [TET]-[DEC]	0.001035	0.000971	0.000889	0.000815	0.000685	0.000622	0.000623

Table B.53. 3: Calculated Gas Concentrations, Experiment #53

Reaction Time (min)	0	19	40	60	90	120
Total calculated moles of gas in sampling bomb (moles)	0.009723	0.009572	0.009672	0.009413	0.010272	0.010662
[H2] (mol/g-liq)	0.001089	0.001059	0.001097	0.001036	0.001033	0.00114
[CO] (mol/g-liq)	0.000548	0.00049	0.000316	0.000209	0.000179	0.000151
[CO2] (mol/g-liq)	0.00117	0.001045	0.00123	0.001263	0.001474	0.001575

Table B.53. 4: GC Gas Analysis, ESTD mol%, Experiment #53

Reaction Time (min)	0	19	40	60	90	120	Final
H2	22.95839	24.99921	25.62321	24.87843	22.7191	24.15569	32.80646
O2	8.268335	8.051985	8.06744	8.19417	8.39063	7.471135	2.282328
N2 Total	31.40914	30.60035	30.68761	31.19481	31.92314	28.49489	9.073648
CH4	0.01928	0.03254	0.0435	0.05066	0.05559	0.066715	0.087865
CO	11.56454	7.391855	5.026945	3.94286	3.207855	2.97844	15.38865
CO2	24.673	28.7361	30.32287	32.42398	33.38339	36.90719	44.59749
C2H4	0.058735	0	0	0	0	0	0
C2H6	0.92627	0.98159	0.980915	1.03945	1.008675	1.072865	1.138975
C2H2	0	0	0	0	0	0	0
H2S	0.752835	0.771125	0.758175	0.795085	0.75038	0.79742	0.459505
COS	0.02803	0.017	0	0	0	0	0.050145
1,2-Prop=	0.0303	0.036965	0.03994	0.04357	0.042225	0.04573	0.03029
Water	0	0	0	0	0	0	0
Propylene	0.03225	0.01664	0.009975	0	0	0	0
C3	0	0	0	0	0	0	0
n-C4	0	0	0	0	0	0	0
i-C4	0	0	0	0	0	0	0
n-C6	0	0	0	0	0	0	0
n-C8	0	0	0	0	0	0	0

Appendix C: Sample Calculations

Derivations and formulas are shown in detail in Section 3.5.

Table C. 1: Gas and Liquid Phase Compositions for Experiment #46 – Sample Calculations

Experiment #46							
Reaction Time (min)	0	20.25	39.75	62.75	104.75	119.75	Final
Average ESTD mol%							
H2	30.07429	27.84524	26.4261	25.43746	24.28098	24.16692	50.30766
O2	9.83826	9.64063	9.91633	9.967585	10.15451	10.13501	2.42214
N2 Total	37.9341	37.05327	37.91671	38.1216	38.79734	38.73345	9.758667
CH4	0.07729	0.09033	0.099635	0.109334	0.116715	0.11857	0.162667
CO	3.43802	2.083535	1.46754	1.184365	0.90609	0.944935	13.54203
CO2	16.50438	18.61863	19.61847	20.6667	21.19443	21.43949	23.8155
C2H4	0	0	0	0	0	0	0
C2H6	0.15326	0.161515	0.164705	0.17026	0.16973	0.169715	0.165677
C2H2	0	0	0	0	0	0	0
H2S	1.349165	1.42875	1.428025	1.46343	1.473405	1.473365	0.993283
COS	0	0	0	0	0	0	0.06518
1,2-Prop=	0	0	0	0	0	0.012005	0
Water	0.40971	0	0	0	0	0	0
Prop	0	0	0	0	0	0	0
C3	0	0	0	0	0	0	0
n-C4	0	0	0	0	0	0	0
i-C4	0	0	0	0	0	0	0
n-C6	0	0	0	0	0	0	0
n-C8	0	0	0	0	0	0	0
Total calculated moles of gas in sampling bomb (moles)	0.008718	0.008577	0.008463	0.008406	0.008421	0.008348	
[H2] (mol/g-liq)	0.001219	0.00111	0.001039	0.000994	0.00095	0.000938	
[CO] (mol/g-liq)	0.000139	8.31E-05	5.77E-05	4.63E-05	3.55E-05	3.67E-05	
[CO2] (mol/g-liq)	0.000669	0.000742	0.000772	0.000807	0.00083	0.000832	
[NPT] (mol/g-liq)	0.000917	0.000805	0.000759	0.000695	0.000626	0.000605	0.000479
[TET] (mol/g-liq)	0.000284	0.000379	0.000478	0.000563	0.000623	0.000644	0.000533
[c-DEC] (mol/g-liq)	1.69E-07	2.89E-07	4.82E-07	7.84E-07	1.08E-06	1.21E-06	9.89E-07
[t-DEC] (mol/g-liq)	3.13E-07	5.79E-07	8.92E-07	1.57E-06	1.88E-06	2.21E-06	3.18E-06
$[NPT] = [NPT]_0 - [TET]-[DEC]$	0.000916	0.00082	0.000721	0.000635	0.000575	0.000553	0.000664

Table C. 2: Recovered Masses and Pressures during and after Experimental Run #46

Experiment #46												
Sample #	Purge	1	2	2B	3	3B	4	4B	5	5B	6	6B
Mass of Empty Vial (g)	16.42	16.59	16.49	16.39	16.37	16.51	16.45	16.49	16.49	16.45	16.58	16.40
Mass of sample + vial (g)	19.01	18.74	17.88	18.70	17.45	18.80	17.56	18.82	17.97	18.69	17.50	18.77
mass of 1st liquid sample	2.59	2.15	1.39	2.31	1.08	2.29	1.11	2.33	1.47	2.24	0.91	2.37
Cumulative Sample Mass Recovered (g)	2.59	4.75	6.14	8.45	9.53	11.82	12.93	15.27	16.74	18.99	19.90	22.27
Cumulative Mass Remaining in Reactor (g)	93.70	91.55	90.16	87.85	86.76	84.47	83.36	81.03	79.55	77.31	76.39	74.02
mass of Liq. Prod. Recovered (g)	71.34											
Final Pressure (psig)	313											
Recovered Aqueous Phase (g)	4.61											

C. 1: Pseudo-first Order Rate Calculations

A plot of concentration (naphthalene concentration, CO mol%) versus time was conducted using Microsoft Excel spreadsheet software. The exponential function was fitted to the data using the Regression Analysis in Excel.

C. 2: Calculation for gas concentration in liquid (Experiment #46)

The mols of initial CO was estimated using the Ideal Gas Law,

$$vol\%\ H_2S = \frac{22.5\ psi}{614.7\ psia} = 3.6\%$$

$$vol\%\ CO\ in\ [CO:H_2] = 50\%$$

$$N_{CO,0} = \left\{\frac{P_{CO,0}V_g}{RT}\right\}$$

$$N_{CO,0} = \left\{\frac{(0.963)x(0.50)x(41.8atm)\,x(0.147L)}{(0.082061atm-L/mol-K)x(300K)}\right\} = 0.1202mol-CO$$

$$\frac{N_{CO,0}}{N_{H2O,0}} = \frac{0.1217\ mol-CO}{\left(\frac{10.0g}{18.02g/mol-H_2O}\right)} = 0.216$$

$$N_{H2O,0} : N_{CO,0} = 4.6$$

Estimate for moles of gas in sampling volume, $n_{gas,sample}$ (mol-gas):

m_{sample}	=	mass of collected sample liquid sample (g-liq)
P_{SB}	=	Pressure in the sampling bomb (psia)
V_{SB}	=	Volume of the sampling bomb (156 x 10^{-6} m^3)
R	=	Molar Gas Constant (8.314 Pa-m^3/mol-K)
T	=	Sampling bomb temperature (K)
Volt	=	Voltage reading of sample pressure transducer (Volts)

$$P_{SB} = \frac{(Volt-1)(100\,psia-0\,psia)}{(5Volt-1Volt)} = 30$$

$$P_{SB,gauge} = P_{SB} - 14.7$$

$$P'_{SB} = P_{SB}\frac{(101325\ Pa\ atm^{-1})}{(14.7\ psi\ atm^{-1})}$$

$$N_{gas} = \frac{(P'_{SB}V_{SB})}{(RT)}$$

$$P_{SB} = \frac{(2.2-1)(100\,psia-0\,psia)}{(5V-1V)}$$

$$P_{SB,gauge} \quad = \quad 30 - 14.7 = 15.3\ psig$$

$$P'_{SB} = 15.3\ psig\ x \frac{(101325\ Pa\ atm^{-1})}{(14.7\ psi\ atm^{-1})} = 1.05461x10^{5}\ Pa$$

$$N_{gas} = \frac{(1.05461x10^{5}\ Pa)\ x\ (156x10^{-6}\ m^{3})}{(8.314\ Pa - m^{3}/mol - K)x(300\ K)} = 0.0066\ mol$$

$$Gas\ Concentration\ \ (mol\ g - Liq^{-1}) = \frac{N_{gas}}{m_{sample}}$$

for sample at time 0 minutes (Experiment #46, sample #1)

$$[H_2] = \frac{(mol\% - H_2)x(total - moles - in - sample - bomb)}{(mass - of - liquid - sample)}$$

$$[H_2] = \frac{(30.07mol\% - H_2)x(8.72mmoles)}{2.15 - g} = 0.00122moles - H_2 / g$$

C. 3: Naphthalene Conversions (Experiment #46)

For naphthalene conversion at 120 minutes:

$$X(\%) = \frac{[NAPH]_0 - [NAPH]_t}{[NAPH]_0} = \frac{[0.00120 - 0.000605]mol/g - liq}{[0.00120]mol/g - liq} = 49.6\%$$

C. 4: Calculation of Pseudo-second order rate constant for hydrogenation (Experiment #46):

k"$_{NAPH}$ is simply approximated by dividing k_{NAPH} by the pseudo-steady state hydrogen concentration.

$$r_{NAPH} = k''_{NAPH}[H_2][NAPH]$$

$$\overline{[H_2]} = \left[\frac{0.001219 + 0.00111 + 0.001039 + 0.000994 + 0.00095 + 0.000938}{6}\right] = 0.00104 mols - H_2 / g - liq$$

$$k''_{NAPH} = \frac{k_{NAPH}}{[H_2]} = \frac{6.93x10^{-5} s^{-1}}{0.00104 mols - H_2 / g - liq} = 0.0665 g - liq / mols - H_2 - s$$

C. 5: Reversible WGS Rate Constant (Experiment #40)

$$K_{eq} = \exp\left\{-4.33 + \frac{4577.8}{T(K)}\right\}$$

$$Ln(A) = Ln\left\{\frac{[CO]_0{}^2 - [CO]_e[CO]_t}{([CO]_t - [CO]_e)[CO]_0}\right\}$$

where,
$[CO]_0$ = initial concentration of CO
$[CO]_e$ = equilibrium concentration of CO
$[CO]_t$ = measured concentration of CO at reaction time t

A plot of Ln A versus time should yield a straight line with slope m, where

$$m = k_i x\left[\frac{[CO]_0 + [CO]_e}{[CO]_0 - [CO]_e}\right]$$

Table C. 3: Normalized mol% CO from Experiment #10 (600 psig, CO/H_2O, 15 psi H_2S, 4.1 °C/min, 340 °C for 4 hours, 18.1 ml H_2O, 52 ml toluene, 87.1 mmol Naph, 1500 rpm impeller speed, 1.16 mmole Mo)

Time (min)	***0.00***	***20.00***	***40.00***	***60.00***	***90.00***	***120.00***
Normalized mol% CO	***9.47%***	***4.39%***	***3.17%***	***2.19%***	***1.92%***	***1.97%***

$$K_{eq} = \exp\left\{-4.33 + \frac{4577.8}{(613K)}\right\} = \exp\{-4.33 + 7.467\} = \exp\{3.138\} = 23.05$$

Calculation for Pure CO feed:

$[CO]_e$ = theoretical equilibrium normalized mol% CO
$[CO]_0$ = normalized mol% CO at 0 minutes
$[CO]_t$ = normalized mol% CO at t minutes

K_{eq} = Equilibrium constant for WGS
$N_{CO,i}$ = Initial mols of CO loaded into reactor (mol)
N_j = mols of species j
$N_{H2}{}^C$ = hydrogen consumed (mol); 2 mol required to form tetralin, 5 mol for decalin

X = Conversion of CO
X_{eq} = Equilibrium conversion of CO
w = initial molar ratio of H_2O:CO, $\frac{molH_2O}{molCO}$
χ_{CO} = normalized dry mol% CO from GC analysis

$$\chi_{CO} = \frac{N_{CO}}{N_T} = \frac{(1-X)N_{CO,0}}{(1+X)N_{CO,0} - N_{H2}^C}$$

where,

The calculation of K_{eq} is thus:

$$K_{eq} = \frac{N_{CO2}N_{H2}}{N_{CO}N_{H2O}}$$

$$K_{eq} = \frac{[N_{CO,i}X_{eq}][N_{CO,i}X_{eq} - N_{H2}^C]}{[N_{CO,i}(1-X_{eq})][N_{CO,i}(w-X_{eq})]}$$

$$K_{eq} = \frac{[N_{CO,i}X_{eq}]^2 - [N_{CO,i}X_{eq}N_{H2}^C]}{[N_{CO,i}{}^2(1-X_{eq})(w-X_{eq})]}$$

Sample Calculation for Experiment #40:

Initial Conditions when Loading Reactor:
P_T = 600 psig
P_{H2S} = 15 psi
V_{H2O} = 18 ml

$V_{toluene}$	=	52 ml
$mass_{NAPH}$	=	11.17 g
V_{gas}	=	187 ml
Temp	=	300 K

$$N_{CO,0} = \frac{PV}{RT} = \frac{(0.975x41.8atm)(187x10^{-3}L)}{(0.082061atmL/molK)(300K)} = 0.310moles$$

$$N_{H2O,0} = \frac{18.0g}{18.02g/mole} = 1.00moles$$

$$w = \frac{1.00\ mol-H_2O}{0.310\ mol-CO} = 3.2$$

$$N_{H2}^{C} = mass_{rxn}\{2[TET]+5[c-DEC]+5[t-DEC]\}$$

$$N_{H2}^{C} = 39.954\ g\ \{2*0.001445\ (mol-NAPH/g)+5*7.917*10^{-6}\ (mol-c-DEC/g)$$
$$+5*1.229*10^{-5}\ (mol-t-DEC/g)\}$$

$$N_{H2}^{C} = 0.1195 \quad mol-H_2 \quad consumed$$

$$K_{eq} = 23.05 = \frac{[N_{CO,i}X_{eq}]^2-[N_{CO,i}X_{eq}N_{H2}^{C}]}{[N_{CO,i}{}^2(1-X_{eq})(w-X_{eq})]}$$

where the GOALSEEK function in Excel was used to solve for X_{eq}.

$$X_{eq} = 0.9877 = 98.7\%$$

$$\chi_{CO} = \frac{(1-X)Ni}{(1+X)N_{CO,0}-N_{H2}^{C}} = \frac{(1-0.988)*(0.310\ mol-CO-initial)}{(1+0.988)*(0.310\ mol-CO-initial)-(0.1195\ mol-H_2-consumed)}$$

$$\chi_{CO} = 0.76\ mole\%$$

$$Ln(A)_{50} = Ln\left\{\frac{[CO]_0{}^2-[CO]_e[CO]_{40}}{([CO]_{40}-[CO]_e)[CO]_0}\right\}$$

$$Ln(A)_{50} = Ln\left\{\frac{[9.47]_0{}^2-[0.78]_e[3.17]_{40}}{([3.17]_{40}-[0.78]_e)[9.47]_0}\right\}$$

$$Ln(A)_{50} = Ln\{4.22\} = 1.44$$

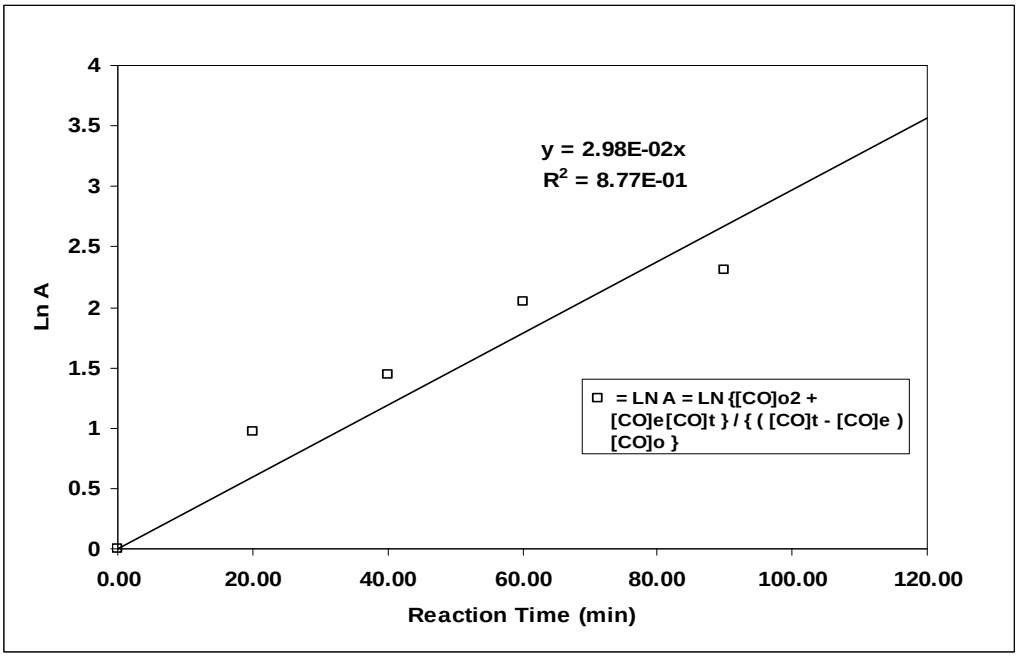

Figure C. 1: Plot of Ln(A) versus Reaction Time for Experiment #40 – Calculation of the reversible WGS Rate Constant

$$m = k_i x \left[\frac{[CO]_0 + [CO]_e}{[CO]_0 - [CO]_e} \right]$$

$$\frac{0.0298 \min^{-1}}{60 s / \min} = k_i x \left[\frac{9.47 + 0.76}{9.47 - 0.76} \right]$$

$$\frac{4.97 x 10^{-4}}{1.24} = k_i = 4.02 x 10^{-4} s^{-1}$$

C. 6: Calculation of Variance (Experiment #5, 5R1, 5R2 - (Isotope Labeling Experiments)

Table C. 4: Means and Variances for first-order rate constants for naphthalene hydrogenation and water-gas shift

Experiment #	**k_{NAPH} (10^{-5} s^{-1})**	**$\overline{k_{NAPH}}$ (10^{-5} s^{-1})**	**k_{NAPH} variance (10^{-10} s^{-2})**	**k_{CO} (10^{-5} s^{-1})**	**$\overline{k_{CO}}$ (10^{-5} s^{-1})**	**k_{CO} variance (10^{-10} s^{-1})**
2	21.0	20.4	0.684			
2R1	19.8					
17	24.3	22.3	8.41			
28	20.2					
5	8.67	7.81	0.561	n/a	n/a	n/a
5R1	7.42			7.50		
5R2	7.33			n/a	n/a	n/a
7	8.55			11.3		
14	7.83			9.58	8.58	0.917
1	20.2			8.50		
1R1	5.33			7.67		

$$s_p^{\,2} = \sum_{i=1}^{n} \frac{(X_i - \overline{X})^2}{n-1}$$

$$s_p^{\,2} = \frac{[(8.67-7.81)x10^{-5}]^2 + [(7.42-7.81)x10^{-5}]^2 + [(7.33-7.81)x10^{-5}]^2}{2}$$

$$s_p^{\,2} = 5.61x10^{-11}s^{-2}$$

C. 7: Calculation of pooled variance for k_{NAPH} (Table C.4)

The pooled variance was calculated from the variance for:

- Experiment #2 and #2R1
- Experiment #17 and #28
- Experiment #5, #5R1 and #5R2

The equation for the pooled variance is shown below:

$$^{naph}s_p^{\,2} = \frac{\sum_i^n \nu_i s_i^{\,2}}{\sum_i^n \nu_i}$$

where,

υ_i = degrees of freedom of mean i

s_i = standard deviation of mean i

$$^{naph}s_p^{\,2} = \left[\frac{0.684 + 8.40 + 2(0.56)}{1+1+2}\right] * 10^{-10}$$

$$^{naph}s_p^{\,2} = 2.55 * 10^{-10}$$

$$^{naph}s_p^{\,2} = MS_e = 2.55 * 10^{-10}$$

C. 8: Calculation of Confidence Interval for k_{CO} (Experiment #1, 1R1 and 14)

$$CI = t_{df,\frac{1-\alpha}{2}} \sqrt{\frac{s^2}{n}}$$

n	=	# of measurements	=	3		
s^2	=	variance	=	$9.17*10^{-11}$		
df	=	degrees of freedom	=	n-1	=	2
α	=	Confidence Level	=	90 %		

from t-tables, $t_{2,0.05}$ = 2.92

$$CI = 2.92\sqrt{\frac{9.17x10^{-11}}{3}} = 1.614x10^{-5}$$

C. 9: Sample Calculation for Analysis of Variance (ANOVA) for ternary VNiMo-sulfides

Table C. 5: (600 psig , 4.0°C/min, 2 hrs, 10 ml H_2O, 100 ml toluene, 10 g NAPH, 1.5 mmoles Mo, 0.91 mmole Ni, 0.91 mmole V, 1500 RPM Stir Speed)

Experiment Number	***Temp***	***H_2S Pressure (psi)***	***Gas Type (CO or H_2)***	***Pseudo-First Order Naphthalene Rate Constant, k_{NAPH} (10^{-5} s^{-1})***	***Final [H2] (mol/g)***
45	380	15	CO	13.03	0.00095
44	340	15	CO	10.1	0.00102
48	380	30	CO	12.2	0.00111
47	340	30	CO	8.93	0.00095
49	380	15	H_2	10.1	0.00075
52	340	15	H_2	8.5	0.00102
51	380	30	H_2	14.27	0.00076
43	340	30	H_2	7.5	0.00083
46	360	22.5	CO/H_2	6.93	0.00094
50	360	22.5	CO/H_2	7.1	0.00104
42	360	22.5	CO/H_2	7.26	0.00114
53	340	15	CO	6.43	0.00114

The example is for the main temperature effect on k_{NAPH}:

$$Effect = \left[\frac{13.03+12.2+10.1+14.27}{4}\right]x10^{-5} - \left[\frac{10.1+8.93+8.50+7.50}{4}\right]x10^{-5}$$

$$Effect = 3.6425x10^{-5}\,s^{-1}$$

$$Sum\,of\ Squares = 2^{f-2}(Effect)^2 = 2^{3-1}(3.6425x10^{-5})^2$$

$$Sum\,of\ Squares = 2.65x10^{-9}$$

$$Mean\,Squares\,(MS) = \frac{SS}{df} = \frac{2.65x10^{-9}}{1} = 2.65x10^{-9}$$

where df = 1 (there are two levels of temperature (380 and 340 °C))

$$Mean\,Square\,Error\,(MSE) = s_p{}^2$$

where $s_p{}^2$ is the variance of the centre-point replicates.

$$F_{experiment} = \frac{MS}{MSE} = \frac{2.65x10^{-9}}{2.72x10^{-12}} = 974.38$$
$$F_{critical} = F_{1,2,0.05} = 18.51$$

$$F_{experiment} > F_{1,2,0.05}$$

therefore we can consider this effect significant.

C. 10: Calculation of Hydrogenation Equilibrium Constant

from (Frye and Weitkamp 1969, 372);

$$K_P = \frac{N_{TET}}{N_{NAPH} * (P_{H2} + 0.00033\ P_{H2}{}^2)^2}$$
$$X_{eq} = 1 - [1 + \frac{N_{TET}}{N_{NAPH}}]^{-1}$$

$$P_{H2} = hydrogen \quad pressure \quad (atm)$$
$$P_{H2} = \frac{[H_2\ mol\ /\ g] * mass_{rxn}(g) * RT}{V_{reactor}}$$

Sample Calculation Experiment #52 ($H_2/H_2O/H_2S$, 340 °C):

$$Log \quad K_P = \frac{6460}{(613.15K)} - 12.4 = -1.86$$

$$K_P = 0.01367$$

$$P_{H2} = hydrogen\ pressure\ (atm)$$

$$P_{H2} = \frac{[H_2\ mol/g] * mass_{rxn}(g) * RT}{V_{reactor}}$$

$$P_{H2} = \frac{[0.001021\, mol - H_2/g] * (73.41g) * (0.082067\ L - atm/K) * (613.15K)}{(0.257\ L)}$$

$$K_P * (P_{H2} + 0.00033{P_{H2}}^2)^2 = \frac{N_{TET}}{N_{NAPH}}$$

$$(0.01367) * (16.38\, atm + 0.00033((16.38\, atm)^2)^2 = \frac{N_{TET}}{N_{NAPH}}$$

$$\frac{N_{TET}}{N_{NAPH}} = 3.71$$

$$X_{eq} = 1 - [1 + \frac{N_{TET}}{N_{NAPH}}]^{-1}$$

$$X_{eq} = 1 - [1 + 3.71]^{-1} = 0.788$$

C. 11: Sample Calculation for Experiment #19, Sample #1 (1.23 minutes reaction time)

$$[NAPH]_{NMR,t} = [NAPH]_{GC,t}\, x\left[\frac{(mass-of-GC-sample)}{mass-of-NMR-sample}\right] = [0.0114g/g-liq]x\left[\frac{(3.1968-2.4903)g}{(2.9198-2.4903)g}\right]$$

$$[NAPH]_{NMR,t} = 0.011361g/g-liq$$

$$\left[\frac{mol-NAPH}{mol-n-Oc\tan e}\right]_{total} = \frac{\left\{\frac{[NAPH]_{NMR,t}}{MW_{NAPH}}\right\}}{\left\{\frac{1-[NAPH]_{NMR,t}-[TET]_{NMR,t}-[c-DEC]_{NMR,t}-[t-DEC]_{NMR,t}-[Ace}{MW_{n-Oc\tan e}}\right.}$$

$$\left[\frac{mol-NAPH}{mol-n-Oc\tan e}\right]_{total} = \frac{\left\{\frac{[0.0114g/g-liq]}{128.17g/mol}\right\}}{\left\{\frac{1-[0.0114g/g-liq]-[0g/g-liq]-[0g/g-liq]-[0g/g-liq]-[0.006536]}{114.21g/mol}\right\}}$$

$$\left[\frac{mol-NAPH}{mol-n-Oc\tan e}\right]_{total} = \frac{\left\{8.864x10^{-5}mol-NAPH\right\}}{\left\{8.599x10^{-3}mol-n-Oc\tan e\right\}} = 0.010308$$

$$\left[\frac{mol-NAPH(^1H)}{mol-n-Oc\tan e(^1H)}\right]_{NAPH-A} = 0.00804$$

$$\%(^1H)-Incorporation_{NAPH-A} = \left[\frac{\left[\frac{mol-NAPH(^1H)}{mol-n-Oc\tan e(^1H)}\right]_{NAPH-A}}{\left[\frac{mol-NAPH}{mol-n-Oc\tan e}\right]_{total}}\right] = \left[\frac{0.00804}{0.010308}\right] = 0.7799 = 78.0\%$$

$[NAPH]_{NMR,t}$ = Concentration of Naphthalene in the NMR sample measured by GC-FID at reaction time t

$[TET]_{NMR,t}$ = Concentration of Tetralin in the NMR sample measured by GC-FID at reaction time t

$[c\text{-}DEC]_{NMR,t}$ = Concentration of c-Decalin in the NMR sample measured by GC-FID at reaction time t

$[t\text{-}DEC]_{NMR,t}$ = Concentration of t-Decalin in the NMR sample measured by GC-FID at reaction time t

$[Acetone]_{NMR,t}$ = Concentration of in the NMR sample measured by GC-FID at

		reaction time t
Subscript t	=	Reaction time sample was collected, t (min)
NMR	=	Sample from NMR tube

C. 12: Sample Calculation of Hydrogenation Index (HI) and Exchange Index (EI)

$mass_{rxn}$	=	mass of liquid in reactor (g)
n_H	=	total moles of hydrogen including D in all products (NAPH and TET)
$n_{1H}°$	=	moles of hydrogen in starting naphthalene
n_{2H}	=	total moles of deuterium in products by hydrogenation and exchange
H	=	net amount of hydrogen added to form tetralin, $n_H - n_{1H}°$
E	=	amount of deuterium incorporated by exchange, $n_{2H} - H$

$$n_H = \{8*[NAPH]+12*[TET]\}*mass_{rxn}$$

$$n_{1H}° = \frac{8*mass_{NAPH,i}}{MW_{NAPH}}$$

$$n_{2H} = mass_{rxn}*\{\{(1-[\%^1H-NAPH-A])+(1-[\%^1H-NAPH-B])\}*4*[NAPH] + \{(1-[\%^1H-TET-AROM])+(1-[\%^1H-TET-SAT]*2\}*4*[TET]\}$$

$$HI = \frac{H}{H+E}$$

$$EI = \frac{E}{H+E}$$

Sample Calculation for HI and EI for Experiment CL5R1 ($CO/D_2O/H_2S$) at 39.3 minutes:

$$[\%^1H-NAPH-A] = 22.95\%$$

$$[\%^1H-NAPH-B])\} = 33.51\%$$

$$[\%^1H-TET-AROM] = 13.85\%$$

$$[\%^1H-TET-SAT] = 34.61\%$$

$$n_H = \{8*[3.868*10^{-4}\ mol-NAPH/g]+12*[5.85*10^{-5}\ mol-TET/g]\}*(70.54g)$$

$$n_{1H}{}^{\circ} = \frac{8*(3.7\quad g-NAPH}{128.17\quad g-NAPH/mol}$$

$$n_{2H} = (70.54g)*\{\{(1-[0.2295])+(1-[0.3351])\}*4*[3.868*10^{-4}\ mol-NAPH/g]$$
$$+\{(1-[0.1385])+(1-[0.3461]*2\}*4*[5.85*10^{-5}\ mol-TET/g]\}$$

$$H = 0.0369$$

$$E = 0.156$$

$$HI = \frac{0.0369}{0.156+0.0369} = 0.191$$

$$EI = \frac{0.156}{0.0369+0.156} = 0.808$$

C. 13: Overall Liquid Mass Balance (Experiment #46)

Assume that naphthalene when dissolved in toluene has a negligible contribution to the volume.

Experiment #46:

Cumulative Mass of all samples collected = 22.74 g
Liquid Recovered at End of Reaction = 71.34 g
Total Mass of Liquid and Solids charged = 107.30 g
Initial mass charged, m_o = $m_{H2O} + m_{NAPH} + m_{toluene} + m_{catalyst}$
$m_{catalyst}$ = $m_{PMA} + m_{NiSO4} + m_{VO(acac)2}$

$$m_0 = 10.0g+10.0g+86.6g+\left\{\begin{array}{l}\left(\dfrac{0.1449g-Mo}{0.65g-Mo/g-PMA}\right)\\ +0.241g-VO(acac)_2+0.240g-NiSO_4*6H_2O\end{array}\right\}$$

$$m_0 = 107.30\ g$$

Theoretical mass at end of reaction = (107.30 – 22.74)g = 84.56 g
Actual mass at end of reaction = 71.34 g

$$\frac{Actual\ Mass\ recovered}{Mass\ Initially\ Charged} = \frac{(71.34+22.74)g}{107.30g} = 87.6\%$$

C. 14: Consumption of water calculated from CO conversion and CO_2 yield (Experiment #46)

$$CO_{(g)} + H_2O_{(g)} \rightleftharpoons CO_{2(g)} + H_{2(g)}$$

Considering a mole balance over the WGS, for every mole of CO consumed 1 mole of water is consumed and 1 mole of CO_2 is produced. Therefore we can calculate the consumption of water indirectly by calculating the moles of CO consumed and CO_2 produced.

Initial Pressure (psig)	=	600 =41.8 atm		
P_{H2S} (psi)	=	22.5		
Volume (ml)				
o Toluene	=	100		
o Water	=	10		
Mass of Naph (g)	=	10		
$V_{g,0}$(ml)	=	257 – (100+10)	=	147
$V_{l,0}$ (ml)	=	100 + 10	=	110

To calculate a normalized mol%, we must subtract the contribution from N_2 and O_2 which represent air that has entered the sampling system. Note: the data in the table is calculated from external calibration gases, one for Refinery gas (Agilent) and one for sulfur gases (Praxair); therefore the total mol% is not exactly 100%.

Total moles excluding air = 101.2328 – (2.42 + 9.75) = 89.06 mol%

Normalized mol%

- $mol\% \quad CO = \frac{13.54}{89.06} = 15.2\, mol\% \quad CO$
- $mol\% \quad CO_2 = \frac{23.82}{89.06} = 26.7\, mol\% \quad CO$

$$P_{CO,0} = 41.8 atm\, x\, 0.50\, x\, 0.963 = 20.135 atm$$

from the Ideal Gas Law,

$$N_{CO,0} = \left\{ \frac{20.135 atm\, x\, 0.147 L}{(0.082061 atm - L/mol - K) x (300 K)} \right\} = 0.1202 mol$$

$$V_{l,final} = V_{toluene,final} + V_{H2O,final} = \frac{(71.34 - 4.61) g}{0.866 g/ml} + 4.61 ml = 81.67 ml$$

$$V_{g,final} = 257 ml - 81.67 ml = 175.3 ml$$

$$N_{gas,\,final} = \left\{ \frac{22.293 atm\, x\, 0.1753 L}{(0.082061 atm - L/mol - K) x (300 K)} \right\} = 0.1587 mol\, total$$

$$N_{CO,\,final} = 0.152 x (0.1587\, mol) = 0.0241 mol - CO$$

moles of CO converted,

$$N_{CO,converted} = (0.1202 - 0.0241) mol - CO = 0.0961 mol - CO$$

$$N_{H2O,consumed} = 0.0961 mol\, x 18.02 g/mol = 1.73 g - H_2O$$

C. 15: Calculation of Water from CO_2 measurement (Experiment #46)

$$N_{CO2,\,final} = \left\{ \frac{22.293 atm\, x\, 0.1753 L}{(0.082061 atm - L/mol - K) x (300 K)} \right\} = 0.1587 mol\, total$$

$$N_{CO2,\,final} = 0.267 x (0.1587\, mol) = 0.0424 mol - CO_2$$

$$N_{CO2,\,produced} = 0.0424 mol - CO_2$$

$$N_{H2O,consumed} = 0.0424 mol\, x 18.02 g/mol = 0.765 g - H_2O$$

The discrepancy between the water balance calculated from CO and CO_2 suggests that significant quantities of CO_2 are absorbed in the liquid phase or to the catalyst surface.

Appendix D: Summary of Reaction Conditions

Table D. 1: Summary of Experimental Conditions

Experiment #	Gas Composition	Molar Ratio	Reactor Temp (°C)	H_2S Pressure (psi)	Solvent	Catalyst Charge	mmoles of metal
1	$CO:H_2:D_2O$	1:1:4.6	340	15	n-Octane	Mo	0.39
1R1	$CO:H_2:D_2O$	1:1:4.6	340	15	n-Octane	Mo	0.39
2	$H_2:D_2O$	1:2.3	340	15	n-Octane	Mo	0.39
2R1	$H_2:D_2O$	1:2.3	340	15	n-Octane	Mo	0.39
5	$CO:D_2O$	1:2.3	340	15	n-Octane	Mo	0.39
5R1	$CO:D_2O$	1:2.3	340	15	n-Octane	Mo	0.39
5R2	$CO:D_2O$	1:2.3	340	15	n-Octane	Mo	0.39
6	$CO:H_2:D_2O$	1:1:4.6	340	15	n-Octane	Mo	0
7	$CO:H_2O$	1:2.3	340	15	n-Octane	Mo	0.39
10*	$CO:H_2O$	1:3.24	340	15	toluene	Mo	1.16
12*	$CO:H_2O$	1:3.24	340	15	toluene	Mo	0
14	$CO:H_2:D_2O$	1:1:4.6	340	15	n-Octane	Mo	0.39
15	$CO:H_2:H_2O$	1:1:4.6	340	15	n-Octane	Mo	0.39
17	$H_2:H_2O$	1:2.3	340	15	n-Octane	Mo	0.39
19	$N_2:D_2O$	1:2.3	340	15	n-Octane	Mo	0.39
24	$CO:H_2O$	1:2.3	340	15	toluene	Mo	0.47
25	$CO:H_2O$	1:2.3	340	15	toluene	Mo	0.39
28	$H_2:H_2O$	1:2.3	340	15	n-Octane	Mo	0.39
29	$N_2:H_2:H_2O$	1:1:4.6	340	15	n-Octane	Mo	0.39
30	$CO:H_2O$	1:2.3	340	15	toluene	none	0
32	$CO:H_2O$	1:2.3	340	15	toluene	Mo	0.47
33	$CO:H_2O$	1:2.3	340	15	toluene	$Ru_3(CO)_{12}$	0.47
34	$CO:H_2O$ ($H_2:H_2O$)	1:2.3	340	15	toluene	$Ru(acac)_3$	0.47
36*	$CO:H_2O$	1:3.24	340	15	toluene	Mo:Ru	0.87 : 0.29
37*	$CO:H_2O$	1:3.24	340	15	toluene	Mo:Fe	1.16 : 0.70
38*	$CO:H_2O$	1:3.24	340	15	toluene	Mo:V	1.16 : 0.70
39*	$CO:H_2O$	1:3.24	340	15	toluene	Mo:Ni	1.16 : 0.70
40*	$CO:H_2O$	1:3.24	340	15	toluene	Mo	1.16
41*	$CO:H_2O$	1:3.24	340	15	toluene	Mo:Ni:V	1.16 : 0.70: 0.70
42**	$CO/H_2/H_2O$	1:1:4.6	360	22.5	toluene	Mo:Ni:V	1.5 : 0.98 0.97
43**	H_2/H_2O	1:2.3	340	30	toluene	Mo:Ni:V	1.5 : 0.91 : 0.91
44**	CO/H_2O	1:2.3	340	15	toluene	Mo:Ni:V	1.5 : 0.91 : 0.91
45**	CO/H_2O	1:2.3	380	15	toluene	Mo:Ni:V	1.5 : 0.91 : 0.91
46**	$CO/H_2/H_2O$	1:1:4.6	360	22.5	toluene	Mo:Ni:V	1.5 : 0.91 : 0.91
47**	CO/H_2O	1:2.3	340	30	toluene	Mo:Ni:V	1.5 : 0.91 : 0.91
48**	CO/H_2O	1:2.3	380	30	toluene	Mo:Ni:V	1.5 : 0.91 : 0.91
49**	H_2/H_2O	1:2.3	380	15	toluene	Mo:Ni:V	1.5 : 0.91 : 0.91
50**	$CO/H_2/H_2O$	1:1:4.6	360	22.5	toluene	Mo:Ni:V	1.5 : 0.91 : 0.91
51**	H_2/H_2O	1:2.3	380	30	toluene	Mo:Ni:V	1.5 : 0.91 : 0.91
52**	H_2/H_2O	1:2.3	340	15	toluene	Mo:Ni:V	1.5 : 0.91 : 0.91
53**	CO/H_2O	1:2.3	340	15	toluene	Mo:Ni:V	0.5 : 0.3 : 0.3

(600 psig, 340 °C for 3 hours, 10 ml water, 100 ml solvent, 5.0 wt% NAPH (organic basis), 1500 rpm impeller speed)

*(600 psig, 340 °C for 4 hours, 18.1 ml H_2O, 52 ml solvent, 11.17 g NAPH, 1500 rpm impeller speed)

**(600 psig, 340 °C for 2 hours, 10 ml H_2O, 100 ml solvent, 10.0 g NAPH, 1500 rpm impeller speed)

Table D. 2: Summary of Experimental Results

Experiment #	k_{NAPH} (10^{-5} s^{-1})	k_{CO} (10^{-5} s^{-1})
1	20.2	8.48
1R1	5.26	7.81
2	21.0	
2R1	19.8	
5	9.25	
5R1	7.42	7.50
5R2	7.33	6.83
6	2.43	5.00
7	8.55	8.65
10	11.1	20.5
12	2.68	10.5
14	7.83	8.92
15	10.1	11.2
17	23.5	
19		
24	13.9	14.5
25	13.0	13.7
28	20.8	
29	8.81	
30	3.02	6.62
32	7.20	9.30
33		4.52
34	3.42	
36	5.40	14.73
37	6.83	22.5
38	6.08	30.3
39	21.0	16.1
40	18.8	40.2
41	13.7	21.9
42	7.26	18.67
43	7.51	
44	10.1	24.9^{rev}
45	13.03	12.2^{rev}
46	6.93	16.03
47	8.93	30.7^{rev}
48	12.2	4.95^{rev}
49	10.1	
50	7.1	15.84
51	14.27	
52	8.53	
53	6.43	19.0

Appendix E: Experimental and Operational Procedures

E. 1: HC 300 cc Liquid Sample Tube Filter Cleaning

Micron sized MoS_2 particles will deposit and accumulate on the sintered 316 SS frit used to prevent solids from entering the liquid sampling lines. In addition, H_2S and the liquid aqueous phase PMA precursor can enter the sintered frit before sufficient temperatures are reached and actually sulfide the PMA precursor to form solid MoS_2 *inside* the frit.

Molybdenum sulfide deposits can be removed from 316 SS and HC-276 surfaces by immersing the metal parts in a well-stirred, dilute solution of 15-30 vol% H_2O_2. **CAUTION!** Hydrogen peroxide can oxidize molybdenum sulfide to produce acids, sulfur oxides and hydrogen sulfide; this procedure must be performed in a fume hood! The parts are immersed for approximately 48 hours, then soaked in water for another 6-12 hours to rinse and decompose any residual H_2O_2.

E. 2: Liquid Sampling Procedure

Weigh and record the empty mass (to .01 g) of 12 sample vials with caps. This is necessary to record an accurate mass balance of species in the system.

Purging the Sample Dip Tube

1. Ensure valves **1, 3, 4, 5, 6, 8, 9** and **11** are closed.
2. Open valve **5** for approximately 10 s to evacuate the previous sample from the sampling volume.
3. Close valve **5** to isolate sampling volume in preparation to take liquid sample to purge the sampling system.
4. Ensure valves **3, 4 and 5** are closed.
5. Take sample from reactor by opening valve **1** quickly and wait until reading on pressure display reaches a minimum. Close valve **1** quickly. Sample should now be isolated between valves **1 and 4 (Figure B1)**. **CAUTION: Valves 1 and 4 should NEVER be opened simultaneously during reactor operation.**
6. Ensure valves **9 and 11** are closed in preparation to depressurize sample. Check that sampling system pressure is at atmospheric or under vacuum on the DAQ system (< 1.6 Volts).
7. Open valve **4** to depressurize sample into sampling bomb. Wait for approximately 30 – 60 s for the sampling temperature and pressure to stabilize.
8. Close valve **7** and Open valve **6**. Open valve **5** to depressurize and vent gas from sample. Collect the liquid sample by opening valve **9** and draining liquid into properly labeled vial. Open valve **7**; Close valve **6** and valve **9**.
9. Weigh the sample vial and record the mass.

Taking the Gas and Liquid Sample

10. Ensure **1, 3, 6, 9 and 11** are **Closed**.
11. Evacuate sampling bomb by opening valve **5**. In sequence, first open valve **9** for 5 s then close valve **9**. Then Open valve **11** for approximately 20 – 30 seconds. This will flush any residual H_2, CO, CO_2, etc. from the sampling bomb. Close valve **11** and check to ensure the pressure in the sampling bomb is below atmospheric. Only N_2 and O_2 should remain in the sample bomb.
12. Close valves **5 and 4**. Ensure valves **3, 11 and 9** are closed also.
13. Repeat steps 5 – 7 to collect a sample from the reactor.
14. Use the gas tight syringe with valve to collect a gas sample from the sampling bomb by inserting the syringe through the rubber septum above valve **11**. Flush and purge the syringe with sample approximately 3 – 5 times. **WARNING:** Pressure in the syringe before injecting into the Agilent MicroGC must be approximately 10 psi. If pressure in the syringe is very high (syringe piston is pushed up rapidly without human help) collect approximately 2 – 3 ml, close the syringe valve and then pull the syringe piston to expand the syringe sample thereby lowering the pressure.
15. Take syringe to the microGC in 1521B. Ensure the septum is installed on the GC sampling inlet.
16. Enter a new sample into the microGC worklist including all relevant details.
17. Insert syringe through septum into sample inlet line, open syringe valve, then start the worklist to begin sample analysis.
18. When you hear the vacuum pumps turn on, slowly inject sample into the microGC line by depressing the piston. Depending upon the syringe pressure, a sufficient rate will be approximately 1 ml / 10 s (you can gauge using the graduations on the syringe). Lower pressures will require a faster injection rate. Closely monitor the microGC status screen on the computer to ensure enough sample is introduced. Too little sample will be accompanied by a message that the pump flow rate is low. Too much sample will be indicated via a message that the column head pressures are high.
19. To ensure accurate analysis, collect another gas sample by repeating steps 13-18.
20. After injecting the second gas sample into the microGC, collect the liquid sample. Close valve **7** and Open valve **6**. Then open valve **5** to vent remaining gas and reduce the sampling bomb pressure.
21. Properly label a vial for the liquid sample, and collect sample into vial by opening valve **9**. Allow the lines to drain for several seconds. Close valve **6 and 9**; Open valve **7**.
22. Record mass of vial and sample.

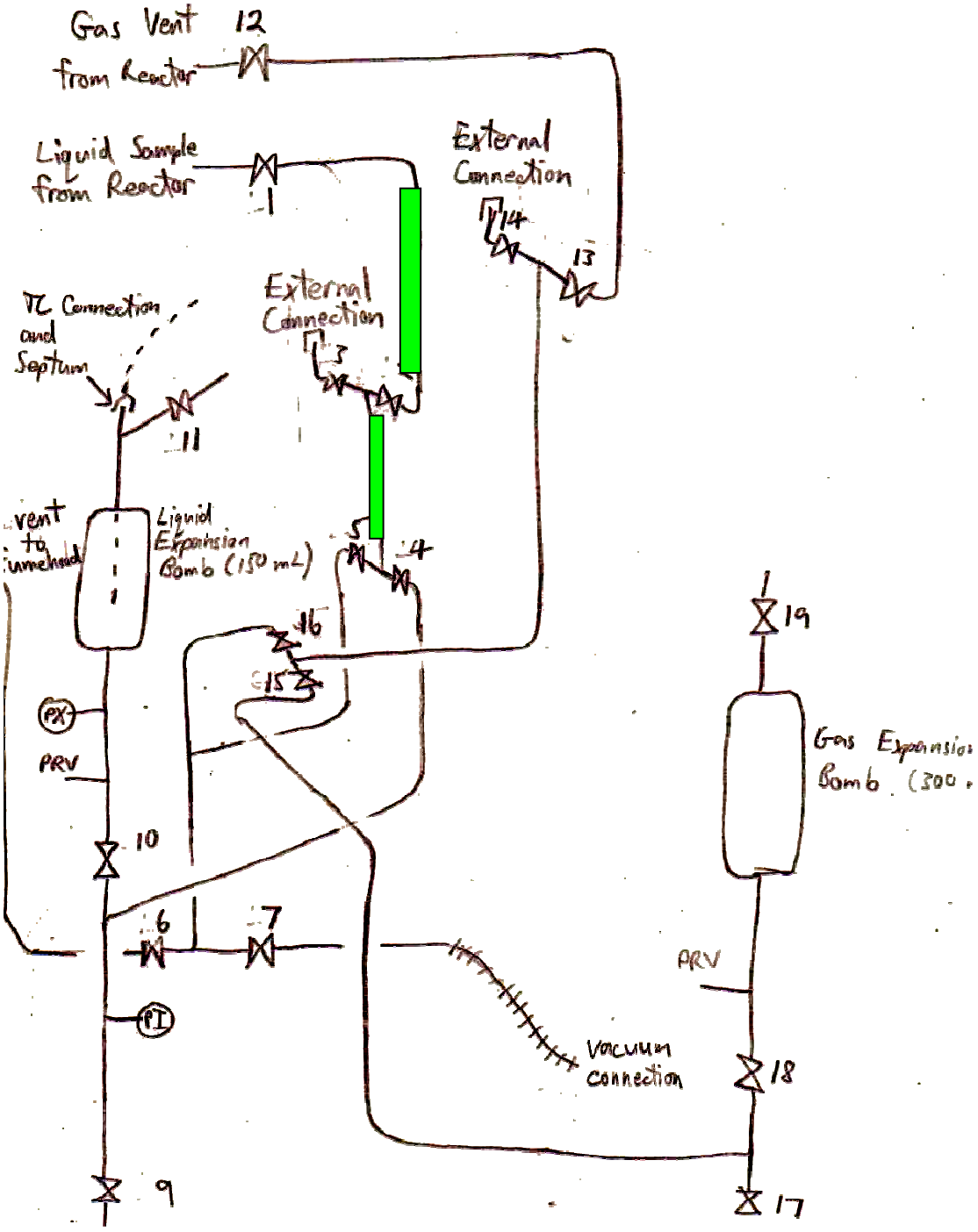

Figure E. 1: Configuration after collection of high pressure reactor sample

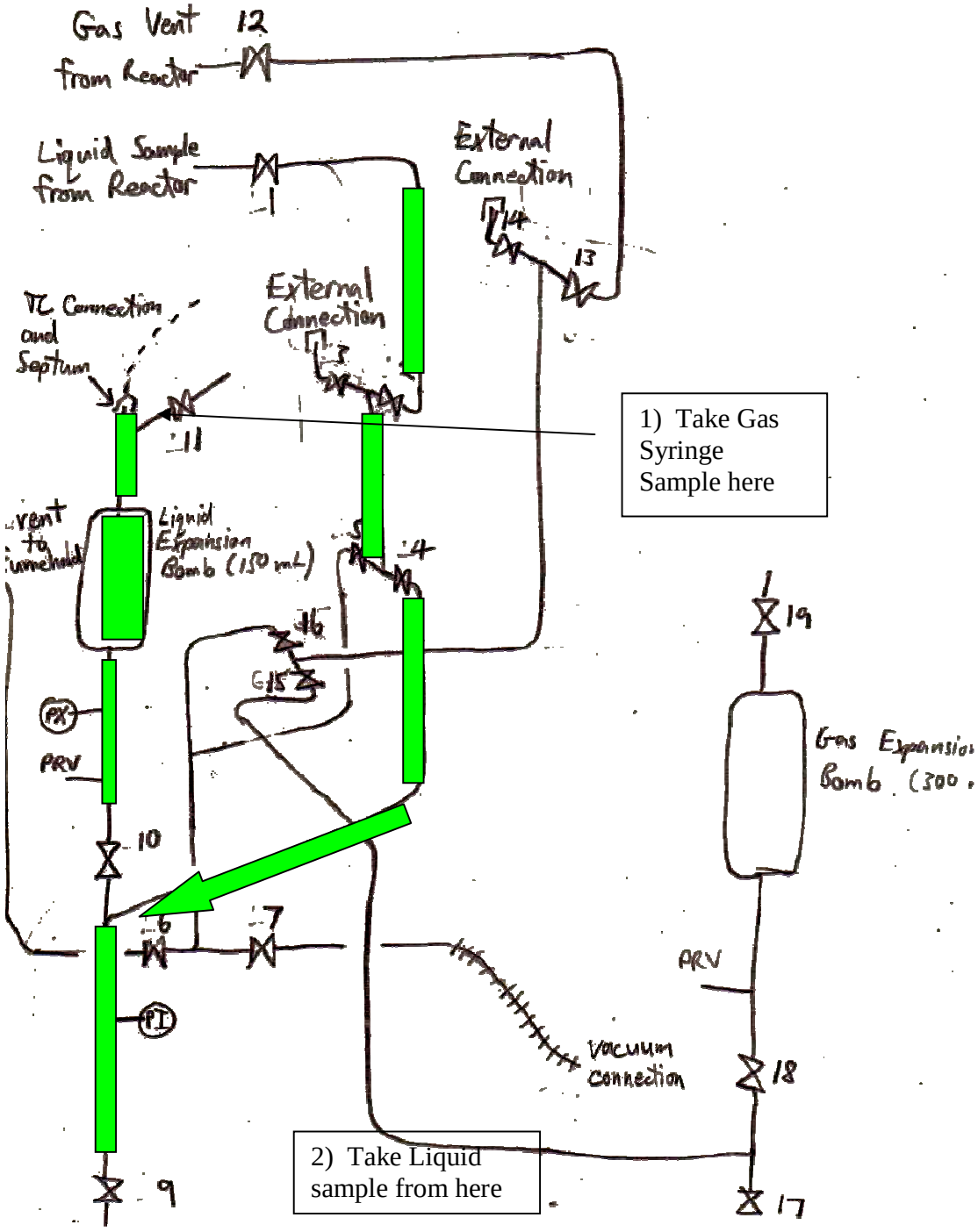

Figure E. 2: Configuration of de-pressurized liquid sample ready for collection

Appendix F: Equipment Specifications and Diagrams

The Data Acquisition System (DAQ) is composed of,

- a power supply (1.5 A, 120 VAC Input, 20 V Output)
- 2 data acquitision boards (USB-TC and USB-1208FS, Measurement and Computing)
- 2 Pressure Transducers (reactor, sampling system = Omega PX209-30V85GI)
- 2 Thermocouples (Omega K-type)
- DAQ Computer that also operates the Agilent Micro-GC Cerity Software
- wiring with associated connectors

Thermocouples are connected to the USB-TC board which is turn is connected to the DAQ computer. The pressure transducers are connected to the USB-1208FS board and operate on a 4-20 mA signal; a 249 ohm resistor bridges the terminals on the USB-1208FS board to convert the 4-20 mA signal into a voltage from 1-5 V. The data is recorded and stored on the computer as a voltage versus time signal; temperature data is recorded directly as a temperature-time signal. The following connection diagrams are included to aid in troubleshooting of the DAQ system if problems arise.

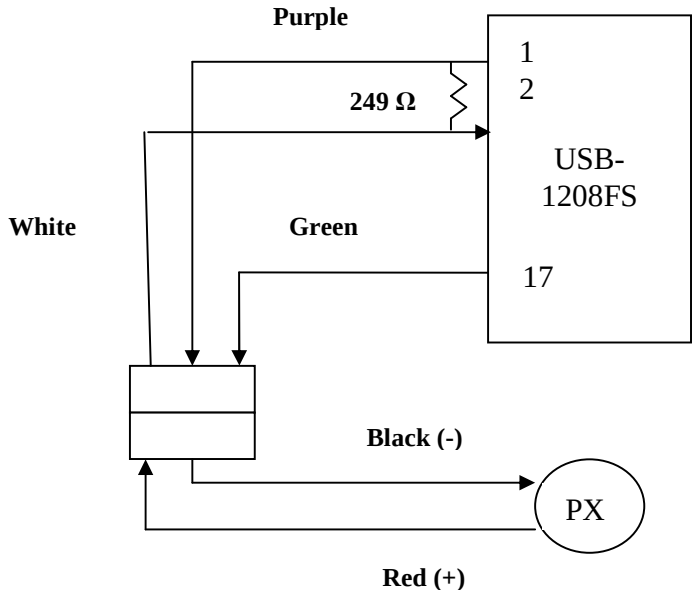

Figure F. 1: Sampling Bomb Pressure DAQ Diagrams

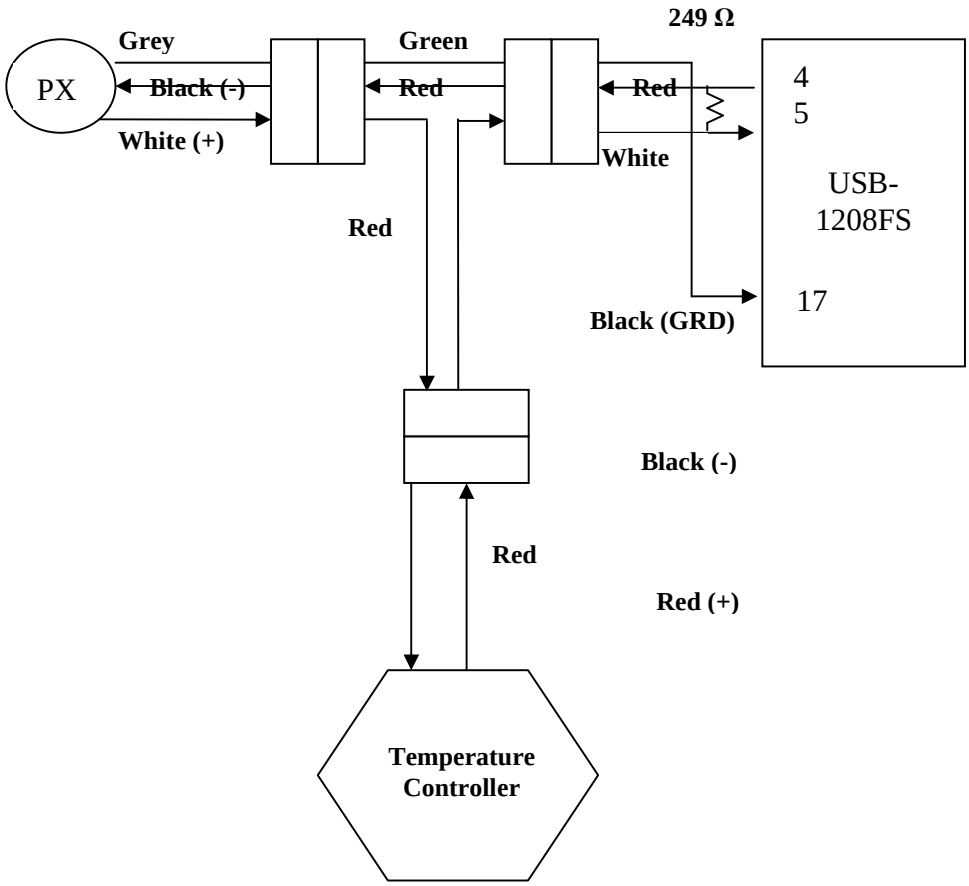

Figure F. 2: Reactor Pressure DAQ Diagrams

Table F. 1: HC-276 300 ml Autoclave DAQ Connections

Description	Channel #	Board
Sample Bomb Temperature	C5	USB-TC
Reactor Temperature	C6	USB-TC
Sample Bomb Pressure	C0	USB-1208FS
Reactor Pressure	C1	USB-1208FS
Instrumentation		
Reactor Pressure Transducer	0-10 000 psig Range	4-20 mA output current
Sample Pressure Transducer	-14.7 – 85 psig Range	4-20 mA output current
Thermocouples	K-type	

Appendix G: Mass Transfer Coefficients

Mass Transfer Limitations

A simple experiment to determine the effect of impeller speed on gas absorption was performed. This involved charging the reactor to 600 psig and then sequentially increasing the stirring rate while measuring the decrease in pressure. This gives an ad-hoc measure of the gas dispersion effectiveness of the impeller.

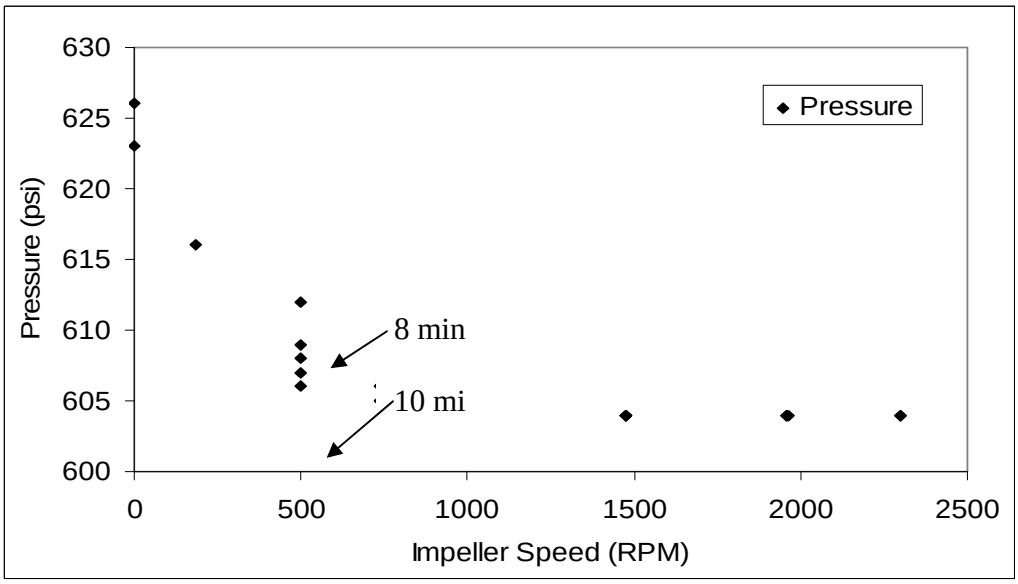

Figure G. 1: Reactor Pressure versus Impeller Speed

Determination of the gas/liquid mass transfer resistance was calculated according published procedures (Fogler 1999). Detailed procedures on calculating mass transfer coefficients for batch reactors have been published elsewhere (Meille et al. 2004, 924-927; Pitaut et al. 2004, 31-42).

$$\frac{C_i}{R_a} = \frac{1}{k_b a_b} + \frac{1}{m}\left(\frac{1}{k_c a_p} + \frac{1}{k\eta}\right)$$

C_i = *Concentration of gas (mol/g-Liq)*
R_a = *Overall rate (min^{-1})*
$k_b a_b$ = *gas absorption coefficient (min^{-1})*
$k_c a_p$ = *mass transfer coefficient from liquid to particle surface*
$k\eta$ = *coefficient of reaction and diffusion within catalyst particle (ppmw Mo min)$^{-1}$*

where,

$$\frac{C_i}{R_a} = r_b + \frac{1}{m}(r_r + r_c)$$

r_b = *resistance to gas absorption (min)*
r_r = *resistance to diffusion within catalyst particle and reaction (ppmwMo-min)*
r_c = *resistance of gas transport from liquid bulk to catalyst surface (ppmw Mo-min)*

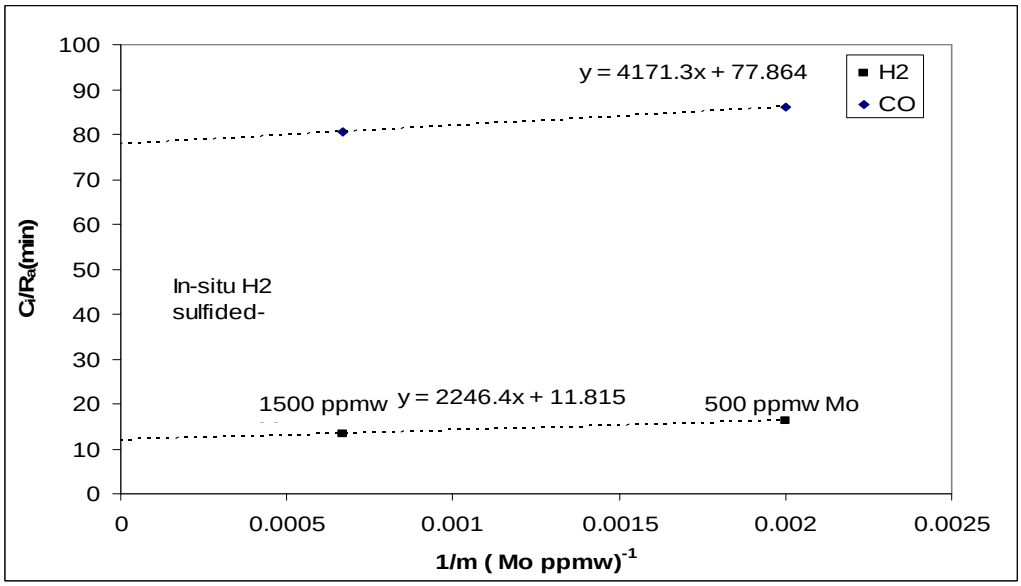

Figure G. 2**:** Estimation of Gas/Liquid Mass Transfer Coefficient under VNiMo-sulfides, Experiment #44 and #53 (1500 RPM Impeller Speed)

From Figure G.2, the estimation of gas absorption resistance is much smaller than the combined resistance of intraparticle diffusion and surface reaction for both hydrogenation and water-gas shift over unsupported, dispersed VNiMo-sulfides.

Appendix H: Selected Examples of Pressure-Temperature Process Data

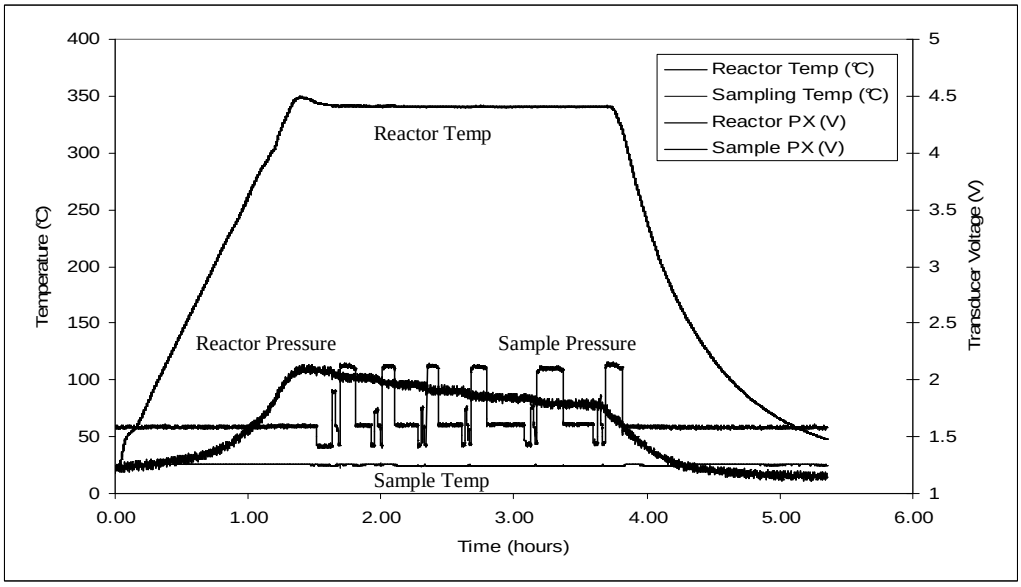

Figure H. 1: Pressure and Time Data for Experiment #53 ($CO/H_2O/H_2S$, 2.5 vol% H_2S, 600 psig, 4.0 °C/min, 340 °C for 2 hrs, 10 ml H_2O, 100 ml toluene, 10 g NAPH, 0.5 mmoles Mo, 0.30 mmoles Ni, 0.30 mmoles V)

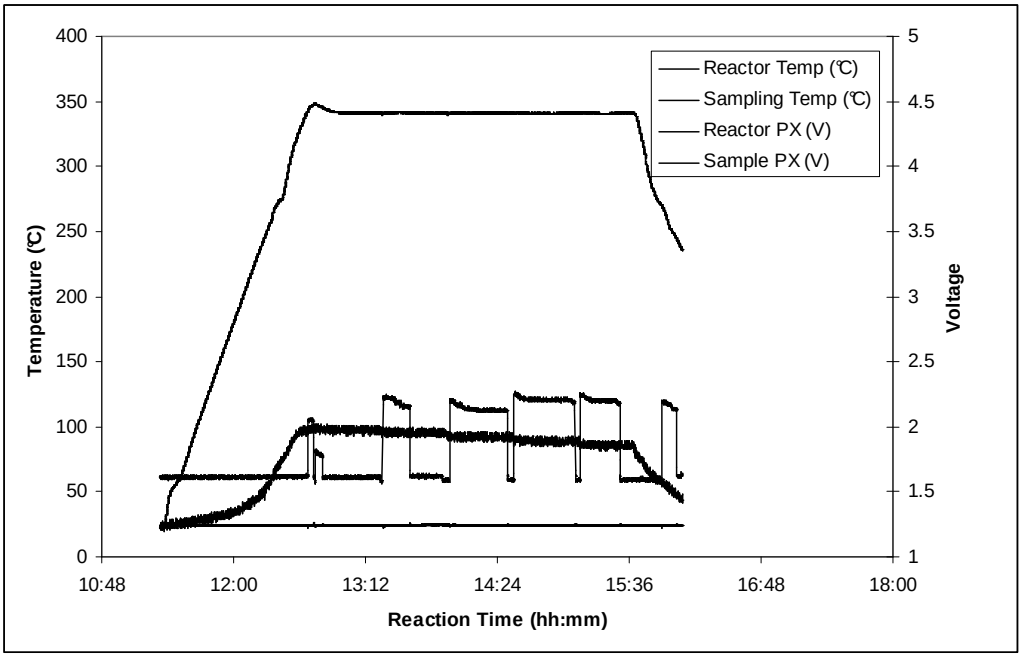

Figure H. 2: Pressure and Time Data for Experiment #1R1 ($COH_2/D_2O/H_2S$, 2.5 vol% H_2S, 600 psig, 4.0 °C/min, 340 °C for 3 hrs, 10 ml D_2O, 100 ml n-octane, 3.7 g NAPH, 0.47 mmoles Mo)